Experimental Investigation of Tornado-Induced Pressures on Low-Rise Buildings

by

Jason Williams

Thesis submitted to the University of Ottawa
in partial Fulfillment of the requirements for the
Master of Applied Science in Civil Engineering

Department of Civil Engineering
Faculty of Engineering
University of Ottawa
Ottawa, Canada
February 2022

Acknowledgements

The past two years have been a great period of personal and professional growth. None of this would have been possible without the help and dedication of many people in my life.

First of all, I would like to thank my supervisor Dr. Elena Dragomirescu. Throughout the last two years, she has been nothing but helpful, positive, and ready to give me guidance. Her availability to discuss experiments and wind engineering made the learning process easy and interesting. Dr. Dragomirescu also introduced me to Dr. Lacasse from the NRC where I was able to secure a graduate student position.

To build on that, I would also like to thank Dr. Lacasse for giving me the opportunity to work at the NRC. I have learned a lot about conducting research and performing experiments while working here. I also appreciate our routine talks about life, academics, and career. It is one of the highlights of my day at work.

Dr. Muslim Majeed and Dr. Gamal Elnabelsya were of great help during the experimental phase of this thesis. They always had an idea of how to fix or build something new and were eager to help. Their good sense of humor and interesting conversations helped with the long days in the lab.

I would like to thank my family, in particular my mom, dad, and grandparents. They have been a great support system, especially during the pandemic, and have financially supported my studies.

I would also like to thank my friends, in particular Jad and Tristan, who have always been by my side and have always been positive influences in my life. This had a significant impact on the completion of this thesis.

I am so lucky to have so many great people in my life and I look forward to the next chapter of my journey.

ABSTRACT

Tornadoes pose a significant danger to human life and structures. Research regarding the effects of tornado-induced loads on residential buildings is in incipient stages and there are no specialized construction standards in place to recommend criteria applicable to structures for withstanding tornadic winds. Three residential house models with different geometries were tested in the Wind-induced Damage Simulator (WDS) built at the University of Ottawa. The WDS is capable of simulating pressures induced by multidirectional and tornadic winds. The peak pressure coefficients were calculated on the walls and roofs of the houses and an analysis was performed on the effects of house model orientation, roof pitch angle, and exposure duration. The peak pressure coefficients were then compared to the NBCC 2015 code to clarify if there were any limitations of the current wind design criteria. It was found that the building orientation did not have a significant effect on pressure coefficient trends and magnitudes on the walls and roofs. For the low roof pitch angle models, it was noticed that the suction on the roof was much greater than the higher roof pitch angle models. An interesting observation was made that found that the leading edge of the walls in the direction of the clockwise tornadic flow were always under greater suction than the trailing edge, which causes a torsional effect on the entire model. When comparing the peak pressure coefficient values to the NBCC 2015 recommended values for the secondary cladding members, it was found that the C_pC_g stipulated in the code were similar to the experimental tornado C_p's for the walls. However, the C_p's on the roof were much greater in the experiments when compared to the NBCC 2015. The C_pC_g of Zones S and Zone R, which are the edges and central regions of the roof, greatly exceed the minimum values in the NBCC 2015. More experiments for residential house models of different geometries should be conducted in order to propose new tornado-induced pressure coefficients to be used in the design of the structure located in tornado-prone areas.

Contents

List of tables

List of figures

Chapter 1 - Introduction

1.1 Background

An average of 60 tornadoes occur each year in Canada; however, in 2021 excessive windstorm activity led to 81 confirmed tornadoes, out of which 46 were reported across Ontario (NTP, 2021). The building design codes, such as National Building Code of Canada (NBCC 2015), do not have specific guidelines for structures' resistance to tornado events. The current building codes have evolved from linear wind models (NBCC, 2015). This is a limitation since the pressures induced by a tornado can exceed those caused by straight-line atmospheric boundary layer (ABL) winds by factors of 3 to 5 (Haan et al., 2008). The devastating effects of tornadoes can be seen in recent tornado events in Dunrobin and Arlington Woods, Ontario, and Gatineau, Quebec, which had estimated wind speeds of 220 km/h to 265 km/h and damaged over 200 buildings (Otis, 2018). The most recent Barrie, Ontario tornado had wind speeds reaching 210km/h, destroyed over 71 houses and caused over $75 million in damages (Paglinawan, 2021). These recent tornadoes correspond to Enhanced Fujita scale EF-2 to EF-3.

The current practice to measure tornado severity is the Enhanced Fujita Tornado Damage Scale. It assigns tornadoes a severity rating depending on the maximum wind speed and the damage caused. It is separated into 6 different categories, EF0 to EF5, which are categorized by wind speed in mph. A wind speed of above 200mph is an EF5 tornado, while a tornado with a wind speed between 65mph and 85mph is an EF0 tornado. Abbreviations linked to specific types of infrastructures are determined based on whether that type of infrastructure was damaged or not and a damage degree is added to the F# notation, for a final EF rating (US Department of Commerce, 2016). Figure 1.1 shows the damage effects of different tornado scale severities on residential houses (Ramseyer et al., 2015).

Figure 1.1: Aerial image of different EF scale tornadoes aftermath (Ramseyer et al., 2015)

The main challenge for determining tornado design procedures lies in the difficulty to predict and track a tornado occurrence. Moreover, it is nearly impossible to obtain data from the full-scale tornadic event (Mishra et al., 2008) due to the damage encountered by the instrumentation deployed in the vicinity of a tornado. Parameters such as velocity, tornado path, and diameter can be determined; however, parameters like the swirl ratio, Reynolds number, and tornado vector field are much more difficult to obtain. Producing physical tornado simulation models that allow engineers and scientists to control these parameters, to test models, and to investigate the shape tendencies of tornado formations could allow for better testing of wind-induced pressures on various types of house models necessary for the optimization of building codes. Currently the pressure coefficients available in NBCC 2015 are determined based on Atmospheric Boundary Layer (ABL) wind tunnel tests. For tornadic events it is not possible to use a straight wind speed profile as a means to measure the forces as the surface pressures measured during experiments are 3 to 5 times higher in a vortex formation when compared to an ABL wind with the same velocity. Therefore, it is important to be able to accurately model a tornado vortex to obtain accurate pressure coefficients results on structures (Haan et al., 2017, Roueche et al., 2020). Several experimental facilities for simulating tornado effects on structures were developed for large-scale testing (Ashraffi et al., 2021) and others for small-scale testing (Haan et al., 2008, Mishra et al., 2008). Results for internal and external pressures induced by tornadoes of different intensities were investigated.

1.2. Research motivation

Research and studies regarding the pressures exerted by tornadoes on residential buildings are limited. Standards and evaluation methods regarding the impacts of tornadoes on pressure coefficients along the surfaces of residential houses in the NBCC 2015 are not yet established. With an increase in severity and quantity of tornadoes in North America, it has become an important topic to determine if the building code is adequate to withstand the greater pressures created by tornadoes. Field studies are not practical in determining the pressures exerted by tornadoes on houses due to the difficulty in capturing data in a full-scale tornado due to their unpredictable and destructive nature. Using experimentally simulated tornadoes in the Wind-induced Damage Simulator (WDS) at the University of Ottawa, which is capable of forming multi-directional winds, the pressures induced by a scaled-down tornado can be obtained and analysed.

1.3. Research objectives

The main objectives of this study are to determine the pressure coefficients exerted by simulated tornadoes on residential houses models and to compare these with the wind-induced pressure coefficients recommended in the current NBCC 2015 building code. With an increase in frequency of occurrence and severity of tornadoes in North America, determining if the building code is adequate to withstand the greater pressures created by tornadoes has become an important topic. For achieving the above research objectives two stages of experimental investigations were planned as follows:

Stage 1: Characterizing the tangential velocity profile along the radius of the tornado.

Stage 2: Obtaining and analyzing the pressure coefficients on the house models for different cases in the simulated tornado.

For both stages of the experiments, a few goals were set and achieved:

- Determining the tangential wind velocity profiles for fan RPM’s ranging from 700RPM to 900RPM in order to determine an adequate simulated tornado to subject the house models to.
- Analyzing the pressure coefficients that were calculated along the house models’ roofs and walls to understand the nature of the pressures along the models’ surfaces.
- Determining the effects of the model’s geometry and orientation on the pressure coefficients on the walls and roofs.
- Comparing the experimentally obtained pressure coefficients to those stipulated in the NBCC 2015 code and determining which zones on the surface of the models exceed the peak pressure coefficient C_p for each zone in the NBCC 2015.
- Studying the effects of exposing the models to the simulated tornado for longer durations by using varying sampling time durations.
- Make recommendations regarding future experiments and emphasizing the most important observations that were noticed during the WDS experiments.
- Recommend important findings regarding pressure coefficient trends and draw conclusions regarding the NBCC 2015 wind pressure coefficients for future tornado design.

1.4. Methodology

The Wind-induced Damage Simulator (WDS) is a wind testing facility at the University of Ottawa, which consists of a 3.65m x 3.65m x 3m cubic reinforced steel box with an outlet fan in the middle of the ceiling that creates a suction in the wind box. Five inlets are found on each wall, and they are strategically placed in the corners and central region at varying heights. By opening different inlets, the flow structure in the WDS changes. The outlet fan causes air to flow through the inlets creating multi-directional wind flows. By opening the inlets in one of the corners of each wall, a tornadic flow can be created. For the current experimental program, the four corner inlets were opened such that a symmetric rotational flow is formed in the WDS chamber to simulate tornadoes. A 12-hole Aeroprobe was employed to characterize the vortex velocity fields at different locations along its radius. By processing the pressure data measured by the Aeroprobe instrument, the

Aeroflow 2 software was used and the horizontal velocity (u), vertical velocity (w) and axial velocity (v) were found. This was performed for different fan RPM's (700 RPM, 750 RPM, 825 RPM, 900 RPM). By comparing the WDS simulated tornado with the Case et al., (2011) study, the 700 RPM was deemed as the best fit for a lab simulated tornado of specific tangential velocity profile. Thereafter, the pressures induced by a simulated tornado on three low-rise house models that had a scale of 1:100 were investigated. The three house models tested in the WDS had different geometries and different roof pitch angles. A total of 96 pressure taps were opened on the walls and roofs of the house models and experiments were conducted by placing the models at different radii of 10 cm, 25 cm and 40 cm, inside the tornado created by the 700 RPM configuration. The models' orientation varied, setting the incoming tangential flow of the tornado approaching the house models at orientation angles of 0°, 45° and 90°. The pressure coefficients were calculated based on the simulated tornado maximum tangential velocity. Peak pressure coefficient contour plots and graphs for each house model and case were made and an analysis of these results was performed.

The tornado that was used for this experiment was stationary. Since tornadoes in nature are translating, simulating a stationary tornado for experimental purposes can lead to different pressures on models. One of the main differences between a simulated translating and stationary tornado is the exposure duration of the tornado to the building. If the tornado is translating, the house will only be exposed to the wind for the extent that it takes for the tornado to pass over it. When simulating tornadoes in a laboratory setting, this is important to take into consideration because a stationary tornado is sitting on the house for the duration of the test. The idea of creating an exposure duration analysis was followed in order to observe the effects of exposure duration on the pressures induced on the surfaces on the house models. Comparing the peak pressure coefficient results (C_p) obtained in the current experiments to the NBCC 2015 recommended pressure coefficients for wind design of residential houses was performed to determine if the delimited C_pC_g zones can be used for tornado design or if these need to be updated.

1.5. Thesis layout

This thesis is separated into 5 chapters, where each chapter will have its own important significance for this research project.

Chapter 1 introduces: the importance of performing research on the impacts of tornadoes on civil engineering infrastructure, the objectives of the experiments performed in this thesis, and the description of the experiments.

Chapter 2 covers the knowledge that was gained to understand the current experimental advancements, which have been done on scaled experimental simulations to understand the effects of tornadoes on residential housing. It starts with a review of some of the important parameters used in simulated tornadoes and introduces the current state-of-the-art tornado simulators. Some experimental methods used by different research institutions are covered and assessed for their practicality related to the experiments carried out for the research project performed at the University of Ottawa. An important section of the literature review is the effect of simulated tornadoes on residential housing. A section on the effects of tornado durations is also introduced and finally, an analysis of the wind design section of the NBCC 2015 is introduced for a comparative analysis between the experimental pressure coefficients and the pressure coefficients in the NBCC 2015.

Chapter 3 presents the method used to obtain an adequate simulated tornado in the WDS at the University of Ottawa, via the use of a 12-hole Aeroprobe sensor used to characterize the tornadic wind profile. The method used to collect pressure coefficients induced by tornadic winds on the residential house models under different test scenarios, where residential house model orientation and positioning along the simulated tornado's radius varied, was introduced. The method employed for processing the experimental data and converting from pressure values to pressure coefficients for further developing the pressure coefficient contour plots and graphs, and the methods used to analyze the data, are also covered.

The experimental pressure coefficient results can be found in Chapter 4 in the form of contour plots and pressure coefficient graphs. An analysis of the house models at different orientation angles and different geometries is made and detailed pressure coefficient results are presented only for most pertinent cases, while the rest of the data is included in Appendices A and B.

Chapter 5 presents a method used to study the sampling duration effect on pressure coefficients. These pressure coefficient results are then compared to the pressure coefficients recommended by NBCC 2015 code, for the stipulated zones along the walls and roofs of the house models. Zones which could potentially exceed the NBCC 2015 criteria are discussed.

Chapter 6 summarizes the important findings and the most interesting discoveries regarding the data analysis and comparison to the NBCC 2015. Future work recommendations are additionally made based on the newly acquired knowledge from this research project.

Chapter 2 - Literature Review

Complex wind flows, such as tornadoes, are still challenging to replicate in laboratories. Design guidelines for structures located in tornado prone regions are still in incipient development. Recreating the strong suction required for design criteria with the laboratory simulated tornadic wind flows and producing tornadoes with accurate parameters such as swirl ratio and Radial Reynolds number are still in need of additional research, especially for new tornado simulators. A lot of research is required in characterizing tornado simulators and comparing one simulator to another can lead to differences and discrepancies. The current chapter summarizes the most representative studies and wind related design codes.

The first attempt to simulate a tornado in a laboratory was carried out by Ward (1972), who employed a cylinder with a fan at the top while at the bottom of the cylinder, guiding plates were installed to redirect the flow into a tornadic formation. However, the Ward simulator had small dimensions and concentrated on determining the shape created by a tornado. Several other researchers have employed the same simulator configuration (Davis-Jones, 1976, Church et al., 1979). It is only in later years that studies were performed to determine the pressures induced on scaled residential buildings (Jischke and Light, 1983).

Haan et al. (2008) performed a study on the tornado inflow at different heights, which showed that the strongest inflow region is at around 10m to 20m. This is the height where civil engineering structures are found. In addition, he emphasized that it is not possible to use an ABL wind as a means to measure the forces created by a tornado, as the surface pressures measured during the experiments are 3 to 5 times higher in a tornado vortex, which has the same velocity as that of a straight wind. Therefore, it is important to be able to accurately model a tornado vortex to obtain accurate pressure results on structures for development of the building code (Haan et al., 2008). This literature review will focus on presenting the most important parameters used in experimental tornado simulations. Three tornado simulating facilities, and the laboratory conditions they employ, are presented along with the experiments that were performed. Knowledge gained from these experiments were taken into account when performing experiments at the WDS at the University of Ottawa. The current study's ideas and approaches were used to define the tornado parameters simulated by the WDS facility. Research that experimented and analyzed pressure trends caused by tornadoes and compared them to the design values recommended by the building codes are also described in this section, as this is the main goal of this thesis.

The three tornado simulators that were described and the experiments that are introduced in this section were from the following tornado simulators: 1) Iowa State University (ISU) Tornado Simulator, 2) Western University WindEEE Dome and 3) Computer Simulation Model of the contaminant vortex box simulator. Two physical models as well as a computer model are introduced. This analysis could help define possible assumptions, methods, parameters, and equations that could be used in similar tornado simulators.

2.1 Tornado parameters

The swirl ratio is the measure of the rotation tendency which develops in a tornado event (Rotunno, 2013). In a tornado, the air is rotating without friction around the cyclone, which is the core of the tornado. When the air tries to enter the tornado vortex, where the pressure is much lower, it may not be able to because of the high centrifugal acceleration of the central vortex. When this occurs, a vertical vortex develops due to the small curvature radius around the low-pressure area. By causing an alteration of the pressure gradient acceleration, an acceleration of the horizontal pressure gradient will cause the formation of a vortex at the Earth's surface. This vortex will cause an inflow of air at a swirl ratio of 1. A low swirl, below 0.4, will develop a single cell vortex as seen in Figure 2.1a. As the swirl ratio increases, the mass of air rotating around the vortex increases and begins to break down into a secondary vortex (Figure. 2.1b). Figure 2.1c and Figure 2.1d exemplify the transition from a single cell tornado to multiple vortices. If the rotating air velocity is increased and the updraft strength is low, there is a tornado with a large swirl ratio. If there is a high updraft strength and a low rotating air mass, this characterizes a lower swirl ratio (Rotunno, 2013; Amit, 2008).

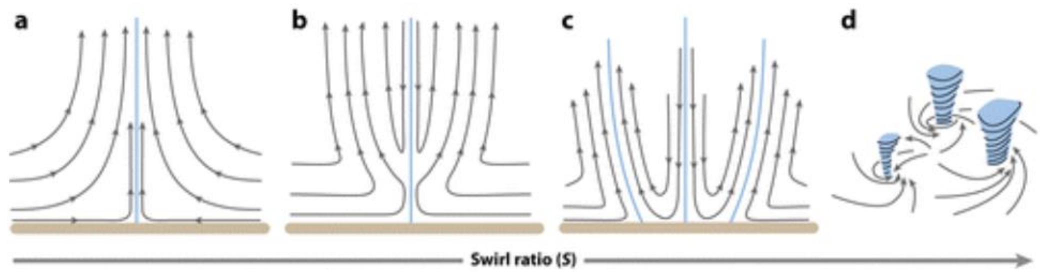

Figure 2.1: Vortex characteristics based on the swirl ratio a) one-cell vortex; b) vortex breakdown; c) two-cell vortex; D) multiple vortices (Rotunno, 2013)

This shows that low swirl ratios create more uniform single vortex tornadoes, and as the swirl ratio increases, the tornado can separate into multiple vortices (Figure 2.1d).

There is a lack of data acquisition for the parameters of full-scale tornadoes. This is due to the destructive power of the winds making it difficult for data acquisition devices to remain undamaged, as well as the unpredictable path and spontaneous development of a tornado. The use of Doppler Radar can be useful in obtaining data, but it is not helpful for civil engineering research as the radar is only useful in obtaining data at an elevation above structures (Kopp et al., 2020). That being said, studies on the effects of simulated tornadoes use different parameters such as swirl ratio, Radial Reynolds number, and tangential and horizontal velocity. These are useful for laboratory-simulated tornadoes and for comparing the results from one simulation to another (Haan et al., 2008; Davies-Jones, 1976).

Most studies used to assess the performance of the experiments carried out in this thesis, were performed at the WindEEE Dome facility located at Western University and the Iowa State University (ISU) tornado simulator. In the Wind EEE Dome from Western University, the swirl ratio is defined as (Refan et al., 2016):

$$S = (1/2a)V_{tan,i}/V_{rad,i} \tag{1}$$

Where S is the swirl ratio, a is the aspect ratio, $V_{tan,i}$ is the tangential velocity and $V_{rad,i}$ is the radial velocity. The aspect ratio, a, stays constant based on the simulator's inlet height and the outlet radius.

$$a = Inflow\ height/Updraft\ radius \tag{2}$$

The aspect ratio is defined as the inflow height over the updraft radius. The inflow height can be determined as the distance from the floor to the inlet, and the updraft radius is the radius of the outlet fan. In the case of the WindEEE Dome, the tornado radius can be set to a specific dimension. For one experiment that they used, the inflow heights were 0.07 m and the updraft radius was set to 0.2 m. Therefore, the aspect ratio a = 0.07/0.2 = 0.35. It was also mentioned that the aspect ratio is independent of the swirl ratio and other tornado parameters, which keeps it constant (Refan et al., 2016).

Also, the $V_{tan,i}/V_{rad,I}$ ratio can be replaced by tan (θ) to create the equation 3 below:

$$S=(1/2a)\ tan\ (\theta) \tag{3}$$

Where θ is the horizontal angle offset of the vane or the inlet and a is the aspect ratio. The WindEEE Dome can control the tornado rotational flows by selecting various angles at the inlet. To create a tornado in the WDS experiment, a 90° inlet angle was the only angle that produced a tornado in the simulator. However, the calculated swirl ratio would be 0. Therefore, Eq. 3 could not be used to determine the swirl ratio for the tornado simulated in the WDS facility. The aspect ratio is also used in the swirl ratio equation.

The Radial Reynolds (*Rer*) number is another physical parameter that is important in characterizing a tornado, especially those in smaller-scale physical vortex models. For full-scale tornadoes, it is not possible to correlate the Radial Reynolds number. However, in a simulated tornado, it can be important to know the Radial Reynolds number to make correlations between it and other vortex parameters. In the WindEEE Dome, the technique to determine the Radial Reynolds number of a vortex, as well as the flow rate, was found using the average axial velocity (*Vax*) in the updraft. The *Rer* number for smooth flows is determined based on the uniaxial wind speed; however, for tornadoes a new formulation was adopted based on the flow rate, thus certain measurements are necessary. A Particle Image Velocimetry (PIV) measurement technique was used to determine the *Rer* number and the swirl ratio. This consists of a high-tech laser, a CCD camera, and 1μm particles that travel in the vortex. The laser would light up the particles and the camera would capture the reflection at intervals of 100 μs and 550 μs. The camera would capture the particle displacement in the vortex. With all the captured images, using the software called TSI, they determined the vector maps based on a time scale. With these, they could determine physical parameters such as velocity, flow, circulation, tornado radius, and swirl ratio (Refan et al., 2016; Hangan, 2014).

The Radial Reynolds number is represented by the equation:

$$Rer = Q/2\pi v \tag{4}$$

Where Q is the volumetric flow rate per unit axial length, v is the kinematic viscosity of the fluid. In a full-size tornado, the *Rer* number is much bigger than that of a simulated scaled-down tornado. It was determined that the *Rer* number does not influence a tornado that transitions from a single vortex to multiple vortices. The swirl ratio is what governs the vortex transition of a tornado; thus it can be deduced that the swirl ratio is what governs a more severe and strong tornado (Refan et al., 2016).

Therefore, in a tornado simulation model, the swirl ratio would be more important to understand and control. However, if knowing the *Rer* number helps determine the swirl ratio or other physical parameters, it can be important to accurately determine it. As mentioned earlier, to determine the *Rer* number of the vortices in the WindEEE Dome, the complex and expensive PIV measurement method was used. In addition, they obtained the flow rate by measuring the axial velocity at the inlet using a rotating vane anemometer. This method is much simpler, less expensive, and quicker compared to the PIV method (Refan et al., 2016). The results of the vane anemometer were very similar to those obtained by the PIV test. The use of a vane anemometer or an Aeroprobe sensor, which can also measure velocity, would be much easier to conduct in the WDS.

2.2 Vortex elimination models for air contaminants

A less known and less researched area of vortex/tornado development is for contaminant elimination in buildings. Testing and computer modeling are done in a room (Yan et al., 2019), which has a very similar configuration to the WDS facility. The research reported by Yan et al. (2019) did not focus on simulating a tornado, but to rapidly evacuate potential air contaminants from a room using a vortex. Numerous vortex contaminant- elimination models use a fan that extracts the air out of the room, and inlets at the base of the room that bring inside new air, which creates a vortex shape in the room. Due to the similarity between the vortex contaminant elimination models (Figure 2.2) and the University of Ottawa WDS facility, methods of determining physical parameters for the WDS tornado could be considered compatible with the ones reported by Yan et al., (2019). The contaminants are sucked into the vortex and are removed from the room through the exhaust fan at the top. This vortex ventilation method proved to remove contaminants much more effectively than the current room ventilation technologies. The physical parameters and the knowledge presented in the papers are beneficial in understanding and determining the vortex physical parameters in a square-shaped vortex simulator (Yan et al., 2019).

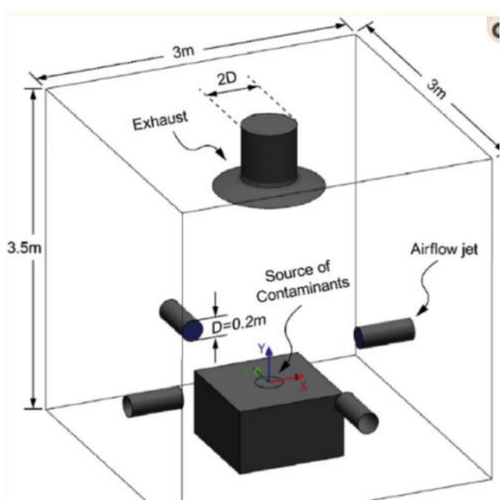

Figure 2.2: Wind box contaminant vortex simulator (Yan et al., 2019)

The design of the WDS is different from that of the WindEEE Dome or the ISU tornado simulator. Therefore, the swirl ratio and the Radial Reynolds *Rer* number expressions used in these papers could not be employed for the WDS experiments. Since the computer model created by Yan et al.,

(2019) has a design that is very similar to the WDS, some methods to measure the swirl ratio could be determined. In the described computer model, different simulations were done where the four airflow jet inlet angles were modified. For the simulations a targeted swirl ratio was considered, for which the horizontal angle of the inlet was changed accordingly. To determine the swirl ratio, the horizontal angle change of the inlet jet flow must be used. The swirl ratio used in this study was defined as the ratio of the tangential velocity to the radial velocity at the inflow (Yan et al., 2019).

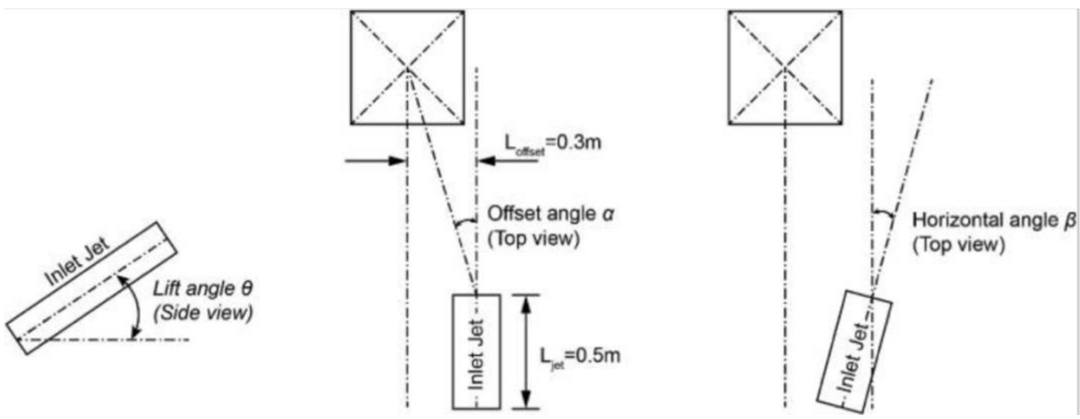

Figure 2.3: Inlet jet angle configuration angle variation possibilities (Yan et al., 2019)

The inlets of the contaminant vortex box simulator were rotated at a horizontal angle, β (Figure 2.3), to create simulations with different swirl ratios. In the 3 m x 3 m x 3.5 m wind box simulation, the swirl ratio was calculated based on the horizontal angle of the inlet jet as summarized in Table 2.1 below (Yan et al., 2019).

Table 2.1: Swirl ratio of the contaminant vortex box simulator

Case No.	Horizontal inlet angle Beta (degrees)	Swirl Ratio
1.1	4.8	0.12
1.2	8.7	0.22
1.3	13.8	0.35

The swirl ratios were obtained by using a set aspect ratio (a) of 0.35 and calculating the swirl ratio by Eq. 3 above. If the horizontal inlets are replaced in the swirl equations, the corresponding swirl ratios from the third column of Table 2.1 will be found (Yan et al., 2019). This is a similar concept to the WDS that is presented in Chapter 3: Methodology and procedures.

2.3 Iowa State University Tornado Simulator and Western University WindEEE Dome

The Iowa State University Tornado simulator uses a different concept for replicating the tornadic wind. The facility consists of a metal bell-shaped chamber, raised from the floor so it can translate. A fan at the top of the simulator creates an updraft, as well as a rotating forced downdraft on the outer portion of the simulator (Haan et al., 2008). The downdraft creates the rotating effect of the vortex and by changing the vane angle between 0° to 55°, the swirl ratio and diameter of the simulated tornado can be modified (Figure. 2.4). The bell-shaped chamber can be moved horizontally by a crane, at a maximum speed of 0.61m/s, over a distance of 3.35m, thus simulating a translating tornado. In addition, the ground area, which is detached from the movable simulator system, can translate vertically by employing a jack, to allow for a change of floor height (H) (Haan et al., 2008). To obtain accurate data, multiple different parameters were altered. The floor height was varied between 0.23m to 0.69m; the vane angles were inclined between 15° and 55°, while the fan speed setting was turned on at 0.33%, 0.50%, and 0.66% of the maximum fan capacity. Multiple tests were performed with different parameter configurations where some remained constant while others were changed. The radius of the tornado core (r_c) was determined as the distance from the center of the simulator to the location of maximum wind speed. This was named Radius of Maximum Winds (RMW) (Haan et al., 2008).

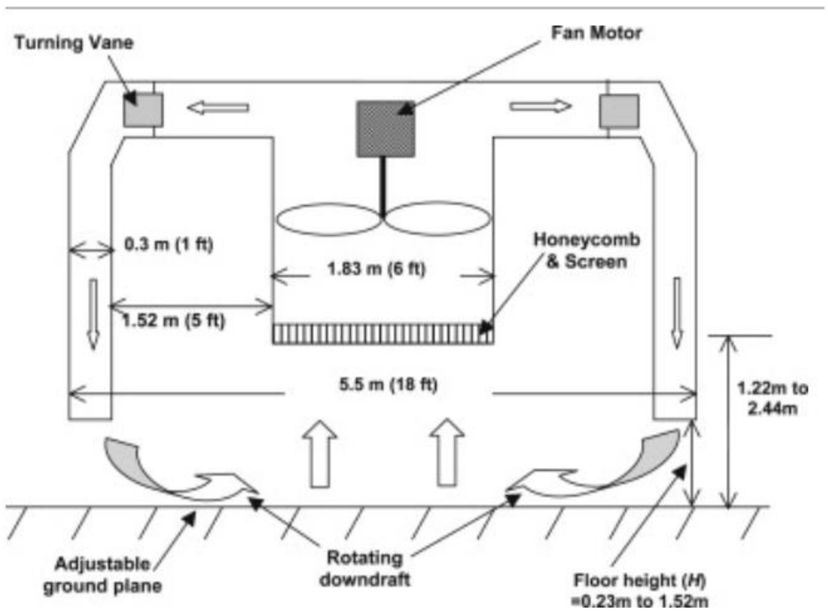

Figure 2.4: Iowa State University tornado simulator (Haan et al., 2008)

The WindEEE Dome built at Western Ontario University is a hexagonal-shaped wind chamber that is capable of simulating tornadoes that have a diameter of up to 4.5 m and a height of 4 m. The dome has an inner section that has a diameter of 25 m and an outer section of 40 m. A total of six fans at the top of the chamber create the suction which produces the updraft. Louver vanes near the floor provide the angle required to produce the rotation of the wind. The incoming flow is controlled by 100 fans distributed mainly on two opposite walls as it can be seen in Figure 2.5a (Refan and Hangan, 2016). Similar to the ISU tornado simulator, a bell mouth connects the low chamber to the upper chamber allowing a tornado to form (Figure 2.5b). Peripheral fans at the base of the six walls increase the angular momentum of the inflow by increasing air circulation through the vanes (Ashrafi et al, 2021; Hu, 2011).

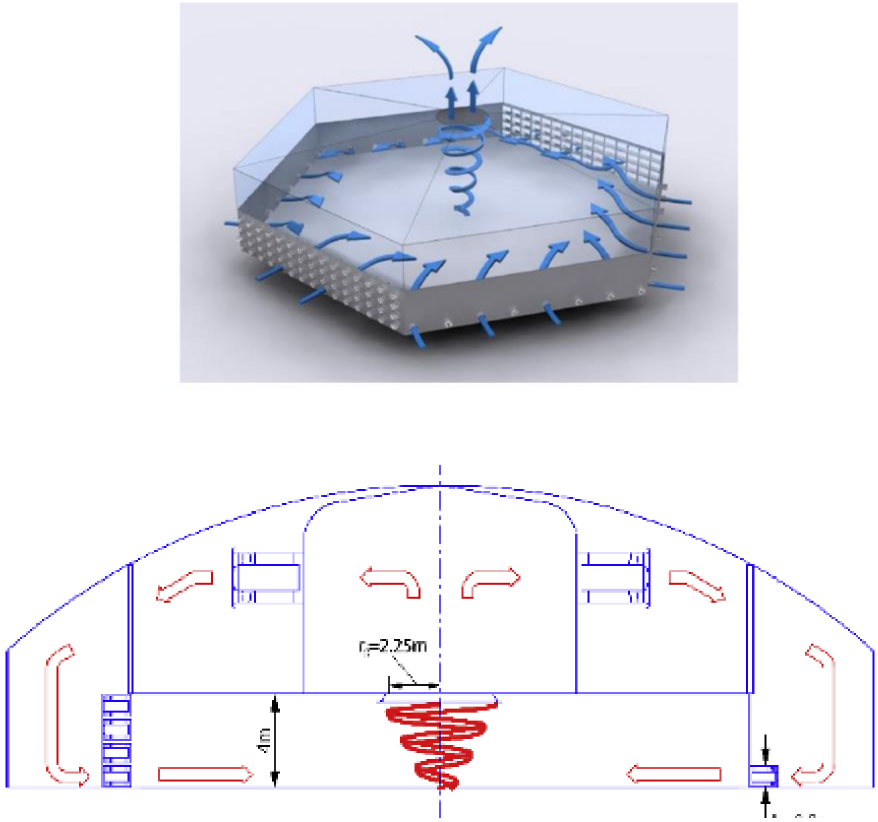

Figure 2.5: a) 3-D visualization of WindEEE Dome simulator; b) Cross-section view of WindEEE the Dome simulator (Refan et al., 2018)

Depending on the experiment type, different procedures are used for the simulators at ISU and the WindEEE Dome at Western University. As detailed in Ssection 2.1, when tornado parameters were introduced, Particle Image Velocimetry (PIV) measurements were conducted at the Western University WindEEE Dome tornado simulator, for determining the velocity vectors and the tornado radius at different heights (Refan et al., 2018). However, these PIV experiments were performed with extensive equipment and a complicated setup to allow capturing the particles in such a large space. The first set of calibrating tests showed that the WindEEE Dome can achieve a tornado with aspect ratios of a = 0.35 – 1, swirl ratios of S = 0.21-1.03 and Radial Reynolds number of $Rer = 10^6$ to 2×10^6 and $V_{tan\ max}$ of 8.8 m/s-16.2 m/s (Refan and Hangan, 2018).

It is also difficult to accurately determine the tornado parameters for the simulated tornadoes, due to their limited size, causing a low resolution. This makes it difficult to find the swirl ratio and the Radial Reynolds Number (Refan et al., 2018). Although the PIV method is very accurate and feasible to obtain results, Haan et al., (2008) stated that it is not ideal for their ISU simulator. The simulator has a height of 2.44 m and a diameter of 4.88 m. This model is very large, which would make it difficult to capture the entire view of the particles throughout the tornado region without numerous equipment and cameras. Also, the PIV particles need to be much larger to be captured by the camera from a further distance, and a very large quantity of particles would be needed to seed the room (Haan et al., 2008). It is first stated that the simulator cylinder is too large to use the PIV method to determine the tornado parameters such as velocities and dimensions.

The ideal method to measure the velocity field at ISU was by using a multi-hole pressure probe to gather velocity data along the vortex field. For the tornado parameters determination in the WDS, this method was considered as a potential alternative because the simulator is of similar dimensions to the one at ISU, and similar equipment is available. This includes a 12 holes Aeroprobe sensor, which is a spherical pressure probe that is similar to the PS18 Omniprobe used by ISU. The ISU pressure probe consists of 18 holes for pressure measurements and allows for flow measurement up to an angle of 165◦ d relative to the probe axis. They used a Scanivalve pressure scanner to record the data. To determine the velocity field, the pressure probe was vertically translated using a vertical traverse, and the horizontal positioning was translated by using the crane. To obtain accurate data, the probe was fixed in the same configuration and mounted horizontally and perpendicular to the crane translation direction (Haan et al., 2008).

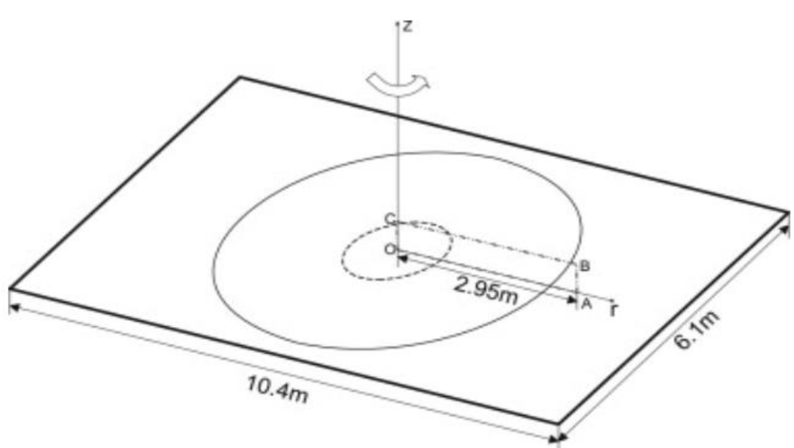

Figure 2.6: Omniprobe measuring field zr plane (Haan et al., 2008)

The pressure probe is placed at a starting position and will gather pressure data for 26 seconds and at a rate of 78Hz. The tornado is then translated to a new location, stopped, and the probe will then record a new set of data during 26 seconds. They determined that the tornado vortex was axisymmetric. Therefore, measurements only need to be taken along the *r* axis, and with varying heights. The OABC region in Figure 2.6 is the rectangle that denotes the testing area where the Omniprobe measured the velocity data. It should be noted that the measurements of data for a given tornado were obtained without stopping the data collection. Once 26 seconds had elapsed, the location of the probe relative to the tornado was altered, a new set of data was obtained during 26 seconds and the probe location relative to the tornado would then be changed again without stopping the tornado or re-setting the experiment (Haan et al., 2008).

The maximum tangential and horizontal velocities used for the experiments reported by Case et al., (2011) used this procedure to obtain the tangential velocity profiles of the tornado simulated on residential housing models installed in the ISU tornado simulator. The velocity profile was determined at different radii using a Cobra probe, which is similar to an Omniprobe. The peak velocity of 11.7 m/s which corresponds to $V_\theta/V_{\theta max}$= 1 in Figure 2.7, was found at 0.56 m corresponding to r/r_c = 1.

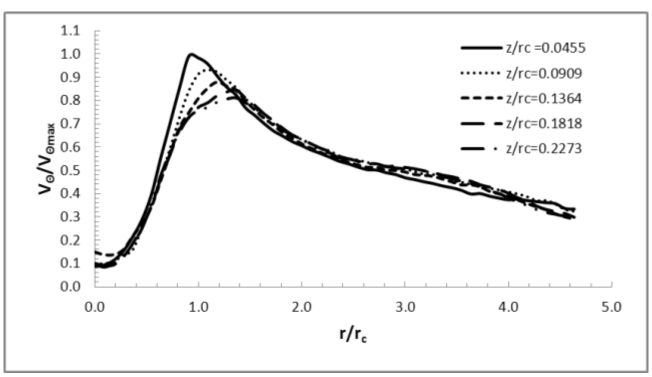

Figure 2.7: Normalized tangential velocity profiles for the ISU simulated tornado (Case et al., 2011)

This method can be used to determine the location of maximum horizontal or tangential velocity, which is also considered the tornado's radius. For experimental simulation of tornadoes, the maximum tangential or horizontal velocity is often used in calculating the pressure coefficient and the radius of maximum wind speeds in tornadoes (e.g., Haan et al., 2010; Wang et al., 2016). Moreover, because the data was obtained using the Omniprobe, velocity vectors could be determined. Using the axial velocity directions and placing each vector into an *rz*-plane (*r* is the *x*-axis), a vector plane can be created as illustrated in Figure 2.8 for a swirl ratio of 1.14 (Haan et al., 2008).

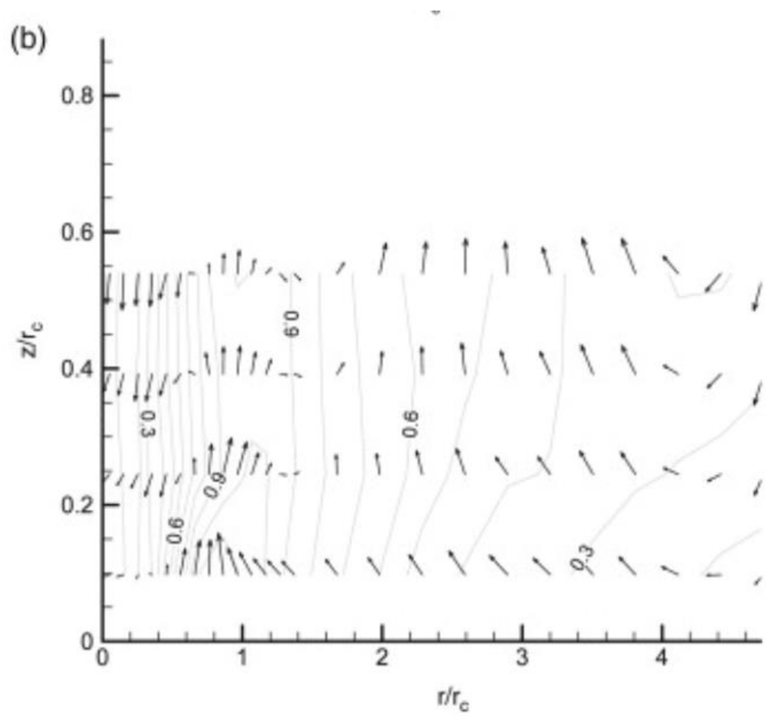

Figure 2.8: Vortex vector map on the z-rc plane, S = 1.14 (Haan et al., 2008)

This allows visualizing the physical formation type of the tornado in the simulation model. The method described above can be used to determine the vortex velocity field, as well as the vortex radius (Haan et al., 2008). The Iowa State University tornado simulator has similar dimensions to the WDS; thus, a similar experimental procedure was sought when performing the current experiments.

2.4 Simulated tornado effects on residential building models

There has been limited efforts in determining the effects of pressures and loadings induced by tornadoes on structures. In this section, a few studies are reviewed and important procedures and methods that were used are introduced, as they are useful for the experiments of this thesis. Studies that present pressure coefficients and their trends on residential house models are also shown.

Most of the literature related to tornadoes' effects on structures that focus on the pressure coefficients display a comparison between different structure types and building geometries. Case et al. (2011) performed experiments on different residential models with geometries corresponding to the ASCE-7 design code, focusing on clarifying: 1) The effects of building geometry such as roof pitch, eave height, and building orientation. 2) Determining the effects of low-rise building geometry and orientation on the failure of roof sheathing. 3) Comparing obtained loads from experimental tornado simulation 4) Proposing recommendations for roof connections.

Using the same tornado profiles from Figure 2.7, Case et al., (2011) carried out experiments in the ISU tornado simulator, to observe the effects of a simulated high-swirl tornado on residential house models. A total of 9 different residential house models, shown in Figure 2.9, with a length scale of 1:100, were tested in a translating tornado with a translation speed of 0.15 m/s and 0.46 m/s. The simulated tornado was based on a full-size EF-3 tornado with a maximum velocity of 73.76 m/s, where the scaled tornado had a horizontal velocity of 11.7 m/s and the vortex velocity scale of $\lambda(v)$ = 11.7/73.76 or $\lambda(v)$ = 1/6.3. This is the full-scale averaging time to the model-scale averaging time. Each scenario was tested for 10 repetitions and up to 124 pressure taps were installed on each model, where pressures were measured at a rate of 390 Hz for the duration that was adequate to measure the entire translation of the simulated tornado. The dimensions of the tested models 1 to 6 are presented in Table 2.2 (Case et al., 2011).

Table 2.2: Model dimensions (Case et al., 2011)

	Θ	B	L	he	ht	h	L/B	h/L
		mm	mm	mm	mm	mm		
model 1	15.95°	98	146	59.7	73.7	66.7	1.5	0.46
model 2	15.95°	98	146	109.7	123.7	116.7	1.5	0.80
model 3	4.6°	98	98	52.8	56.8	52.8	1.0	0.54
model 4	15.95°	98	98	47.7	61.7	54.7	1.0	0.56
model 5	35.5°	98	98	37.1	72.1	54.6	1.0	0.56
model 6	35°	221	221	37.1	114.1	75.6	1.0	0.34

ht = total height he = eave height h = mean roof height as defined in ASCE 7-05
L = longer plan dimension B = shorter plan dimension Θ = roof pitch

Once installed at a certain location in the simulated tornado, the models were rotated around the vertical axis, for a total of 7 building orientation angles for each model scenario, as summarized in Table 2.3 (Case et al., 2011).

Table 2.3: Different scenarios for models 1 to 6 (Case et al., 2011)

	VT= 0.15 m/s							VT= 0.46 m/s						
Model	0°	15°	30°	45°	60°	75°	90°	0°	15°	30°	45°	60°	75°	90°
Model 1	1	2	3	4	5	6	7	8	9	10	11	12	13	14
Model 2	15	16	17	18	19	20	21	22	23	24	25	26	27	28
Model 3	29	30	31	32	33	34	35	36	37	38	39	40	41	42
Model 4	43	44	45	46	47	48	49	50	51	52	53	54	55	56
Model 5	57	58	59	60	61	62	63	64	65	66	67	68	69	70
Model 6	71	72	73	74	75	76	77	78	79	80	81	82	83	84

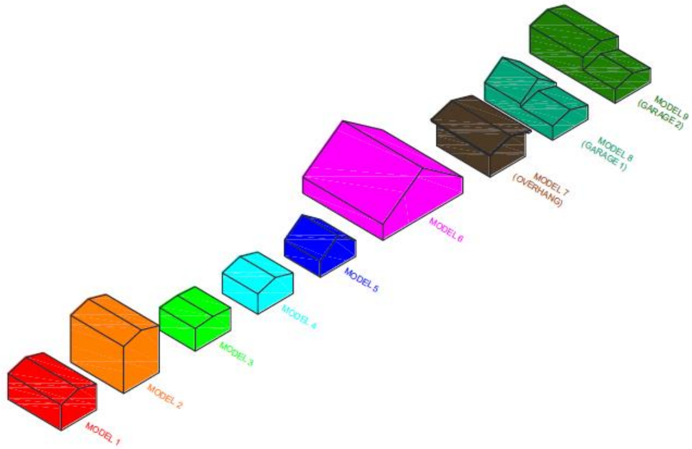

Figure 2.9: House models tested by Case et al. (2011)

With the pressures obtained from these experiments, the force coefficients *CFx, CFy*, and *CFz* were computed, where *CFx* was the component parallel to the tornado's translation direction, *CFy* was perpendicular to the tornado's translation direction, and *CFz* was along the vertical direction. The forces for each house model were calculated by summing the average pressure for *x*, *y*, *z* components for each time step of the 10 repeated trials. This was then multiplied by the tributary area of each pressure tap. The force coefficients were plotted as a function of the force coefficient vs time. Finally, the time corresponding to the total translation duration of the tornado is considered and the peak force coefficients are calculated based on the force acting on the models under *x*, *y*, and *z* directions. Pressure coefficients were then plotted using a contour plot as seen in Figure 2.10 (Case et al., 2011). This type of plot helps visualize the high and low suction zones on the walls and roofs of the residential house models.

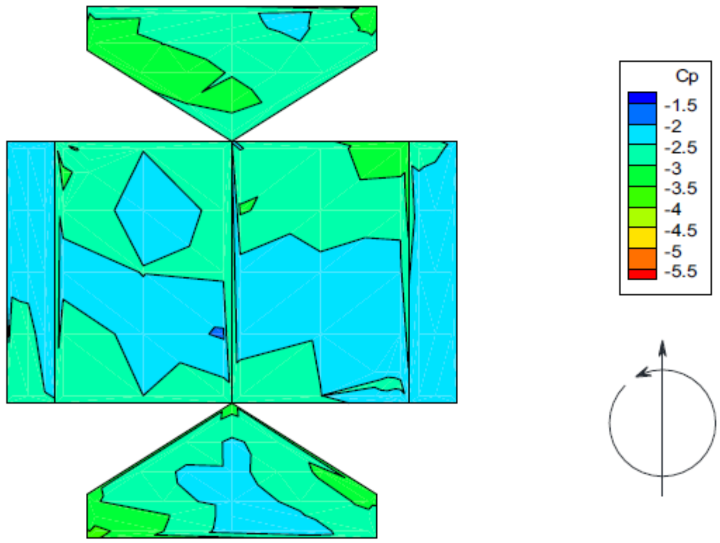

Figure 2.10: Peak pressure coefficient contour plot, model 6, inclination 0° (Case et al., 2011)

Haan et al., (2010) found that building orientation affected the peak horizontal force coefficients but not the vertical force coefficient. The uplift force is largely influenced by the pressure deficit of the vortex core. The peak uplift on the roof of the model was greatest when the model was in the center of the tornado. The peak horizontal force occurred when the tornado was at the radius of maximum tangential velocity, also known as the RMW. Vertical forces on the roof are much higher than the horizontal forces acting on the walls. This shows the important effect the simulator's updraft has on the pressure induced at the models' surfaces.

Sabareesh et al., (2012) studied the effects of a stationary vortex with a peak velocity of around 2.75 m/s on a 25 mm cube on which 45 pressure taps were installed. The cube was tested at different locations along the radius of the tornado, $r/r_c = 0$ (center vortex), $r/r_c = 0.68$ (cube inside vortex core), $r/r_c = 1.62$ and $r/r_c = 2.7$, which are outside of the vortex. High suctions were found when the cube was at the center of the tornado. This is where the minimum C_p coefficients of -10 to -11 were found on the roof, while the min C_p coefficients on the walls were between -6 and -11. When the cube was offset from the center, but still in the tornado core, the C_p coefficients on the roof registered fewer negative values between -8 and -11. The cube faces that were perpendicular to the tangential flow were under less suction, between -1 and -4.5, for both the $r/r_c = 0.68$ and $r/r_c = 1.62$ locations. It was noticed that the leading edge to the clockwise flow of each wall was under a greater C_p compared to the trailing edge. The walls that are parallel to the tangential flow are under greater suction than those perpendicular to the flow for model location $r/r_c = 1.62$ and higher. However, inside the vortex core, the effects of tangential velocity are not seen on the wall faces.

2.5 Determining peak pressure coefficients for different time durations

Haan et al. (2017) analysed the pressure coefficient data on a house model tested in the ISU simulator employing a different data interpretation method. In the previous section, where the peak pressure coefficients were presented in the form of contour plots (Figure 2.10), the peak pressure coefficient of each pressure tap was found as the peak C_p value of the entire time length of the test. For the data interpretation method used by Haan et al. (2017), the C_p values were calculated in different ways to show the effects of duration sampling time on the pressures induced by the tornado. This could help simulate and understand the effects of a tornado that is sitting at the same location for a short or long amount of time. In the experiments performed at the University of Ottawa, the house models were only tested in a stationary tornado. Sampling from different time durations could help determine similarities or trends to a translating tornado and could help determine the adequacy of the National Building Code of Canada (NBCC, 2015) relative to tornadic winds. As mentioned in the study performed by Haan et al. (2017), testing a model in a stationary tornado creates greater pressure peaks and gusts when compared to a translating tornado. Thus, the presented data interpretation method could simulate a worst-case scenario where the tornado persists for an extended amount of time on the same house. Also, it was previously shown that the pressures generated by a stationary tornado had magnitudes 45% larger than the translating vortex (Haan et al., 2017).

The test performed by Haan et al., (2017) consisted of finding the pressures on a house model in a translating tornado and then a stationary tornado. The translating tornado's duration was estimated as the time that it takes the core of the vortex to translate past a point on the house model. The following equation was used to estimate the duration, τ:

:

$$\tau = \frac{2R_c}{V_t} \tag{5}$$

Translation speeds of 0.15 m/s to 0.61 m/s were used, which correspond to exposure durations of 0.7 s to 2.9 s for a tornado with a radius of 0.22 m. For each translation speed, the C_p was found for each of the 10 repeated trials and the median value for the 10 trials was found (Haan et al., 2017).

For the stationary tornado, each trial lasted 48s and the time series were divided into segments of 0.1s to 10s. The peak C_p was found for each segment and the median C_p was determined for the entire 48s time series. This was repeated for each r/r_c value, and the median C_p value was chosen from all of the peak C_p values out of all the duration segments at each r/r_c location. This would replicate the concept of exposure duration caused by different tornado translation speeds. The C_p peaks found from the stationary vortex for different durations were then compared to the C_p peaks from the translating vortex. The peaks for different r/r_c locations could be used to predict the pressure coefficients of a translating tornado by using a C_p obtained from a stationary tornado test. Since the peaks are chosen based on duration, a smaller duration would simulate a faster translating tornado while a longer length would simulate a slow-moving tornado (Haan et al., 2017).

Once the experiments were performed for the translating and stationary tornadoes, the static pressure was removed from the pressures that diminished the large peaks. The peak pressure coefficients that were calculated in this study were different from other similar studies on experimental tornadoes. The peak pressure coefficients were calculated based on the equation:

$$C_{p_{\text{peak}}}(x) = \frac{(p(x)-p_{\text{ref}})_{\text{peak}}}{\frac{1}{2}\rho\left[V^{\text{t}}_{H_{\text{peak}}}(x)\right]^2} - \frac{p_{\text{static}}(x)-p_{\text{ref}}}{\frac{1}{2}\rho\left[V^{\text{t}}_{H_{\text{peak}}}(x)\right]^2} = \frac{(p(x)-p_{\text{ref}})_{\text{peak}}}{\frac{1}{2}\rho\left[V^{\text{t}}_{H_{\text{peak}}}(x)\right]^2} - C_{p_{\text{static}}}(x) \tag{6}$$

Where $(p(x)-p_{ref})_{peak}$ is the peak pressure measured at a pressure tap, $p_{static}(x)- p_{ref}$ is the static pressure induced by the vortex minus the reference pressure and it was determined by finding the average of the 89 pressure taps on the model for each time step. V_{Hpeak} is the peak horizontal velocity of the translating tornado and ρ is the air density (Haan et al., 2017). The peak C_p for the stationary and translating tornado was normalized with the median. The outcome consisted of a peak to median ratio for each pressure tap on the model.

For the experiments performed at the University of Ottawa, the static pressure was not removed from the results. A comment by Haan et al., (2017) stated that when comparing the C_p values experimentally obtained for simulated tornadoes on a house model to the ASCE-7 design recommended values, the static pressure must be included in the pressure coefficients acting on a building model. Therefore, for the University of Ottawa experimental results, the static pressure was not removed from the results as one of the main goals is to compare the pressure coefficients to the NBCC 2015. This being said, Haan et al., (2017) and Kopp and Wu., (2020), both experimented to remove the static pressure from tornado induced pressures to see its effect. The static pressure is attributed to the increase in magnitude of the pressure seen in tornado winds versus the ABL winds. Haan et al., (2017) removed the static pressure from the $C_{p\ peak}$ as seen in Eq. (6).

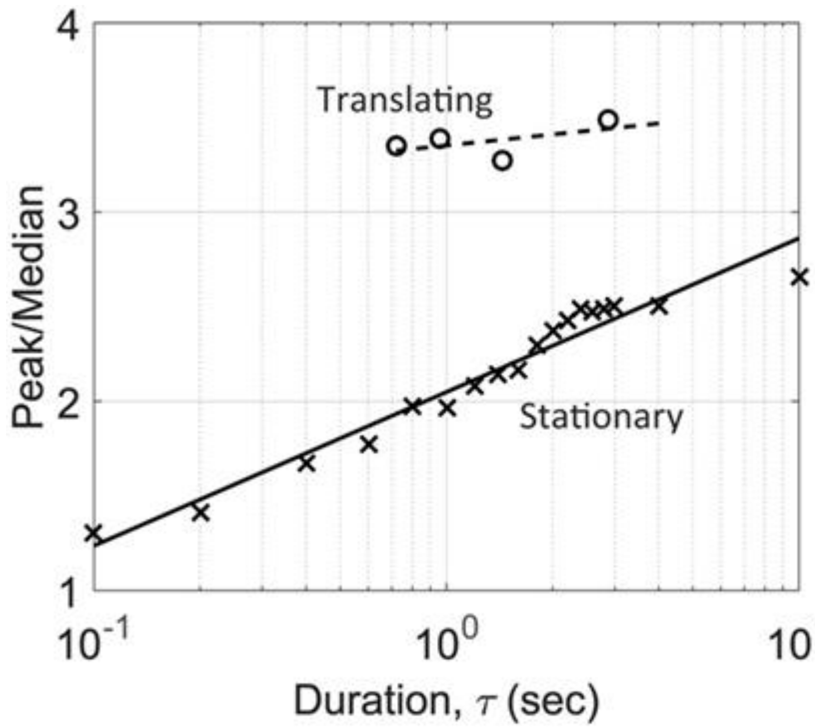

Figure 2.11: Ratio of peak C_p to median C_p as a function of event duration, T, for translating and stationary vortex tests on pressure tap #66 (Haan et al., 2017)

Figure 2.11 shows that as duration increases, so does the peak/median ratio. This means that the C_p peak pressure value becomes more significant with an increase in duration. To present the pressure taps' results by regions of magnitude at the surface of the models, these were separated into zones as shown in Figure 2.12. The rotating arrow represents the direction of the simulated tornado. For each zone, the upper and lower bounds of the peak pressure coefficient envelope curves, $C_{p\ peak}$ (x), were plotted. These were based on finding the C_p peaks in the 1s segment durations and using the peak of the data set for the pressure taps at specific r/r_c locations. The results for each r/r_c location were presented in zone groups as seen in Figure 2.12.

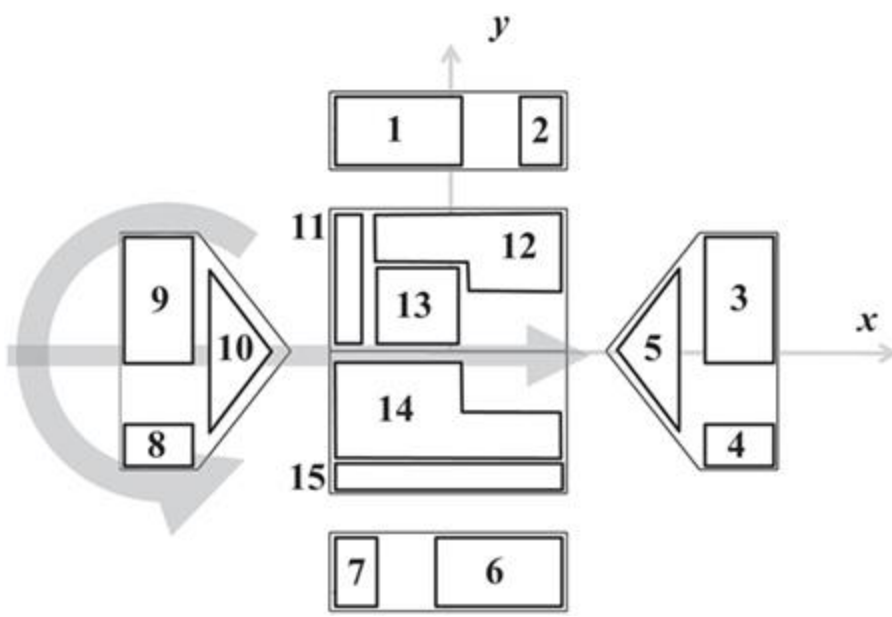

Figure 2.12: Zoning used for duration effect analysis on pressure coefficient (Haan et al., 2017)

The zones were created based on similarities in C_p peak pressures. NBCC 2015 design code has pressure recommendations for different zones of the roofs; however, these were aligned with the edges and corners of the roof, while the C_p values were determined based on Atmospheric Boundary Layer (ABL) winds simulated in wind tunnels. Therefore, the method described above was employed for the current experiments, as well as to help determine if the NBCC 2015 zones used for wind design can be employed for defining the regions to withstand tornadoes. It was also employed to determine if changes are required to be made to zoning configurations. The peak/median values reported by Haan et al., (2017) for some of the zones can be seen in Figure 2.13.

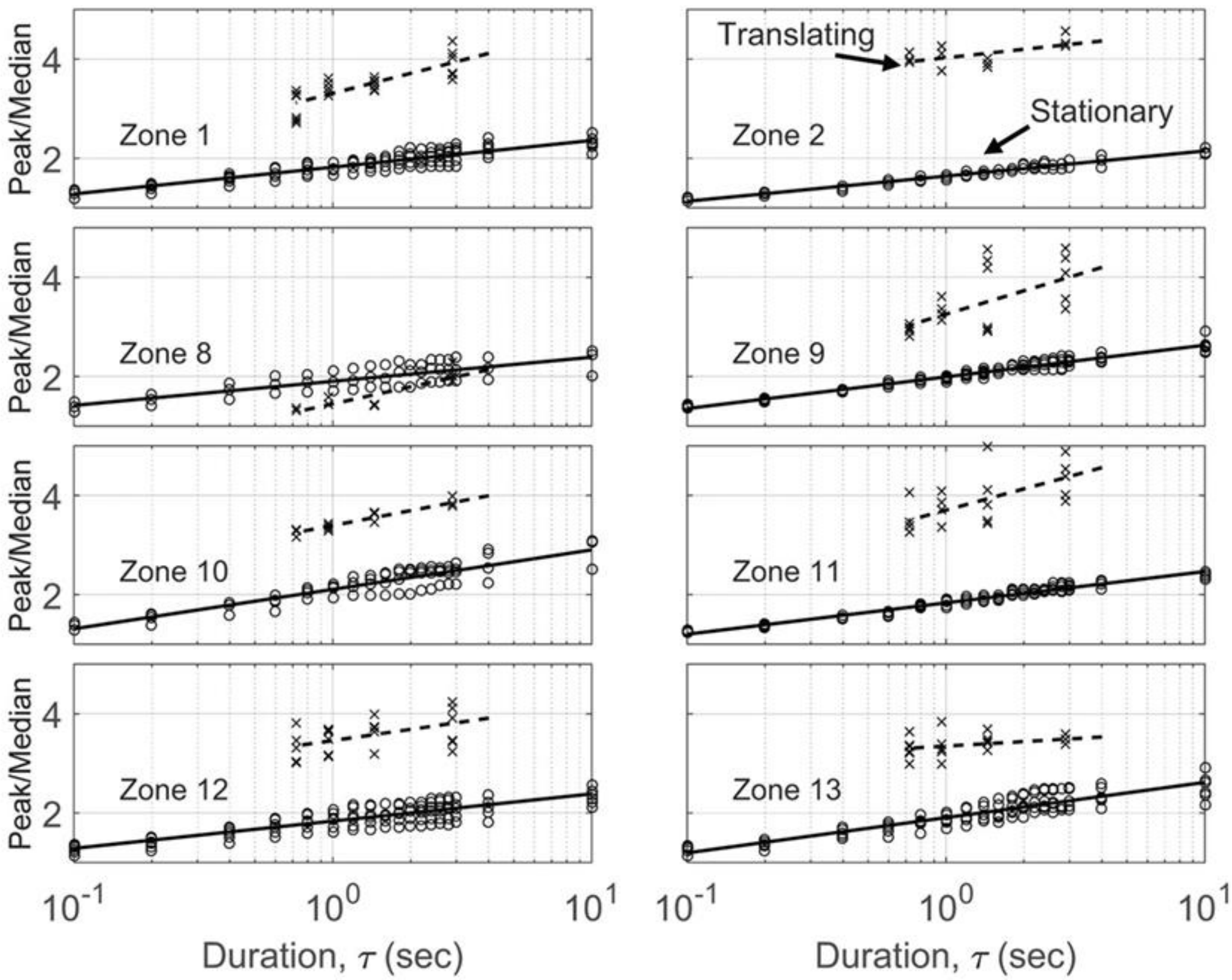

Figure 2.13: Pressure coefficient peak/median for different durations (Haan et al., 2017)

With the graphs from Figure 2.13, the peak/median ratio curve was found, and the following expression was used to quantify the pressure coefficient trend:

$$PM = m \times ln(T) + b \quad (7)$$

Where m and b are the fit constants and T is the time in seconds. The peak/median ratio was compared for 10s and 100s to show its change with the tornado exposure duration. The factors between peak values at 10s and 100s were 1.1 and 1.4 respectively.

Conclusive statements could not be made regarding the pressure coefficients and forces induced by translating tornadoes, however, it was conclusively shown that the peak pressure coefficient increased as exposure duration increased. It was observed that the peak pressure coefficient occurred in or near the tornado vortex core and that these peaks could be due to strong vertical gusting and static pressure fluctuations.

2.6 Wind Design Building Codes: NBCC 2015 and ASCE-7

One of the main loads that buildings need to be able to withstand is the wind-induced load. Two of the main design standards in North America are the NBCC (National Building Code of Canada) and the ASCE (American Society of Civil Engineers). Low-rise buildings are the area of study for this report, as low-rise buildings are found in the lower part of the atmospheric boundary layer. Due to the smaller area of components in secondary structural members and cladding, the winds produce loads that are much larger than those acting on main structural elements (Aldoum, 2018). This results in high magnitudes of pressure, which is therefore important to consider when adequately designing these areas of a building (Prevatt et al., 2011). There are no design standards for tornadoes, so the pressure coefficients recommended by the current building codes, which are based on ABL winds, are used when analysing tornado loads on residential houses (NBCC, 2015). The current design standards in North America may not be adequate due to their limited consideration of the effects of loads created by tornadoes on structures (Kopp et al., 2020).

When an ABL wind flow hits sharp building edges, the flow will separate into an inner domain flow and an outer domain flow, with small vortices separating the two flow regions. These are called bluff bodies. In the middle of a wall where the wind hits perpendicularly (windward wall), the dynamic pressure is zero, this being the region with the maximum compressive pressure. After hitting the center region of a wall, the flow will deviate around the building corner and will accelerate, producing a negative pressure or suction around the corners (Aldoum, 2018). For ABL winds on roofs, large suctions occur on the windward edges and corners. Much lower suctions are found in the middle region of the roof. The greatest suction is found on the corners, followed by the edges and then the center area of the roofs.

Canada's building code and design guidelines for different loads are found in the NBCC 2015. The NBCC 2015 section addressing the wind design is separated into low-rise buildings, where $H/D < 1$ m and $H < 20$ m, or mid-rise buildings where the height is larger than 20 m or $H/D > 1$ m. The dimension H is the height and D is the smallest plan dimension. Different zoning at the surface of the model and minimum pressure coefficients are used for low-rise buildings with different roof types, and roof slopes (NBCC, 2015). The pressures for different zones of the roofs recommended by NBCC 2015 are expressed as the product C_pC_g where C_p is the pressure coefficient, while C_g is the gust coefficient. For the walls of low-rise buildings, the C_pC_g values for different zones on a wall are found in Figure 2.14 (NBCC, 2015). The two zones on the walls are E and W, where E is the side section of the wall and W is the central section. As defined in the NBCC 2015, Zone E is taken as the lesser of the 10% of the least horizontal dimension and 40% of the height, H, but not less than 4% of the least horizontal dimension or 1 m. The W Zone is the remainder of the area in between the two E zones. Zone E has a greater minimum C_pC_g of -2.1 to the W Zone (NBCC, 2015).

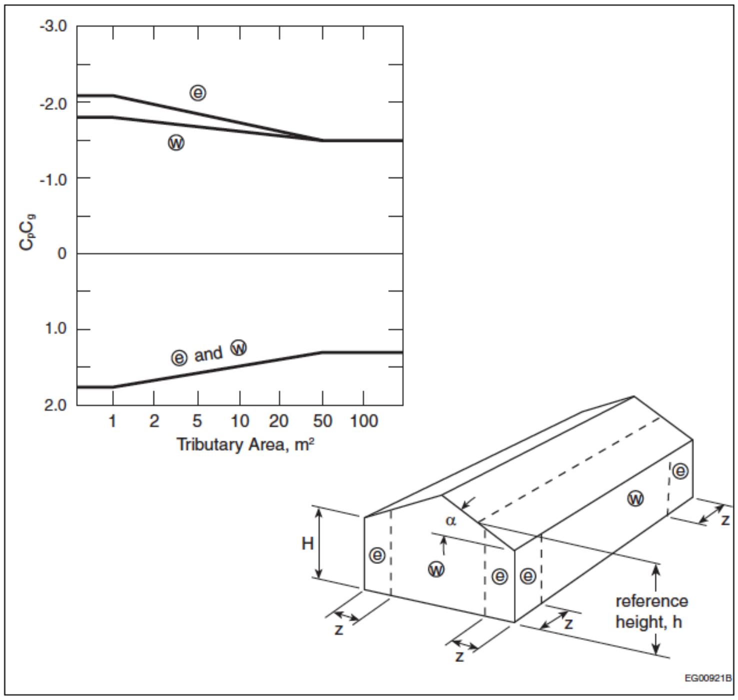

Figure 2.14: 4.1.7.6.-B External peak values of C_pC_g on individual walls for the design of cladding and secondary structural members (NBCC, 2015)

For Figure 4.1.7.6 from the NBCC 2015, the peak pressure coefficient C_pC_g was developed based on the most critical load created by the wind blowing at the critical angle. The critical wind angle is the angle that produces the greatest loads on the building. The C_pC_g values already consider the effect of the directionality of the wind, therefore the recommended C_pC_g in the

NBCC 2015 are based on the critical angle. Wind directionality is only used in choosing the correct figure to obtain the correct peak pressure coefficient values (Aldoum, 2018).

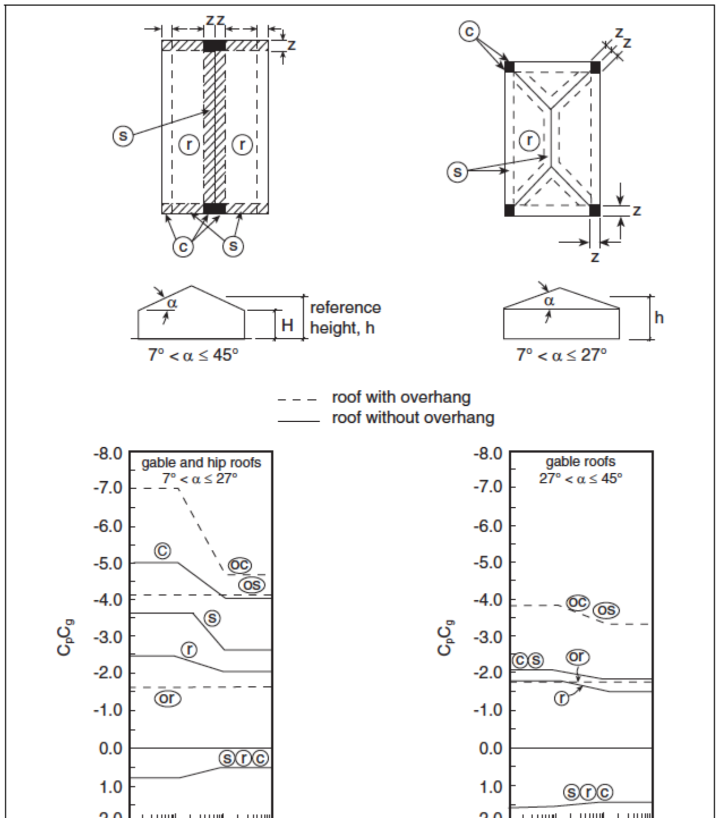

Figure 2.0.15: 4.1.7.6.-E External peak values of C_pC_g on single-span gabled and hipped roofs with a slope greater than 7° for the design of structural components and cladding (NBCC, 2015)

For the roof of low-rise buildings, the C_pC_g values for different zones on a wall are found in Figure 2.15. The zones are separated into C for the corner zones, S for the edge zone, and R for the central area of the roof zone. In this case, NBCC 2015 defines the end zone width, z, of the roof as the lesser of 10% of the least horizontal dimension and 40% of the height, *H*, but not less than 4% of the least horizontal dimension or 1 m. The corner zone c has the greatest minimum C_pC_g requirement followed by Zone s and Zone r (NBCC, 2015).

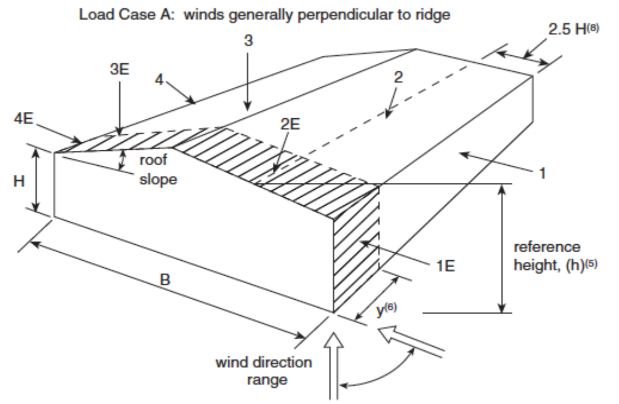

Roof Slope	Building Surfaces							
	1	1E	2	2E	3	3E	4	4E
0° to 5°	0.75	1.15	-1.3	-2.0	-0.7	-1.0	-0.55	-0.8
20°	1.0	1.5	-1.3	-2.0	-0.9	-1.3	-0.8	-1.2
30° to 45°	1.05	1.3	0.4	0.5	-0.8	-1.0	-0.7	-0.9
90°	1.05	1.3	1.05	1.3	-0.7	-0.9	-0.7	-0.9

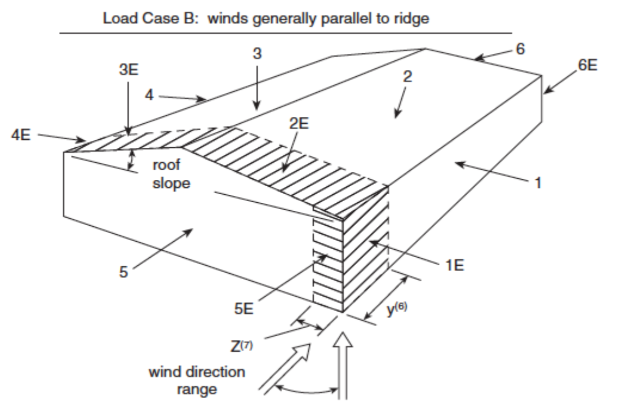

Roof Slope	Building Surfaces											
	1	1E	2	2E	3	3E	4	4E	5	5E	6	6E
0° to 90°	-0.85	-0.9	-1.3	-2.0	-0.7	-1.0	-0.85	-0.9	0.75	1.15	-0.55	-0.8

EG00920B

Figure 2.16: 4.1.7.6.-A External peak values of C_pC_g for primary structural actions arising from wind load acting simultaneously on all surfaces of low buildings (H ≤ 20 m), (NBCC, 2015)

2.7 Other studies

A tornado simulator very similar to the ISU one was built at Tongji University (Wang et al., 2018) and internal pressures for a gable roof of a low-rise building with roof openings of different sizes, were investigated by Wang et al., (2021) for a stationary tornado. It was found that for an 8% increase in the opening, the mean internal pressure coefficient decreases when the model is in the core of the tornado.

A tornado wind velocity hazard map for Canada, was developed by Hong et al., (2021) using the wind velocity at 10 m height above the ground surface employing two historical tornado catalogues. One of the historical tornado catalogues reported tornado events from 1980 to 2009 and the second one was developed based on the Poisson model, for tornadoes reported between 1980 to 2019.

Velocity profiles for a single-cell simulated tornado and the tangential and radial velocities (Figure 2.17) were experimentally determined by Mishra et al., (2008) for a Ward Type tornado simulator built at Texas Institute of Technology (TTU). The TTU simulator has a blower connected at the top and underneath the floor has a plenum where inclined vanes control the incoming flow. Near the simulator chamber, there are slants that allow the airflow to enter the convection area.

Comparison with real tornado data reported for the Spencer Tornado showed that a radial velocity outflow within the core was observed for $r/r_0<0.27$, as shown in Figure 2.18. The WDS is not a Ward Type simulator. Therefore, further similarity conditions from the TTU simulator were not employed for the current research.

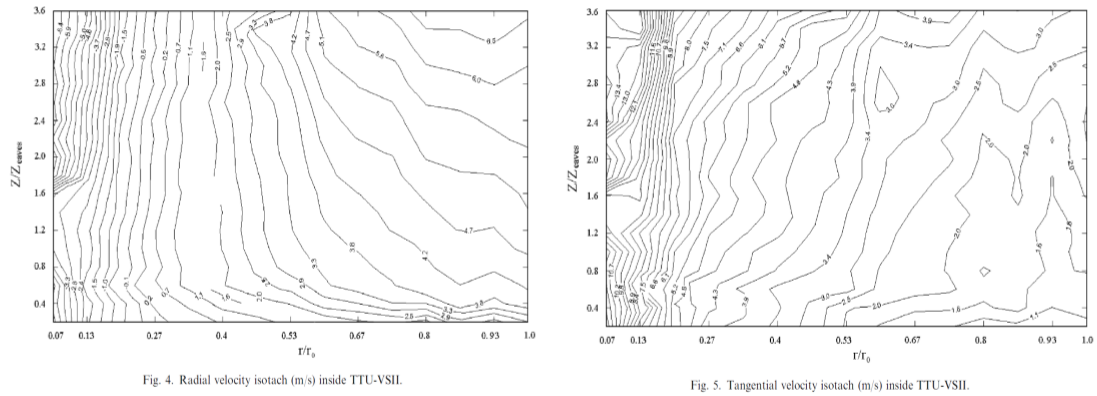

Figure 2-17: Tangential and radial velocity profiles for a Ward type simulator (Mishra et el., 2008)

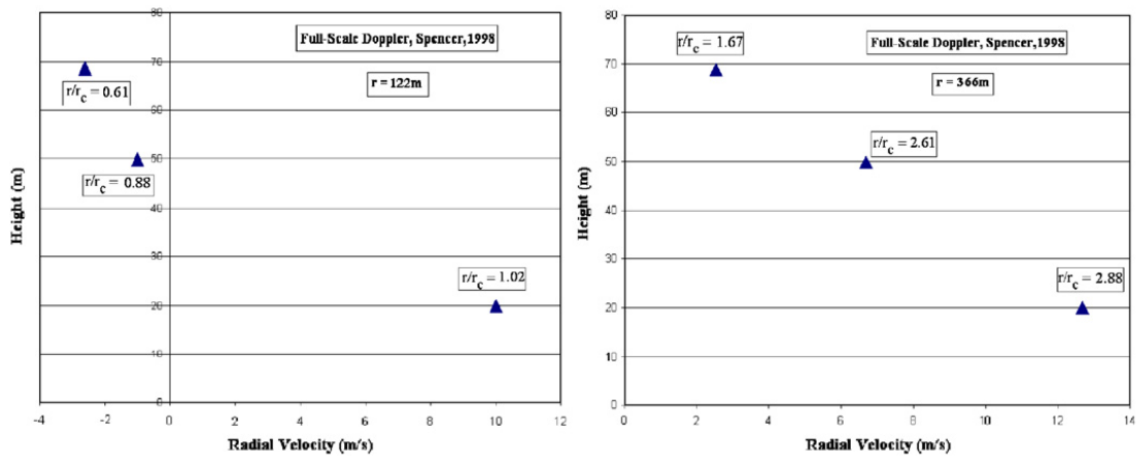

Figure 2.18: Radial velocity data from the Spencer tornado (Mishra et el., 2008)

Another CFD-LES simulation was created for a 3.76 m diameter tornado simulator, similar to the ISU simulator, by Yuan et al., (2019). The streamlines represented by pressure intensity colour have shown the tornado formation (Figure. 2.19), while the parametric study revealed the parameters of the tornado as: S = 0.47 to 0.89, r_{cmax}/r_{cmin} = 435 to 341, and h_{max}, $r/h_{max,s}$ = 460 to 478.

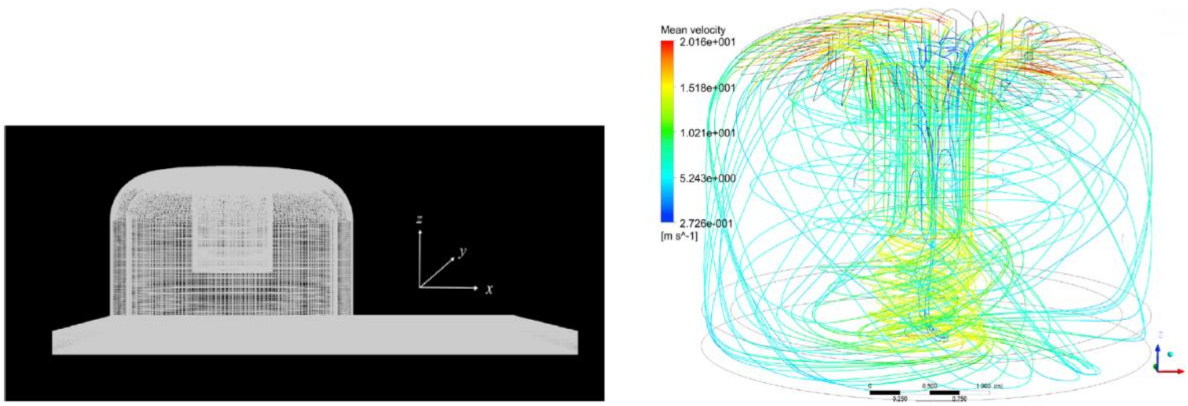

Figure 2.19: CFD simulation of tornado flows (Yuan et al., 2019)

Kopp and Wu, (2020) found that pressures measured on the ground are at a minimum in the core of a simulated vortex and increase radially from the center. Negative radial flow is significant at distances larger than r_c at ground level. The flow is entering the vortex near the ground level and as height increases, the radial flow component decreases. At high swirl ratios, multiple vortices form inside the central vortex core, while in a low swirl ratio a single vortex forms. Wang et al., (2016) experimentally found that translating tornadoes, and their pressures measured at a single point, act in a quasi-steady manner when compared to a stationary tornado. This means that the static tornado vortex, in combination with the vortex translation speed, creates the translating tornado wind field. The WDS is currently capable of simulating only stationary vortices. However, with additional knowledge on quasi-steady manner tornadoes, discoveries and similarities could be made between translating and stationary tornadoes. This ties into the idea used by Haan et al., (2017) in Section 2.5 and Section 4.4 of this research paper.

The lift forces or suction on the house is affected by the building aerodynamics and by the static pressure induced by the tornado. Haan et al., (2010) experimentally showed that the peak pressure coefficient is 1.8 to 3.2 times greater than that of the ASCE 7-05 and is mainly attributed to the static pressure. The study performed by Kopp and Wu, (2020) incorporated this concept in their research and hypothesized on the fact that the wind loads induced by tornadoes can be separated into an aerodynamic load and a static pressure load

.

2.8 Literature important implications to experiments

The research articles that are described in this literature review are helpful in learning the basic methodology and concepts used in laboratory-simulated tornadoes and the pressures they created on building models. However, a few articles were used as guidelines for the experiments and data analysis performed for this thesis. The three house models used for the WDS experiments had the same dimensions as the ones used by the Case et al., (2011) experiments. A similar tangential velocity profile was found in the current WDS experiments, while the procedure to obtain the tangential velocity profiles was based on the method used by the Haan et al., (2008) experiment. Section 4.4 and Chapter 5 of this thesis also cover the effects of tornado exposure duration on the magnitude of pressure coefficients. Although the procedure to process the data was different for the WDS study, as it was intended to create a comparison to the NBCC 2015 criteria, the method originated from the Haan et al., (2017) experiment.

No method has yet to be established to determine the swirl ratio in the WDS facility. The methods used for the Ward Simulator Type, the ISU simulator and the WindEEE Dome, all used the vane angle in the swirl ratio equation. However, the WDS does not employ the same concept. The circular inlets located at the bottom corner of each wall let the flow in, while the ceiling fan causes the updraft, thus creating the swirl. Since the inlets' pipes are perpendicular to the WDS wall, the flow has a 0º angle. If an angle of 0º is employed in the swirl ratio equation, an indeterminate swirl ratio value is found. The simulator concept used in the study by Yan et al., (2019) as seen in Figure 2.2 and Figure 2.3, is similar to that of the WDS facility. However, the inlet horizontal angle is used as the angle in the swirl ratio equation. This is also not practical for the experiment performed at the WDS because there is no horizontal angle. One idea that could be more practical in determining the swirl ratio could be the angle that the flow enters the vortex. However, measuring this angle inside the WDS testing chamber is challenging, as further detailed in the experimental procedure of Chapter 3.

Chapter 3 Experiment Set-up and Methodology

3.1 Wind Damage Simulator (WDS)

Recently, a Wind-induced Damage Simulator (WDS) was built at the University of Ottawa (Figure 3.1b) that can simulate turbulent winds, shear winds, and tornadic wind flows. With a varying speed industrial blower, with RPM ranging from 350 RPM to 3650 RPM, the WDS can simulate low wind speeds necessary for small-scale experiments on scaled models of structures. It can also replicate larger scale turbulent winds capable of displacing roofs' shingles and mock-ups. The WDS testing section has dimensions of 3.0 m x 3.6 m x 3.6 m and the WDS outlet positioned in the middle of the ceiling has a diameter of 31cm and draws the air upwards. To create different flow directions and vortices, five circular inlets, each with a diameter of 20 cm, are found at different locations on each wall of the WDS box (Figure 3.1a). Depending on the experimental purposes, these inlets can be opened or closed to produce different flow patterns. To simulate the tornado vortex required for the experiments conducted as part of this research, the bottom left corner inlet from each wall of the WDS was opened, thus creating a rotating vortex in the center of the box.

The fan updraft forces the air outside of the WDS to be directed through the inlets of each corner. The wind enters the chamber at the angle of the inlets and converges towards the center of the room. The combination of the updraft and the wind velocity entering as symmetric inflows that converge towards the middle produces a vortex. As the outlet is fixed, the WDS facility cannot simulate a translating tornado, but only stationary tornadoes. Other parameters, such as the inlet inclination angle, can be varied; however, additional testing needs to be done to simulate different tornadoes, to understand the different sizes of the simulated vortices and their parameters such as swirl ratio and Radial Reynolds number.

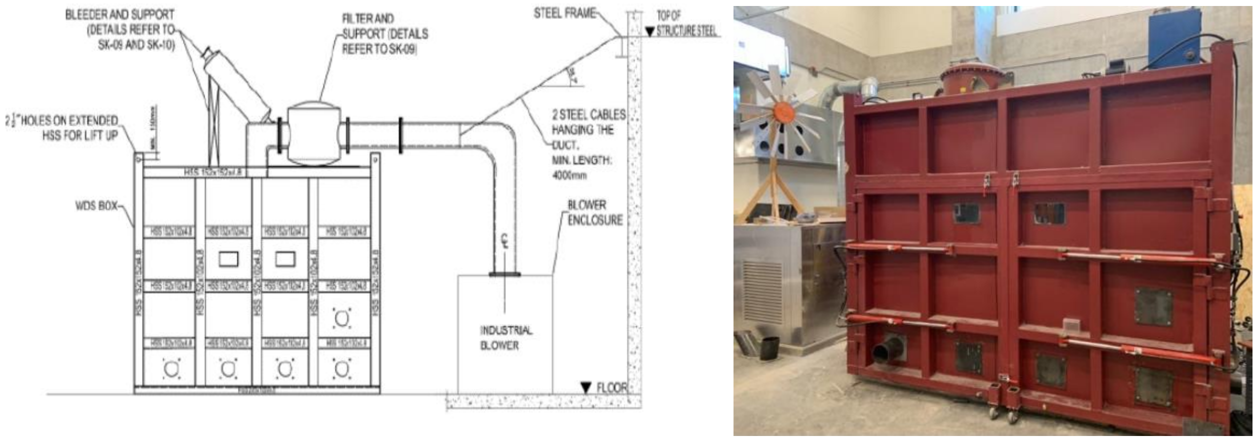

Figure 3.1: a) Wind Induced Damage Simulator Dimensions b) Wind Damage Simulator Facility

The goal of the current experiment is to assess the external pressures on three scaled house models, caused by a tornadic wind. The experimental program was conducted in two phases: the first part of the experiment consisted of measuring the tangential wind speed at different distances from the vortex center, based on a similar procedure as the one used in the experiments performed by Haan et al., (2008). This would determine the properties of the WDS simulated tornado, such as: tangential velocity, vertical and radial velocity of the vortex along its cross-section. The second phase consisted of testing three scaled house models in a stationary vortex, and obtaining external pressure coefficients along the surface of the houses. Two of the houses had the same dimensions, but different roof pitch angle, as detailed in Subsection 3.4 below, while the third house had bigger dimensions but same roof pitch angle as the second model, such that the effect of the geometry and of the roof angle can be analysed and discussed.

3.2 Tangential velocity profiles of the tornado (Phase 1)

To find the velocity parameters of the tornado flow, a 12-hole Omniprobe sensor, by Aeroprobe, was used (Aeroprobe PS12 / PL12 Omniprobe, 2020). It was attached to an L bracket that was anchored to a threaded rod mounted beneath the floor. Standard tubing connected the Omniprobe to a DSA3217 pressure scanner, and data was acquired at a sampling rate of 40 Hz for 30 s, at each 5 cm interval to a range of 45 cm from the center of the tornado. The velocity parameters were measured at an elevation of 5 cm as this was the approximate height of the roof to wall connection of the models. The tornado was assumed to be symmetric about the center of the floor which was directly under the fan outlet. The Omniprobe, as seen in Figure 3.2, was positioned facing the tangential velocity component of the tornado. The Aeroflow computer software transforms the pressure data and produces three velocity vectors, *x*, *y*, *z* directions. The horizontal velocity parameter was determined from the Aeroflow software and was used to find the maximum horizontal velocity. However, due to the tornado rotationary flow hitting perpendicular to the house models, it was decided to use the term tangential velocity instead of horizontal velocity as they would be very similar, or the same. The velocity data obtained during these tests had some fluctuation with short high and low-velocity peaks. To avoid errors caused by the sensors, the velocities were averaged every 0.1 seconds, to determine the 0.1s average tangential velocity $V_{t.0.1s.avg}$. The maximum 0.1-second average tangential velocity was taken for each 5 cm interval. Multiple tests were done for different RPMs to determine an adequate tornado tangential velocity, and each test was repeated three times. The tornado wind speed cross-section measurements were taken for fan speeds of 700 RPM, 750 RPM, 825 RPM, and 900 RPM. With the velocity data, the location of maximum tangential wind speed was found for the four different tornadoes generated by the four different fan RPM's. Using the tangential velocity and tornado radius data, a choice was made for the test locations to subject the house models to different velocity zones of the tornado: max velocity, mid velocity, and low velocity regions, in the second phase of the experiment.

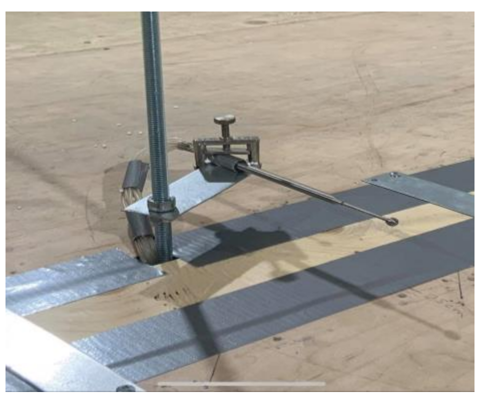

Figure 3.2: Omniprobe sensor used to determine velocity parameters of experimental vortex

When the updraft starts inside the WDS facility, the wind speed will not have a uniform distribution across the testing chamber: the main vortex core will be formed underneath the outlet, in the center of the box, while, the airflow jets incoming from the inlets dominate the flow patterns before merging with the central vortex (Figure 3.3b). Also, the *x*, *y*, *z* components of the velocities will be very different, thus it is necessary to carefully measure the velocities in the WDS testing chamber. Tangential velocities measured in Phase 1 at nine locations along the tornado radius, at 5 cm intervals and at an elevation of 5 cm above the floor, are reported in Figure 3.3a. These measurements were recorded for four different fan RPMs: 700 RPM, 750 RPM, 825 RPM, and 900 RPM. As expected, higher velocities, of up to 16.5 m/s, were recorded for higher RPM, of 900 RPM, and lower velocities were recorded for 700 RPM. Also, as a general trend, high velocities were noticed in the central region of the tornado, at a radius up to 10 cm away from the center; however, these decreased gradually further away from the location of greatest tangential velocity and from the vortex's core. The tangential velocity tapers off to a common value of 3.0 m/s, 40 cm from the center of the vortex, for all tested RPM's. Similar evolutions of tangential wind velocity in a tornadic flow were shown in previous studies (Haan et al., 2008). Therefore, the tornado simulated in the WDS facility is considered adequate for testing scaled house models. The tangential velocities for 825 RPM and 900 RPM were considered too high while the 750 RPM tornado was too low. This is because the goal was to obtain a tangential velocity close to 11.7 m/s which was used in a study performed by Case et al., (2011). An interesting aspect is that a critical point was identified at 700 RPM, where the flow regime changes unexpectedly, yielding velocities higher than the 750 RPM case. No conclusive reasoning was identified for the greater peak tangential velocity measured at lower fan RPM of 700, compared to the 750 RPM test, since a higher tangential velocity would be expected for a higher RPM value. However, the simulator geometry probably had an influence on the flows that created the vortex, resulting in different tornado flows, thus different velocities.

As it can be noticed in Figure 3.4, a simulated tornado at 700 RPM was performed, and the peak tangential velocity was 12.2 m/s at a radius of 10 cm. This tornado was considered adequate as the tangential velocity was close to the goal of 11.7 m/s for which the wind speed curve profile was similar to the ones obtained by Haan et al., (2008) and Case et al., (2011) for the ISU simulated tornado. The 700 RPM was used for the experiments in this study; however, there were three differences between this tornado and the lab simulated tornado reported by Case et al., (2011). The tangential velocity profile in the core of the vortex, up to $1 = r/r_c$ (where r is the radius of the tornado and r_c is the radius of the tornado core) does not register a large positive increase in velocity where the tangential velocity is near 0 m/s at the center; instead, it starts at a high velocity and has only a slight increase in velocity where it peaks at 1 = r/r_c (Figure 3.4). This could be due to the tornado oscillating flow. The second difference is the small tornado diameter of only 20 cm. This is a small diameter compared to the tornado simulated by Case et al., (2011) that had a diameter of 1.12 m. Thirdly, the tornado flowed in a clockwise direction at the WDS while it flowed in a counterclockwise direction for the Case et al., (2011) study. This creates a different tornado, and the pressure coefficient results obtained on the surface of the models will be different from one surface to the other. The diameter of the WDS simulated tornado was considered as 20 cm, as from the middle (0 cm) and up to this distance the highest wind speeds were recorded for all RPM values tested. From 20 cm and up to the 45 cm span, the tangential velocity is much lower due to the wall effect and the peripheral shear layers which do not constitute the tornado vortex (Figure 3.3b). It was noticed that the central outlet diameter of the WDS, which is the source of suction, may be affecting the diameter of the vortex as the diameter remained unchanged for different RPM values and inlet angle configurations.

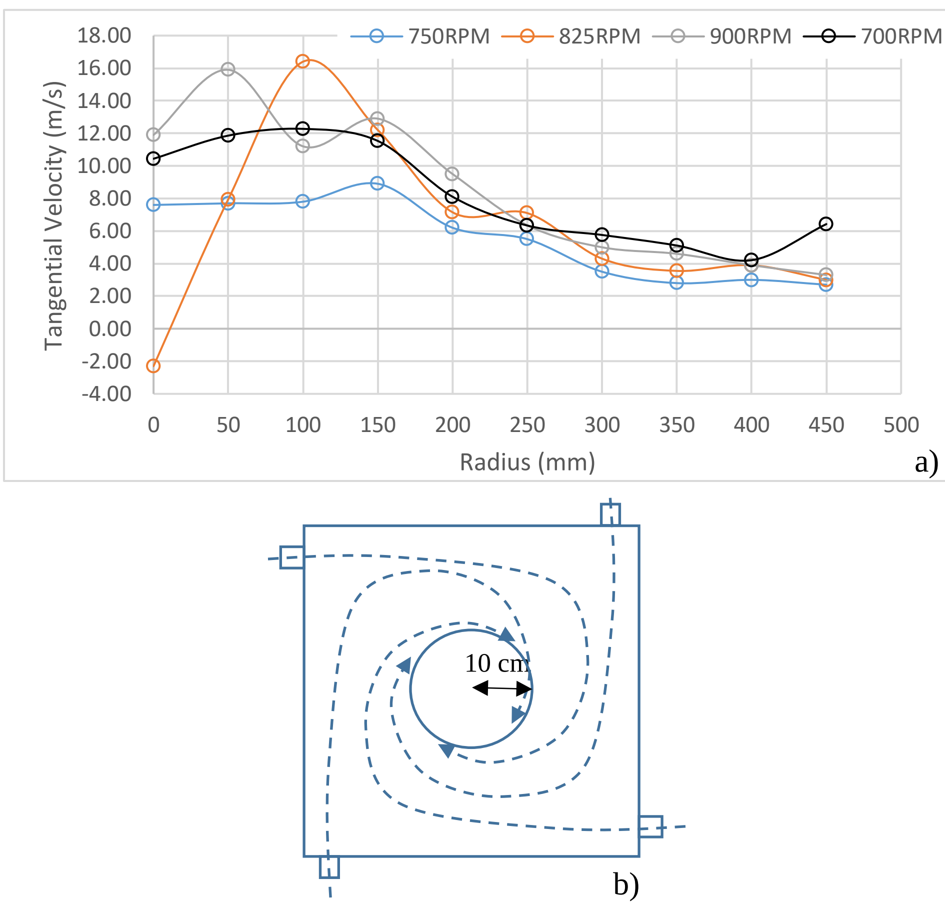

Figure 3.3: a) Maximum tangential velocity vs radius for different RPMs b) Inlets and shear layers peripheral to the 10cm vortex core radius

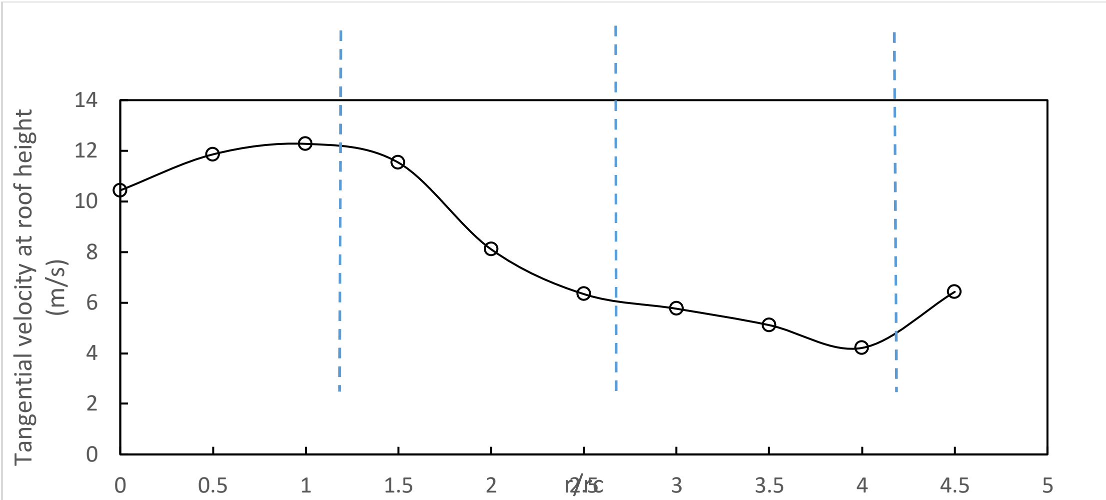

Figure 3.4: Maximum tangential velocity vs radius for 700 RPM

When trying to define the tornado parameters of the WDS simulated vortex, such as swirl ratio, Radial Reynolds number, and aspect ratio, several challenges were encountered. It was found that opening the four outer inlets and using 0° inlet orientation would form a vortex with a distinct core with a radius of 10 cm. However, the problem with this setup is that by using the defined equations for swirl ratio (Eq. 1), which is dependent on the inlet inclination angle, a swirl ratio of 0 is found. Actually, the angle where the shear layers merge with the core should be used in the current experiment; however, there were no means available to accurately measure this parameter in the WDS. An obvious initial concern when using a different tornado simulator is the difficulty in producing a similar vortex to those obtained by other researchers. Because the WDS facility is large, 3 m x 3 m x 3.65 m, and the inlets that were used are located on the outer corners of the box, the vortex is formed in the center of the box. The flow that comes through the inlets, curves toward the center where the vortex is formed. The inlet angle is 0°, which leads to an undetermined swirl ratio; however, the flow that comes through an inlet merges with the center vortex at a certain angle. Obtaining an accurate swirl ratio requires determining the angle at which the flow converges and to view the possibility of using that convergence angle. For this reason, the swirl ratio for the currently simulated tornado was not specified. However, future goals consist of performing additional experiments to characterize the swirl ratios and vortices of various tornadoes that can be produced in the WDS.

3.3 Wind induced pressure coefficients (Phase 2)

Three residential house models, scaled 1:100, were tested in the WDS at 700 RPM to determine the tornado-induced pressures. This RPM generates the highest tangential velocities of 12.2 m/s at a radius of 10 cm, 6.3 m/s at 25 cm, and 4.2 m/s at 40 cm from the center of the tornado. The walls A, B, C, and D and the roof sides B and D were instrumented with 96 pressure taps, as represented in Figure 3.5. DSA3217 Scanivalve pressure scanners recorded pressure measurements at a rate of 400 Hz relative to a reference pressure. Each of the scanners had an individual reference pressure input. Three DSA3217 Scanivalve pressure scanners were connected to 48 pressure tap sensors through individual 40 cm tubing to record all 96 pressure taps. The experiment was conducted in 2 stages. The first stage consisted of 48 pressure taps affixed to all the wall sections. For the second stage, the 48 pressure taps were removed from the walls and were affixed to the roof and the triangular gable at the ends of the model (Figure 3.6). Figure 3.5 represents the layout of the 96 pressure taps affixed to the roof and wall sections of the model. Data from the 2 stages were compiled and grouped to represent the conditions for which all house surfaces were tested for the same wind conditions.

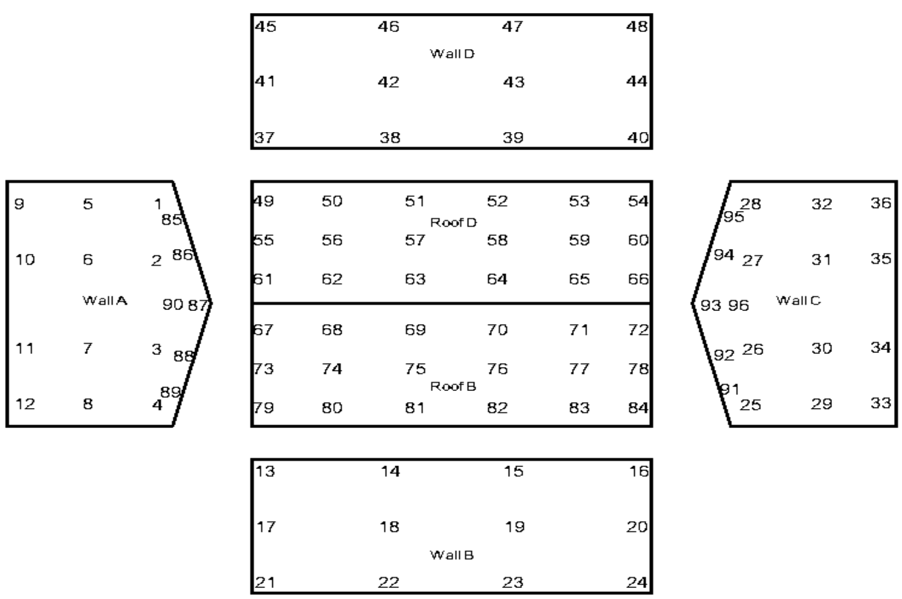

Figure 3.5: Pressure taps layout on the model’s roof and walls

Figure 3.6: Pressure taps installed on the roof of the model for phase 2 experiments

Each test was repeated 3 times and every scenario was run for 30 seconds. The peak pressure value was taken from each of the 3 repeated tests and the peak pressure coefficients were calculated. The maximum average pressure coefficient (C_p) was calculated by averaging the C_{p_max} values (Eq. 2.1) for each of the three repeated tests. C_{p_max} was determined for each of the 96 pressure taps for all of the 9 cases tested (3 house models each tested 3 times).

$$C_{p\_max} = \frac{(p_{max} - p_{ref})}{\frac{1}{2}\rho(V_{t.0.1s.avg})^2{}_{max}} \qquad (2.1)$$

Where is the air density, pmax is the peak pressure measured at the pressure tap, pref is the atmospheric pressure measured outside the WDS chamber in a static pressure bottle, and Vt.0.1s.avg is the maximum tangential velocity from the 30 second intervals found at the radius where the model was tested. The approach of using the maximum mean tangential velocity at the building height as V_{ref} and measuring p_{ref} outside of the tornado simulator was used in the study by Haan et al. (2010). As seen in Chapter 2.4, Case et al., (2011) used an approach that calculated the force coefficient and presented the variation of the force coefficient, C_F, with time. However, since one of the main goals of the current experiment is to observe the C_p trends on residential housing as well as to compare the peak pressure coefficient values to the NBCC 2015, calculating the pressure coefficient was considered instead of determining the force coefficients.

As the full-scale tangential velocity of an EF-3 tornado is 73.76 m/s, and the measured tangential velocity of the ISU tornado employed by Case et al., (2011) was 11.7 m/s, the vortex velocity scale is $\lambda(v)$=11.7/73.76 or 1/6.3 for the full-scale averaging time equivalent to the model-scaling averaging time. If the same scaling similarity principle is used for the WDS simulated tornado, then the vortex velocity scale factor is very similar: $\lambda(v)$=12.2/73.76 or 1/6. Therefore, the tornado tested in the WDS for these sets of experiments is representative to a full scale EF-3 tornado, as is the one simulated by Case et al. (2011). The scales used for the tornado and of the models were based off of Case et al. (2011)'s study as the WDS has not been characterized yet. Therefore, the similar tornado formed in the WDS and was considered comparable to the Case et al. (2011) tornado and thus, same model scaling factor was used.

EF-3 tornadoes and below are considered to be the range of tornado scale that would be important to adapt the building code in order to withstand them. They are the most common tornado, and adapting the building code could be possible, while for higher EF-4 and EF-5 tornadoes, the wind velocities are too severe to withstand.

3.4 Residential house models

The current study has selected the models used for the WDS experiments following the same dimensions as the ones recommended by the ASCE 7-05 and were also included in the experiments performed at Iowa State University by Case et al., (2011). The same models are compatible with the dimensions recommended in the I7 Commentary of the National Building Code of Canada 2015 (NBCC, 2015), therefore an extensive interpretation can be drawn when discussing the current results. Case et al., (2011) focused on determining the force coefficients, while the current study will measure the pressure coefficients in order to compare them with the NBCC 2015. It was decided to perform the experiments on 3 models of residential buildings, scaled at 1:100, which were chosen to observe the effect of the roof pitch angle, and building geometry (Figure 3.7). The scale of 1:100 was chosen, as the tornado dimension of 20 cm would encompass the entire model, and the experiment performed by Case et al. (2011) had a similar tornado dimension and 1:100 scaled models. Model 2 and Model 3 had the same dimensions but different roof pitch angles of 16° and 36° respectively, and Model 1 had the same roof pitch angle as Model 2, but had a longer depth, L, and height, H, thus the aspect ratios were L/B = 1.5 and H/L = 0.46. Table 3.1 and Table 3.2 present the geometries of the three house models and Figure 3.7 shows the image of the three house models tested.

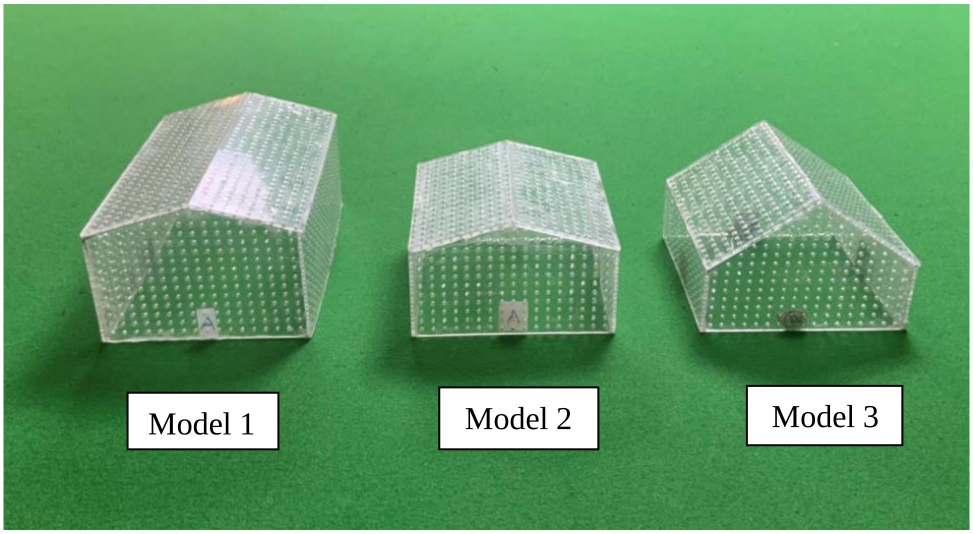

Figure 3.7: Residential house models 1, 2 and 3

Table 3.1: Model dimensions

	Θ	B	L	He	ht	h	L/B	h/L
Model	Degrees	mm	mm	mm	mm	mm	-	-
1	15.95	98	146	59.7	73.7	66.7	1.5	0.46
2	15.95	98	98	47.7	61.7	54.7	1	0.56
3	35.5	98	98	37.1	72.1	54.6	1	0.56

ht = total height he = eave height h = mean roof height
L = longer plan dimension B = shorter plan dimension Θ = roof pitch

Table 3.2: Full-Scale dimensions in meters

	Θ	B	L	he	ht	h	L/B	h/L
Model	Degrees	m	m	m	m	m	-	-
1	16	9.76	14.64	5.97	7.37	6.67	1.5	0.46
2	16	9.76	9.76	4.77	6.17	5.47	1	0.56
3	35.5	9.76	9.76	3.71	7.21	5.46	1	0.56

ht = total height he = eave height h = mean roof height
L = longer plan dimension B = shorter plan dimension Θ = roof pitch

3.5 Experimental cases

The three house models were tested at three different locations from the center of the tornado. In addition, each model was turned around its own axis to achieve three different tornado incidence angles of 0°, 45°, and 90°. A total of 9 test cases per model were performed, as summarized in Table 3.3. Locations along the radius of the tornado were based on the maximum, medium, and minimum tangential velocities measured in Phase 1 of the experiment. The 0° and 90° angle orientations were chosen because these represent a perpendicular incident wind relative to the windward wall and roof. The 45° angle orientation was chosen to represent a test condition where the incident wind could be split by the corner of the house, which could create different wind effects on the house. For the three different house angles tested, 0°, 45° , and 90°, the house Wall A was facing the center of the tornado while the tangential velocity of the tornado was perpendicular to Wall D at 0°. At the 90° orientation, Wall B was facing the center of the tornado vortex while the tangential velocity was perpendicular on the Wall A. In Figure 3.8, the building orientation angles (BOA) are represented, at 10cm for the BOA = 0° case, at 25cm for the BOA = 45° case, and 40cm for the BOA = 90° case.

Table 3.3: Test cases for different angles and model locations

Tornado zone	Max Velocity			Mid Velocity			Min Velocity		
Case	1	2	3	4	5	6	7	8	9
Angle (°)	0	45	90	0	45	90	0	45	90
Location (cm)	10	10	10	25	25	25	40	40	40

The three ranges of tangential velocity correspond to three radii as positions where the house models were placed (Figure 3.8): the 10cm radius as the location of maximum tangential velocity of 12.2 m/s, the 25 cm radius as the location of mid-velocity of 6.3 m/s location, and the 40 cm radius as the location of low-velocity of 4.2m/s location. As the tornado simulated in the current experiment is stationary, these three model locations give a better understanding of the peak pressures on the house model at different locations in the tornado; however, these cannot replace the effect of a translating tornado.

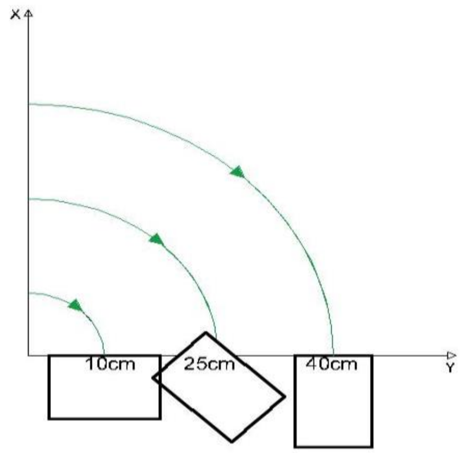

Figure 3.8: Top view of a quarter of the tornado showing model locations and orientations

Figure 3.8 shows schematically the experimental Case 1 (BOA = 0°, D = 10 cm), Case 5 (BOA = 45°, D = 25 cm) and Case 9 (BOA = 90°, D = 40 cm) as detailed in Table 3.3.

3.6 Simulated tornado duration effect

Since the tornado simulated in the WDS was stationary, an interesting way of organizing the stationary tornado pressure data was employed, as consulted in Haan et al. (2017). The peak pressure coefficient was found for different tornado exposure durations to the house model. This generated the idea of studying the effects of tornado exposure duration, as well as presenting the results on zones at the surface of the model; however, there are differences between the Haan et al., (2017) method presented in the literature review and the one performed for the WDS tornado experiments. Duration intervals of 0.1 s, 0.5 s, 1 s, 2 s, 3 s, 4 s, 5 s, 6 s, 7 s, 8 s, 9 s 10 s, 15 s, 30 s, 60 s and 90 s were chosen from the three 30 s tests, and the peak pressure was selected from each respective time interval *x(s)*. The three 30 s trials were combined, and 100 random selections of *x(s)* duration segments were chosen, where the peak pressure coefficient of that segment was considered. The average of all the 100 pressure coefficient selections was then found. This procedure was repeated for each duration (0.1 s, 0.5 s, 1 s to 10 s, 15 s, 30 s and 60 s) and for each pressure tap. The value of the pressure coefficient measured for the 90 s exposure duration, was the peak Cp value from the three repetitions, therefore the sampling method was not used for this exposure duration. Increasing the amount of selection from 100 to 1000 was attempted; however, the computational time to process the data was not realistic for this set of experiments relative to the small reduction of error percentage. Such data organization can bring information regarding the exposure duration effect on the intensity of the peak pressure coefficients. Also, since the WDS facility is limited to stationary tornadoes, establishing a testing protocol to correlate the pressures on a model caused by a stationary tornado to those of a translating tornado could be helpful for future experiments. It has been previously mentioned that the stationary tornadoes could be used to determine worst-case scenarios where a tornado would stagnate on the same point for an extended amount of time and would produce greater pressures than those caused by translating tornadoes. Studying the peak pressures and the effects of duration for a stationary tornado will be used for comparison of peak pressure coefficients to the C_pC_g coefficients recommended by NBCC 2015 and it could prove important for future experiments. As detailed in Chapter 2.5, Haan et al., (2017) mentioned that the static pressure should not be removed when calculating the C_p values if a comparison to the ASCE 7-05 design code is sought. Therefore, the peak pressure coefficients were calculated using the C_p values (Eq. 2.1).

The C_pC_g values were taken from the zonal system of the NBCC 2015, described in Figure 2.14 to 2.16 of Section 2.6. Figure 2.16 (4.1.7.6-A) are the external peak values of C_pC_g for primary structural members while Figure 2.14 and Figure 2.15 (4.1.7.6 B, E) are the external peak values of C_pC_g for cladding and secondary structural members. Since there are no provisions for tornadoes in the NBCC 2015, no gust factors have been determined specifically for tornadoes. Pressure coefficients obtained from experimental ABL wind tunnel tests are presented as C_pC_g values (Aldoum, 2018). However, since studies on the C_g values were not found for tornadoes, it was decided that the pressure coefficient values obtained from the WDS tornado experiments would be presented as C_T values (Pressure Coefficient “Tornado”) and would be compared to the C_pC_g values of the building code. The peak C_T value of each zone and for different exposure durations was used to compare the recommended peak C_pC_g values of the NBCC 2015 provisions. Analysis of the zone locations on the house models that exceed the NBCC 2015 provisions are discussed in Chapter 5.

Chapter 4 Results and analysis

This chapter summarizes the pressure coefficient results for the three house models tested in the WDS facility with 9 different cases per model for a total of 27 different test cases. However, it was found that the experiments that were performed at the 25 cm and 40 cm radius were too far outside of the tornado vortex. Since the tornado's diameter was of similar size to the house models, the models were exposed to the flows from a large radius. The tornado's tangential velocity profile is greatest at the 10 cm location and significantly decreases further away from the tornado's core. At the 25 cm and 40 cm location, the model was placed in a region where the portion of the house closest to the core was experiencing a greater tangential velocity, while the tangential velocity on the other side of the house was much less. Since the tangential velocity in the center of the house was used to calculate the pressure coefficient, the C_p nearest the tornado core were very high due to the increased pressures caused by the greater velocity parameter, while the other side of the house experienced smaller magnitudes of pressures due to the lower velocity parameter. This resulted in the calculation of the C_p value that was very different from one side of the model to the other. Therefore, only the results from the tests that were performed at the radius of 10 cm, corresponding to the maximum velocity (r_c) were presented and discussed, while the cases at the 25 cm and 40 cm radii were presented in the appendix. These tests could be used for analysis in future studies if a more precise tangential velocity is used to calculate the pressure coefficients at different locations along the model. Therefore, the tangential velocity found on the side of the house nearest the core should be used to calculate that side of the house, while the tangential velocity found on the opposite side should be used to calculate those pressure coefficients. The pressures measured at each pressure tap were transformed to a pressure coefficient and were illustrated in three different representations

In Section 4.1; colour scaled contour plots and graphs of the C_p for each pressure tap along 1 horizontal row were plotted. In Section 4.2 and Section 4.3, graphs of the averaged C_p value from the 3 vertical pressure taps are used to present the pressure coefficients of different cases as multiple cases and can be presented in one graph, making it easier to visualize pressure trends and make a comparison between different models or orientation angles. Colour-scaled contour plots help visualize the pressure coefficient magnitudes on each wall and roof; the average C_p graphs show the average of all three rows are presented for all three models under the same BOA and location, and for a specific model at a different BOAs. This helps understand the effects of the roof pitch angle, building orientation, and house geometry on the tornado-induced pressure coefficient distributions. The C_p graphs that show the results along each horizontal pressure tap row allow us to see the C_p of each pressure tap as well as the trends and the regions of greater or lesser suction on the surface of the model. This is ideal to analyze the results from a single house model under one scenario.

In Section 4.4, the effects of tornado exposure duration on the pressure coefficient results were investigated and an analysis was performed on each house model, where the pressure coefficients' results were organized by the zones corresponding to the NBCC 2015 recommendations. A comparison of the C_p pressure coefficients obtained in the current experiments to the NBCC 2015 recommended minimum C_pC_g was performed to identify the potential limitations of the code for applicability to the tornado prone regions. In the NBCC 2015, the recommended C_pC_g values are given for different scenarios based on atmospheric boundary layer (ABL) wind tunnel experiments. It was decided to present the pressure coefficients of the tornado experiments in the WDS as C_T since no standard or procedure has been determined for tornado loading in the NBCC 2015, nor has a gust factor been found for a tornado event. Therefore, C_T will be the C_pC_g obtained experimentally, and C_pC_g will be the one obtained from the NBCC 2015.

4.1 Peak pressure coefficients for pressure tap rows

In the current section, an analysis of the low and high suction areas on the walls is presented. The pressure contour plots show a visual representation of the high and low pressures along the walls and roofs of the tested models, which are followed by the C_p values and plot trends. The graphs that show the plots for each pressure taps' row (bottom, middle, and top rows) are used for this analysis.

There is a similar pressure coefficient trend occurring on all the walls in all three models. Due to the similarity of the pressure coefficients on the walls of the different models and cases, the main analysis for the walls will be presented in Section 4.1.1. The analysis for the roof is presented after each graph for the respective model and case number as the graphs are different for all the cases.

When comparing the peak pressure coefficients for the roofs of different models it was noticed that Model 1 and Model 2 compared better to each other than to Model 3, due to their same roof pitch angles but different base dimensions. Model 2 and Model 3 were compared to each other since they have the same base dimensions but different roof pitch angles, which could help understand the effects of roof pitch angle.

4.1.1 Peak pressure coefficients trend on the walls of Model 1

As the pressure coefficients, C_p are non-dimensional, the graphs were represented by a function of the non-dimensional length of the walls and roofs by dividing the distance where each pressure tap is located (x) by the length of the wall or roof (L) on the corresponding surface where the pressure tap is found. For Model 1, x/L spans from 0 to 1 for Wall B and Wall D and from 0 to 0.9 for Wall A and Wall C. In general, for all the cases performed, the models were under suction and low magnitude positive pressures were noticed on the walls or on the roofs. The dominant suction and the absence of pressure could be explained by the fact that the models were immersed in the tornadic funnel, which creates an updraft on all of the exposed surfaces. However, the induced suction was not the same for all the roofs and walls on which the tornado acted. The peak pressure coefficients recorded for Model 1, tested at BOA = 0° and at a distance of 10 cm from the center of the vortex (Case 1), are represented in Figure 4.1 and Figure 4.2. When the horizontal wind was approaching perpendicular to Wall D (BOA = 0°), it was noticed that Wall A and Wall C were under opposing high and low suction distributions. The vortex was rotating in a clockwise flow and the leading wall edge to the clockwise flow was under a greater suction than the trailing edge, thus creating a torsional effect on the entire model. The leading edge of Wall A at $0 = x/L$ (corner with Wall D) registered the lowest suction, while the trailing edge at $0.9 = x/L$ (corner with Wall B), encountered much more suction, for the three rows of pressure taps (Figure 4.2). Wall C, which was parallel to Wall A, was experiencing opposite high and low suction areas when compared to Wall A: the leading edge was under greater suction than the trailing edge.

For Wall A and Wall C, which were parallel to the horizontal flow, a similar flow pattern around the two walls was expected. However, the pressure coefficients had different evolutions, because Wall A was located towards the center of the vortex where vertical, axial, and horizontal velocity components were higher than the velocities further away from the center of the vortex, where Wall C is located. Also, one of the reasons for which Wall A and Wall C have opposite pressure coefficient distributions could be due to the flow, which was deviating off of Wall D, creating a suction zone near the corner of the model and at the leading edge of Wall C. This is known as the "separation bubble" and was signaled around the corners of the walls and roofs exposed to incoming wind flow. Thereafter, the flow re-attached on the Wall C around 0.6 = *x*/*L* region, which led to a lower suction zone at the windward edge and a higher suction at the leeward edge of Wall C. However, for Wall A, the vortex layers detached at around 0.5 = *x*/*L*, thus the low suction occurred first, and it was followed by the region of high suction after detachment.

Similarly, Wall D and Wall B recorded opposing suction intensities on opposing wall edges. Wall D had a higher suction at the 0 = *x*/*L* compared to the suction at 1 = *x*/*L*, while Wall B had higher suction at the 1 = *x*/*L* than at the 0 = *x*/*L* location. As the flow approached the edge of Wall B, another high suction zone was created near the 1 = *x*/*L* edge and the flow touched down again near the 0.4 = *x*/*L* location, which led to a lower suction zone.

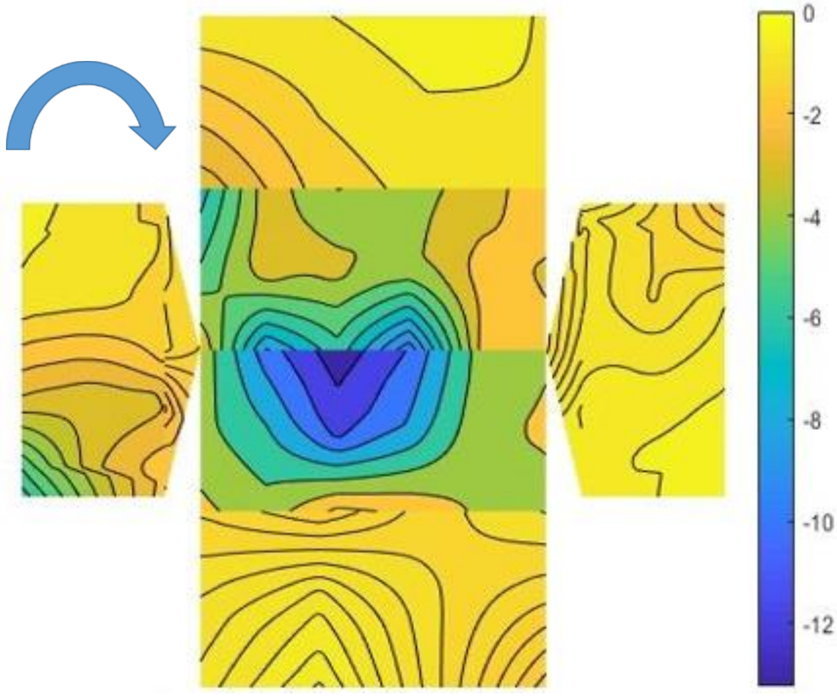

Figure 4.1: Model 1, Case 1 (BOA: 0°, D: 10cm) Peak pressure coefficient contour plot

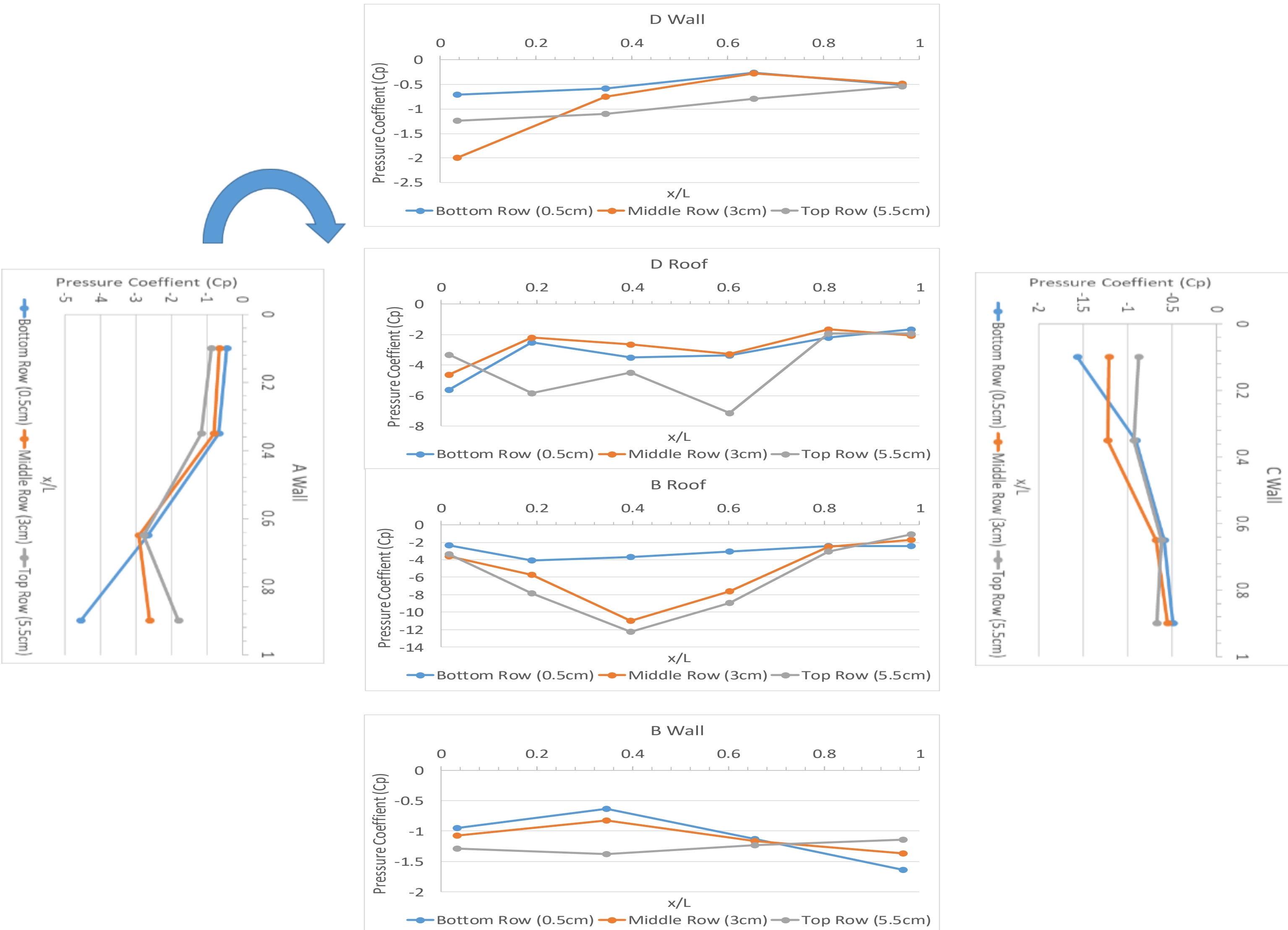

Figure 4.2: Model 1, Case 1 (BOA: 0°, D: 10cm) Peak pressure coefficient plots

For Case 2 (BOA = 45°, *D* = 10cm), as can be seen in Figure 4.3 and Figure 4.4, when the building orientation is 45° in relation to the incoming wind direction, similar peak pressure coefficient patterns were observed for the walls: at 1 = *x*/*L* Wall A experienced the highest suction out of the four walls, while at 0 = *x*/*L* the lowest suction was recorded. Wall C had an opposite pressure distribution compared to Wall A, but overall lower suction values. For Wall D and Wall B, suction was dominant, especially for the 1 = x/L region of Wall D, where, due to layers of flow detachments and reattachments, the flow became too complex to assign an explanation. However, it can be concluded that the wall that was the nearest to the center of the vortex, Wall A in this case, had the region with the greatest suction.

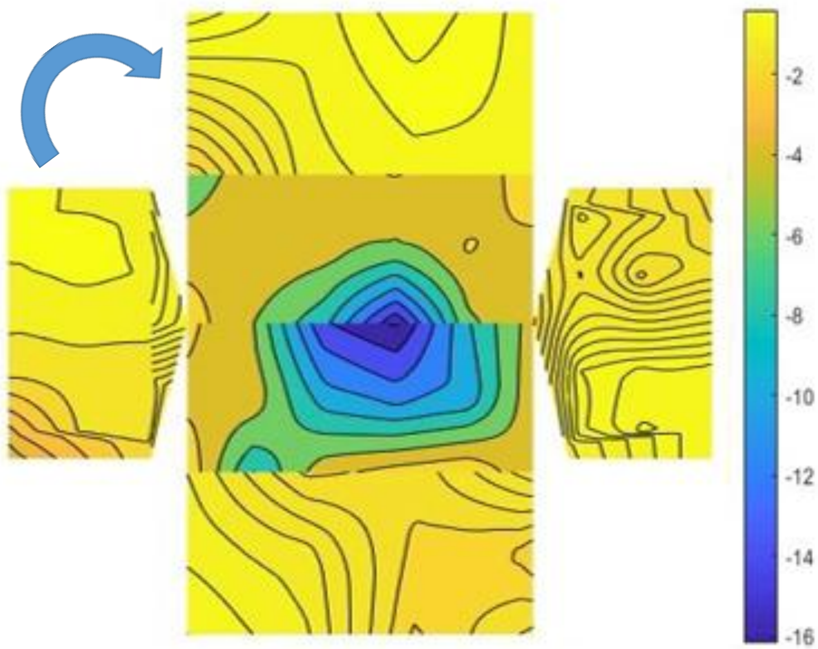

Figure 4.3: Model 1, Case 2 (BOA: 45°, D: 10cm) Peak pressure coefficient contour plot

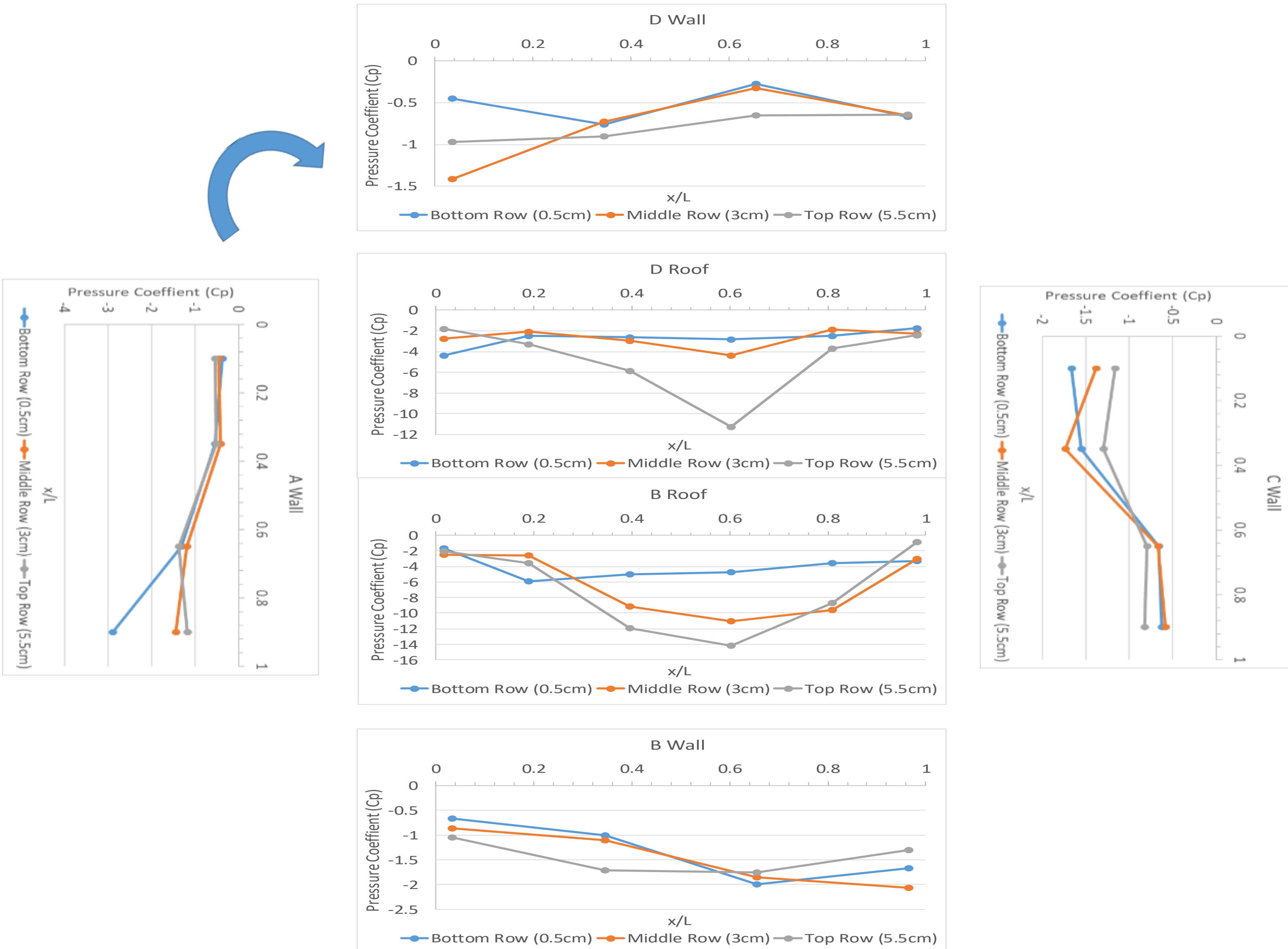

Figure 4.4: Model 1, Case 2 (BOA: 45°, D: 10cm) Peak pressure coefficient plots

For Model 1, Case 3 (BOA = 90°, D = 10cm), the building orientation was at 90°. Therefore, Wall A was directly exposed to the incoming flow, while Wall B was the one closest to the vortex and parallel to the incoming flow. As represented in Figure 4.5 and Figure 4.6, it was noticed that Wall B had the greatest suction (greatest negative peak pressure coefficient), while Wall B and Wall D had opposite distributions of suction intensities from one another.

As a general observation, it was also noticed that all the peak suctions of the four walls were most commonly found at the bottom row of pressure taps on the wall, except for the windward walls (Wall D for Case 1 and Case 2, and Wall A for Case 3). The windward wall always had the greatest suction at the middle or top row instead of the bottom row of pressure taps. This could be due to the horizontal velocity parameter being greater at the midpoint elevation of the house wall. It could also be due to the flow created when this impacts the wall or runs over the roof and towards the wall connection, resulting in a higher suction on the portion of the upper wall. There was more variance in terms of the row elevation (Bottom, Middle, Top) and the greatest suction on the other walls. Therefore, a trend could not always be established

.

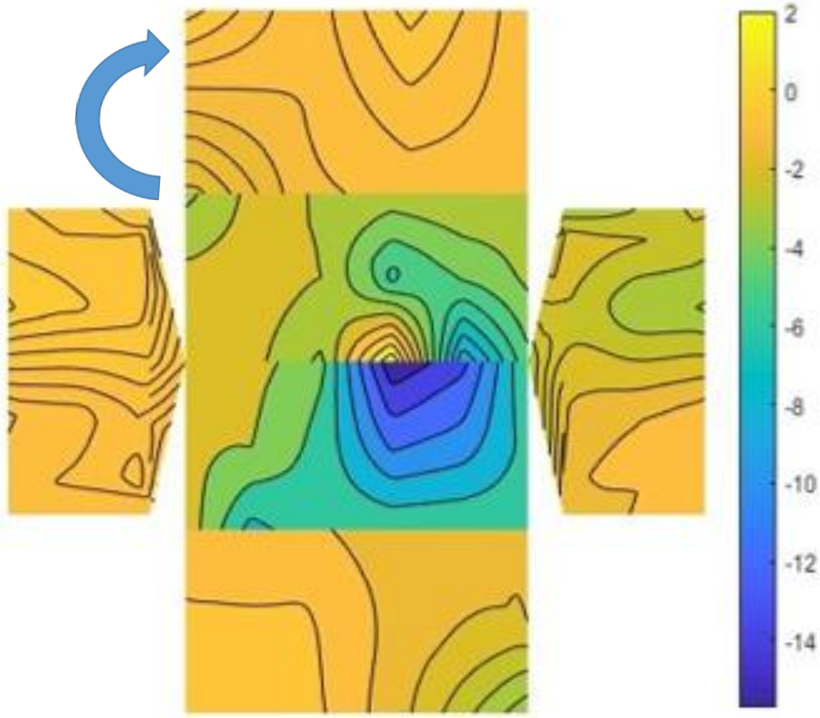

Figure 4.5: Model 1, Case 3 (BOA: 90°, D: 10cm) Peak Pressure coefficient contour plot

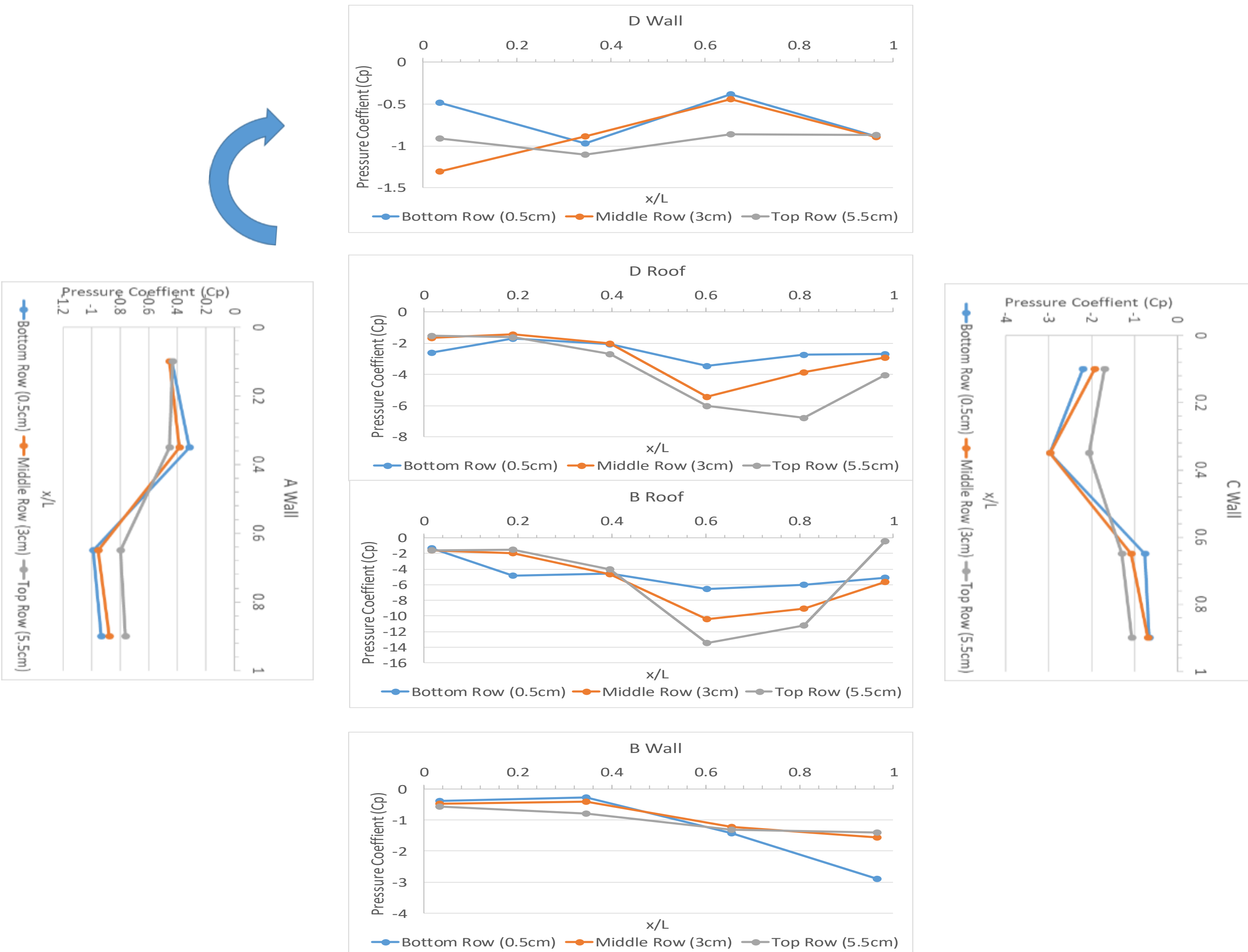

Figure 4.6: Model 1, Case 3 (BOA: 90°, D: 10cm) Peak pressure coefficient plots

4.1.2 Peak pressure coefficients trend on the roofs of Model 1

The roof of Model 1 appeared to have very high suctions, with peak pressure coefficients of up to -15, especially when compared to the walls where the maximum pressure coefficient was measured to be -4.5. For Model 1, Case 1 (BOA = 0°, *D* = 10cm), for which the incoming horizontal wind approached perpendicularly to Wall D and the edge of the windward Roof D, the location of the highest suction was on Roof D and was recorded on the top row of pressure taps, which were parallel and very near to the ridge of the roof (Figure 4.1 and Figure 4.2). High levels of suction were also signaled along the middle of the roof and there were high levels of suction at the 0 = *x/L* region for both the bottom and middle rows of pressure taps. This is near the corner of the leading edge of the roof nearest to the vortex's core. On the leeward Roof B, the middle and top row of pressure taps were very similar throughout the 0 = *x/L* to the 1 = *x/L* region; however, the suction was higher than on the windward Roof D. The greatest suction was again found in the center of the roof, while the lowest suctions were found at the 0 = *x/L* and 1 = *x/L* on Roof B's edge. The peak pressure coefficient from 0 = x/L to 0.4 = *x/L* (location of peak suction) augmented linearly and then gradually decreased to the right of 0.4 = *x/L* to 1 = *x/L* (Figure 4.1 and Figure 4.2).

As it can be noticed in Figure 4.3 and Figure 4.4, for Model 1, Case 2 (BOA = 45°, *D* = 10 cm), the windward Roof D once again had the highest suction in the center of the roof at 0.6 = *x/L*, along the top row of pressure taps near the ridgeline. The bottom and middle rows of pressure taps had lower suction. The leeward roof had a similar suction to the 0° = BOA, Case 1; however, the highest peak suction shifted slightly to 0.6 = *x/L*, instead of 0.4 = *x/L*. The horizontal velocity was approaching the roof corner instead of the center of the roof edge, which could be the reason for the shift of the suction areas. The region from 0 = *x/L* to 0.2 = *x/L* of Roof D was under much lower suction until it suddenly increased at the 0.4 = x/L, and the 0.6 = x/L regions. For the windward Roof D, the region with the least amount of suction was at the bottom row of pressure taps that were along the edge of the length of the roof, increasing gradually towards the ridge of the roof. The edge of the leeward Roof B had the lowest levels of suction on the bottom row, which was along the edge of the roof, specifically at 0 = *x/L*, and 1 = *x/L*. A sudden increase was noticed at the ridge of Roof B, between 0.6 = x/L, and 0.8 = x/L, pointing out a further shift in the highest suction location when the BOA angle increased.

Figure 4.5 and Figure 4.6 represent the peak pressure coefficients for Model 1, Case 3 (BOA = 90°, D = 10cm) for which the incoming horizontal wind was approaching perpendicular to the Wall A and the gable peak of the roof, compared to the side/diagonal of the roof for Case 1 and Case 2. Thus, Wall B and Wall D were parallel to the flow and were facing towards the vortex and further away from the vortex, respectively. From 0 = x/L to 0.4 = x/L there was a relatively stable low suction; however, after 0.4 = x/L there was a much greater suction on both Roof B and Roof D. One probable cause for this was the deviation of the flow over the triangular wall peak, which detached after the 0.4 = x/L region, where it gained a faster velocity resulting in increased suction. It was noticed that the two roofs had similar pressure coefficient trends; however, Roof B records the highest suction, much higher compared to Roof D and Wall A, Wall B, Wall C, Wall D. This could be due to the closer proximity of Roof B to the vortex core of the tornado.

4.1.3 Peak pressure coefficients trend on the walls and roofs of Model 2, Cases 1 and 2

When investigating the peak pressure coefficients for Model 2, it was noticed that the peak pressure coefficients on the walls and roofs of Model 1 and Model 2 were similar for each respective case. Therefore, in the current subsection the suction distributions for both cases, Case 1 (BOA = 0°, D = 10 cm) and Case 2 (BOA = 45°, D = 10 cm), are discussed for both Model 1 and Model 2. The comparison between the walls will also be made as Model 1 is longer than Model 2.

The roof pitch angles of the roofs were the same for Model 1 and Model 2; however, Model 1 was longer (L = 146mm) than Model 2 (L = 98mm). Slight differences between the peak pressure coefficients were noticed for the windward Roof B, which was under slightly less suction for Model 2 compared to Model 1 for Case 1 and Case 2. The middle row of pressure taps on Model 1 had a decrease in suction after 0.2 = x/L while the longer house Model 2 had a decrease in suction at 0.4 = x/L, as it can be seen in Figure 4.7 and Figure 4.8. This could be due to the longer roof length that allowed the flow to accelerate over a longer distance, creating a greater negative pressure. The bottom row of pressure coefficients nearest the roof edges were similar for both houses while the gradual increase of suction could be noticed towards the ridge of the roof, with a peak on the leeward Roof B, as reported for Model 1 as well.

The walls of Model 1 and Model 2 were very similar from one another for Case 1. The Wall A of Model 1 had a more gradual decrease of the pressure coefficient between 0.1 = x/L and 0.35 = x/L while Model 2's decrease was more significant. The trailing edge of Wall A for both models end up at a very similar suction magnitude. Wall D was slightly different between Model 1 and Model 2, where the pressure coefficients between 0.025 = x/L and 0.325 = x/L were very similar from one another for Model 2, while there is a larger spread of magnitudes for Model 1. Wall B of Model 2 is under a slightly greater suction between 0.65 = x/L and 0.95 = x/L compared to Model 1. This was most likely due to the difference between the two models' dimensions, leading to a slightly different positioning in the simulated tornado.

Figure 4.7: Model 2, Case 1 (BOA: 0°, D: 10cm) Peak pressure coefficient contour plot

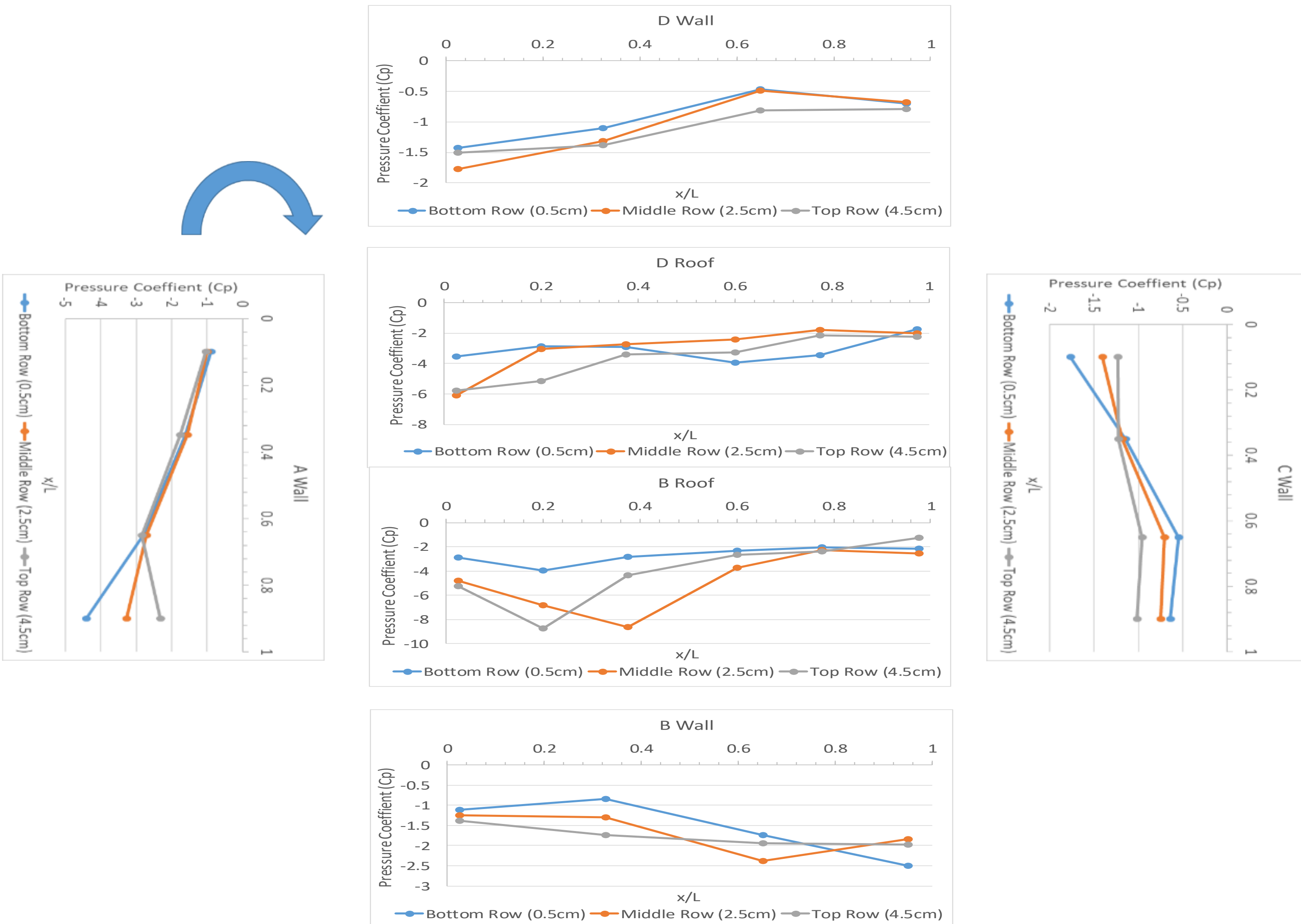

Figure 4.8: Model 2, Case 1 (BOA: 0°, D: 10cm) Peak pressure coefficient plots

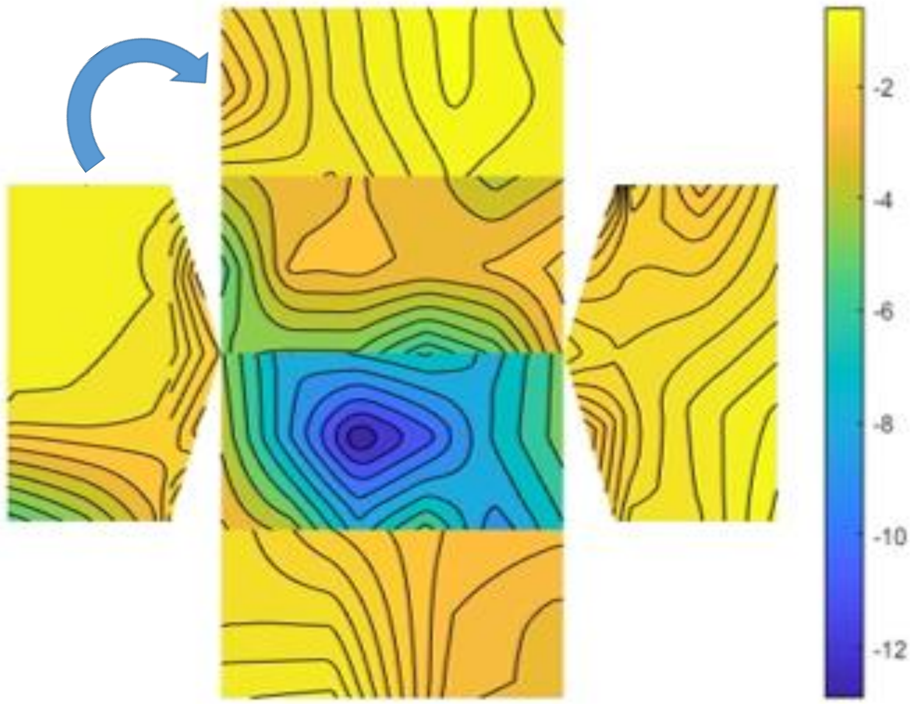

Figure 4.9: Model 2, Case 2 (BOA: 45°, D: 10cm) Peak pressure coefficient contour plot

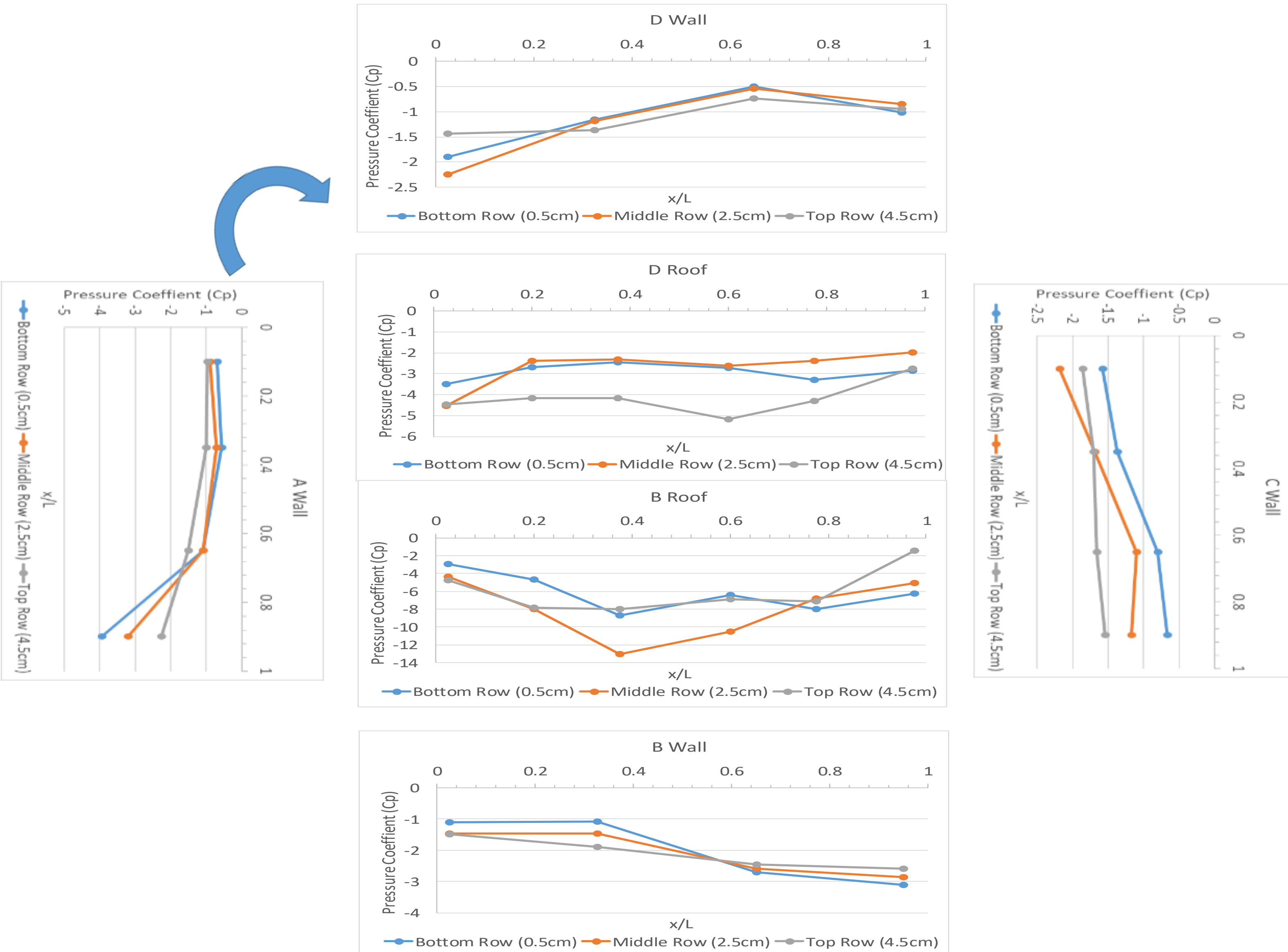

Figure 4.10: Model 2, Case 2 (BOA: 45°, D: 10cm) Peak pressure coefficient plots

The trends of the pressure coefficients between Model 1 and Model 2 for Case 2 were once again quite similar. It was noticed that the magnitudes of the pressure coefficients were greater on the walls of Model 2 compared to Model 1. There is a slight difference in the trend of Wall C of Model 1, where the C_p between 0.025 = x/L and 0.35 = x/L remains at a similar magnitude. The C_p values then increase between 0.325 = x/L and 0.65 = x/L. The peak pressure coefficients of Model 2 were steadily increasing until slightly after 0.65 = x/L.

For Model 2, Case 3, (BOA = 90°, D = 10 cm), the peak pressure coefficients on Roof B and Roof D were similar for Model 1 and Model 2. The shorter roof of Model 2 did not seem to affect the locations of greatest and lowest suction regions; however, there was a slight decrease in the magnitude of suction for Roof D of Model 2, as seen in Figure 4.11 and Figure 4.12. On Roof B of Model 2, there was a shift in the location of greatest suction, which was found at 0.4 = x/L instead of 0.6 = x/L for Model 1. The greatest suction was also found on the middle row instead of the top row near the ridgeline.

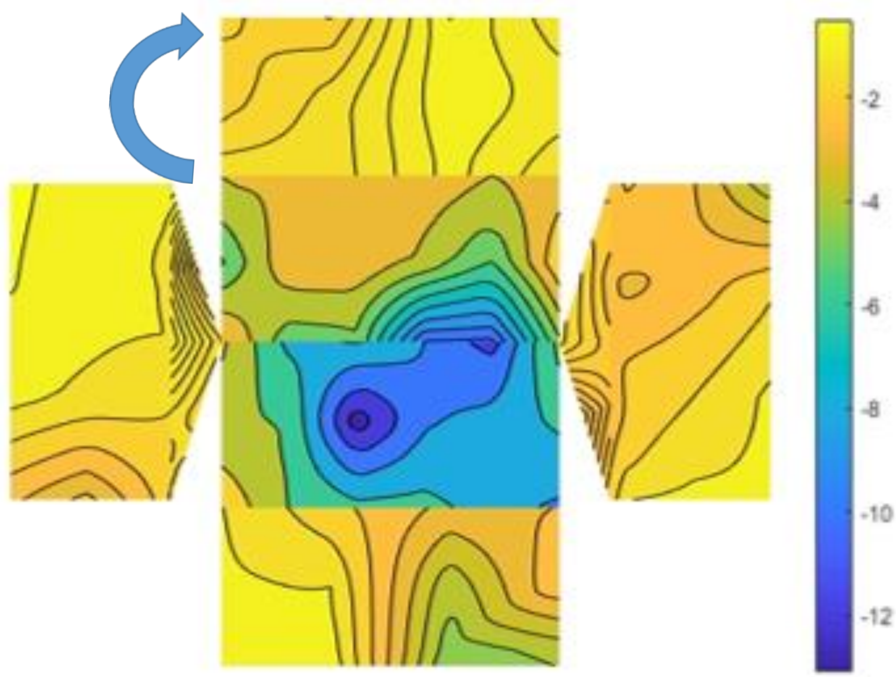

Figure 4.11: Model 2, Case 3 (BOA: 90°, D: 10cm) Peak pressure coefficient contour plot

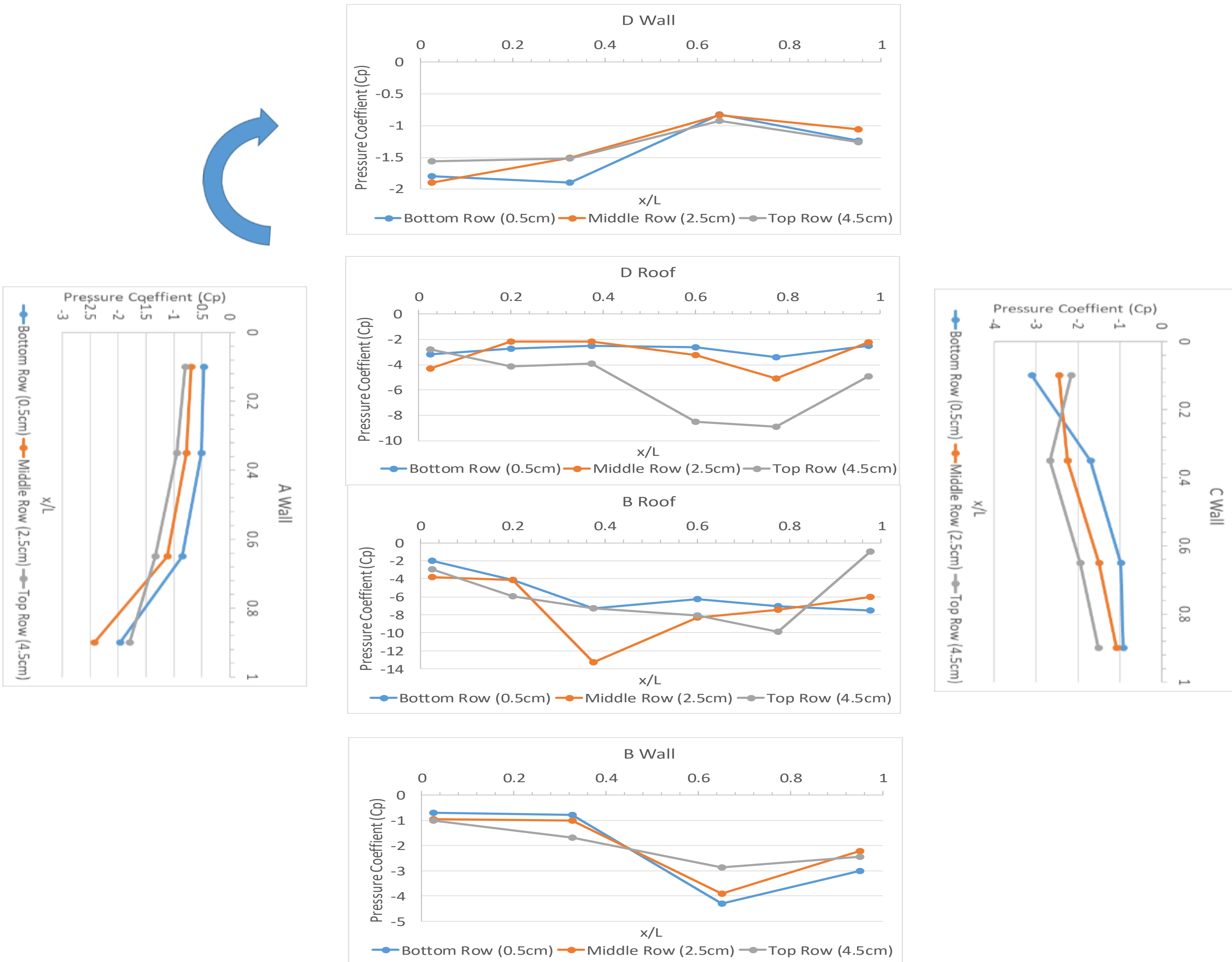

Figure 4.12: Model 2, Case 3 (BOA: 90°, D: 10cm) Peak pressure coefficient plots

Wall A of Model 2 was similar in trend to Model 1; however, the region nearest to 1 = *x*/*L* is under a much greater magnitude of Cp compared to Wall A of Model 1. Wall D was similar near the 1 = *x*/*L* region; however, there was a large spread between the C_p values for the three rows near 0 = *x*/*L* for Model 1, while Model 2's C_p values were very similar to one another. For Wall C of Model 2, the bottom row of C_p values were of lesser magnitudes near 0.1 = *x*/*L;* however, for the regions after 0.2 = *x*/*L* the middle and top row of C_p values were of greater magnitude. Once again, the walls of Model 2 were under a greater negative C_p value compared to Model 1.

4.1.4 Peak pressure coefficients trend on the walls and roofs of Model 3 Cases 1, 2 and 3

In this section, Model 3 will be compared to Model 2, as these two had similar dimensions but different roof pitch angles. For Model 3 Case 1 (BOA = 0°, *D* =10 cm), the windward Roof D of Model 3 had similar trends for all 3 rows of pressure taps compared to Model 2; however, Model 3 had slightly lower suction, as depicted in Figure 4.13 and Figure 4.14. Thus, the higher roof pitch angle caused a lower suction on the roof surfaces. The leeward Roof B of Model 3 had different pressure coefficient trends for all of the rows of pressure taps when compared to those of Model 2. The corner at 0 = *x*/*L* for Model 3 was under much less suction compared to Model 2. The greatest suction was between 0.6 = *x*/*L* and 0.8 = *x*/*L* while the highest suction of Roof B for Model 2 was found at the 0.2 = *x*/*L* and 0.4 = *x*/*L* locations. The magnitude of the suction was also much lower for Model 3. The bottom and middle rows of pressure taps of Model 3 were under much less suction and were under very similar suction compared to Model 2. Model 2's middle and top rows of pressure taps were under a much higher suction than the bottom row.

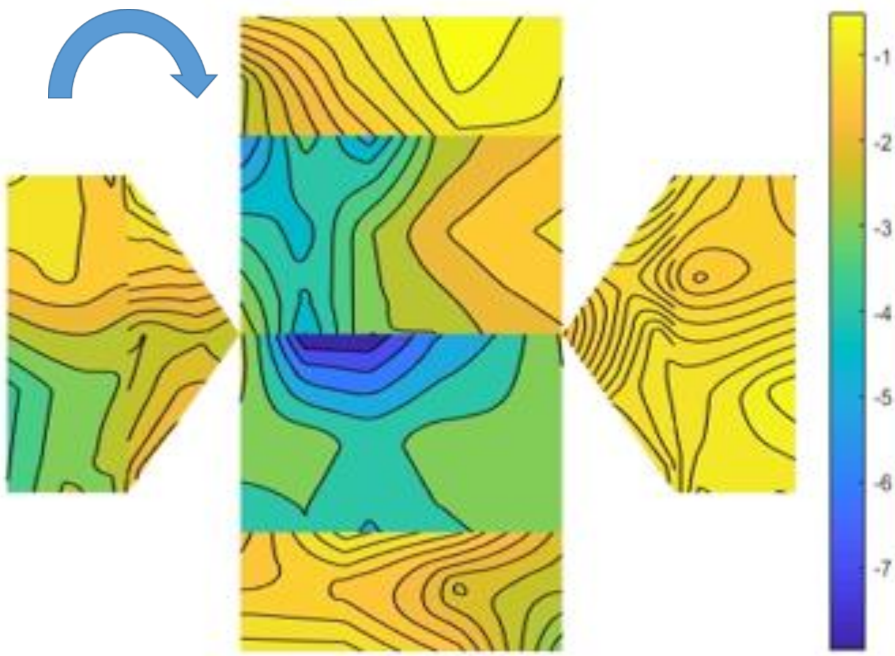

Figure 4.13: Model 3, Case 1 (BOA: 0°, D: 10cm) Peak pressure coefficient contour plot

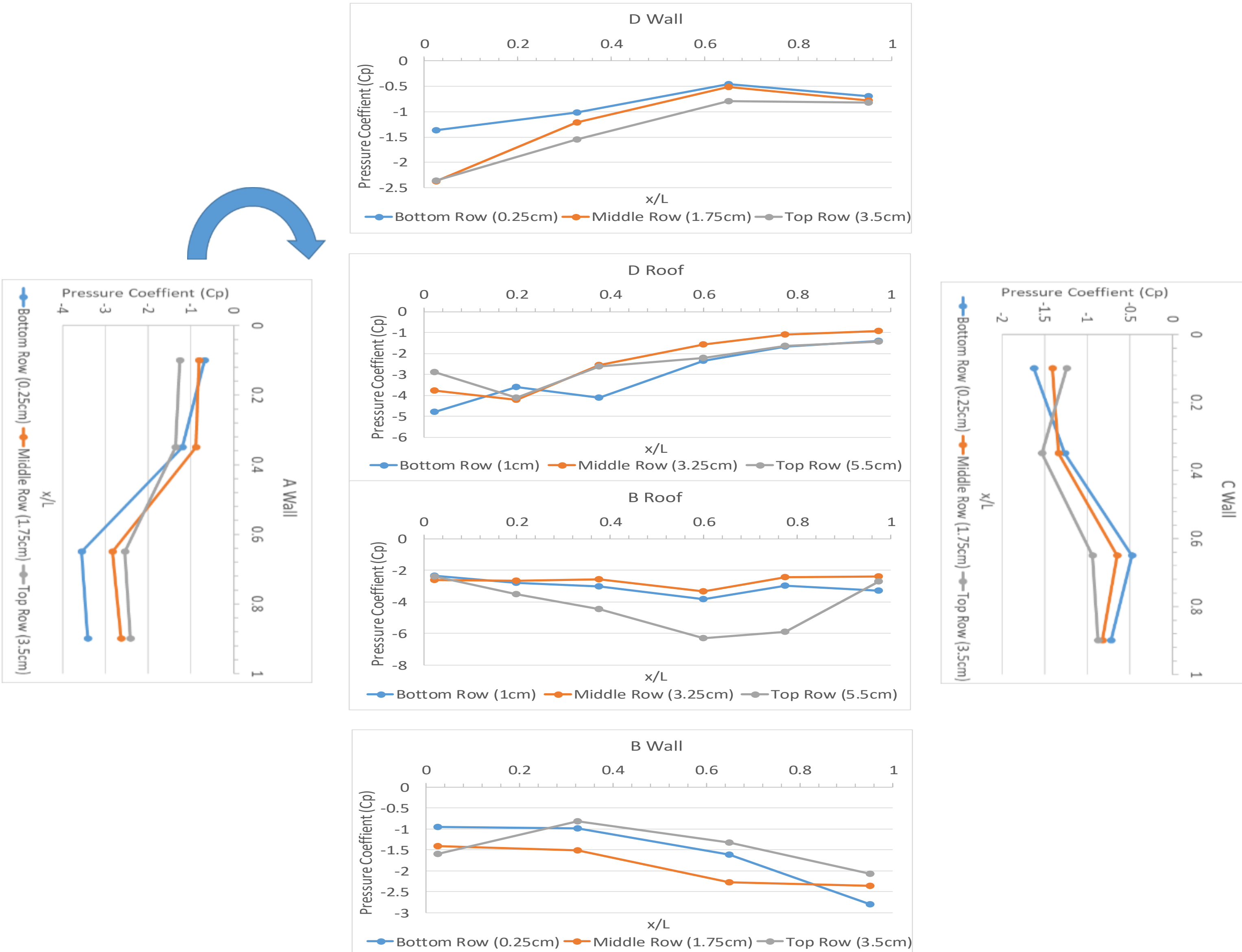

Figure 4.14: Model 3, Case 1 (BOA: 0°, D: 10cm) Peak pressure coefficient plots

For Case 2 (BOA = 45°, D = 10 cm) of Model 3, Figure 4.15 and Figure 4.16 show that the windward Roof D had the greatest suction on the leading edge of the roof between $0.2 = x/L$ and $0.4 = x/L$ at the top row of pressure taps, before it reduced until the trailing edge of the roof. This is different from Model 2, which had a 16° roof pitch angle, since the top row pressure taps stayed at a high suction over most of the length of the roof, from $0 = x/L$ to $0.8 = x/L$, as seen in Figure 4.15 and Figure 4.16. Another difference is that the bottom row of pressure taps at $0 = x/L$, which represents the corner where the wind initially hits, was the location of the greatest suction for the 36° roof pitch angle Model 3. However, for Model 2 with the 16° roof pitch angle, the bottom and middle rows of pressure taps were all under a similar high suction throughout $0 = x/L$ to $1 = x/L$. This could signify that a higher roof pitch angle is more affected at the corner part of the roof, while a lower roof pitch angle has a more constant high suction on the entire edge of the roof.

The C_p magnitudes on the walls for both Model 2 and Model 3 were very similar to each other. The trend of Wall A of Model 2 is different to that of Model 3. The Model 2 pressure coefficient trend had a gradual decrease of the C_p value from $0.1 = x/L$ to $0.65 = x/L$ and then a large C_p increase that stabilizes at $0.95 = x/L$. Model 3 Wall A, had similar C_p values between $0.1 = x/L$ and $0.35 = x/L$, then significantly decreased between $0.35 = x/L$ and $0.65 = x/L$ before plateauing at its greatest negative C_p value between $0.65 = x/L$ and $0.95 = x/L$. The other walls were similar in trend.

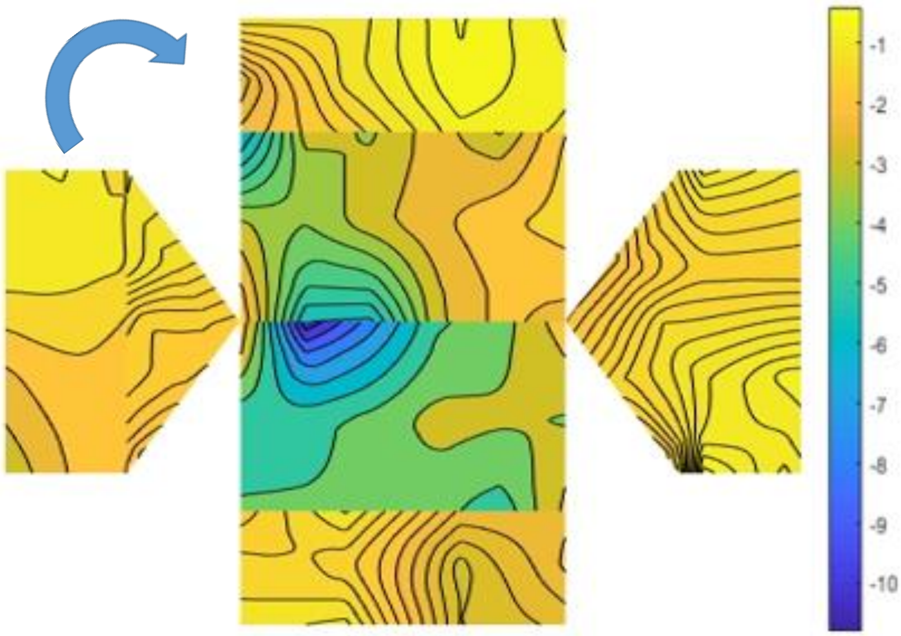

Figure 4.15: Model 3, Case 2 (BOA: 45°, D: 10cm) Peak pressure coefficient contour plot

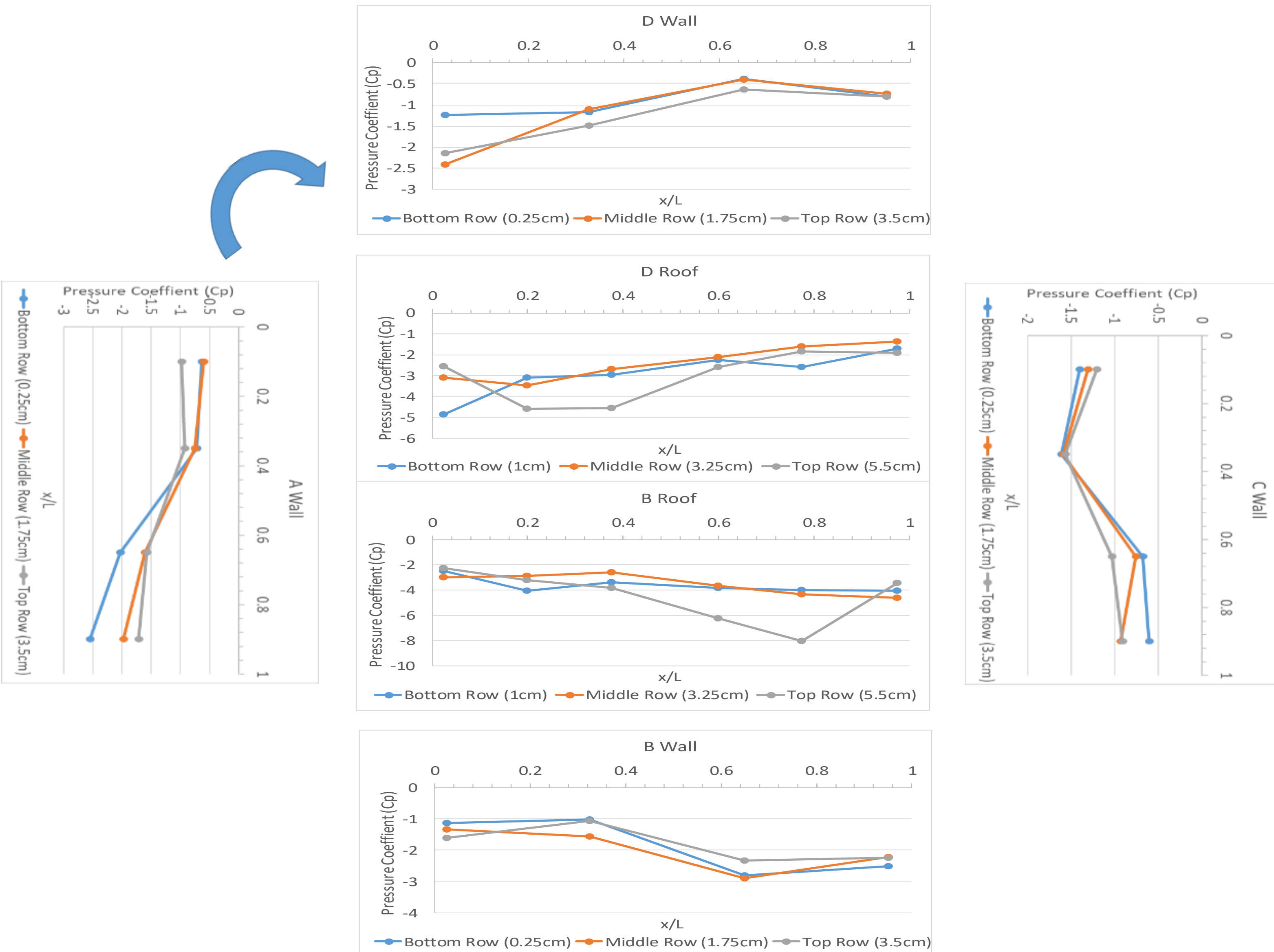

Figure 4.16: Model 3, Case 2 (BOA: 45°, D: 10cm) Peak pressure coefficient plots

The leeward roof of Model 3 was under less suction on the leading edge of the roof compared to the trailing edge. The peak suction is found at 0.8 = *x*/*L* on the side furthest away from the initial point of contact with the incoming wind. This was different from Model 2, where the peak suction was found at the 0.4 = *x*/*L* location. Thus, a higher roof pitch angle could lead to the formation of a higher suction zone further away from the leading edge on the leeward roof once the wind hits the windward Roof B due to the trajectory of the flow. After the peak suction at the 0.8 = *x*/*L* location for house Model 3, at the top row pressure taps, there was a significant drop in suction that was not seen in Model 2. This drop could be due to the flow detaching from the trailing roof edge in a different pattern.

Once again, the pressure coefficient trends and magnitudes at each pressure tap row were similar from Model 2 to Model 3. Wall A of Model 2 had stable C_p values between 0.1 = *x*/*L* and 0.65 = *x*/*L* but the C_p magnitude significantly increased to a much greater suction between 0.65 = *x*/*L* and 0.9 = *x*/*L*. Although there was an increase in the C_p values' magnitude between 0.65 = *x*/*L* and 0.9 = *x*/*L* for Model 3, it was not nearly as significant as the increase seen in Model 2.

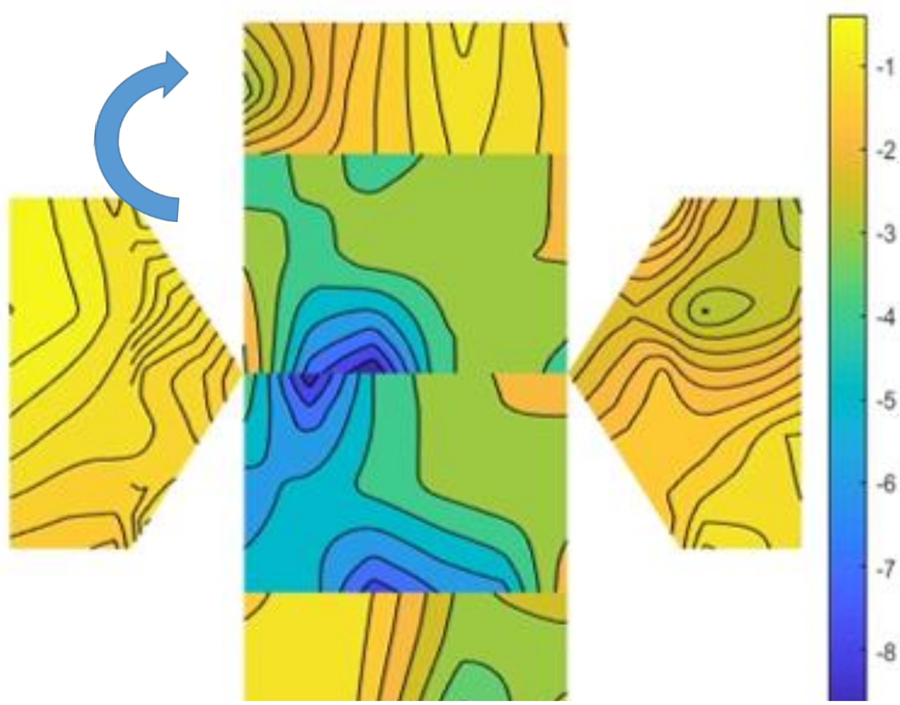

Figure 4.17: Model 3, Case 3 (BOA: 90°, D: 10cm) Peak pressure coefficient contour plot

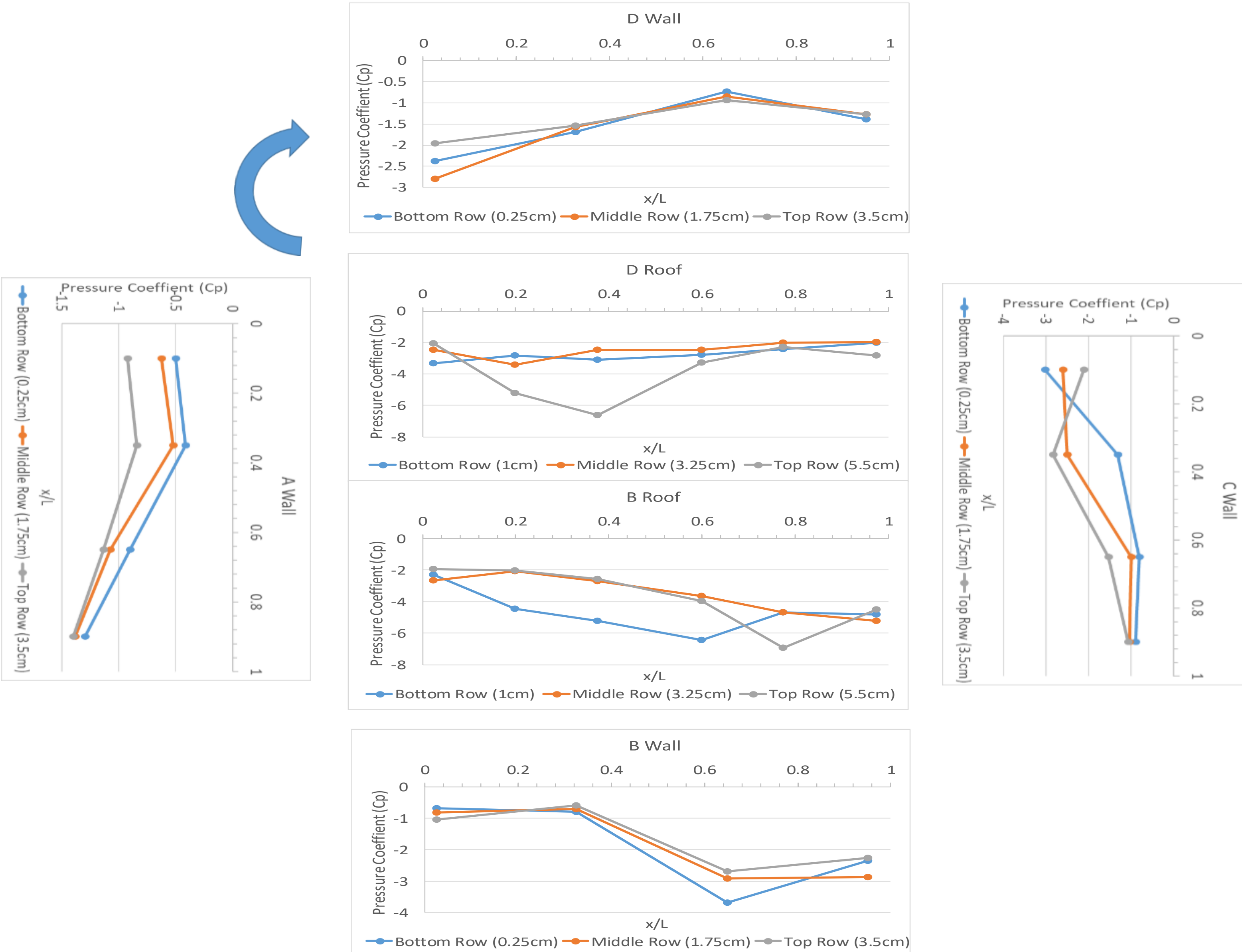

Figure 4.18: Model 3, Case 3 (BOA: 90°, D:10cm) Peak pressure coefficient plots

For Model 3 Case 3 (BOA = 90°, D = 10cm), the incoming wind flow was directed parallel to the roof ridge, so there were no windward or leeward roofs for this case. Roof D, which was facing the outer layers of the tornado, had a peak suction at the 0.4 = x/L location, while Roof B's peak suction, which was facing the vortex of the tornado, was found at 0.8 = x/L. The pressure's peak magnitudes were reported on the top row of pressure taps near the ridge of the roof for both Roof B and Roof D. One difference between Roof D and Roof B was that the bottom row pressure taps were under high suction on Roof B, while they were under much lower suction on Roof D. This could be due to Roof B being nearer to the vortex's core. The bottom row of pressure taps were under a higher suction than the middle and top row from 0 = x/L to 0.6 = x/L; however, the peak suction was found at 0.8 = x/L at the top row. Once again, there was a decrease in suction after 0.8 = x/L, which was the location of peak suction. The pressure coefficient of the top row augments to a value closer to the values obtained at the bottom and middle row.

Wall A of Model 2 for Case 3 was under a much greater magnitude of C_p than Model 3. However, Wall D of Model 3 was under a greater magnitude of C_p compared to Model 2, which has yet to be seen when comparing the walls of Model 2 to Model 3.

4.2 Building orientation effect on tornado-induced average pressure coefficients

This section compares the average of each column of pressure taps along the walls and roofs. of the 3 rows of pressure coefficients on the walls and roofs for each case. Thus, Figure 4.19 to Figure 4.21 compare the average values of the C_p for the 3 pressure taps from the bottom row, middle row, and top row of each column of pressure taps, for each BOA case. The 3 row average, $C_{p\text{avg}}$, is then plotted relative to the x/L position for each row of pressure taps on the walls and roofs of the models, Case 1 (BOA = 0°), Case 2 (BOA = 45°) and Case 3 (BOA = 90°). This method helped simplify the data from 3 rows of pressure taps to only 1, thus making it easier to compare Case 1, Case 2, and Case 3 to each other to visualize the effects of building orientation.

For the walls of all three house models (Figure 4.19 to Figure 4.21), it was noticed that Case 1 and Case 2 did not differ much in terms of the $C_{p\text{avg}}$ magnitude and the trend of the plot. The pressure distributions were very similar for Wall B, Wall C, and Wall D. However, it was noticed that on Wall A there was a large difference in pressure magnitude, where the $C_{p\text{avg}}$ registered for Case 1 was nearly two times the one recorded for Case 2. It seems that for Case 1, where Wall A was parallel to the horizontal velocity and was facing the central vortex of the tornado, there was a greater suction, while in Case 2, where the house was oriented at a 45° BOA, there was a reduction in suction. However, for the other walls, Case 1 was under the least amount of suction. Wall A might have been under greater suction because the incoming horizontal velocity was accelerating along the wall, which was closer to the tornado vortex where the highest wind speeds were recorded. The $C_{p\text{avg}}$ values of Case 3 for Wall B demonstrated that Wall B was under the greatest suction, and that the magnitude of the suction was similar to that of Case 1 for Wall A. Wall B in Case 3 was at the same position as Wall A in Case 1 (parallel to horizontal velocity). This shows that the wall nearest to the core of the vortex was under the greatest suction. The remainder of the plots for each case are very similar to each other and the building orientation did not seem to have a significant effect on the trends and the $C_{p\text{avg}}$ values' magnitudes on the walls. In addition, as mentioned in Section 4.1, the leading edge to the clockwise flow was under greater suction than that of the trailing edge on the walls.

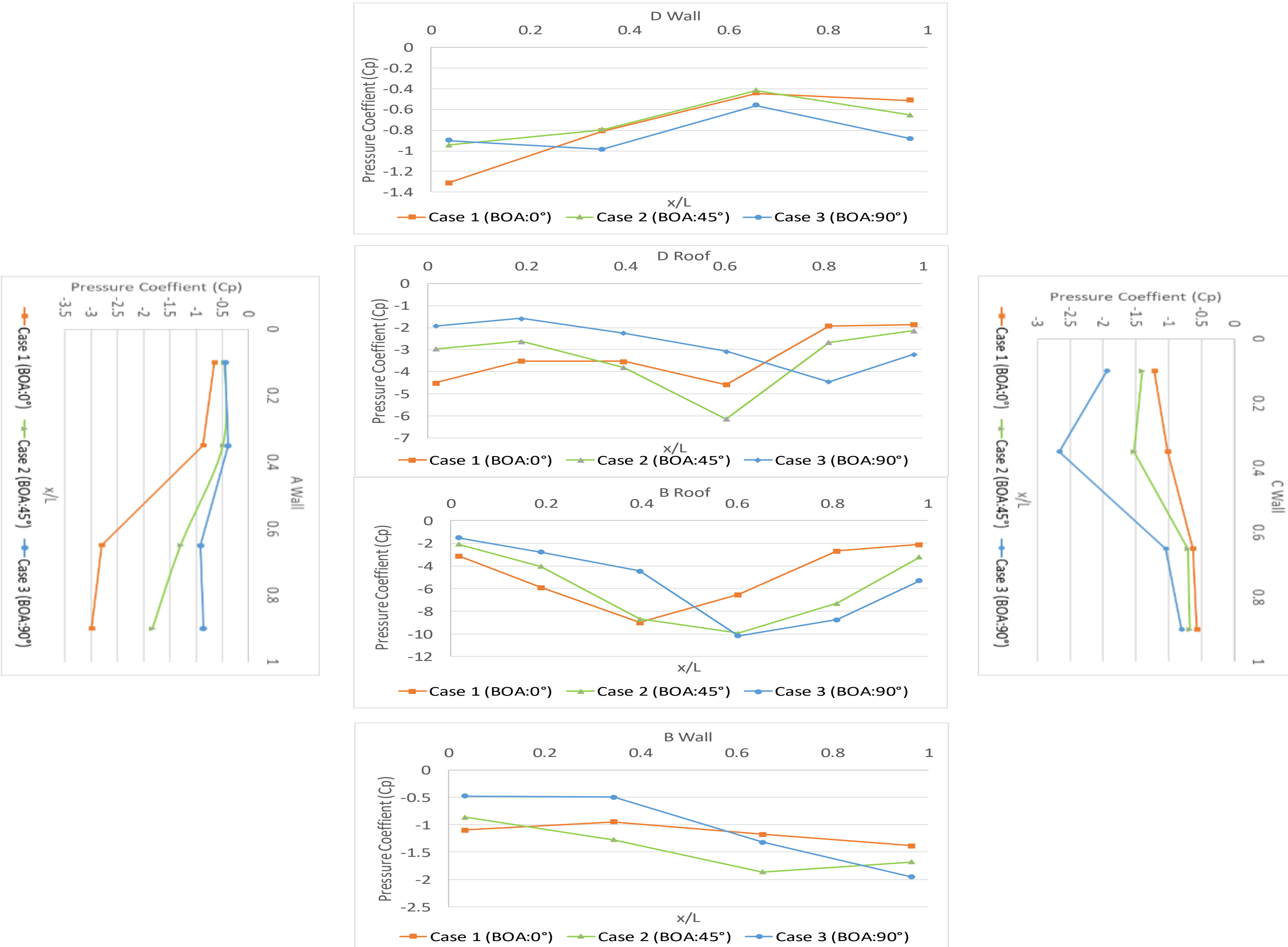

Figure 4.19: Three row average pressure coefficients, C_{pavg} for Model 1, Cases 1, 2, 3

For Roof D of Model 1 in Figure 4.19, the C_{pavg} values' trends were similar for all three cases; however, there was a large difference in terms of the C_{pavg} value's magnitude. Case 2 had a more significant decrease in the C_{pavg} values and the highest suction was 1.33 times higher than for the other cases. Case 3 had a decrease in the C_{pavg} values, however, due to the horizontal velocity parameter being parallel to the ridge, the highest suction was found at $0.8 = x/L$. For Roof B, the C_{pavg} values' trends and magnitudes were very similar to one another. The only significant difference was that for Case 1, the C_{pavg} values were higher between $0.4 = x/L$ and $1 = x/L$, while for Case 3, the highest C_{pavg} value was registered between $0 = x/L$ and $0.4 = x/L$.

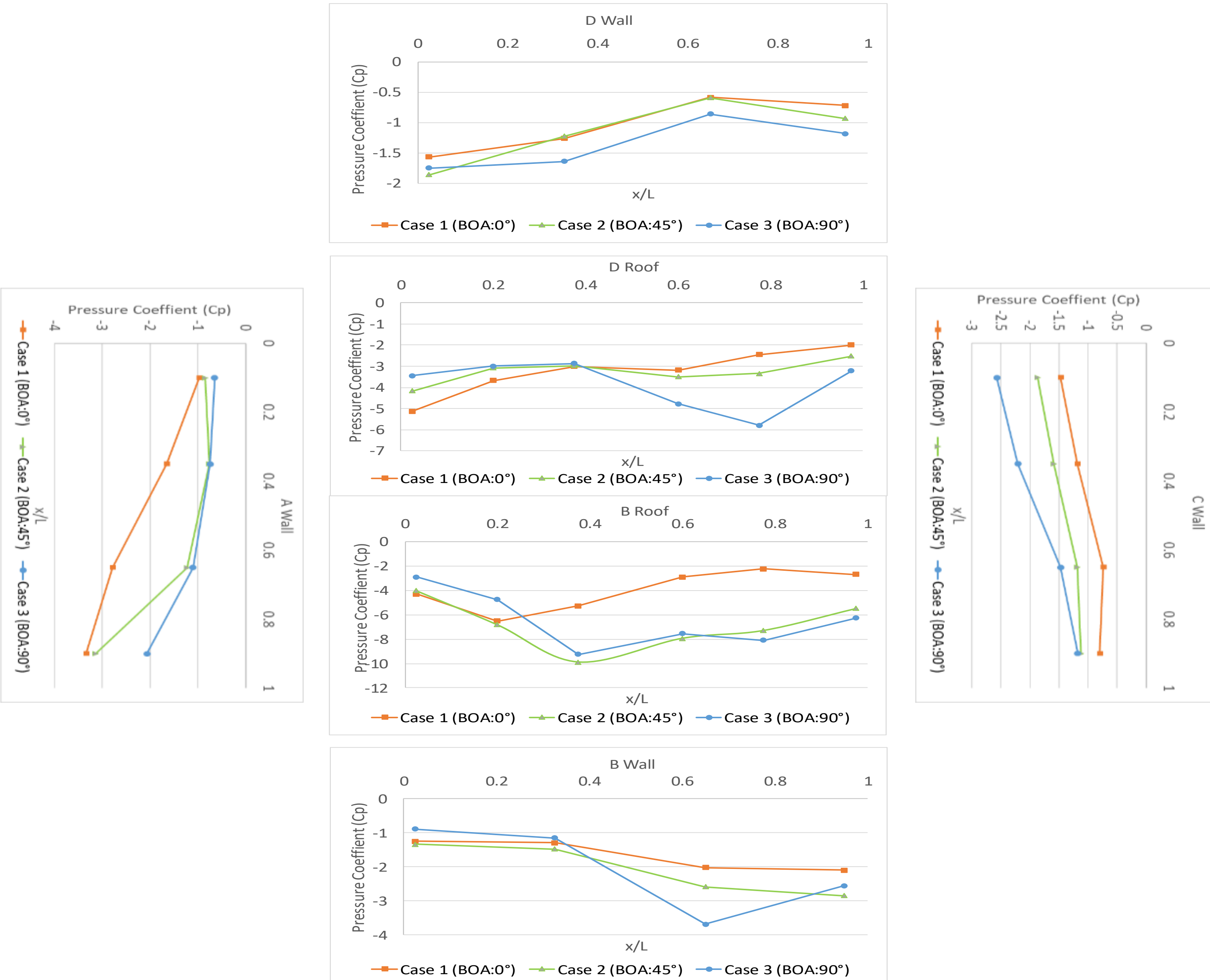

Figure 4.20: Three row average pressure coefficients, C_{pavg} for Model 2, Cases 1, 2, 3

For the windward Roof D of Model 2, (Figure 4.20), the $C_{p\mathrm{avg}}$ values' trends seemed to be very similar for Case 1 and Case 2. Case 3 had a large decrease in the $C_{p\mathrm{avg}}$ values where it was under a much greater suction at $0.8 = x/L$. The incoming horizontal velocity was parallel to the roof ridge thus the wind was creating a different type of flow due to the deviation of the triangular section of the wall and reattaching on the trailing side of the Roof D ($0.8 = x/L$). Other than this decrease in the $C_{p\mathrm{avg}}$ values, the average pressure trends for all of the cases look similar to each other. It was also noticed that for Case 1, the magnitude of the $C_{p\mathrm{avg}}$ values at $0 = x/L$ on the windward Roof D was lower, causing greater suction compared to Case 2 and Case 3. This was most likely due to the vertical velocity directly under the WDS outlet, in the center of the vortex core, that was associated with the highest suction. Roof B, Case 2 and Case 3 were very similar to each other in terms of plot trend and in the $C_{p\mathrm{avg}}$ values magnitude; however, Case 1 had a very different trend. This could mean that when the incoming horizontal velocity was oriented perpendicular to the roof ridge, the roof was under less suction. This is contradictory to the results shown in Section 4.1, where the peak pressure coefficients measured at the pressure taps on the top roof row were under the greatest suction out of all pressure taps on the house models. However, due to the averaging technique used in this section, the highly negative C_p values were being averaged with much lesser negative C_p values for the other rows of pressure taps, dampening the magnitude of the reported $C_{p\mathrm{avg}}$ values. This discrepancy between the C_p values and $C_{p\mathrm{avg}}$ values also implies that there was intensive pressure fluctuation around the ridge of the roof.

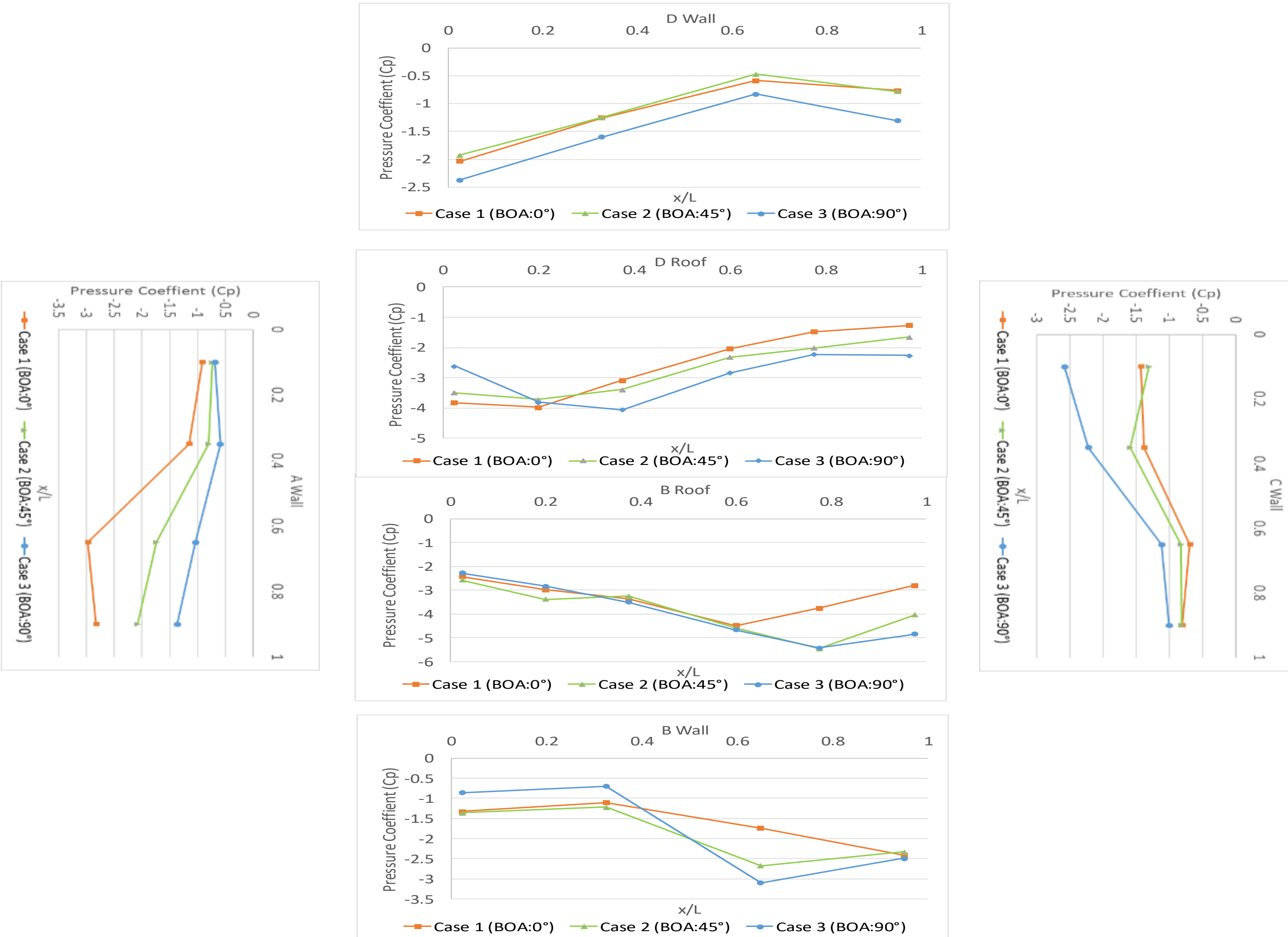

Figure 4.21: Three row average pressure coefficients, C_{pavg} for Model 3, Cases 1, 2, 3

For Roof B and Roof D of Model 3, as can be seen in Figure 4.21, there was very little difference in terms of trends and magnitudes of C_{pavg} values for all three cases. Moreover, the average suction is much smaller than for the Models 1 and 2. Also, no significant difference was noticed between the values measured for peak pressures coefficients, C_p, and the current averaged coefficients, C_{pavg}. Thus, it can be concluded that the higher roof pitch angle of Model 3 can decrease the pressure coefficient magnitude, while also reducing the pressure fluctuation on the roof, for all building orientations. For the walls of Model 3, it was noticed that the average pressure coefficients had opposite distributions on Wall A, Wall C, Wall D, and Wall B respectively. The suctions started from low values and increased to high values in the second halves of Wall A and Wall B and the opposite started from high values and decreased to lower magnitudes for Wall D and Wall C. This pattern was consistent with the C_{pavg} values' distributions determined for the other models and it was the main cause of inducing a torsion of the body of the tested building models.

4.3 Roof pitch angle and building geometry effect on tornado-induced average pressure coefficients

The same pressure averages of the bottom, middle, and top rows are compared in Figure 4.22 to Figure 4.24 for Model 1, Model 2, and Model 3 to visualize the effects of roof pitch angle and building geometry.

The C_{pavg} values' distribution along the walls was presented in detail in the previous section, Section 4.2. It can be mentioned that the opposite pressure distribution pattern was present for all tested cases. Thus, an imminent conclusion is that the walls of the models experienced torsion, regardless of the dimensions of the walls.

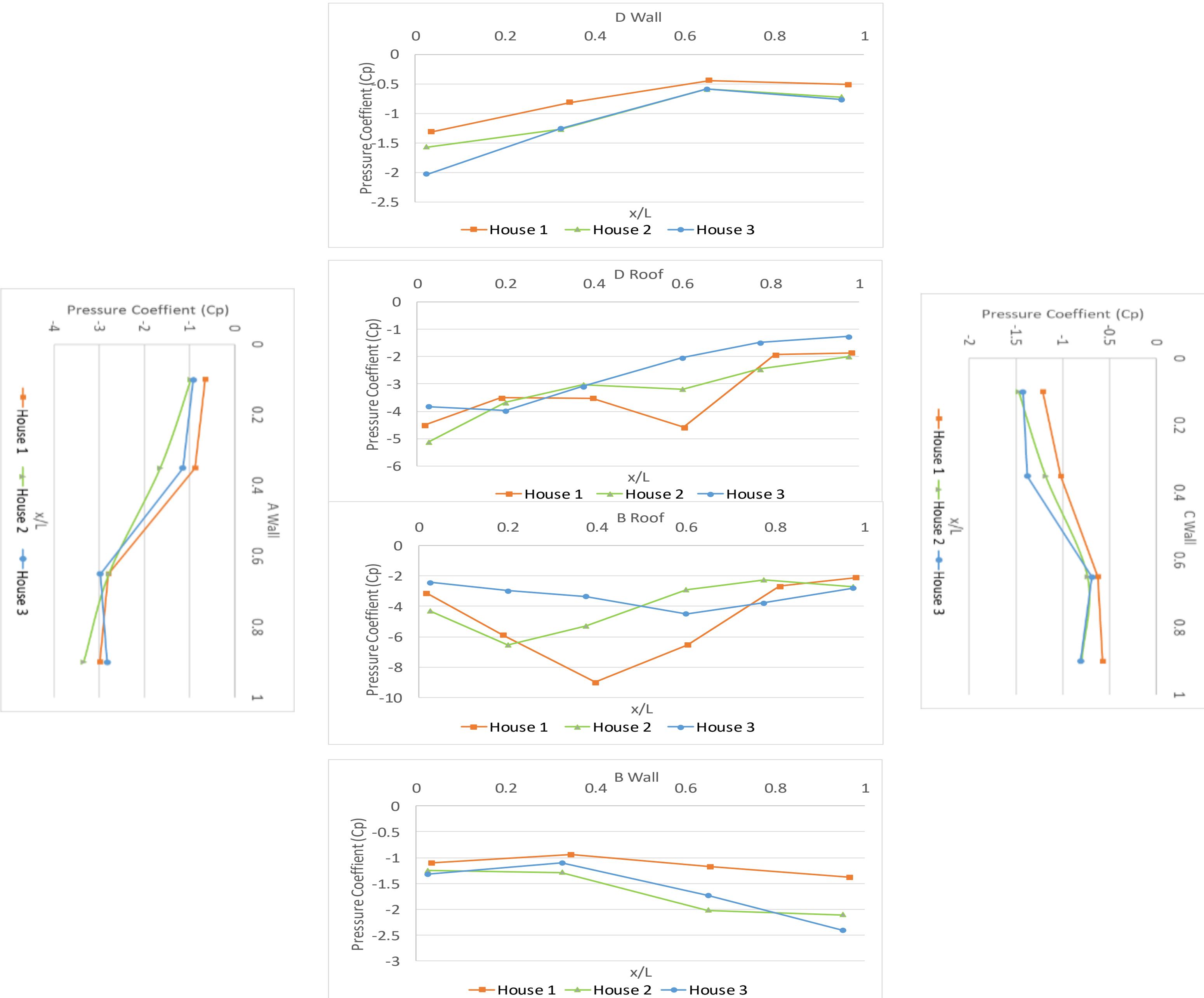

Figure 4.22: Three row average pressure coefficients, C_{pavg} for Model 1, 2, 3, Case 1 BOA: 0°

As seen in Figure 4.22, the windward Roof D, which was the nearest to the center of the vortex at 0 = x/L, had a higher suction than the side of the roof furthest from the center of the vortex. Moreover, at 0.4 = x/L of Model 1, there was an increase in suction at the center of the Roof D, which was much greater than the other two models. Model 3 with 36° roof pitch angle, was under the least suction for nearly all locations when compared to Model 1 and Model 2 that had 16° roof pitch angles. Therefore, lower sloped roof pitch angles produced an increased magnitude of negative pressures on the windward roof, and therefore, a stronger suction. The leeward Roof B was under greater suction than the central region of Roof D. The peak pressure near the center of the tornado was more than two times higher on the windward side than the leeward side for Model 1.

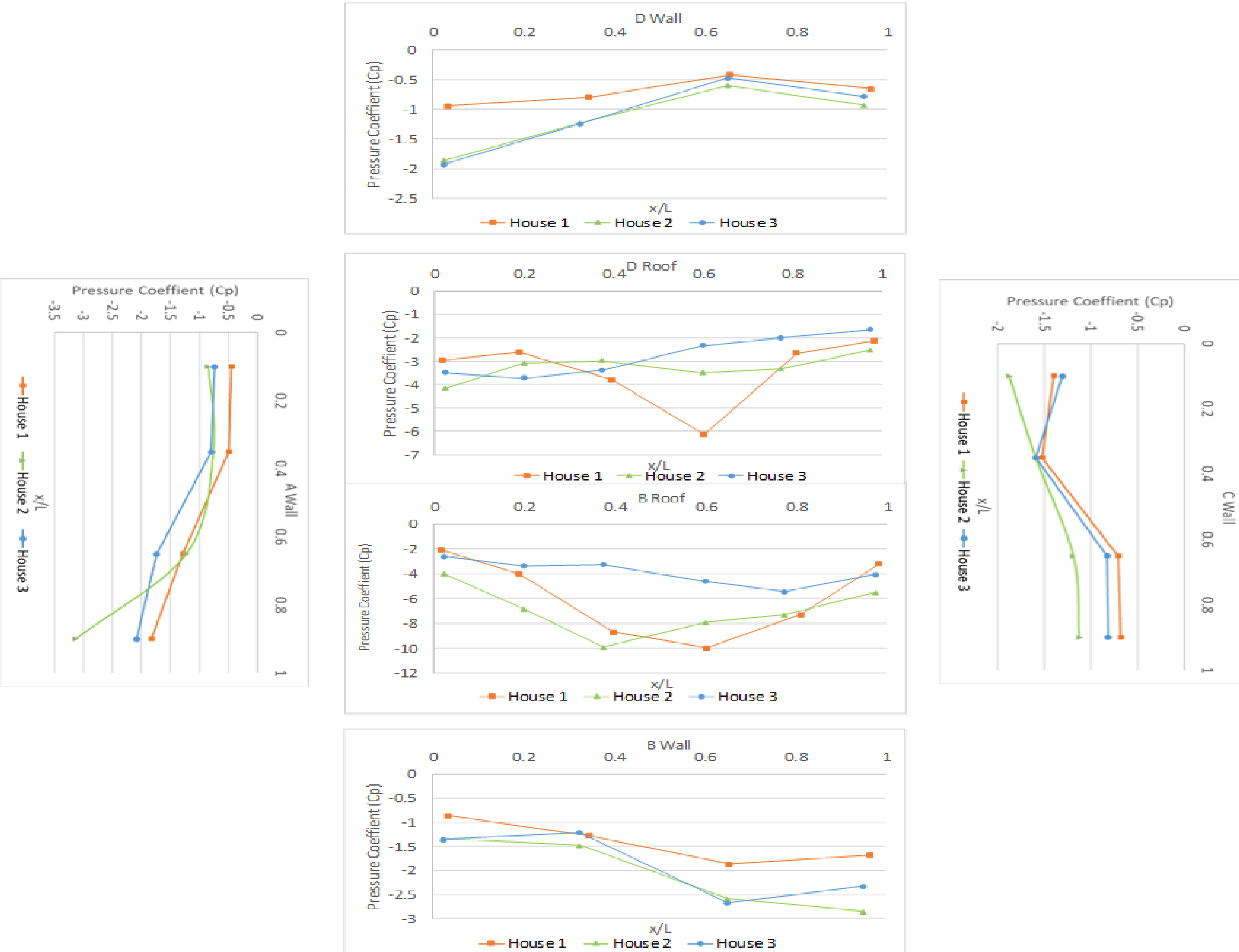

Figure 4.23: Three row average pressure coefficients, C_{pavg} for Model 1, 2, 3, Case 2 BOA: 45°

For the BOA = 45° (Figure 4.23), the highest C_{pavg} values on the windward Roof D shifted towards 0.6 = x/L for Model 1, away from the location where the wind initially hit the roof. Model 1 had the greatest magnitude of negative C_{pavg} values for Roof D. Both Model 1 and Model 2 had similar C_{pavg} plot values and trends on the leeward Roof B. This would be due to the same roof pitch angle of 16°. The central region of Roof B (Leeward) was under a greater negative pressure coefficient than the central region of Roof D (Windward). The highest C_{pavg} values located near the center of the roof were nearly two times on the windward side of the roof than on the leeward side of the roof. Model 3 with the 36° roof pitch angle had much lower C_{pavg} values, and therefore, less suction.

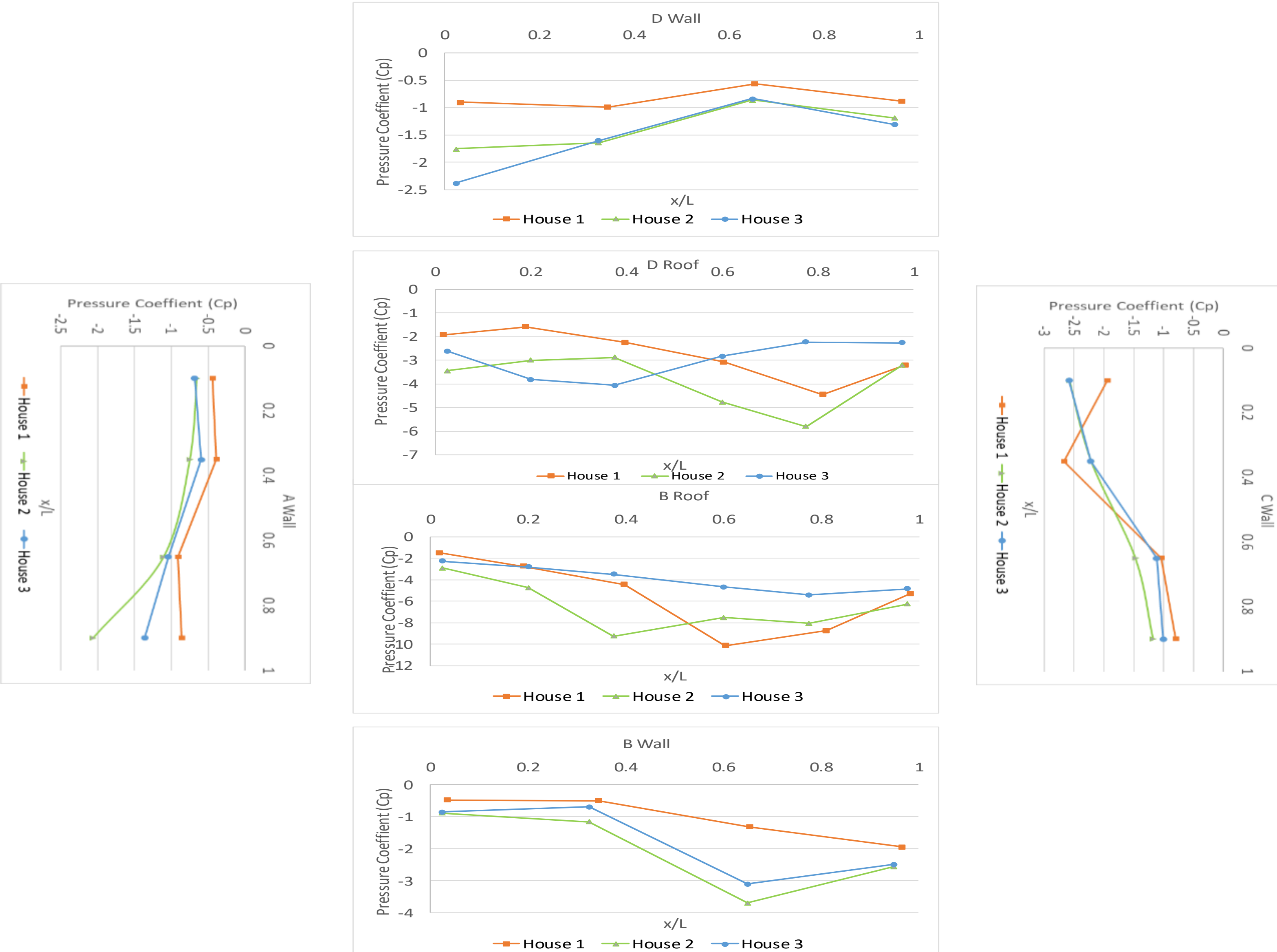

Figure 4.24: Three row average pressure coefficients, C_{pavg} for Model 1, 2, 3, Case 3 BOA: 90°

The C_{pavg} values for the BOA = 90° in Figure 4.24, where the flow was hitting perpendicular to the roof ridge. Roof D of Model 3, had a greater suction on the leading half of the roof from 0.2 = x/L to 0.4 = x/L compared to the other two models that had a lower roof pitch angle of 16°. Roof D of Model 3 had a greater suction between 0.2 = x/L and 0.4 = x/L compared to the other two models. This could be caused by the incoming wind, which was directly hitting the inner portion of Roof B towards the vortex, while the section of Roof D that was further away from the vortex was protected by the high ridge of the roof. This effect was not observed on Model 1 and Model 2, which had low roof pitch angles. When the incoming wind approached perpendicular to the ridge of the roof (BOA = 90°), the higher ridge could cause the flow to detach from the highest roof point, creating a separation bubble on the leading edge, when compared to the second trailing half of the roof. Therefore, additional testing would need to be performed to draw a conclusive statement.

Model 1 and Model 2, with 16° roof pitch angles, had two to three times greater negative C_{pavg}, values respectively after 0.4 = x/L. This could be due to the low roof pitch angle allowing for a flow separation zone to develop after 0.4 = x/L, leading to a high suction zone. Model 3, with the greater roof pitch angle of 36°, had a roof gable perpendicular to the flow. This might be preventing a separation bubble from developing on the roof causing the region between 0.4 = x/L and 1 = x/L of Roof B and Roof D to be under less suction than the other two models.

4.4 Tornado Duration Analysis

The stationary vortex peak pressure results of Model 2 Case 2 were investigated for different exposure time durations. The peak C_p values were extracted for different durations of exposing the model to the tornadic vortex in an attempt to clarify the effect of the tornado stagnation at one location. The procedure used to determine the peak pressure coefficient, C_p, for different durations is described in Chapter 3.6. Thus, the peak C_p values were plotted as a function of the tornado exposure duration as represented for Model 2 Case 2 in Figure 4.25 to Figure 4.42.

Moreover, the results are presented in zoning groups as recommended by the NBCC 2015. Figures 4.1.7.6-B, -E used for the design of secondary structural components and cladding, as well as NBCC 2015 Figure 4.1.7.6-A used for load Case A and Case B from the NBCC wind provisions, for primary structural actions arising from wind load acting simultaneously on all surfaces of low-rise buildings. Load Case A is for wind loads that are generally perpendicular to the roof ridge, while Case B is for wind loads generally parallel to the roof ridge. Since the horizontal velocity of Case 2 (BOA = 45°) is approaching the Model 2 diagonally to the roof ridge, a comparison with both NBCC 2015 load Case A and Case B was conducted. The peak C_p values from all the building orientations (360°) used for design are found in Figures 4.1.7.6-B, E of the NBCC 2015 for different zones. Figures 4.1.7.6 A, B, and E can be seen in Chapter 2.6 (Figure 2.14, Figure 2.15, and Figure 2.16).

The results for the peak pressure coefficients for each pressure tap were organised as per the zoning recommended in NBCC 2015 Figures 4.1.7.6-A and 4.1.7.6-B, -E and were reported in Figure 4.26 to Figure 4.31, for different durations. However, the NBCC 2015 graphs, 4.1.7.6-A, depict the external pressure multiplied with a gust coefficient: C_pC_g acting simultaneously on all surfaces of the house. Thus, the C_pC_g values already consider the effect of the directionality of the wind. In the current experiment, the gust, or the effect of wind directionality was not measured separately; however, the overall pressure recorded at the surface of the models was induced by the fluctuating tornadic vortex. Thus, the obtained pressure coefficients were considered to be directly comparable with the C_pC_g values denoted in NBCC 2015. To avoid confusion, only for this section, the peak pressure coefficients determined from the current experiment are denoted as C_T when compared with C_pC_g from NBCC 2015.

When comparing the external peak pressure coefficients for Figure 4.1.7.6-B, -E, which are for the design of cladding and secondary structural members, the C_pC_g is provided based on area-averaged C_pC_g, where the peak C_pC_g is given based on the minimum tributary area of the surface of that wall or roof. In Figure 4.1.7.6-B, -E, the C_pC_g value becomes less conservative when the tributary area increases. In this study, the tributary area was considered as 1 m^2 as this is the minimum area resulting in the most conservative pressure coefficients.

The concept of separating the stationary tornadoes' pressure data into duration segments, used initially by Haan et al. (2017), could serve to better understand the effects of the tornado duration on the induced peak pressures. It could also be used to compare the pressure coefficients exerted for different exposure durations to the NBCC 2015 criteria. If the results found using this method correlate well with results reported from translating tornado experiments, it could even be used to replicate a translating tornado with a stationary one in future experiments.

Figure 4.25 and Figure 4.26 below show the zonation recommended by NBCC 2015 for determining the wind pressure coefficients. Model 2, Case 2 was divided into similar zones and the E and W notations were added for Wall A, Wall B, Wall C, and Wall D to represent the respective zones stipulated in NBCC 2015 (Figure 4.25a), while for the roof notations Roof DC, DS, DR and BC, BS, BR were used (Figure 4.25b). When pressure coefficients were calculated on the E Zone, W Zone, C Zone, S Zone, and R Zone of Model 2, only the pressure taps from the designated zones were considered. Figure 4.26 to Figure 4.42 below represent the peak pressure coefficients for the different zones of Wall A, Wall B, Wall C, and Wall D as well as Roof B and Roof D

.

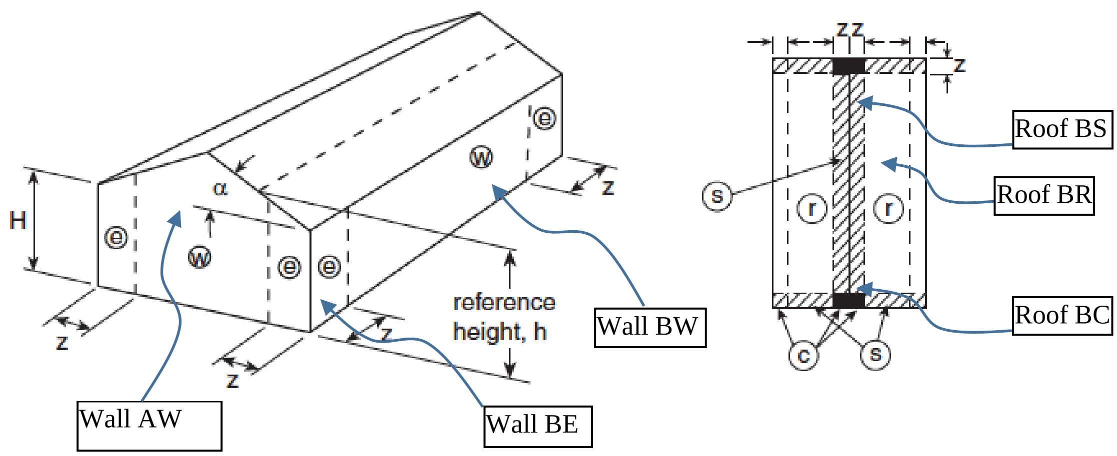

Figure 4.25: NBCC'15 zones for pressure coefficients on cladding and secondary structural members adapted for Model 2 Case 2 a) Walls zones (NBCC 2015 4.1.7.6-B), b) Roof zones (NBCC 2015 4.1.7.6 E)

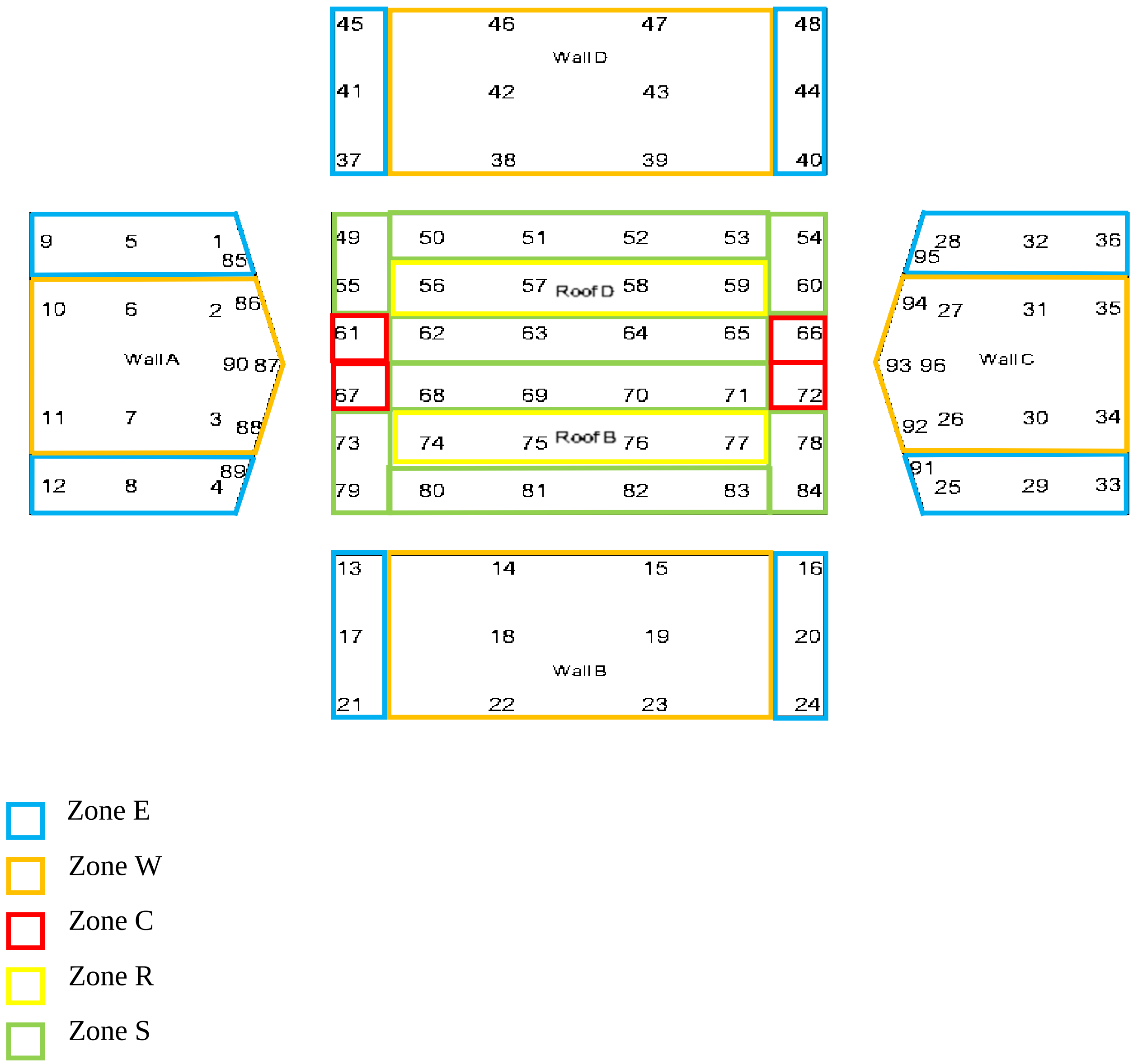

Figure 4.26: Pressure taps encompassed by the different NBCC'15 zones for pressure coefficients on cladding and secondary structural members (NBCC 2015 4.1.7.6-B-E)

The pressure tap numbers in Figure 4.27 to Figure 4.32 can be seen in Figure 4.27. The colour-coded legend as well as wall or roof letters can be used to determine where on the pressure tap was found on the models' surfaces.

For the Wall AE zone of Model 2, Case 2 (BOA = 45°, D = 10 cm) a total number of 8 pressure taps were identified and the peak pressure coefficients, C_T, were plotted in Figure 4.27a for the durations of tornado exposure between 0.1 s and 100 s. It was noticed that the C_T values decreased with the increase of exposure duration, thus inducing higher suction on the investigated surface. The pressure taps 1 to 4, located at the lower base of the Wall A, registered a lower decrease, while the other four pressure taps, which were located on the upper side of the Wall A and reaching the roof, had a more accentuated decrease.t A similar pattern was noticed for the Wall AW zone, where a total of 10 pressure taps were reported (Figure 4.27b). For the zone Wall BE (Figure 4.28a), where the incoming wind doesn't approach the corner, a similar behavior was noticed; however, a clear distinction appears between the upper pressure taps and lower pressure taps placed along the corner strips. For the inside region of the wall (zone Wall BW) the same pattern was noticed with peak pressure coefficients gradually decreasing with duration of tornado exposure, thus increasing the suction on the wall surface. When comparing Wall A and Wall B, the strongest suction, with a C_T value of up to -4.2, was noticed on the corner strip of Wall A (zone Wall AE), followed closely by the corner strip of Wall B (zone Wall BE), with C_T values of up to -3.2, then Wall BW, with C_T values of up to -3.1, and Wall AW, with C_T values of only -2.5.

For Roof B of the Model 2, Case 2, the same tendency of the magnitude of the peak pressure coefficients to gradually increase with an increase of exposure duration was noticed for all the three regions: corners (Roof BC in Figure 4.31a), edges (Roof BS in Figure 4.31b) and interior roof zone (Roof BR in Figure 4.31c). Only 4 pressure taps were identified for the corner zone Roof BC, for which the C_T value was lower for the leeward corner taps, when compared with the ones located on the windward corner (Figure 4.31a). Initially, consistent values were noticed for the 10 pressure taps located on the edges of the roof, zone Roof BS, but with the increase of tornado exposure duration, more discrepancy was noticed with pressure taps situated on the windward edge registering lowest C_T value of up to -12, while the ones located on the leeward edge had C_T values of up to -4.7. Along the ridge of the roof C_T values of up to -7 were recorded (Figure 4.31b). The inside zone of the roof, (zone of Roof BR), recorded a decrease of C_T values with the increase of the tornado exposure duration for each of the 4 pressure taps. However, the decrease accentuated the region near the windward edge, reaching a C_T value of up to -13.2, when compared with the leeward side of, which registered a C_T value of up to – 7.1 (Figure 4.31c). In general, for both the walls and roofs at smaller exposure durations, smaller suctions were recorded, which could lead to an underestimation of tornado-induced pressures and, only if the exposure period is increased, the suction on the roofs and walls will increase as well.

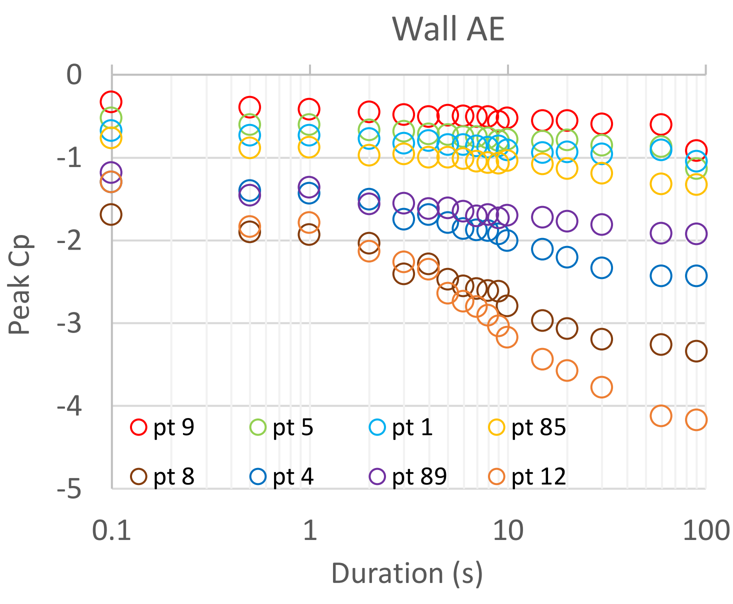

Figure 4.28: Peak pressure coefficients C_T for different durations on the Wall A for cladding and secondary structural members for zones a) AE and b) AW for Model 2, Case 2 (BOA:45°)

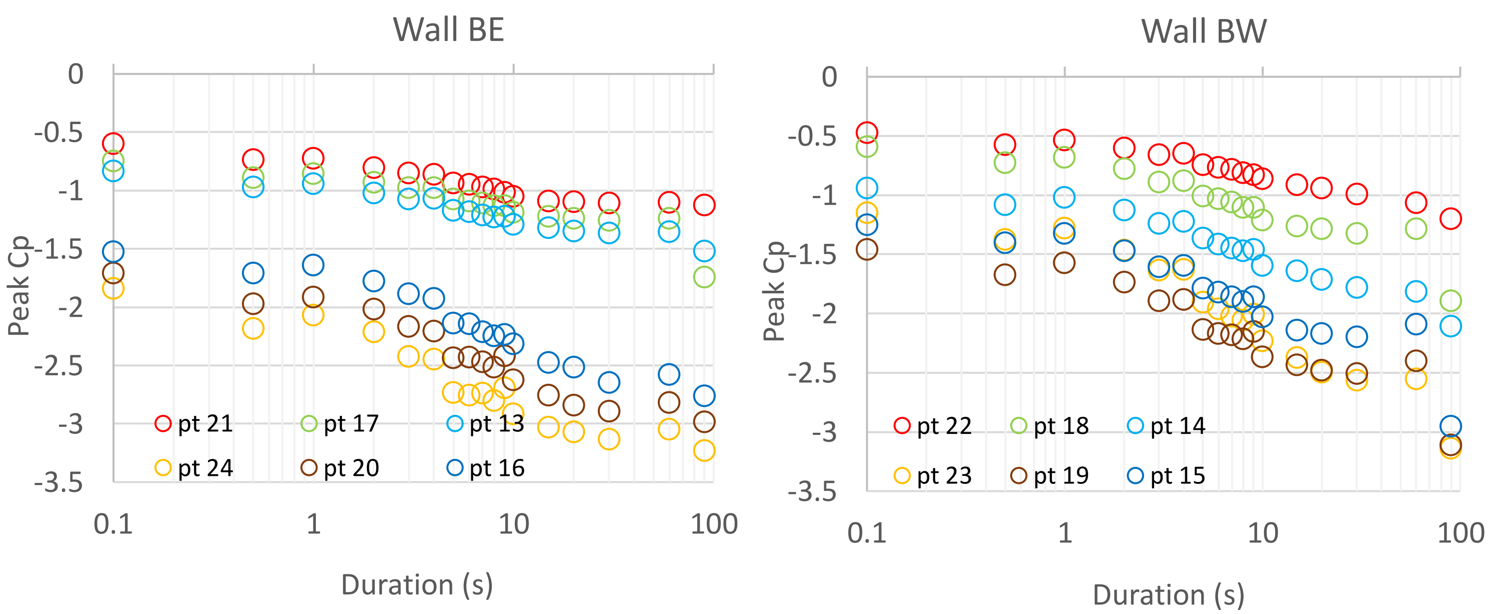

Figure 4.27: Peak pressure coefficients C_T for different durations on Wall B for cladding and secondary structural members for zones a) BE and b) BW for Model 2, Case 2 (BOA: 45°)

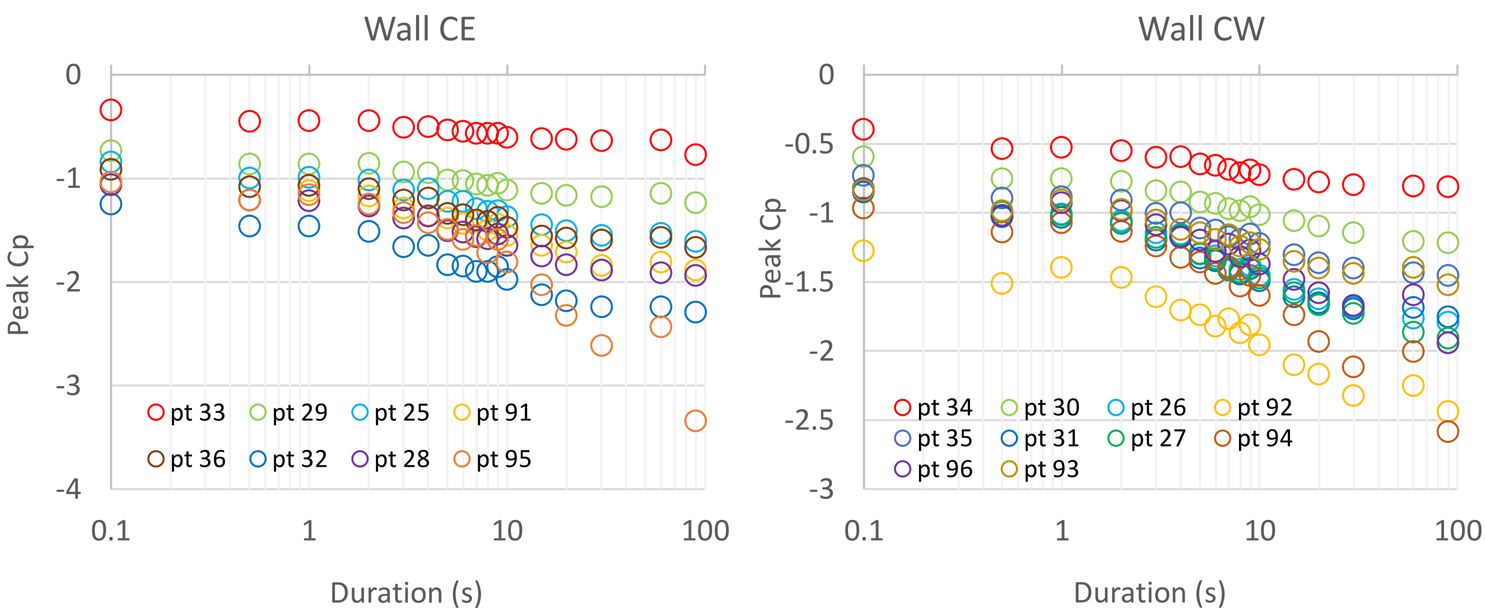

Figure 4.30: Peak pressure coefficients C_T for different durations on Wall C for cladding and secondary structural members for zones a) CE and b) CW for Model 2, Case 2 (BOA:45°)

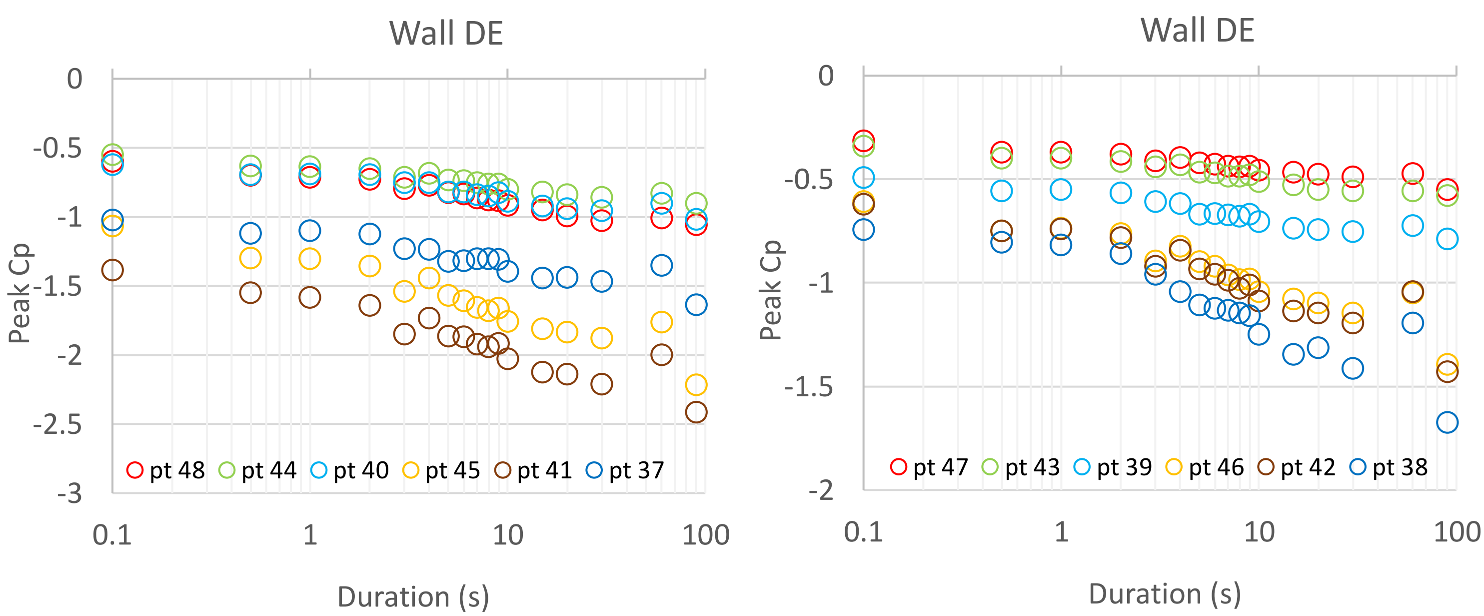

Figure 4.29: Peak pressure coefficients C_T for different durations on Wall D for cladding and secondary structural members for zones a) DE and b) DW for Model 2, Case 2 (BOA: 45°)

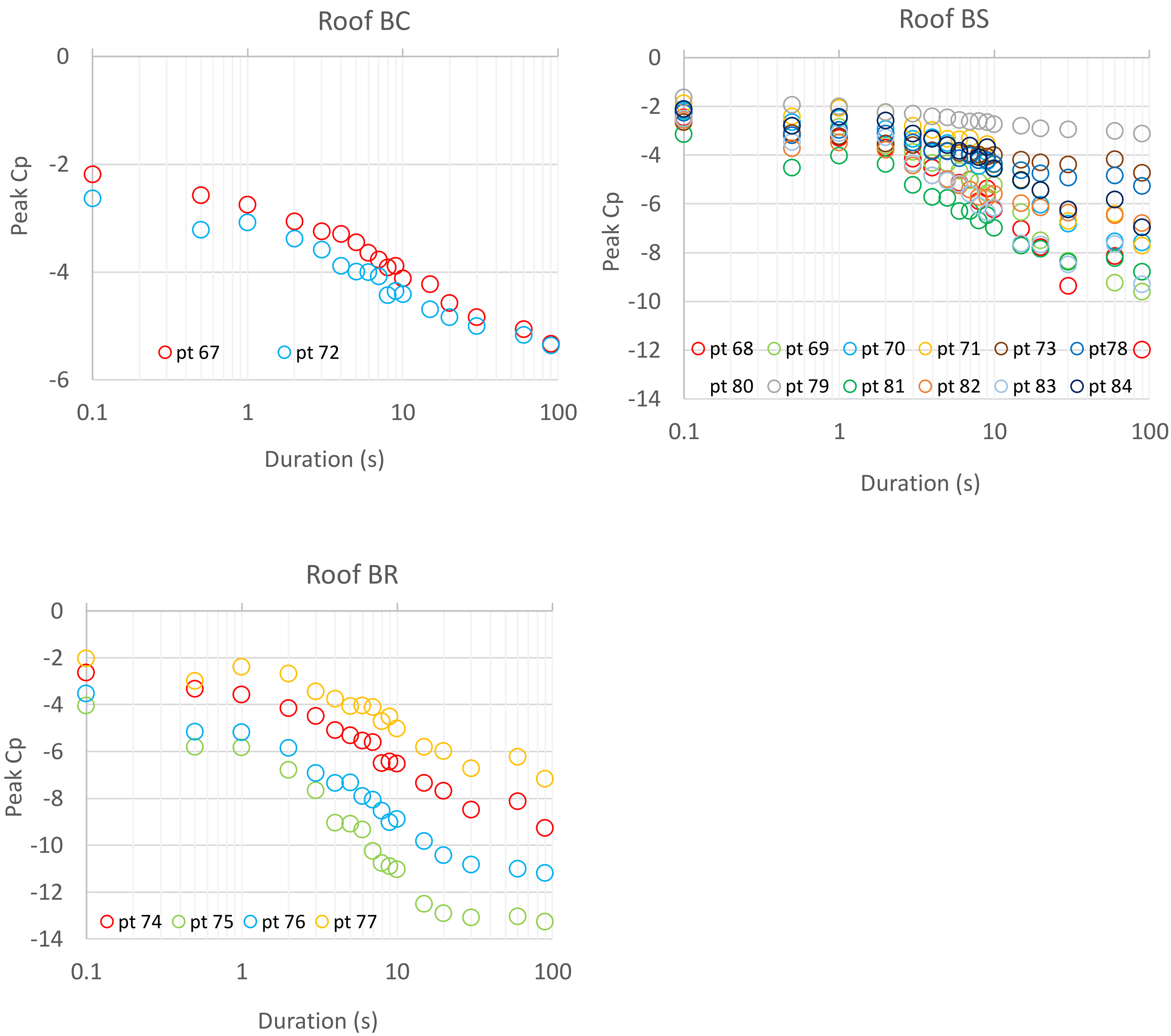

Figure 4.31: Peak pressure coefficients C_T for different durations on Roof B for structural components and cladding for single-span gabled roof for zones a) BC, b) BS and c) BR for Model 2, Case 2 (BOA: 45°)

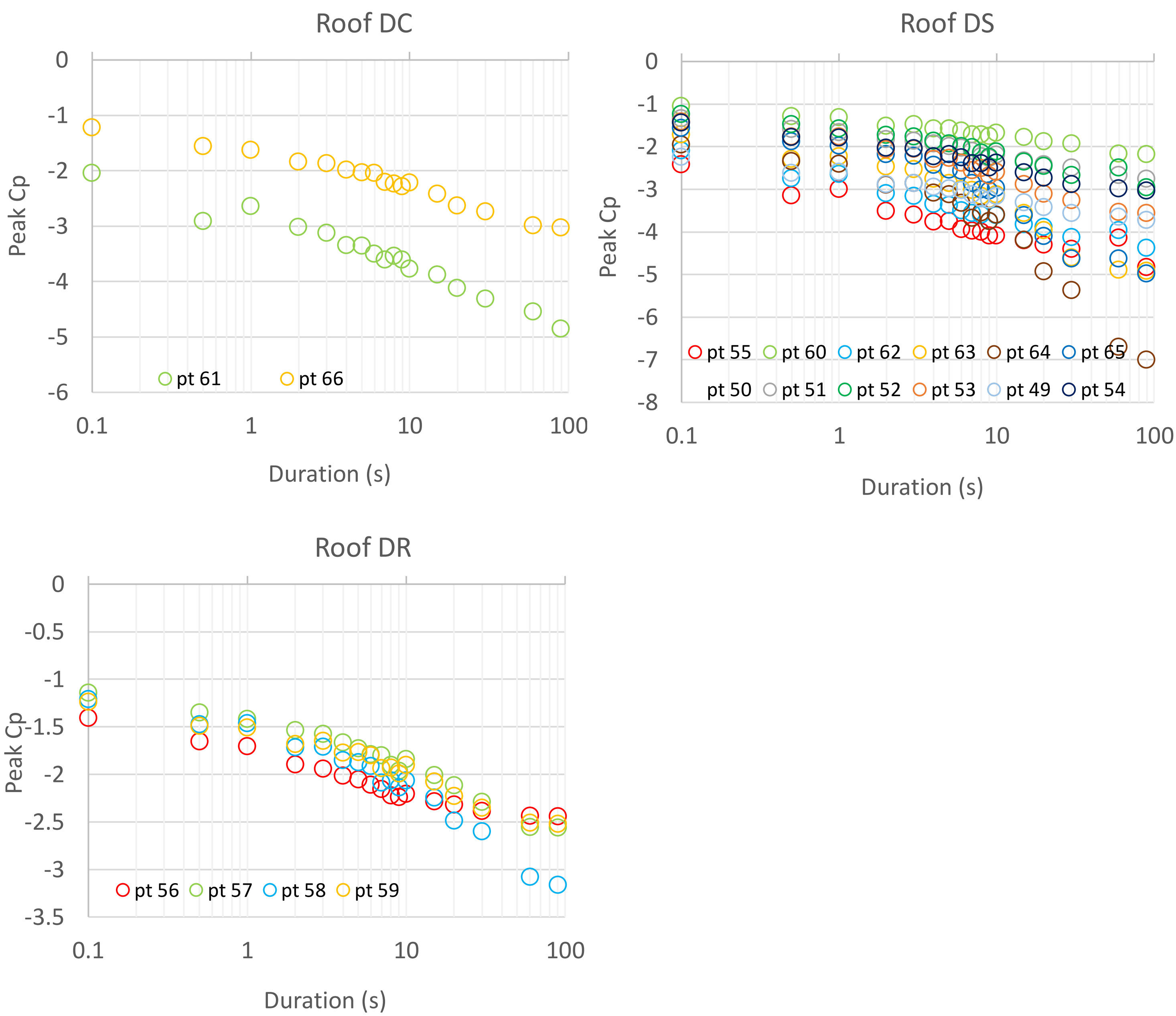

Figure 4.32: Figure 4.32: Peak pressure coefficients C_T for different durations on Roof B for structural components and cladding for single-span gabled roof for zones a) DC, b) DS and c) DR for Model 2, Case 2 (BOA: 45°)

The results obtained in the current experiment cannot be compared with the ones reported in similar studies (Haan et al., 2017, Case et al., 2011) due to different methods employed for delimiting the zones on the models. The Haan et al., (2017) study had a different approach in plotting their data, as well as the peak/median pressure coefficient values vs duration were reported, while in the current research the peak pressure coefficient, C_T, variation with the tornado exposure duration was plotted in Figure 4.27 to Figure 4.32. Reporting the peak pressures was preferred because the goal of this study is to find the C_T values for the pressure taps and organize them by zones, which can then be compared to the NBCC 2015 recommended C_pC_g values, as detailed in Chapter 5.

One of the main observations drawn from Figure 4.27 to Figure 4.32, is the large difference between the greatest magnitude of peak pressure coefficients, C_T, to the lowest ones in some of the graphs. Therefore, in Table 4.1, and Table B1 and Table B2 in the appendix, the ratio between the highest and lowest magnitude for the C_T values determined at each time step for each zone were reported. Although there are no other studies to compare these values with, these could be used as a baseline for future experiments. If the C_{Tmax} / C_{Tmin} magnitude is too large, it could signify that the zones in the NBCC 2015 are not adequate for tornadoes. A better zone configuration might be needed for residential buildings designed to withstand tornadoes. More experiments and research would need to be performed to prove and to make accurate conclusions regarding a new zonation which should include the tornadoes' effects on residential buildings.

Table 4.1: The ratio $C_{T\max} / C_{T\min}$ for Walls and Roofs zones as per NBCC 4.1.7.6-B, E, for Model 2, Case 2

	0.1s	0.5s	1s	2s	3s	4s	5s	6s	7s	8s	9s	10s	15s	20s	30s	3-pk Avg
AE	5.1	4.8	4.6	4.7	5.0	4.7	5.4	5.4	5.5	5.7	5.4	6.0	6.2	6.4	6.3	5.7
AW	4.5	4.6	4.2	4.3	4.2	4.1	4.3	4.3	4.3	4.3	4.0	4.3	4.1	4.3	4.1	3.8
BE	3.1	3.0	2.9	2.7	2.9	2.8	2.9	2.9	2.8	2.8	2.7	2.8	2.8	2.8	2.8	2.8
BW	3.1	2.9	2.9	2.9	2.9	2.9	2.9	2.8	2.8	2.7	2.6	2.7	2.7	2.6	2.6	2.5
CE	3.6	3.2	3.3	3.4	3.3	3.3	3.4	3.4	3.4	3.3	3.3	3.3	3.4	3.7	4.1	3.5
CW	3.2	2.8	2.6	2.7	2.7	2.9	2.7	2.8	2.6	2.6	2.6	2.7	2.8	2.8	2.9	2.9
DE	2.5	2.5	2.5	2.5	2.6	2.5	2.5	2.5	2.6	2.5	2.5	2.5	2.6	2.5	2.6	2.7
DW	2.3	2.2	2.2	2.3	2.3	2.6	2.6	2.6	2.6	2.6	2.6	2.7	2.9	2.8	2.9	2.7
DC	1.8	1.9	1.6	1.6	1.7	1.7	1.7	1.7	1.6	1.6	1.6	1.7	1.6	1.6	1.6	1.6
DS	2.3	2.4	2.3	2.3	2.4	2.4	2.4	2.4	2.3	2.3	2.3	2.4	2.4	2.6	2.8	2.6
DR	1.3	1.3	1.2	1.3	1.2	1.4	1.3	1.3	1.4	1.3	1.4	1.4	1.4	1.5	1.4	1.4
BC	1.6	1.6	1.5	1.5	1.6	1.6	1.6	1.6	1.6	1.7	1.6	1.7	1.8	1.9	2.1	2.1
BS	1.4	1.3	1.6	1.6	1.5	1.5	1.5	1.5	1.5	1.5	1.6	1.6	1.7	1.8	2.1	1.8
BR	2.0	1.9	2.4	2.5	2.2	2.4	2.2	2.3	2.5	2.4	2.4	2.5	2.7	2.8	2.8	2.8

In Table 4.1, it was noticed that Zone E and Zone W for the walls have higher C_{Tmax} / C_{Tmin} ratio, compared to Zone C, Zone S, and Zone R for the roof. The leading edge of the clockwise flow was under much greater suction than the trailing edge, which led to a large difference between the highest and lowest magnitudes for the peak pressure coefficients, C_T. Therefore, the C_{Tmax} / C_{Tmin} ratio was significantly higher for the wall zones ranging from 2.5 to 5.7, or zone Wall AE, where the corner strip is directly exposed to the incoming horizontal velocity (BOA = 45°), the ratio C_{Tmax} / C_{Tmin} increased with the exposure time, while all the other wall regions experienced a slight decrease for longer exposure times. The roof zones cover areas where the C_T values were more consistent to each other in spite of the much higher suction registered on the roof when compared to the walls. Therefore, the C_{Tmax} / C_{Tmin} ratio for the Roof Zone C, Zone S, and Zone R ranged from 1.4 to 2.6. This was likely due to the zones encompassing an area where the C_T values were similar throughout that area. Also, it was noticed that the roof corner zones (Roof DC and Roof BC) and edge zones (Roof DS and Roof BS) had a slightly lower C_{Tmax} / C_{Tmin} ratio, while the interior of the roof (Roof DR and Roof BR) had a higher difference between the maximum and minimum peak pressure coefficients. This might be caused by the shifting of the separation bubble which creates a stronger suction depicted in the contour plots above (Figure 4.9).

4.5 Comparison with other studies

The results obtained in the current experiment cannot be compared with the ones reported in similar studies (Haan et al., 2017, Case et al., 2011) due to the different methods employed for delimiting the zones on the models. The Haan et al., (2017) study had a different approach in plotting their data, as the peak/median pressure coefficient values vs duration were reported, while in the current research, the peak pressure coefficient, C_T, variation with the tornado exposure duration was plotted in Figure 4.27 to Figure 4.32. Reporting the peak pressures was preferred because the goal of this study was to find the C_T values for the pressure taps and organize them by zones that can be compared to the NBCC 2015 recommended C_pC_g values, as detailed in Chapter 5.

Sabareesh et al., (2012) performed a tornado experiment, as described in Chapter 2, although the model was a small cube with a flat roof; however, some common features can be compared to the models with a gable roof. This is a pertinent study to compare results with the ones obtained in the current WDS experiment because it was done with a stationary tornado that had a clockwise flow, such as the one simulated in the WDS. Although the tornado velocity, model locations, and model geometry were different from the one performed at the WDS, significant similarities can be found. In the Sabareesh et al., (2012) study, the walls that were perpendicular to the flow were under less suction than the walls that were parallel to the tangential/horizontal flow. This is similar to the phenomena identified in Section 4.1 of this thesis, where the discussion of building orientation on walls was completed. The C_{pmin} values found on the walls from the Sabareesh et al., (2012) experiment were a much greater magnitude than those obtained in the WDS facility. The C_p values on the walls from the Sabareesh et al., (2012) study ranged from -6 to -11, while those for the WDS experiments did not surpass a C_p value of -4.56 on the walls. This could be due to the use of a different tornado simulator and a different tornado, leading to different flows and different peak velocities. A significant similarity between the WDS experiment and the Sabareesh et al., (2012) experiment is that there are greater minimum C_p values on the leading edges to the clockwise flow than the trailing edge. This creates a torsional effect on the tested models. Although the top of the cube did not have a gable roof, thus no roof pitch angle, some similarities and differences were found between the experiment by Sabareesh et al., (2012) and the experiment of this thesis. In the Sabareesh et al., (2012) study, it was found that the greatest negative C_p values were found on the corners of the roof. This is different from the results obtained from the WDS experiment, where the greatest negative C_p values were found in the center of each roof section. This could be due to the addition of a sloped roof in the models tested in the WDS. For both studies, the roof was under greater suction than the walls.

A different study performed by Hu et al., (2011) also reported the effects of a simulated tornado on a residential model. However, they performed PIV testing that was coordinated with the pressure tap pressure readings over the same time period. This allowed viewing trends between the flows and the pressure readings. In the WDS experiment, it was noticed that the wall nearest to the vortex core was under greater suction. This was also seen in the Hu et al., (2011) study, and a larger suction on one side of the model's wall created an unbalance and caused a pulling of the building towards the center of the vortex. It was also mentioned that all surface pressures on the roof were negative, thus under suction. This coincides with the results obtained from the WDS experiments. Another significant comparison is the lack of positive pressure on the windward wall where the tangential wind velocity was hitting perpendicularly, where a positive pressure is seen where ABL winds hit a surface. This is due to the low pressure in the core region of the tornado. It was also found that a high-velocity region on the windward roof led to a large separation bubble that formed over the leeward roof. Both roofs would have high magnitudes of negative pressure, but the leeward roof was under greater suction.

One of the main observations drawn from Figure 4.27 to Figure 4.32, was the large difference between the greatest magnitude of peak pressure coefficients, C_T, to the lowest ones in some of the graphs. Therefore, in Table 4.1 to Table 4.3 the ratio between the highest and lowest magnitude for the C_T values determined at each time step for each zone were reported. Although there are no other studies to compare these values with, these could be used as a baseline for future experiments. If the C_{Tmax} / C_{Tmin} magnitude is too large, it could signify that the zones in the NBCC 2015 are not adequate for tornadoes. Ideally, the zones encompass a region where the pressure coefficients are similar throughout that roof zone. However, if the pressure coefficient variance is very large, and does not compare well to the NBCC wind provision *CpCg, it could* mean that the zones' geometries do not capture and consider the correct areas. As tornadoes are causing peak pressure coefficient magnitudes at different locations than ABL winds, a better zone configuration might be needed for residential buildings designed to withstand tornadoes. More experiments and research would need to be performed to prove and to make accurate conclusions regarding a new zonation, which should include the tornadoes effects on residential building.

4.6 Concluding remarks on tornado induced pressure coefficients

Based on the results and analysis on the effects of building orientation on pressure coefficients presented in section 4.2, a few observations were made based on the WDS experiments. Some of these have already been reported in other studies. Haan et al. (2010) found that building orientation affected the peak horizontal force coefficient, but not the peak vertical force coefficient. This was due to the pressure deficit phenomenon created by the uplift force in the center of the tornado vortex core. In Section 4.2, the plot trends of the peak pressure coefficient values on the roof differed when changing the building orientation angles; however, the peak C_p values on the roofs were very similar to each other. However, the results presented in Section 4.2 and Section 4.3 are the averages of the bottom, middle, and top row pressure taps. Thus, singular peak pressure coefficients at 1 single pressure tap cannot be reflected. For the contour plots introduced in Section 4.1, peak pressure coefficients, C_p**,** magnitudes are consistent along the surface of each roof. The peak values for different durations and the different sections of the walls and roof can be seen in Section 4.3.

When comparing Model 1 to Model 2, which have the same dimensions, but a different roof pitch angle, no significant effect was noticed on the trends and magnitudes of the pressure coefficient plots. The peak suction on each wall was found on the leading edge facing the clockwise flow. Also, it was noticed that the wall facing the vortex's core had the greatest suction. The bottom row of pressure taps on the trailing corner of the wall nearest the vortex's core usually had the greatest suction out of all the four walls.

The highest suction on the roof of the models was usually on the top row of pressure taps located near the roof ridge (peak negative pressure coefficient).

- For Model 1, peak suction was on the top row for Roof B and Roof D for all cases.
- For Model 2, the top row was under greater pressure on roof D for all cases, while the middle row was under greater suction on Roof B for two of the three cases.
- For Model 3: Roof D peak suction varied from row to row depending on the case, while Roof B had the greatest suction for two of the three cases.

-After a peak suction on the roof, the suction significantly decreased until the roof edge.

-Edges of the roof on the leading and trailing edge were under much less suction than the rest of the roof.

-For the case with a building orientation angle of 45°, the leading corner pressure tap (bottom row) was under greater suction than the other rows of pressure taps on the roof.

-The leeward roof was under greater suction than the windward roof.

-Building orientation angle did not have a significant effect on trends and magnitudes of pressure coefficients.

-Model 1 and Model 2 with the 16° roof pitch angle experienced greater suctions than Model 3 with the 36° roof pitch angle.

Chapter 5 Design Code Interpretation

5.1 NBCC 2015 Comparison and Analysis

One of the goals of this study is to compare the peak pressure coefficient, C_T, obtained experimentally, to the minimum C_pC_g values stipulated in NBCC 2015. This will help determine if the NBCC 2015 recommended design criteria is suitable or not to withstand tornado-induced pressures. A general conclusion on the applicability of NBCC 2015 for tornado prone areas is not sought because this is not a full analysis since the experiments performed did not consider enough building orientation angles and locations along the radius of the vortex. However, this research could be used as a stepping-stone for future studies on comparing pressures caused by tornadic winds with various design codes criteria. The C_T coefficients presented in Table 5.1 to Table 5.21 represent the peak pressure coefficients for each zone and for tornado exposure durations between 0.1 s to 30 s. The peaks were taken from the data found in Figure 4.26 to Figure 4.31 in Section 4.4 and in Figure B.1 to Figure B.10 in Appendix B. The *3pk-Avg* column corresponds to the average of the peak pressure of the three trial runs for each case. These are the C_p values presented in Figure 4.1 to Figure 4.18 in Section 4.1. The results presented in the current chapter does not compare directly to the graphs in Section 4.2 to Section 4.3, as the pressure coefficient data is the average for the bottom, middle and top row of data. This averaging leads to an attenuation of the data which does not reflect the peak pressure coefficient in each zone.In the tables below the green cells represent C_T values that do not exceed the NBCC 2015 minimum C_pC_g values, orange cells were assigned for the C_T values that exceed the NBCC minimum C_pC_g values by 0% to 20%, while the red cells are used for the C_T values exceeding the NBCC 2015 minimum C_pC_g values by more than 20%. The Figure 5.1 to Figure 5.9 are for Zone W, Zone E, Zone C, Zone S, and Zone R that correspond to NBCC 2015 Figure 4.1.7.6 -B, -E, for cladding and secondary structural members. The last column represents the minimum C_pC_g values determined from the NBCC 2015 Figure 4.1.7.6-B, -E, and -A from the NBCC 2015 (Figure 2.14 and Figure 2.15 from Section 2.6 in Chapter 2) for the corresponding zone and house geometry. A direct comparison between the results currently obtained for the scaled model, and the ones recommended by NBCC 2015 is possible because both the non-dimensional wind-induced pressure coefficients were used. Figure 5.10 to Figure 5.21 are for the zones that correspond to NBCC 2015 Figures 4.1.7.6-A for load case A and B, for primary structural members from the NBCC 2015 (Figure 2.16 from Section 2.6 in Chapter 2). The values in Zone 1 and Zone 1E of load case A and Zone 5 and Zone 5E of load case B have been crossed out because the NBCC 2015 recommended pressure coefficients are positive values and the pressures obtained experimentally were only negative.

5.2 Wall pressure coefficients comparison as per 4.1.7.6-B, E cladding and secondary structural elements

Model 1, which had a rectangular house footprint and greater wall areas than the other two models, had fewer zones that exceed the NBCC 2015 C_pC_g values compared to Model 2 and Model 3, which had a square house footprint and smaller roof and wall areas. For all three orientations of Model 1, as it can be noticed in Table 5.1 to Table 5.3, zone Wall DE and Wall DW, which correspond to the edge of the wall leeward from the incoming tangential wind flow and the edge of the leeward edge of the roof respectively, are the only zones that did not exceed the NBCC 2015 recommended values for all the exposure durations investigated (0.1 s – 30 s). The C_T values exceeded the C_pC_g values of the NBCC 2015 for all the other zones in at least one of the three orientation angles. Also, for all Model 1 cases, the *3pk-Avg* C_p value, which is very close to the 30 s value, is the second most negative C_T value. Interestingly, even the two most extreme C_T values do not exceed the C_pC_g from the NBCC 2015 for some zones such as Zone BE, Zone BW, Zone CE, Zone CE, Zone DE and Zone DW. Zones where the C_T values exceed the NBCC 2015 recommended C_pC_g values changed depending on the building orientation case. This shows that orientation angle could affect the magnitude of the C_T values as well as the zones of high suction. This is a significant finding because in Section 4.2 of Chapter 4 it was shown that the building orientation did not have a significant effect on the pressure coefficient trends, but the results derived from the duration analysis show that this could affect the magnitude of the pressure coefficient. It can also be seen that for some smaller tornado exposure durations, C_T values did not exceed the NBCC 2015 criteria, however the 3-peak average and the 30 s values of the C_T values exceeded the NBCC 2015 recommendations. For the walls of Model 1, the pressure coefficient did not exceed those of the NBCC 2015 for most of the exposure durations and cases, and for the few cases where these were greater, C_T values did not exceed the NBCC 2015 values by a large factor. Both Model 2 and Model 3 (Table 5.4 to Table 5.6, and Table 5.7 to Table 5.9, respectively) had similar zones that exceed the C_pC_g of the NBCC 2015 due to the similar wall dimensions. For all building orientations of both models, there were more wall zone cases for which C_T values exceeded the C_pC_g of the NBCC 2015. It seems that the pressure coefficient for these scenarios was consistently high, which could signify that a building code which groups these different building geometries under the same recommendations, would not be conservative enough to withstand the tornado that was produced for the current experiment. Most of the walls were exceeding the C_pC_g values recommended by NBCC 2015, for at least one or all orientation angles. The only wall that did not exceed the C_pC_g value limitations was Wall D for both Zone E and Zone W. This is most likely due to being the furthest away from the tornado core, facing the leeward side of the incoming tangential velocity. Thus, the wind flows were creating fewer negative pressures on its surface. However, since the C_pC_g value is determined for the worst-case scenarios in NBCC 2015, many more building orientations would have to be experimentally investigated to determine if the NBCC 2015 building code recommendations are adequate for tornado resistance design.

For all the tested models, the C_T values for Zone E and Zone W on the walls often do not exceed by a large factor compared to the NBCC 2015 minimum values. Out of the C_T values of the 3-peak average, for the three models at BOA = 0°, BOA = 45°, and BOA = 90°, the greatest exceedance factor on the walls was 2.1 for Zone E and 2.38 for Zone W. Moreover, if the exposure durations are reduced from 30 s, then this factor will also decrease.

Table 5.1: Pressure coefficients comparison for Model 1, Case 1 and NBCC 2015

	0.1s	0.5s	1s	2s	3s	4s	5s	6s	7s	8s	9s	10s	15s	20s	30s	3pk-Av	CpCg
AE	-2.24	-2.90	-2.98	-3.11	-3.49	-3.59	-3.66	-3.69	-3.93	-3.77	-4.06	-4.17	-4.38	-4.42	-4.51	-4.56	-2.1
AW	-1.37	-1.60	-1.65	-1.73	-1.90	-2.01	-1.93	-2.01	-2.21	-2.11	-2.20	-2.39	-2.54	-2.77	-3.04	-2.92	-1.8
BE	-1.04	-1.14	-1.16	-1.23	-1.23	-1.31	-1.34	-1.37	-1.35	-1.46	-1.42	-1.44	-1.51	-1.61	-1.67	-1.64	-2.1
BW	-0.89	-1.01	-1.01	-1.06	-1.14	-1.17	-1.21	-1.20	-1.22	-1.25	-1.28	-1.29	-1.32	-1.34	-1.36	-1.38	-1.8
CE	-0.69	-0.82	-0.78	-0.92	-0.91	-1.00	-1.02	-1.07	-1.04	-1.12	-1.09	-1.09	-1.20	-1.28	-1.46	-1.56	-2.1
CW	-0.64	-0.72	-0.72	-0.79	-0.81	-0.86	-0.93	-0.91	-0.96	-0.97	-1.01	-1.02	-1.11	-1.16	-1.26	-1.23	-1.8
DE	-1.24	-1.50	-1.51	-1.55	-1.64	-1.66	-1.71	-1.73	-1.74	-1.75	-1.81	-1.83	-1.88	-1.95	-2.05	-1.99	-2.1
DW	-0.74	-0.86	-0.84	-0.89	-0.93	-0.95	-0.96	-0.98	-0.99	-1.01	-1.01	-1.03	-1.06	-1.07	-1.09	-1.10	-1.8
DC	-1.61	-1.93	-2.20	-2.29	-2.37	-2.52	-2.51	-2.55	-2.65	-2.75	-2.82	-2.82	-3.07	-3.15	-3.22	-3.53	-5.0
DS	-2.95	-2.57	-3.05	-3.13	-3.34	-3.64	-3.81	-3.91	-4.07	-4.25	-4.24	-4.43	-4.81	-5.53	-6.53	-7.15	-3.6
DR	-1.43	-1.73	-1.80	-1.89	-2.00	-2.10	-2.14	-2.10	-2.21	-2.36	-2.31	-2.30	-2.48	-2.81	-3.16	-3.26	-2.4
BC	-1.83	-2.11	-2.07	-2.26	-2.38	-2.44	-2.59	-2.67	-2.80	-2.79	-2.79	-2.87	-3.08	-3.15	-3.22	-3.36	-5.0
BS	-3.27	-5.23	-5.79	-6.78	-7.62	-8.76	-9.92	-9.27	-10.41	-10.51	-11.03	-11.43	-12.25	-12.28	-12.42	-12.56	-3.6
BR	-2.32	-3.57	-3.95	-4.69	-5.55	-6.35	-6.77	-6.35	-7.88	-7.40	-8.28	-8.56	-9.66	-10.32	-10.65	-11.03	-2.4

Table 5.2: Pressure coefficients comparison for Model 1, Case 2 and NBCC 2015

	0.1s	0.5s	1s	2s	3s	4s	5s	6s	7s	8s	9s	10s	15s	20s	30s	3pk-Av	CpCg
AE	-1.16	-1.40	-1.50	-1.61	-1.61	-1.93	-2.12	-2.04	-2.28	-2.33	-2.30	-2.43	-2.63	-2.86	-2.97	-2.89	-2.1
AW	-0.88	-1.04	-1.08	-1.12	-1.19	-1.32	-1.35	-1.38	-1.40	-1.42	-1.44	-1.48	-1.53	-1.55	-1.56	-1.59	-1.8
BE	-1.02	-1.25	-1.20	-1.35	-1.52	-1.44	-1.51	-1.56	-1.54	-1.62	-1.66	-1.63	-1.83	-1.97	-1.97	-2.07	-2.1
BW	-1.05	-1.21	-1.28	-1.38	-1.48	-1.59	-1.70	-1.74	-1.71	-1.82	-1.80	-1.85	-1.89	-1.95	-2.02	-1.99	-1.8
CE	-0.78	-0.89	-0.89	-0.95	-1.00	-1.04	-1.03	-1.11	-1.09	-1.14	-1.19	-1.31	-1.46	-1.68	-1.73	-1.66	-2.1
CW	-0.85	-1.00	-0.99	-1.10	-1.13	-1.21	-1.22	-1.30	-1.30	-1.32	-1.40	-1.49	-1.61	-1.72	-1.76	-1.73	-1.8
DE	-0.73	-0.92	-0.94	-1.04	-1.08	-1.12	-1.18	-1.20	-1.25	-1.29	-1.28	-1.31	-1.36	-1.38	-1.41	-1.41	-2.1
DW	-0.56	-0.68	-0.65	-0.71	-0.75	-0.78	-0.76	-0.78	-0.79	-0.80	-0.81	-0.82	-0.85	-0.89	-0.91	-0.90	-1.8
DC	-1.73	-2.31	-2.34	-2.57	-2.90	-3.34	-3.40	-3.57	-3.57	-3.68	-3.73	-3.90	-4.09	-4.11	-4.17	-4.34	-5.0
DS	-2.12	-3.15	-3.09	-3.71	-4.27	-4.80	-5.33	-5.66	-5.81	-6.14	-5.93	-6.30	-7.04	-8.89	-10.12	-11.24	-3.6
DR	-1.61	-1.98	-1.95	-2.12	-2.19	-2.39	-2.50	-2.60	-2.67	-2.68	-2.70	-2.70	-2.82	-3.20	-3.44	-4.37	-2.4
BC	-1.70	-2.01	-2.02	-2.23	-2.31	-2.37	-2.54	-2.61	-2.64	-2.72	-2.81	-2.70	-2.97	-3.18	-3.27	-3.32	-5.0
BS	-3.57	-5.96	-6.07	-7.45	-8.05	-8.87	-9.47	-10.14	-10.69	-11.45	-11.45	-12.20	-12.97	-13.23	-14.34	-14.14	-3.6
BR	-2.83	-4.48	-4.40	-6.26	-7.18	-7.32	-8.03	-8.78	-8.81	-8.98	-9.11	-10.03	-10.94	-11.33	-11.61	-10.99	-2.4

Table 5.3: Pressure coefficients comparison for Model 1, Case 3 and NBCC 2015

	0.1s	0.5s	1s	2s	3s	4s	5s	6s	7s	8s	9s	10s	15s	20s	30s	3pk-Av	CpCg
AE	-0.53	-0.60	-0.62	-0.64	-0.67	-0.72	-0.74	-0.75	-0.75	-0.75	-0.77	-0.78	-0.85	-0.92	-0.95	-0.93	-2.1
AW	-0.49	-0.57	-0.59	-0.62	-0.65	-0.76	-0.75	-0.75	-0.82	-0.82	-0.81	-0.84	-0.91	-0.98	-1.02	-0.99	-1.8
BE	-1.18	-1.42	-1.61	-1.59	-1.85	-1.81	-1.88	-1.99	-2.01	-2.06	-2.18	-2.16	-2.48	-2.60	-2.84	-2.90	-2.1
BW	-0.87	-0.95	-0.99	-1.01	-1.07	-1.09	-1.12	-1.14	-1.16	-1.18	-1.20	-1.19	-1.36	-1.32	-1.47	-1.44	-1.8
CE	-1.12	-1.40	-1.38	-1.47	-1.53	-1.65	-1.72	-1.72	-1.79	-1.87	-1.88	-1.92	-2.09	-2.11	-2.29	-2.20	-2.1
CW	-1.44	-1.77	-1.80	-1.90	-2.05	-2.20	-2.27	-2.31	-2.39	-2.50	-2.50	-2.56	-2.77	-2.81	-3.09	-2.98	-1.8
DE	-0.56	-0.67	-0.66	-0.73	-0.73	-0.85	-0.87	-0.90	-0.95	-0.93	-0.94	-0.94	-1.06	-1.11	-1.17	-1.30	-2.1
DW	-0.57	-0.67	-0.66	-0.70	-0.73	-0.81	-0.79	-0.80	-0.85	-0.86	-0.88	-0.89	-0.94	-1.01	-1.07	-1.10	-1.8
DC	-1.61	-2.18	-2.25	-2.58	-2.66	-2.82	-2.92	-2.99	-3.20	-3.13	-3.31	-3.52	-3.57	-3.75	-3.98	-4.02	-5.0
DS	-2.67	-3.72	-3.68	-4.54	-4.68	-5.16	-5.09	-5.30	-5.74	-5.61	-5.76	-6.21	-6.36	-6.87	-7.06	-6.78	-3.6
DR	-1.74	-2.30	-2.13	-2.50	-2.74	-2.83	-2.90	-3.13	-3.32	-3.34	-3.74	-3.57	-4.36	-4.54	-4.72	-5.43	-2.4
BC	-2.44	-2.94	-3.03	-3.25	-3.63	-3.78	-3.97	-3.97	-4.19	-4.35	-4.37	-4.53	-4.76	-4.96	-5.25	-5.13	-5.0
BS	-3.47	-6.04	-5.46	-6.55	-7.46	-8.25	-9.13	-9.38	-10.20	-10.56	-9.91	-10.98	-12.33	-12.91	-13.60	-13.49	-3.6
BR	-2.60	-4.18	-3.85	-4.39	-4.85	-5.87	-6.12	-6.42	-6.64	-7.20	-6.86	-7.15	-8.72	-9.78	-10.37	-10.42	-2.4

Table 5.4: Pressure coefficients comparison for Model 2, Case 1 and NBCC 2015

	0.1s	0.5s	1s	2s	3s	4s	5s	6s	7s	8s	9s	10s	15s	20s	30s	3pk-Av	CpCg
AE	-2.34	-2.89	-2.66	-3.11	-3.40	-3.64	-3.79	-3.85	-3.85	-3.96	-4.01	-4.11	-4.22	-4.40	-4.47	-4.42	-2.1
AW	-1.75	-2.00	-2.08	-2.26	-2.52	-2.55	-2.71	-2.72	-2.77	-2.77	-2.82	-2.91	-3.07	-3.11	-3.19	-3.17	-1.8
BE	-1.43	-1.78	-1.58	-1.80	-1.95	-1.88	-2.01	-2.06	-2.11	-2.20	-2.22	-2.26	-2.37	-2.48	-2.59	-2.50	-2.1
BW	-1.30	-1.60	-1.42	-1.63	-1.76	-1.71	-1.80	-1.88	-1.92	-2.03	-2.00	-2.03	-2.17	-2.29	-2.44	-2.38	-1.8
CE	-0.93	-1.19	-1.12	-1.15	-1.28	-1.25	-1.37	-1.42	-1.45	-1.52	-1.53	-1.53	-1.64	-1.73	-1.87	-1.77	-2.1
CW	-0.63	-0.74	-0.78	-0.86	-0.90	-0.95	-0.97	-1.00	-1.05	-0.99	-1.10	-1.08	-1.14	-1.18	-1.21	-1.23	-1.8
DE	-1.07	-1.30	-1.27	-1.29	-1.42	-1.48	-1.57	-1.57	-1.58	-1.64	-1.66	-1.68	-1.73	-1.77	-1.81	-1.78	-2.1
DW	-0.79	-0.90	-0.85	-0.96	-1.04	-1.05	-1.12	-1.15	-1.19	-1.20	-1.23	-1.20	-1.27	-1.33	-1.42	-1.38	-1.8
DC	-3.29	-3.89	-3.82	-4.23	-4.68	-4.60	-5.06	-4.98	-4.99	-5.02	-5.16	-5.27	-5.53	-5.62	-5.83	-5.43	-5.0
DS	-3.43	-3.96	-4.13	-4.47	-4.87	-4.90	-5.21	-5.23	-5.28	-5.22	-5.53	-5.63	-5.80	-5.94	-6.13	-6.08	-3.6
DR	-1.27	-1.54	-1.71	-1.78	-2.08	-2.14	-2.36	-2.37	-2.41	-2.47	-2.53	-2.52	-2.76	-2.83	-3.05	-3.02	-2.4
BC	-2.98	-3.53	-3.73	-4.11	-4.25	-4.42	-4.56	-4.62	-4.67	-4.68	-4.82	-4.90	-5.06	-5.17	-5.23	-5.24	-5.0
BS	-3.20	-4.08	-4.07	-4.66	-5.24	-5.33	-5.48	-5.92	-6.02	-6.07	-6.49	-7.05	-7.10	-7.95	-9.48	-6.62	-3.6
BR	-2.30	-3.07	-3.07	-3.50	-3.89	-4.11	-4.36	-4.48	-4.56	-4.67	-4.93	-5.34	-5.88	-6.33	-6.87	-8.65	-2.4

Table 5.5: Pressure coefficients comparison for Model 2, Case 2 and NBCC 2015

	0.1s	0.5s	1s	2s	3s	4s	5s	6s	7s	8s	9s	10s	15s	20s	30s	3pk-Av	CpCg
AE	-1.69	-1.90	-1.94	-2.14	-2.41	-2.35	-2.64	-2.74	-2.81	-2.91	-3.04	-3.18	-3.44	-3.57	-3.77	-3.94	-2.1
AW	-1.29	-1.58	-1.48	-1.67	-1.71	-1.79	-1.78	-1.88	-1.91	-1.89	-1.94	-1.93	-1.96	-2.02	-2.04	-2.11	-1.8
BE	-1.84	-2.18	-2.07	-2.21	-2.42	-2.45	-2.73	-2.76	-2.74	-2.80	-2.69	-2.92	-3.03	-3.07	-3.13	-3.11	-2.1
BW	-1.46	-1.68	-1.57	-1.73	-1.90	-1.88	-2.14	-2.17	-2.18	-2.22	-2.15	-2.37	-2.44	-2.50	-2.56	-2.71	-1.8
CE	-1.25	-1.46	-1.46	-1.52	-1.66	-1.65	-1.84	-1.85	-1.90	-1.90	-1.86	-1.98	-2.13	-2.33	-2.61	-2.32	-2.1
CW	-1.28	-1.51	-1.40	-1.47	-1.61	-1.70	-1.74	-1.82	-1.77	-1.87	-1.81	-1.96	-2.10	-2.17	-2.33	-2.36	-1.8
DE	-1.39	-1.55	-1.59	-1.64	-1.85	-1.73	-1.86	-1.87	-1.92	-1.94	-1.92	-2.03	-2.13	-2.14	-2.21	-2.25	-2.1
DW	-0.74	-0.81	-0.82	-0.86	-0.96	-1.05	-1.11	-1.13	-1.14	-1.15	-1.16	-1.25	-1.35	-1.32	-1.42	-1.36	-1.8
DC	-2.24	-2.91	-2.64	-3.02	-3.12	-3.34	-3.35	-3.50	-3.61	-3.54	-3.61	-3.77	-3.88	-4.12	-4.31	-4.46	-5.0
DS	-2.41	-3.14	-3.00	-3.51	-3.60	-3.76	-3.74	-3.93	-3.98	-4.00	-4.08	-4.09	-4.20	-4.92	-5.37	-5.19	-3.6
DR	-1.45	-1.76	-1.76	-2.07	-2.05	-2.29	-2.27	-2.38	-2.56	-2.50	-2.68	-2.59	-2.88	-3.10	-3.25	-3.30	-2.4
BC	-2.64	-3.22	-3.09	-3.39	-3.59	-3.89	-4.00	-4.01	-4.08	-4.44	-4.35	-4.55	-5.03	-5.43	-6.24	-6.27	-5.0
BS	-2.65	-3.20	-3.30	-3.69	-4.16	-4.52	-4.99	-5.15	-5.04	-5.90	-5.57	-6.25	-7.03	-7.78	-9.37	-7.98	-3.6
BR	-4.04	-5.82	-5.83	-6.78	-7.67	-9.05	-9.09	-9.33	-10.25	-10.76	-10.90	-11.04	-12.51	-12.91	-13.09	-13.01	-2.4

Table 5.6: Pressure coefficients comparison for Model 2, Case 3 and NBCC 2015

	0.1s	0.5s	1s	2s	3s	4s	5s	6s	7s	8s	9s	10s	15s	20s	30s	3pk-Av	CpCg
AE	-1.23	-1.51	-1.47	-1.55	-1.68	-1.76	-1.85	-1.88	-2.00	-2.03	-2.12	-2.08	-2.23	-2.38	-2.55	-2.43	-2.1
AW	-1.09	-1.30	-1.26	-1.33	-1.41	-1.43	-1.48	-1.50	-1.54	-1.55	-1.58	-1.63	-1.65	-1.65	-1.69	-1.69	-1.8
BE	-1.69	-1.96	-1.98	-2.17	-2.10	-2.30	-2.38	-2.43	-2.48	-2.64	-2.63	-2.57	-2.76	-2.91	-2.95	-3.01	-2.1
BW	-1.61	-2.03	-1.94	-2.13	-2.15	-2.42	-2.51	-2.71	-2.68	-2.76	-3.04	-2.72	-3.60	-4.04	-4.73	-4.30	-1.8
CE	-1.91	-2.16	-2.21	-2.33	-2.45	-2.55	-2.61	-2.72	-2.70	-2.74	-2.78	-2.76	-2.92	-2.99	-3.06	-3.09	-2.1
CW	-1.69	-2.04	-1.97	-2.16	-2.29	-2.37	-2.41	-2.52	-2.48	-2.52	-2.56	-2.48	-2.71	-2.78	-2.87	-2.85	-1.8
DE	-1.17	-1.38	-1.38	-1.43	-1.47	-1.57	-1.55	-1.59	-1.65	-1.69	-1.67	-1.73	-1.75	-1.79	-1.85	-1.90	-2.1
DW	-0.98	-1.14	-1.11	-1.24	-1.40	-1.46	-1.51	-1.57	-1.61	-1.63	-1.58	-1.71	-1.82	-1.85	-1.95	-1.89	-1.8
DC	-2.12	-3.01	-2.88	-3.11	-3.30	-3.28	-3.64	-3.63	-3.93	-4.03	-4.00	-4.10	-4.41	-4.54	-4.85	-4.25	-5.0
DS	-3.38	-5.09	-4.89	-5.49	-5.82	-5.90	-6.55	-6.70	-7.20	-7.64	-7.08	-7.42	-8.47	-9.32	-10.26	-8.92	-3.6
DR	-1.89	-2.50	-2.34	-2.53	-2.88	-2.75	-3.10	-3.01	-3.65	-3.68	-3.55	-3.70	-4.35	-4.50	-5.03	-5.07	-2.4
BC	-3.16	-3.96	-3.89	-4.25	-4.46	-4.52	-4.65	-4.73	-4.76	-4.81	-4.83	-4.75	-5.00	-5.11	-5.18	-5.28	-5.0
BS	-4.03	-5.36	-5.07	-6.38	-7.48	-7.40	-8.13	-8.25	-8.64	-8.72	-9.02	-9.32	-9.53	-9.71	-10.19	-9.94	-3.6
BR	-3.45	-4.60	-4.72	-5.26	-6.11	-7.27	-6.96	-7.92	-7.39	-8.32	-7.84	-9.39	-10.35	-10.91	-12.25	-13.25	-2.4

Table 5.7: Pressure coefficients comparison for Model 3, Case 1 and NBCC 2015

	0.1s	0.5s	1s	2s	3s	4s	5s	6s	7s	8s	9s	10s	15s	20s	30s	3pk-Av	CpCg
AE	-2.04	-2.27	-2.33	-2.50	-2.70	-2.73	-2.81	-2.93	-2.97	-3.02	-3.01	-3.07	-3.18	-3.26	-3.49	-3.41	-2.1
AW	-1.63	-1.77	-1.80	-1.98	-2.29	-2.17	-2.28	-2.65	-2.45	-2.68	-2.78	-2.92	-3.23	-3.39	-3.59	-3.56	-1.8
BE	-1.68	-1.93	-1.94	-2.06	-2.06	-2.16	-2.26	-2.16	-2.35	-2.32	-2.37	-2.40	-2.59	-2.68	-2.77	-2.79	-2.1
BW	-1.31	-1.60	-1.57	-1.76	-1.77	-1.83	-1.89	-1.85	-1.96	-1.96	-1.99	-2.00	-2.09	-2.16	-2.26	-2.27	-1.8
CE	-0.92	-1.16	-1.12	-1.18	-1.23	-1.29	-1.37	-1.30	-1.42	-1.43	-1.44	-1.48	-1.55	-1.60	-1.62	-1.62	-2.1
CW	-0.82	-0.97	-0.93	-1.01	-1.07	-1.11	-1.18	-1.18	-1.23	-1.24	-1.27	-1.30	-1.40	-1.47	-1.50	-1.53	-1.8
DE	-1.66	-1.96	-1.91	-2.00	-2.06	-2.14	-2.14	-2.11	-2.16	-2.20	-2.19	-2.21	-2.27	-2.31	-2.38	-2.36	-2.1
DW	-0.99	-1.20	-1.15	-1.28	-1.30	-1.36	-1.41	-1.39	-1.45	-1.46	-1.46	-1.47	-1.55	-1.57	-1.63	-1.54	-1.8
DC	-1.69	-2.01	-2.04	-2.14	-2.18	-2.31	-2.37	-2.39	-2.49	-2.45	-2.47	-2.51	-2.58	-2.61	-2.69	-2.77	-5.0
DS	-3.09	-2.81	-2.94	-3.13	-3.14	-3.29	-3.40	-3.37	-3.54	-3.58	-3.58	-3.57	-3.72	-3.77	-3.89	-4.12	-3.6
DR	-2.89	-3.28	-3.34	-3.42	-3.52	-3.78	-3.77	-3.78	-3.88	-3.90	-3.94	-3.94	-4.18	-4.25	-4.42	-4.23	-2.4
BC	-1.72	-2.01	-1.99	-2.13	-2.24	-2.28	-2.36	-2.42	-2.39	-2.43	-2.50	-2.54	-2.59	-2.66	-2.74	-2.72	-5.0
BS	-3.86	-4.36	-4.66	-4.86	-4.99	-5.13	-5.24	-5.21	-5.48	-5.46	-5.57	-5.51	-5.86	-6.02	-6.30	-6.06	-3.6
BR	-1.81	-2.07	-2.06	-2.12	-2.21	-2.31	-2.37	-2.52	-2.47	-2.47	-2.66	-2.75	-2.98	-3.12	-3.42	-3.33	-2.4

Table 5.8: Pressure coefficients comparison for Model 3, Case 2 and NBCC 2015

	0.1s	0.5s	1s	2s	3s	4s	5s	6s	7s	8s	9s	10s	15s	20s	30s	3pk-Av	CpCg
AE	-1.20	-1.55	-1.40	-1.54	-1.77	-2.00	-1.88	-2.08	-2.16	-2.17	-2.19	-2.27	-2.36	-2.57	-2.72	-2.55	-2.1
AW	-1.11	-1.24	-1.23	-1.29	-1.39	-1.41	-1.44	-1.49	-1.50	-1.51	-1.53	-1.63	-1.79	-1.96	-2.03	-2.03	-1.8
BE	-1.40	-1.73	-1.75	-1.73	-1.88	-1.91	-2.03	-2.02	-2.07	-2.12	-2.16	-2.18	-2.37	-2.45	-2.57	-2.51	-2.1
BW	-1.30	-1.61	-1.65	-1.68	-1.86	-2.00	-2.00	-2.11	-2.16	-2.21	-2.27	-2.35	-2.60	-2.70	-2.90	-2.89	-1.8
CE	-1.00	-1.12	-1.10	-1.11	-1.17	-1.21	-1.22	-1.21	-1.24	-1.28	-1.28	-1.30	-1.38	-1.40	-1.61	-1.42	-2.1
CW	-1.14	-1.33	-1.28	-1.30	-1.39	-1.45	-1.48	-1.47	-1.50	-1.55	-1.57	-1.59	-1.74	-1.79	-1.90	-1.88	-1.8
DE	-1.30	-1.80	-1.68	-1.71	-1.89	-1.87	-2.01	-2.00	-2.04	-2.13	-2.12	-2.17	-2.33	-2.47	-2.66	-2.41	-2.1
DW	-0.78	-1.02	-0.99	-1.06	-1.18	-1.18	-1.26	-1.26	-1.28	-1.32	-1.33	-1.34	-1.47	-1.52	-1.66	-1.48	-1.8
DC	-3.22	-3.72	-3.76	-3.99	-4.16	-4.30	-4.49	-4.41	-4.49	-4.48	-4.53	-4.57	-4.72	-4.73	-4.83	-4.84	-5.0
DS	-2.08	-2.53	-2.68	-2.83	-2.98	-3.31	-3.33	-3.40	-3.53	-3.62	-3.69	-3.85	-4.22	-4.39	-4.72	-4.59	-3.6
DR	-2.27	-2.68	-2.67	-2.84	-2.98	-3.08	-3.19	-3.23	-3.26	-3.24	-3.25	-3.31	-3.31	-3.35	-3.46	-3.48	-2.4
BC	-2.38	-2.85	-2.82	-2.87	-3.13	-3.29	-3.33	-3.29	-3.43	-3.54	-3.60	-3.64	-3.91	-4.02	-4.09	-4.04	-5.0
BS	-2.96	-4.33	-4.07	-4.28	-4.95	-5.18	-5.33	-5.65	-5.62	-5.99	-6.28	-6.46	-7.00	-7.12	-7.73	-8.04	-3.6
BR	-2.37	-2.89	-2.87	-2.98	-3.27	-3.42	-3.45	-3.52	-3.61	-3.77	-3.78	-3.80	-4.09	-4.12	-4.57	-4.33	-2.4

Table 5.9: Pressure coefficients comparison for Model 3, Case 3 and NBCC 2015

	0.1s	0.5s	1s	2s	3s	4s	5s	6s	7s	8s	9s	10s	15s	20s	30s	3pk-Av	CpCg
AE	-0.87	-1.00	-1.01	-1.06	-1.05	-1.17	-1.17	-1.20	-1.22	-1.26	-1.27	-1.28	-1.36	-1.38	-1.44	-1.40	-2.1
AW	-0.94	-1.01	-1.01	-1.09	-1.11	-1.16	-1.17	-1.18	-1.18	-1.20	-1.22	-1.21	-1.26	-1.30	-1.30	-1.32	-1.8
BE	-1.73	-2.16	-2.19	-2.22	-2.27	-2.45	-2.41	-2.51	-2.49	-2.63	-2.65	-2.63	-2.78	-2.85	-2.88	-2.87	-2.1
BW	-1.71	-2.09	-2.08	-2.39	-2.77	-2.72	-2.81	-2.91	-3.02	-3.05	-3.16	-3.35	-3.50	-3.55	-3.77	-3.70	-1.8
CE	-1.90	-2.11	-2.14	-2.24	-2.39	-2.45	-2.57	-2.57	-2.66	-2.66	-2.65	-2.70	-2.78	-2.89	-2.99	-3.02	-2.1
CW	-1.70	-1.90	-1.95	-2.03	-2.19	-2.22	-2.35	-2.35	-2.49	-2.46	-2.45	-2.51	-2.59	-2.69	-2.82	-2.83	-1.8
DE	-1.47	-1.88	-1.92	-1.95	-2.01	-2.28	-2.22	-2.32	-2.34	-2.50	-2.47	-2.44	-2.66	-2.77	-2.86	-2.79	-2.1
DW	-0.95	-1.13	-1.11	-1.23	-1.35	-1.32	-1.44	-1.48	-1.53	-1.53	-1.54	-1.56	-1.66	-1.74	-1.83	-1.69	-1.8
DC	-1.56	-1.78	-1.83	-1.91	-1.98	-2.09	-2.14	-2.25	-2.31	-2.32	-2.43	-2.43	-2.65	-2.71	-2.83	-2.73	-5.0
DS	-2.95	-3.60	-3.59	-3.92	-4.20	-4.82	-4.87	-5.18	-5.33	-5.18	-5.34	-5.50	-5.81	-6.18	-6.50	-6.60	-3.6
DR	-1.62	-2.00	-2.08	-2.30	-2.52	-2.73	-2.75	-2.73	-2.75	-2.97	-2.97	-2.99	-3.24	-3.35	-3.46	-3.40	-2.4
BC	-2.27	-2.81	-2.79	-3.07	-3.21	-3.40	-3.46	-3.56	-3.64	-3.57	-3.60	-3.71	-3.88	-4.11	-4.30	-4.50	-5.0
BS	-4.05	-4.85	-4.86	-5.16	-5.38	-5.67	-5.57	-5.70	-5.73	-5.92	-5.86	-5.98	-6.15	-6.38	-6.40	-7.50	-3.6
BR	-3.10	-3.46	-3.52	-3.69	-3.97	-4.03	-4.06	-4.17	-4.13	-4.20	-4.29	-4.29	-4.51	-4.65	-4.75	-4.69	-2.4

5.3 Roof pressure coefficients comparison as per 4.1.7.6-B, E cladding and secondary structural elements

The peak pressure coefficients, C_T**,** along the roof zones were very similar for all three of the models tested. Zone C, which were on the corners of the roofs, were usually within the minimum C_pC_g values of the NBCC 2015. Thus, the tornadic flows were creating similar pressures on the roof corners compared to ABL flows, which the C_pC_g values in the NBCC 2015 are designed for. The corners of the roof are susceptible zones in ABL flows due to the separation of ABL flows. Conservative C_pC_g values are used in the NBCC 2015, thus Zone C is the only zone where the C_T values did not always exceed the C_pC_g values of the NBCC 2015 criteria. However, there were cases at higher exposure durations for Model 1 and Model 2 that had a roof pitch angle of 16°, where the C_T values for Zone C exceeded the C_pC_g in the NBCC 2015. It was also shown in Chapter 4 (Section 4.3) that the lower roof pitch angles created greater suctions when exposed to lab-simulated tornadoes. There was no exceedance of the C_T values for Zone C of Model 3, which had a bigger roof pitch angle of 36° compared to the NBCC 2015. Therefore, for lower roof pitch angles, Zone C intervals in NBCC 2015 need slight modifications to be more conservative. For Zone S and Zone R, the experimental C_T values greatly exceeded the C_pC_g values found in NBCC 2015 for most of the tornado exposure durations. The suctions were much greater in the center sections of the roofs (R zones), as well as on the edges (S zones). The tornado core was under much greater suction due to the updraft and pressure differential. This is not seen in the ABL wind flows, which might be the reason why the C_pC_g values of the NBCC 2015 are so far from being adequate for tornado resistant design of residential houses. The zones on the roof exceeded the minimum C_pC_g values of the NBCC 2015 by much larger factors than the walls. For the roof's Zone S, the 3-peak average values exceeded the NBCC 2015 by a maximum factor of 3.92, while for Roof Zone R, the 3-peak average C_T values exceeded by a factor of 5.52. Once again, a reduction of the exposure duration results in a lower exceedance factor. Similar conclusions were formulated by Haan et al. (2010) when he compared the experimentally obtained tornado induced pressure coefficients to the ASCE 7-05 building code and found that the peak uplift coefficients are about 1.8–3.2 times bigger than the ASCE 7-05 recommended values. The same study pointed out that this discrepancy might be caused by the significant drop in static pressure created by the vortex of the tornado. As such, their results relate only to the particular building geometry under the tornado vortex conditions they examined. There are also scenarios where the static pressure will have minimal effect, such as the case of a relatively small building in a large tornado, for which the static pressure gradient is considered negligible, as argued by Gavanski and Kopp (2017). However, by not separating effects of the aerodynamic and static pressure loads which can occur in a tornado, such considerations cannot be reflected in the design provisions.

The effects of the tornado exposure duration analysed in the current study are not conclusive in determining an ideal duration time for tornado exposure to be used in experiments, because most of the C_T values on the roof zones exceeded the minimum C_pC_g values of the NBCC 2015. However, it can be noticed that the C_T values exceed the minimum code recommendation in the NBCC 2015 for different durations at different zones. Numerous times this exceedance occured at durations larger or equal to 0.5 s; however, there were instances where exceedance only occurred at higher exposure durations. In the case of the tornado tested in the current study, the NBCC 2015 for low-rise buildings is not adequate for structures intended to withstand an EF-3 tornado. However, the use of a duration method, where tornado exposure duration can be selected and altered, could have benefits for future scaled laboratory tornado experiments, for example, when testing EF-1, EF-2 and lower velocity EF-3 tornadoes, or if the C_pC_g values of the building code are increased so they can lead to more conservative design.

Table 5.10: Pressure coefficients comparison for Model 1, Case 1 and NBCC 2015 (4.1.7.6-A Load Case A)

	0.1s	0.5s	1s	2s	3s	4s	5s	6s	7s	8s	9s	10s	15s	20s	30s	3-peak Avg	CpCg
1	-0.74	-0.86	-0.84	-0.89	-0.93	-0.95	-0.96	-0.98	-0.99	-1.01	-1.01	-1.03	-1.06	-1.07	-1.09	-1.10	0.93
1E	-1.24	-1.50	-1.51	-1.55	-1.64	-1.66	-1.71	-1.73	-1.74	-1.75	-1.81	-1.83	-1.88	-1.95	-2.05	-1.99	1.41
2	-1.47	-1.73	-1.78	-1.82	-1.86	-1.94	-2.00	-2.02	-2.02	-2.08	-2.06	-2.08	-2.13	-2.18	-2.21	-2.21	-1.3
2E	-2.95	-3.62	-4.05	-4.14	-4.27	-4.45	-4.54	-4.53	-4.58	-4.79	-4.86	-4.88	-5.18	-5.53	-6.53	-7.15	-2
3	-1.30	-1.50	-1.53	-1.59	-1.67	-1.75	-1.93	-2.01	-2.04	-2.18	-2.19	-2.26	-2.46	-2.68	-2.99	-3.08	-0.85
3E	-3.27	-5.23	-5.79	-6.78	-7.62	-8.76	-9.92	-9.27	-10.41	-10.51	-11.03	-11.43	-12.25	-12.28	-12.42	-12.25	-1.22
4	-1.04	-1.14	-1.16	-1.23	-1.23	-1.31	-1.34	-1.37	-1.35	-1.46	-1.42	-1.44	-1.51	-1.61	-1.67	-1.64	-0.73
4E	-0.89	-1.01	-1.01	-1.06	-1.14	-1.17	-1.21	-1.20	-1.22	-1.25	-1.28	-1.29	-1.32	-1.34	-1.36	-1.38	-1.09

Table 5.11: Pressure coefficients comparison for Model 1, Case 2 and NBCC 2015 (4.1.7.6-A Load Case A)

	0.1s	0.5s	1s	2s	3s	4s	5s	6s	7s	8s	9s	10s	15s	20s	30s	3-peak Avg	CpCg
1	-0.56	-0.68	-0.65	-0.71	-0.75	-0.78	-0.76	-0.78	-0.79	-0.80	-0.81	-0.82	-0.85	-0.89	-0.91	-0.90	0.93
1E	-0.73	-0.92	-0.94	-1.04	-1.08	-1.12	-1.18	-1.20	-1.25	-1.29	-1.28	-1.31	-1.36	-1.38	-1.41	-1.41	1.41
2	-1.61	-1.98	-1.95	-2.06	-2.29	-2.42	-2.51	-2.64	-2.68	-2.80	-2.88	-2.88	-3.12	-3.30	-3.52	-3.67	-1.3
2E	-2.12	-3.15	-3.09	-3.71	-4.27	-4.80	-5.33	-5.66	-5.81	-6.14	-5.93	-6.30	-7.04	-8.89	-10.12	-11.24	-2
3	-2.25	-3.13	-3.06	-4.40	-4.78	-5.08	-5.66	-5.97	-6.36	-6.37	-6.86	-6.82	-7.57	-8.49	-9.35	-9.56	-0.85
3E	-3.57	-5.96	-6.07	-7.45	-8.05	-8.87	-9.47	-10.14	-10.69	-11.45	-11.45	-12.20	-12.97	-13.23	-14.34	-14.14	-1.22
4	-1.05	-1.25	-1.28	-1.38	-1.52	-1.59	-1.70	-1.74	-1.71	-1.82	-1.80	-1.85	-1.89	-1.97	-2.02	-2.07	-0.73
4E	-0.77	-0.91	-1.01	-1.02	-1.06	-1.22	-1.31	-1.37	-1.40	-1.49	-1.45	-1.56	-1.67	-1.73	-1.78	-1.72	-1.09

Table 5.12: Pressure coefficients comparison for Model 1, Case 2 and NBCC 2015 (4.1.7.6-A Load Case B)

	0.1s	0.5s	1s	2s	3s	4s	5s	6s	7s	8s	9s	10s	15s	20s	30s	3-peak Avg	CpCg
1	-1.05	-1.25	-1.28	-1.38	-1.52	-1.59	-1.70	-1.74	-1.71	-1.82	-1.80	-1.85	-1.89	-1.97	-2.02	-2.07	-0.85
1E	-0.77	-0.91	-1.01	-1.02	-1.06	-1.22	-1.31	-1.37	-1.40	-1.49	-1.45	-1.56	-1.67	-1.73	-1.78	-1.72	-0.9
2	-1.61	-1.98	-1.95	-2.06	-2.29	-2.42	-2.51	-2.64	-2.68	-2.80	-2.88	-2.88	-3.12	-3.30	-3.52	-3.67	-1.3
2E	-3.57	-5.96	-6.07	-7.45	-8.05	-8.87	-9.47	-10.14	-10.69	-11.45	-11.45	-12.20	-12.97	-13.23	-14.34	-14.14	-2
3	-2.25	-3.13	-3.06	-4.40	-4.78	-5.08	-5.66	-5.97	-6.36	-6.37	-6.86	-6.82	-7.57	-8.49	-9.35	-9.56	-0.7
3E	-2.12	-3.15	-3.09	-3.71	-4.27	-4.80	-5.33	-5.66	-5.81	-6.14	-5.93	-6.30	-7.04	-8.89	-10.12	-11.24	-1
4	-0.56	-0.68	-0.65	-0.71	-0.75	-0.78	-0.76	-0.78	-0.79	-0.80	-0.81	-0.82	-0.85	-0.89	-0.91	-0.90	-0.85
4E	-0.73	-0.92	-0.94	-1.04	-1.08	-1.12	-1.18	-1.20	-1.25	-1.29	-1.28	-1.31	-1.36	-1.38	-1.41	-1.41	-0.9
5	-0.88	-1.04	-1.08	-1.12	-1.19	-1.32	-1.35	-1.38	-1.40	-1.42	-1.44	-1.48	-1.53	-1.55	-1.56	-1.59	0.75
5E	-1.16	-1.40	-1.50	-1.61	-1.61	-1.93	-2.12	-2.04	-2.28	-2.33	-2.30	-2.43	-2.63	-2.86	-2.97	-2.89	1.15
6	-0.85	-1.00	-0.99	-1.10	-1.13	-1.21	-1.22	-1.30	-1.30	-1.32	-1.40	-1.49	-1.61	-1.72	-1.76	-1.73	-0.55
6E	-0.69	-0.78	-0.78	-0.84	-0.86	-0.89	-0.92	-0.95	-0.95	-0.98	-1.00	-0.99	-1.05	-1.07	-1.10	-1.11	-0.8

Table 5.13: Pressure coefficients comparison for Model 1, Case 2 and NBCC 2015 (4.1.7.6-A Load Case B)

	0.1s	0.5s	1s	2s	3s	4s	5s	6s	7s	8s	9s	10s	15s	20s	30s	3-peak Avg	CpCg
1	-1.18	-1.42	-1.61	-1.59	-1.85	-1.81	-1.88	-1.99	-2.01	-2.06	-2.18	-2.16	-2.48	-2.60	-2.84	-2.90	-0.85
1E	-0.49	-0.56	-0.56	-0.57	-0.60	-0.63	-0.63	-0.65	-0.66	-0.66	-0.68	-0.70	-0.77	-0.81	-0.88	-0.81	-0.9
2	-2.67	-3.72	-3.68	-4.54	-4.68	-5.16	-5.09	-5.30	-5.74	-5.61	-5.76	-6.21	-6.36	-6.87	-7.06	-6.78	-1.3
2E	-3.47	-6.04	-5.01	-6.55	-7.46	-8.25	-9.13	-9.38	-10.20	-10.56	-9.91	-10.98	-12.33	-12.91	-13.60	-13.49	-2
3	-3.44	-5.46	-5.46	-5.98	-7.45	-7.81	-7.95	-8.42	-8.76	-9.28	-9.36	-9.24	-10.70	-10.67	-11.45	-11.17	-0.7
3E	-1.74	-2.30	-2.13	-2.50	-2.74	-2.83	-2.90	-3.13	-3.32	-3.34	-3.74	-3.57	-4.36	-4.54	-4.72	-5.43	-1
4	-0.57	-0.67	-0.66	-0.70	-0.73	-0.81	-0.79	-0.80	-0.85	-0.86	-0.88	-0.89	-0.94	-1.01	-1.07	-1.10	-0.85
4E	-0.57	-0.67	-0.66	-0.73	-0.73	-0.85	-0.87	-0.90	-0.95	-0.93	-0.94	-0.94	-1.06	-1.11	-1.17	-1.30	-0.9
5	-0.49	-0.57	-0.59	-0.62	-0.65	-0.76	-0.75	-0.75	-0.82	-0.82	-0.81	-0.84	-0.91	-0.98	-1.02	-0.99	0.75
5E	-0.53	-0.60	-0.62	-0.64	-0.67	-0.72	-0.74	-0.75	-0.75	-0.75	-0.77	-0.78	-0.85	-0.92	-0.95	-0.93	1.15
6	-1.44	-1.77	-1.80	-1.90	-2.05	-2.20	-2.27	-2.31	-2.39	-2.50	-2.50	-2.56	-2.77	-2.81	-3.09	-2.98	-0.55
6E	-0.80	-0.93	-0.92	-0.96	-1.03	-1.06	-1.11	-1.12	-1.14	-1.16	-1.16	-1.22	-1.31	-1.36	-1.44	-1.47	-0.8

Table 5.14: Pressure coefficients comparison for Model 2, Case 1 and NBCC 2015 (4.1.7.6-A Load Case A)

	0.1s	0.5s	1s	2s	3s	4s	5s	6s	7s	8s	9s	10s	15s	20s	30s	3-peak Avg	CpCg
1	-0.79	-0.90	-0.85	-0.96	-1.04	-1.05	-1.12	-1.15	-1.19	-1.20	-1.23	-1.20	-1.27	-1.33	-1.42	-1.38	0.93
1E	-1.07	-1.30	-1.27	-1.29	-1.42	-1.48	-1.57	-1.57	-1.58	-1.64	-1.66	-1.68	-1.73	-1.77	-1.81	-1.78	1.41
2	-1.91	-2.33	-2.43	-2.76	-2.89	-2.96	-2.94	-3.02	-3.10	-3.06	-3.17	-3.23	-3.28	-3.36	-3.45	-3.44	-1.3
2E	-3.43	-3.96	-4.13	-4.47	-4.87	-4.90	-5.21	-5.23	-5.28	-5.22	-5.53	-5.63	-5.80	-5.94	-6.13	-6.08	-2
3	-1.47	-1.82	-1.93	-2.23	-2.35	-2.49	-2.55	-2.63	-2.77	-2.64	-2.94	-2.90	-3.06	-3.17	-3.25	-3.32	-0.85
3E	-3.20	-4.08	-4.07	-4.66	-5.24	-5.33	-5.48	-5.92	-6.02	-6.07	-6.49	-7.05	-7.10	-7.95	-9.48	-8.76	-1.22
4	-1.43	-1.78	-1.58	-1.80	-1.95	-1.88	-2.01	-2.06	-2.11	-2.20	-2.22	-2.26	-2.37	-2.48	-2.59	-2.50	-0.73
4E	-1.01	-1.20	-1.08	-1.21	-1.31	-1.27	-1.37	-1.47	-1.48	-1.56	-1.50	-1.53	-1.59	-1.72	-1.85	-1.74	-1.09

Table 5.15: Pressure coefficients comparison for Model 2, Case 2 and NBCC 2015 (4.1.7.6-A Load Case A)

	0.1s	0.5s	1s	2s	3s	4s	5s	6s	7s	8s	9s	10s	15s	20s	30s	3-peak Avg	CpCg
1	-0.74	-0.81	-0.82	-0.86	-0.96	-1.05	-1.11	-1.13	-1.14	-1.15	-1.16	-1.25	-1.35	-1.32	-1.42	-1.36	0.93
1E	-1.39	-1.55	-1.59	-1.64	-1.85	-1.73	-1.86	-1.87	-1.92	-1.94	-1.92	-2.03	-2.13	-2.14	-2.21	-2.25	1.41
2	-1.57	-1.88	-1.98	-2.18	-2.21	-2.43	-2.54	-2.57	-2.86	-3.00	-3.04	-2.97	-3.61	-4.10	-4.62	-4.31	-1.3
2E	-2.41	-3.14	-3.00	-3.51	-3.60	-3.76	-3.74	-3.93	-3.98	-4.00	-4.08	-4.09	-4.20	-4.92	-5.37	-5.19	-2
3	-2.64	-3.46	-3.10	-3.39	-4.35	-4.84	-5.05	-5.18	-5.60	-6.08	-6.36	-6.18	-7.63	-7.68	-8.49	-7.98	-0.85
3E	-4.04	-5.82	-5.83	-6.78	-7.67	-9.05	-9.09	-9.33	-10.25	-10.76	-10.90	-11.04	-12.51	-12.91	-13.09	-13.01	-1.22
4	-1.84	-2.18	-2.07	-2.21	-2.42	-2.45	-2.73	-2.76	-2.74	-2.80	-2.69	-2.92	-3.03	-3.07	-3.13	-3.11	-0.73
4E	-0.94	-1.08	-1.02	-1.13	-1.24	-1.22	-1.37	-1.41	-1.45	-1.47	-1.46	-1.59	-1.64	-1.72	-1.78	-1.89	-1.09

Table 5.16: Pressure coefficients comparison for Model 2, Case 2 and NBCC 2015 (4.1.7.6-A Load Case B)

	0.1s	0.5s	1s	2s	3s	4s	5s	6s	7s	8s	9s	10s	15s	20s	30s	3-peak Avg	CpCg
1	-1.84	-2.18	-2.07	-2.21	-2.42	-2.45	-2.73	-2.76	-2.74	-2.80	-2.69	-2.92	-3.03	-3.07	-3.13	-3.11	-0.85
1E	-0.94	-1.08	-1.02	-1.13	-1.24	-1.22	-1.37	-1.41	-1.45	-1.47	-1.46	-1.59	-1.64	-1.72	-1.78	-1.89	-0.9
2	-1.57	-1.88	-1.98	-2.18	-2.21	-2.43	-2.54	-2.57	-2.86	-3.00	-3.04	-2.97	-3.61	-4.10	-4.62	-4.31	-1.3
2E	-4.04	-5.82	-5.83	-6.78	-7.67	-9.05	-9.09	-9.33	-10.25	-10.76	-10.90	-11.04	-12.51	-12.91	-13.09	-13.01	-2
3	-2.64	-3.46	-3.10	-3.39	-4.35	-4.84	-5.05	-5.18	-5.60	-6.08	-6.36	-6.18	-7.63	-7.68	-8.49	-7.98	-0.7
3E	-2.41	-3.14	-3.00	-3.51	-3.60	-3.76	-3.74	-3.93	-3.98	-4.00	-4.08	-4.09	-4.20	-4.92	-5.37	-5.19	-1
4	-0.74	-0.81	-0.82	-0.86	-0.96	-1.05	-1.11	-1.13	-1.14	-1.15	-1.16	-1.25	-1.35	-1.32	-1.42	-1.36	-0.85
4E	-1.39	-1.55	-1.59	-1.64	-1.85	-1.73	-1.86	-1.87	-1.92	-1.94	-1.92	-2.03	-2.13	-2.14	-2.21	-2.25	-0.9
5	-1.29	-1.58	-1.48	-1.67	-1.71	-1.79	-1.78	-1.88	-1.91	-1.89	-1.94	-1.93	-1.96	-2.02	-2.04	-2.11	0.75
5E	-1.69	-1.90	-1.94	-2.14	-2.41	-2.35	-2.64	-2.74	-2.81	-2.91	-3.04	-3.18	-3.44	-3.57	-3.77	-3.94	1.15
6	-1.28	-1.51	-1.46	-1.52	-1.66	-1.70	-1.84	-1.85	-1.90	-1.90	-1.86	-1.98	-2.13	-2.33	-2.61	-2.36	-0.55
6E	-1.04	-1.21	-1.12	-1.18	-1.29	-1.36	-1.39	-1.44	-1.42	-1.50	-1.44	-1.56	-1.65	-1.71	-1.84	-1.86	-0.8

Table 5.17: Pressure coefficients comparison for Model 2, Case 3 and NBCC 2015 (4.1.7.6-A Load Case B)

	0.1s	0.5s	1s	2s	3s	4s	5s	6s	7s	8s	9s	10s	15s	20s	30s	3-peak Avg	CpCg
1	-1.69	-2.03	-1.98	-2.17	-2.15	-2.42	-2.51	-2.71	-2.68	-2.76	-3.04	-2.72	-3.60	-4.04	-4.73	-4.30	-0.85
1E	-0.87	-1.06	-1.04	-1.10	-1.07	-1.19	-1.23	-1.28	-1.26	-1.28	-1.40	-1.28	-1.49	-1.66	-1.77	-1.68	-0.9
2	-3.38	-5.09	-4.89	-5.49	-5.82	-5.90	-6.55	-6.70	-7.20	-7.64	-7.08	-7.42	-8.47	-8.94	-10.26	-8.92	-1.3
2E	-3.48	-4.60	-4.72	-5.26	-6.11	-7.27	-6.96	-7.92	-7.39	-8.32	-7.84	-9.39	-10.35	-10.91	-12.25	-13.25	-2
3	-4.03	-5.36	-5.07	-6.38	-7.48	-7.40	-8.13	-8.25	-8.64	-8.72	-9.02	-9.32	-9.53	-9.71	-10.19	-9.86	-0.7
3E	-3.10	-3.90	-3.93	-4.63	-4.92	-4.93	-5.62	-5.93	-6.63	-7.29	-6.82	-7.33	-8.16	-9.32	-10.26	-8.50	-1
4	-0.98	-1.08	-1.11	-1.16	-1.25	-1.25	-1.29	-1.29	-1.33	-1.35	-1.31	-1.38	-1.41	-1.49	-1.51	-1.51	-0.85
4E	-1.17	-1.38	-1.38	-1.43	-1.47	-1.57	-1.55	-1.59	-1.65	-1.69	-1.67	-1.73	-1.82	-1.85	-1.95	-1.90	-0.9
5	-1.09	-1.30	-1.26	-1.33	-1.41	-1.43	-1.48	-1.50	-1.54	-1.55	-1.58	-1.63	-1.65	-1.65	-1.69	-1.69	0.75
5E	-1.23	-1.51	-1.47	-1.55	-1.68	-1.76	-1.85	-1.88	-2.00	-2.03	-2.12	-2.08	-2.23	-2.38	-2.55	-2.43	1.15
6	-1.91	-2.16	-2.21	-2.33	-2.45	-2.55	-2.61	-2.72	-2.70	-2.74	-2.78	-2.76	-2.92	-2.99	-3.06	-3.09	-0.55
6E	-1.29	-1.53	-1.51	-1.63	-1.70	-1.73	-1.77	-1.84	-1.83	-1.85	-1.88	-1.83	-1.96	-2.01	-2.03	-2.02	-0.8

Table 5.18: Pressure coefficients comparison for Model 3, Case 1 and NBCC 2015 (4.1.7.6-A Load Case A)

	0.1s	0.5s	1s	2s	3s	4s	5s	6s	7s	8s	9s	10s	15s	20s	30s	3-peak Avg	CpCg
1	-0.99	-1.20	-1.15	-1.28	-1.30	-1.36	-1.41	-1.39	-1.45	-1.46	-1.46	-1.47	-1.55	-1.57	-1.63	-1.54	0.93
1E	-1.66	-1.96	-1.91	-2.00	-2.06	-2.14	-2.14	-2.11	-2.16	-2.20	-2.19	-2.21	-2.27	-2.31	-2.38	-2.36	1.41
2	-1.17	-1.28	-1.26	-1.33	-1.38	-1.44	-1.48	-1.46	-1.52	-1.55	-1.57	-1.57	-1.65	-1.69	-1.75	-1.68	-1.3
2E	-3.09	-3.65	-3.69	-3.85	-3.89	-4.19	-4.30	-4.32	-4.47	-4.53	-4.51	-4.56	-4.73	-4.78	-4.91	-4.79	-2
3	-2.45	-3.37	-3.27	-3.62	-4.07	-3.99	-4.19	-4.43	-4.40	-4.46	-4.64	-4.75	-4.86	-4.99	-5.38	-5.89	-0.85
3E	-3.86	-4.36	-4.66	-4.86	-4.99	-5.13	-5.24	-5.21	-5.48	-5.46	-5.57	-5.51	-5.86	-6.02	-6.30	-6.30	-1.22
4	-1.68	-1.93	-1.94	-2.06	-2.06	-2.16	-2.26	-2.16	-2.35	-2.32	-2.37	-2.40	-2.59	-2.68	-2.77	-2.79	-0.73
4E	-1.17	-1.27	-1.25	-1.33	-1.37	-1.39	-1.41	-1.44	-1.44	-1.46	-1.46	-1.48	-1.54	-1.56	-1.59	-1.60	-1.09

Table 5.19: Pressure coefficients comparison for Model 3, Case 2 and NBCC 2015 (4.1.7.6-A Load Case A)

	0.1s	0.5s	1s	2s	3s	4s	5s	6s	7s	8s	9s	10s	15s	20s	30s	3-peak Avg	CpCg
1	-0.78	-1.02	-0.99	-1.06	-1.18	-1.18	-1.26	-1.26	-1.28	-1.32	-1.33	-1.34	-1.47	-1.52	-1.66	-1.48	0.93
1E	-1.30	-1.80	-1.68	-1.71	-1.89	-1.87	-2.01	-2.00	-2.04	-2.13	-2.12	-2.17	-2.33	-2.47	-2.66	-2.41	1.41
2	-1.43	-1.71	-1.71	-1.81	-1.83	-2.01	-1.97	-1.96	-2.04	-2.09	-2.18	-2.18	-2.47	-2.48	-2.60	-2.58	-1.3
2E	-3.22	-3.72	-3.76	-3.99	-4.16	-4.30	-4.49	-4.41	-4.49	-4.48	-4.53	-4.57	-4.72	-4.73	-4.83	-4.84	-2
3	-2.96	-4.33	-4.07	-4.28	-4.95	-5.18	-5.33	-5.65	-5.62	-5.99	-6.28	-6.46	-7.00	-7.12	-7.73	-8.04	-0.85
3E	-2.58	-3.50	-3.63	-4.01	-4.35	-4.59	-4.98	-5.07	-5.01	-5.07	-5.17	-5.19	-5.50	-5.72	-5.94	-6.26	-1.22
4	-1.40	-1.73	-1.75	-1.73	-1.88	-2.00	-2.03	-2.11	-2.16	-2.21	-2.27	-2.35	-2.60	-2.70	-2.90	-2.89	-0.73
4E	-0.84	-0.92	-0.89	-1.00	-1.05	-1.12	-1.10	-1.18	-1.20	-1.23	-1.29	-1.31	-1.33	-1.38	-1.43	-1.61	-1.09

Table 5.20: Pressure coefficients comparison for Model 3, Case 2 and NBCC 2015 (4.1.7.6-A Load Case B)

	0.1s	0.5s	1s	2s	3s	4s	5s	6s	7s	8s	9s	10s	15s	20s	30s	3-peak Avg	CpCg
1	-1.40	-1.73	-1.75	-1.73	-1.88	-2.00	-2.03	-2.11	-2.16	-2.21	-2.27	-2.35	-2.60	-2.70	-2.90	-2.89	-0.85
1E	-0.84	-0.92	-0.89	-1.00	-1.05	-1.12	-1.10	-1.18	-1.20	-1.23	-1.29	-1.31	-1.33	-1.38	-1.43	-1.61	-0.9
2	-1.43	-1.71	-1.71	-1.81	-1.83	-2.01	-1.97	-1.96	-2.04	-2.09	-2.18	-2.18	-2.47	-2.48	-2.60	-2.58	-1.3
2E	-2.58	-3.50	-3.63	-4.01	-4.35	-4.59	-4.98	-5.07	-5.01	-5.07	-5.17	-5.19	-5.50	-5.72	-5.94	-6.26	-2
3	-2.96	-4.33	-4.07	-4.28	-4.95	-5.18	-5.33	-5.65	-5.62	-5.99	-6.28	-6.46	-7.00	-7.12	-7.73	-8.04	-0.7
3E	-3.22	-3.72	-3.76	-3.99	-4.16	-4.30	-4.49	-4.41	-4.49	-4.48	-4.53	-4.57	-4.72	-4.73	-4.83	-4.84	-1
4	-0.78	-1.02	-0.99	-1.06	-1.18	-1.18	-1.26	-1.26	-1.28	-1.32	-1.33	-1.34	-1.47	-1.52	-1.66	-1.48	-0.85
4E	-1.30	-1.80	-1.68	-1.71	-1.89	-1.87	-2.01	-2.00	-2.04	-2.13	-2.12	-2.17	-2.33	-2.47	-2.66	-2.41	-0.9
5	-1.11	-1.24	-1.23	-1.29	-1.39	-1.41	-1.44	-1.49	-1.50	-1.51	-1.53	-1.63	-1.79	-1.96	-2.03	-2.03	0.75
5E	-1.20	-1.55	-1.40	-1.54	-1.77	-2.00	-1.88	-2.08	-2.16	-2.17	-2.19	-2.27	-2.36	-2.57	-2.72	-2.55	1.15
6	-1.14	-1.33	-1.28	-1.30	-1.39	-1.45	-1.48	-1.47	-1.50	-1.55	-1.57	-1.59	-1.74	-1.79	-1.90	-1.88	-0.55
6E	-1.00	-1.12	-1.10	-1.11	-1.17	-1.21	-1.22	-1.21	-1.24	-1.28	-1.28	-1.30	-1.38	-1.39	-1.44	-1.42	-0.8

Table 5.21: Pressure coefficients comparison for Model 3, Case 3 and NBCC 2015 (4.1.7.6-A Load Case B)

	0.1s	0.5s	1s	2s	3s	4s	5s	6s	7s	8s	9s	10s	15s	20s	30s	3-peak Avg	CpCg
1	-1.73	-2.16	-2.19	-2.39	-2.77	-2.72	-2.81	-2.91	-3.02	-3.05	-3.16	-3.35	-3.50	-3.55	-3.77	-3.70	-0.85
1E	-0.65	-0.70	-0.75	-0.77	-0.82	-0.84	-0.87	-0.89	-0.91	-0.94	-0.96	-0.98	-1.01	-1.04	-1.06	-1.06	-0.9
2	-1.69	-1.86	-1.91	-1.98	-2.05	-2.18	-2.18	-2.25	-2.31	-2.32	-2.43	-2.43	-2.65	-2.71	-2.83	-2.81	-1.3
2E	-4.05	-4.85	-4.86	-5.16	-5.38	-5.67	-5.57	-5.70	-5.73	-5.92	-5.86	-5.98	-6.15	-6.38	-6.40	-6.41	-2
3	-3.41	-3.83	-3.80	-4.20	-4.29	-4.93	-5.16	-5.14	-5.16	-5.19	-5.32	-5.58	-5.82	-6.09	-6.18	-6.91	-0.7
3E	-2.95	-3.60	-3.59	-3.92	-4.20	-4.82	-4.87	-5.18	-5.33	-5.18	-5.34	-5.50	-5.81	-6.18	-6.50	-6.60	-1
4	-0.95	-1.13	-1.11	-1.18	-1.19	-1.28	-1.28	-1.33	-1.33	-1.38	-1.37	-1.38	-1.45	-1.50	-1.55	-1.54	-0.85
4E	-1.47	-1.88	-1.92	-1.95	-2.01	-2.28	-2.22	-2.32	-2.34	-2.50	-2.47	-2.44	-2.66	-2.77	-2.86	-2.79	-0.9
5	-0.94	-1.01	-1.01	-1.09	-1.11	-1.16	-1.17	-1.18	-1.18	-1.20	-1.22	-1.21	-1.26	-1.30	-1.30	-1.32	0.75
5E	-0.87	-1.00	-1.01	-1.06	-1.05	-1.17	-1.17	-1.20	-1.22	-1.26	-1.27	-1.28	-1.36	-1.38	-1.44	-1.40	1.15
6	-1.90	-2.11	-2.14	-2.24	-2.39	-2.45	-2.57	-2.57	-2.66	-2.66	-2.65	-2.70	-2.78	-2.89	-2.99	-3.02	-0.55
6E	-1.07	-1.15	-1.14	-1.18	-1.20	-1.24	-1.23	-1.24	-1.24	-1.26	-1.25	-1.27	-1.30	-1.33	-1.34	-1.35	-0.8

5.4 Concluding remarks for 4.1.7.6 B, E for cladding and secondary structural elements and 4.1.7.6 A Load Case A and B for primary structural members

For the current WDS experiment, the C_T values usually exceeded the C_pC_g values (NBCC, 2015) for one of the four walls, while most of the roof cases performed showed higher C_T values than the corresponding C_pC_g values (NBCC, 2015). Since it is important for the walls and roofs not to exceed the design recommended pressure coefficients for all orientations, an exceedance for only one of the experimentally tested orientations would mean that the NBCC 2015 is not adequate to withstand the EF-3 tornado tested in the lab. This implies that for tornadoes of smaller intensities and smaller velocities, such as an EF-1 or EF-2 category tornado, the exposure duration analysis could be more useful in determining the C_pC_g values found in a stationary tornado experiment due to expected small magnitude pressure coefficient values. Several studies (Haan et al., 2017, Case et al., 2011) showed that the stationary tornado is capable of producing much higher peak pressures than the translating tornado. Therefore, the worst-case pressure coefficient would be determined when stationary tornado experiments are conducted. Using the worst-case scenario for a stationary tornado may not be the best alternative since it could be too conservative. Using the worst-case scenario of a translating tornado might also not be the best alternative because the faster the tornado translates, the less magnitude the pressure coefficients will have, possibly leading to an underestimation of the peak pressure coefficients' C_pC_g values. Finding a balance between a conservative C_pC_g value and a value that is realistic to adopt in the building codes while providing more resistance to tornadic winds is very important. The method of sampling the stationary tornado-induced pressures for different durations could prove to be useful when determining the C_pC_g values for each wall and roof zone recommended in the NBCC 2015, as it will alterations to the data in order to find a balance between conservative and realistic C_pC_g values for designing structures to withstand tornadoes of different intensities.

The current NBCC zones might not be adequate for design of buildings that should withstand tornadoes. The pressure coefficient values measured for the zones delimited as per the NBCC guidelines have a large variability shows that these zones might not be encompassing the areas of the roof and walls of similar tornado-induced pressures. Changing the zone areas could lead to pressure coefficient values that are more consistent for each specific zone.

For a complete adaptation of the C_T values to the C_pC_g values and for a concrete amendment proposal for the new version of the NBCC 2015, a vast experimental program should be conducted, while the current study performed experimental investigations for only three models. Additional scenarios with different building orientation angles would need to be performed under tornadic flow conditions simulated in the WDS facility. In order to determine an adequate time exposure duration to find a C_T value, a complete analysis would need to be performed. Determining a value that is conservative enough, without being unrealistic, to adopt the building code is important. The potential solution to withstand tornadic winds needs to be effective and realistic in terms of cost and material availability. Therefore, a full analysis would need to be done in order to prove that the level of conservativeness.

The pressure coefficients experimentally obtained are not always exceeding the C_pC_g value for the NBCC and a time duration of 10 s could be conservative enough, as most of the experimental data is not exceeding the NBCC requirement at this duration. In practice, determining this exposure duration value should be based on historic data of tornadoes events in North America. The dimensions, translation speeds and maximum wind velocities should all be taken into consideration when determining the duration that a house would be exposed to these tornadoes, as well as the level of damage expected.

An alternative to study exposure duration's effects on the pressure coefficient values is to use a probabilistic method instead of finding the average of the 100 samples. For instance, if the 100 samples are taken, and the 95th percentile value is taken considered for the C_T of that exposure duration, it could lead to a more practical approach to finding a C_pC_g value for the NBCC. A probabilistic approach could also be paired with current historic tornado data in order to find a tornado translation speed that is adequate to consider in design codes.

After comparing the experimental C_T results to those of the minimum values for cladding and secondary structural members as well as for primary structural members, the following conclusions can be made:

-The duration effects were a useful analysis of pressure coefficients for cladding and secondary structural members design, but proved to be less applicable for the primary structural members because the building code criteria might not be conservative enough for the tornado intensity that was tested. However, for the cladding and secondary structural members, the duration effect could be more useful since, at lower durations, the experimental C_T values did not exceed the NBCC 2015 values.

-Further research needs to be conducted to improve the method and to determine if it is possible and practical to use a similar duration analysis when studying experimental stationary tornadoes.

- For the secondary structural members, NBCC 2015 criteria for Zone C of the WDS experiments were the most conservative of the zones on the roof because, for nearly all durations and for the 3-peak average, the values are within the limit of the code C_pC_g.

-The tornado-induced pressure coefficients for Zone S and especially Zone R were much greater than the NBCC 2015's limit C_pC_g values. This shows that there is a large difference between ABL straight-line winds and tornadic winds. The roof is more prone to high suction pressures compared to the walls. The exceedance factor between experimental C_T values and NBCC 2015 C_pC_g values was up to 5.5 on the roof. Additional research should be performed to determine the adequacy of the NBCC 2015 values for tornadic winds, especially for the roof zones.

-The tornado-induced pressure coefficients registered on the walls were much closer to the minimum C_pC_g values of the NBCC 2015, but there were still many cases where some of the walls were under greater suction than the limit specified in the NBCC 2015. For walls, the difference between the NBCC 2015 values and the experimental values were not significant. The exceedance factor was, at most, 2.1. The NBCC 2015 could include future improvements to create a more conservative C_pC_g for the wall zones subjected to tornadoes.

Only a few conclusions could be made regarding the primary structural members, since almost all the C_T values exceeded the NBCC 2015 recommended C_pC_g pressure coefficients.

-There was a much greater exceedance factor in the primary structural members when compared to the cladding and secondary members. The maximum exceedance factor on the roof was 11.6 for Load case A and 15.9 for Load case B. The maximum exceedance factor on the walls is 4.2 for Load case A and 5 for Load case B.

-The large difference between experimentally determined peak pressure coefficients and the NBCC 2015 C_pC_g values show that additional research is required to find the best methodology of analysing tornadic winds on the primary structure components.

Chapter 6 Conclusions

6.1. Experimental program conclusions

The pressure coefficient results from the tornado simulation experiments were used to investigate the effects of a simulated EF-3 tornado on three residential house models. A tornado was simulated in the WDS by setting the fan at 700 RPM while opening one inlet at each corner of the testing chamber. The models were tested at radii of 10 cm, 25 cm and 40 cm from the center of the tornado. The results for the 10 cm radius were discussed in detail as these recorded the most significant pressure trends and magnitudes observed on the models.

Based on the analysis of the roof, the greatest suction, corresponding to the highest negative pressure coefficient, was found near the roof ridge as well as in the middle area of the roof for all the tested models. This is an interesting result since, for ABL straight-line wind tests, the peak pressure coefficients are found on the corners or edges of the roof. Another observation drawn from the performed experimental program, was that the leeward roof was always under greater suction than the windward roof. Conclusive reasoning for this was difficult to formulate without visually matching the tornado flow parameters with the pressure tap data, which is recommended to be done in future experiments. The leading edge of the roof was under less suction than the center and trailing edge sections of the roof. This could be attributed to the flow deviating from the wall or roof edge and creating a greater negative pressure coefficient zone in the central part of the roof, resulting in an increased suction. Another finding was that Model 1 and Model 2, with a 16° roof pitch angle had greater suctions by a factor of 1.5 to 2x to those found on Model 3, which had a higher pitch angle of 36°.

For the comparison of Model 1 to Model 2, it was noticed that Model 1 had a lower magnitude of pressure coefficients on the walls compared to Model 2. This could be due to the smaller base dimensions of Model 2, and consequently Model 3, that has the same base dimensions as Model

2. One reason for this is that Model 1, with the large base dimension, is in a slightly different region of the vortex compared to Model 2 and Model 3. Especially for the Model 1, Case 2 and Model 1, Case 3, where the BOA of the models were 45° and 90° respectively, since this causes portions of the walls to be further away from the vortex core than Model 2 and Model 3. Therefore, building geometry could have an effect on the pressure coefficient magnitudes on models due to the effects of the positioning of the house relative to the tornado.

When comparing Model 2 to Model 3, the walls of Model 2 were almost always under greater suction. There are two different hypotheses as to why this is the case. The first is the wall height of Model 3 is 47.7 mm compared to the 37.1 mm height of Model 3. This could result in the formation of a greater sized negative pressure zone on the walls of Model 2. The second hypothesis is that the effect of the roof pitch angle could be influencing the C_p values' magnitudes. The greater roof pitch angle could potentially lead to the tapering off of the negative pressure zone due to the increased roof slope, while the low roof pitch angle could allow the formation of a greater negative pressure zone. There were no significant observations regarding the C_p values' magnitudes of the bottom, middle, and top pressure tap rows of the walls so this hypothesis cannot be proven. However, this could be an interesting area to further research, where obtaining pressure data at a higher concentration on certain regions of the walls could help understand the pressure trends near the connection of the wall to the edge of the roof.

For the walls, the effect of the BOA did not seem to have a significant effect on the trends of the pressure coefficient measurements. A redistribution of the pressure coefficient trends was observed when the BOA changed from 0° to 90°, but the magnitude was not significantly impacted. For all BOA's tested, the wall nearest to the center of the vortex was under the greatest suction, most likely due to the increased suction and velocities in the core of the tornado. One observation that was made for every house model, was that the peak suction was on the leading edge of each wall relative to the clockwise flow direction of the tornado. This creates a torsional effect on the house models. The torsional forces exerted by full-scale tornadoes have been observed to cause failures of houses by tearing out the anchors connecting the sill plate to the foundation (Prevatt et al., 2012) and this may have been observed in the experimental scaled-down setting employed in the current research.

6.2 NBCC 2015 analysis conclusions

With the pressure data obtained from the experiments, a tornado exposure duration analysis was performed. For each pressure tap, the peak C_p value was taken from duration segments that were randomly selected 100 times from the combined three 30 s trials. The duration segments were 0.1 s, 0.5 s, 1-10 s, 15 s, 30 s, 60 s and 90 s. The average of all 100 C_p values were then found for each duration and was reported as C_T. The pressure taps were grouped by the zoning defined in the NBCC 2015 Figure 4.1.7.6-A, -B for primary structural member design and Figure 4.1.7.6-B, -E for cladding and secondary structural members. The experimental peak pressure coefficient, C_T, was compared to the C_pC_g values in the NBCC 2015 wind provision. For the shorter exposure durations of 0.1 s, the C_pC_g value was about 2 times smaller, compared to the full 90 s duration. The use of different exposure durations could be employed to find a conversion between the pressures induced by stationary and translating tornadoes. Also, the tornado exposure duration analysis could serve as a better estimating method for the C_pC_g values adapted for tornado resistant design in NBCC 2015; for instance, a larger duration could be similar to a larger factor of safety.

When following the NBCC 2015, procedure for cladding and secondary structural members, the peak pressure coefficients, C_T, on the walls measured in the current experiment were adequate when compared to the code C_pC_g recommended values for most durations. However, for the zones of certain walls, the exceedance factor was up to 2.1. This could warrant additional studies as the exceedance factor was significant. The NBCC 2015 could need amendments in order to adopt more conservative C_pC_g values for the walls of residential houses located in tornado-prone regions. The interior section and the edges of the roof recorded experimental peak pressure coefficients, C_T, which were much greater than the C_pC_g values' provisions in the NBCC 2015, with an exceedance factor of up to 5.5. For the roof corners, the NBCC 2015 provisions seemed adequate when compared to the peak pressure coefficients, C_T, determined in the experiments. Results showed that the experimental C_T values were much greater than the C_pC_g values in the NBCC 2015 for the primary structural elements for all duration intervals. This is not surprising as the building code is not adapted to withstand EF-3 tornadoes. However, the magnitude of the experimental C_T values for some of the zones was significant when compared to the NBCC 2015 recommended C_pC_g. This leads to the question of the necessity of updating the building code to reflect wind design for structures in tornado-prone regions. Another conclusion that is drawn when making a parallel between the NBCC 2015 provisions and the results from the current tornado experiment is that NBCC 2015 is using positive C_pC_g values for some loading zones. For tornado-induced pressures, the house models were almost always under suction except for a few locations where the C_T value was 0 or slightly positive, but still near 0. This requires additional work to determine if more flexible NBCC 2015 criteria's are required to be changed to plan for positive pressures caused by ABL winds and negative pressures when designing structures to withstand tornado-induced pressures.

6.3 Recommended future work

The current research experimentally investigated the tornado-induced pressure coefficients at the surface of three scaled residential house models, and compared these values with the NBCC 2015 recommended pressure coefficients for wind design of low-rise buildings. Some of the tornadic flow and building geometry parameters were not considered. Thus, the following aspects can be recommended for further in-depth analysis.

- Additional WDS tests should be performed to simulate EF-1 and EF-2 tornadoes, in order to see if the wind provisions in the NBCC 2015 are adequate for lower EF tornadoes. In addition, more models of different and complex geometries should be tested to generate more experimental data for comparison with the building code recommended criteria.
- Additional research should be performed to determine the adequacy of the NBCC 2015 recommended pressure coefficients for tornadic winds, especially for the roof Zone s and roof Zone r (edges and middle of the roof), where for the current analysis high exceedance factors of up to 5.5 were found.
- Further research could help improve the exposure duration method and help determine if it is possible to compare stationary tornado pressures to a translating tornado by influencing the exposure duration.
- A method of accurately determining the swirl ratio in the WDS needs to be determined. This could be done by using a PIV method or a more thorough flow analysis.

- The large difference between experimental CT values and the NBCC 2015 CpCg values for primary structural elements could require additional research to find a better way of analysing tornadic winds on the primary structure.
- One last scenario that should be tested is the effects of the model placement perpendicular to the expected translation path. In the current experiments, the model is placed directly perpendicular to the horizontal velocity parameter. However, shifting the model away from the expected tornado path at small increments, 5 cm or less, could result in different flows on the house, thus creating different CpCg values along the walls and roofs. If an in-depth analysis were to be made, these ideas should be taken into more consideration.

Reference

Aeroprobe PS12 / PL12 Omniprobe. (2020, September). Retrieved from https://www.chell.co.uk/pressure/motorsport/multi-hole-probe/aeroprobe-ps12---pl12-omniprobe

Aldoum, Murad. “Wind Loads on Low-Slope Roofs of Low-Rise and Mid-Rise Buildings with Large Plan Dimensions.” Concordia University, 2018.

Amit R. Mishra, Darryl L. James,, Chris. W. Letchford (2008). Physical simulation of a single-celled tornado-like vortex, Part A: Flow field characterization. Journal of Wind Engineering and Industrial Aerodynamics 96 (2008) 1243–1257

Ashrafi, Arash., et al. “Experimental investigation of large-scale tornado-like vortices.” Journal of Wind Engineering and Industrial Aerodynamics, vol 208, 2021, p. 104449

Case, Jeremy Michael. “Effect of Building Geometry on Wind Loads on Low-Rise Buildings in a Laboratory-Simulated Tornado with a High Swirl Ratio.” Iowa State University, 2011

Church, C.R., J.T. Snow, G.L. Baker, E.M. Agee, “Characteristics of tornado-like vortices as a function of swirl ratio: A laboratory investigation,” Journal of the Atmospheric Sciences, v. 36, (1979) 1755-1776.

Davies-Jones, R.P., “Laboratory Simulation of Tornadoes,” Proceedings of the Symposium on Tornadoes, Assessment of Knowledge and Implications for Man, ed. R.E. Peterson, Texas Tech University, (1976) 151-174.

Engineering, O. (2020, July 29). Pitot Tubes. https://www.omega.ca/en/resources/pitot-tube

H.P. Hong*, Q. Huang, W.J. Jiang, Q. Tang, P. Jarrett. 2021. Tornado wind hazard mapping and equivalent tornado design wind profile for Canada, Structural Safety 91 (2021) 102078

Haan, F. L., Balaramudu, V. K., & Sarkar, P. P. (2010). Tornado-induced wind loads on a low-rise building. *Journal of Structural Engineering*, *136*(1), 106–116. https://doi.org/10.1061/(asce)st.1943-541x.0000093

Haan, F. L., Sarkar, P. P. and Gallus W. A. (2008). Design, construction, and performance of a large tornado simulator for wind engineering applications. Engineering Structures 30 (2008) 1146–1159

Haan, Fred L. (April 2017) "An Examination of Static Pressure and Duration Effects on Tornado-Induced Peak Pressures on a Low-Rise Building." Frontiers in Built Environment, vol. 3, Article 20

Hangan, H., 2014. The wind engineering energy and environment (WindEEE) dome at western university, Canada. Wind Engineers, JAWE, 39(4), Volume 39 Issue 4 Pages 350-351https://doi.org/10.5359/jawe.39.350

Hu, H., Yang, Z., Sarkar, P., & Haan, F. (2011). Characterization of the wind loads and flow fields around a gable-roof building model in tornado-like winds. Experiments in Fluids, 51(3), 835–851. https://doi.org/10.1007/s00348-011-1102-6

Jischke, M. C., Light, B. D., "Laboratory Simulation of Tornadic Wind Loads on a Rectangular Model Structure," Proc. Sixth International Conference on Wind Engineering, v. 1, Australia & New Zealand (1983).

Kopp, G. A., & Wu, C.-H. (2020). A framework to compare wind loads on low-rise buildings in tornadoes and atmospheric boundary layers. Journal of Wind Engineering and Industrial Aerodynamics, 204, 104269. https://doi.org/10.1016/j.jweia.2020.104269

NBCC 2015, CANADIAN COMMISSION ON BUILDING AND FIRE CODES, NATIONAL RESEARCH COUNCIL CANADA & NATIONAL REEARCH COUNCIL OF CANADA. (2015). *National building code of Canada (NBCC).* Ottawa, Associate Committee on the National Building Code, National Research Council

Otis, J. R. and D. (2018, September 23). *Twin tornadoes damage dozens of homes, wipe out power across Ottawa-gatineau*. CTVNews. Retrieved January 29, 2022, from https://www.ctvnews.ca/canada/twin-tornadoes-damage-dozens-of-homes-wipe-out-power-across-ottawa-gatineau-1.4105213

Paglinawan, D. (2021, August 18). Tornado that hit Barrie caused $75 million in insured damages: Insurance Bureau. The Canadian Press. Retrieved from https://www.C_p24.com/news/tornado-that-hit-barrie-caused-75-million-in-insured-damages-insurance-bureau-1.5552266.

Prevatt, D. O., Coulbourne, W., Graettinger, A. J., Pei, S., Gupta, R., & Grau, D. (2012). Joplin, Missouri, Tornado of May 22, 2011. https://doi.org/10.1061/9780784412503

Ramseyer, C., Holliday, L., & Floyd, R. (2016). Enhanced Residential Building Code for tornado safety. Journal of Performance of Constructed Facilities, Volume 30(4), 04015084.

Refan, M., & Hangan, H. (2016, February 23). Characterization of tornado-like flow fields in a new model scale wind testing chamber. Journal of Wind Engineering and Industrial Aerodynamics Volume 151, April 2016, Pages 107-121

Refan, Maryam, and Horia Hangan. (April 2018) “Near Surface Experimental Exploration of Tornado Vortices.” Journal of Wind Engineering and Industrial Aerodynamics, vol. 175, 2018, pp. 120–135.

Rotunno, Richard. “The Fluid Dynamics of Tornadoes.” Annual Review of Fluid Mechanics, vol. 45, no. 1, 2013, pp. 59–84., https://doi.org/10.1146/annurev-fluid-011212-140639

Sabareesh, G. R., Matsui, M., & Tamura, Y. (2012). Dependence of surface pressures on a cubic building in tornado like flow on building location and ground roughness. Journal of Wind Engineering and Industrial Aerodynamics, vol. 103, pp. 50–59. https://doi.org/10.1016/j.jweia.2012.02.011

Stevenson SA, Kopp GA and El Ansary AM (2020) Prescriptive Design Standards for Resilience of Canadian Housing in High Winds. Front. Built Environ. 6:99. doi: 10.3389/fbuil.2020.000992

Wang, J., & Kopp, G. A. (2021). Comparisons of aerodynamic data with the main wind force–resisting system provisions of ASCE 7-16. I: Low-rise buildings. *Journal of Structural Engineering*, *147*(3), 04020347. https://doi.org/10.1061/(asce)st.1943-541x.0002925

Wang, J., Cao, S.Y., Pang, W.C., Cao, J.X., 2018. Experimental study on tornado-induced wind pressures on a cubic building with openings. J. Struct. Eng. 144.

Wang, Jin, and Gregory A. Kopp. "Comparisons of Aerodynamic Data with the Main Wind Force–Resisting System Provisions of ASCE 7-16. I: Low-Rise Buildings." Journal of Structural Engineering, vol. 147, no. 3, 2021, p. 04020347

Wang, Jin, et al. (November 2016) "Wind-Load Characteristics of a Cooling Tower Exposed to a Translating Tornado-like Vortex." Journal of Wind Engineering and Industrial Aerodynamics, vol. 158, 2016, pp. 26–36., doi.org/10.1016/j.jweia.2016.09.008.

Ward, N.B. (1972) The Exploration of Certain Features of Tornado Dynamics using a Laboratory Model. J. of the Atmospheric Sciences, 29, 1194-1204.

Yan, Y., Li, X., Tu, J., Feng, P., & Zhang, J. (2019). Characterisation and analysis of indoor tornado for contaminant removal and emergency ventilation. Building and Environment, 164, 106345. https://doi.org/10.1016/j.buildenv.2019.106345

Appendix A: Pressure coefficient on residential model surfaces

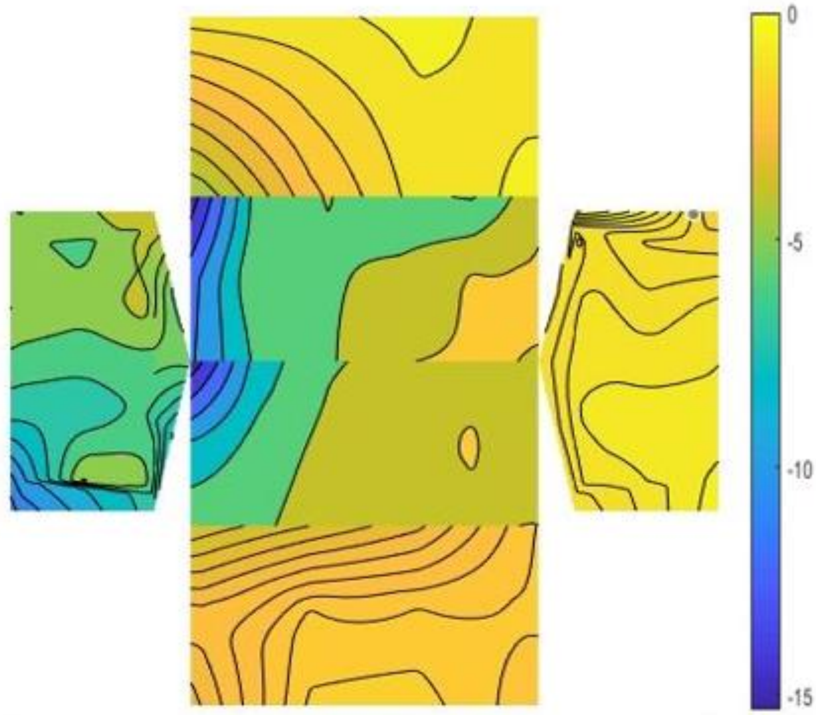

Figure A.1: Model 1, Case 4 (BOA:0°, D:25cm) Peak pressure coefficient contour plot

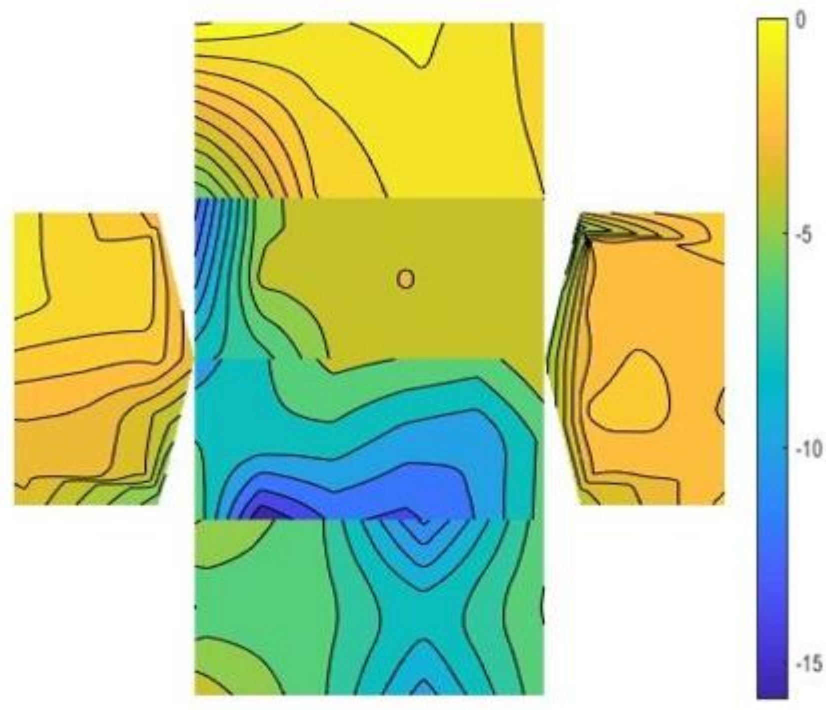

Figure A.2: Model 1, Case 5 (BOA:45°, D:25cm) Peak pressure coefficient contour plot

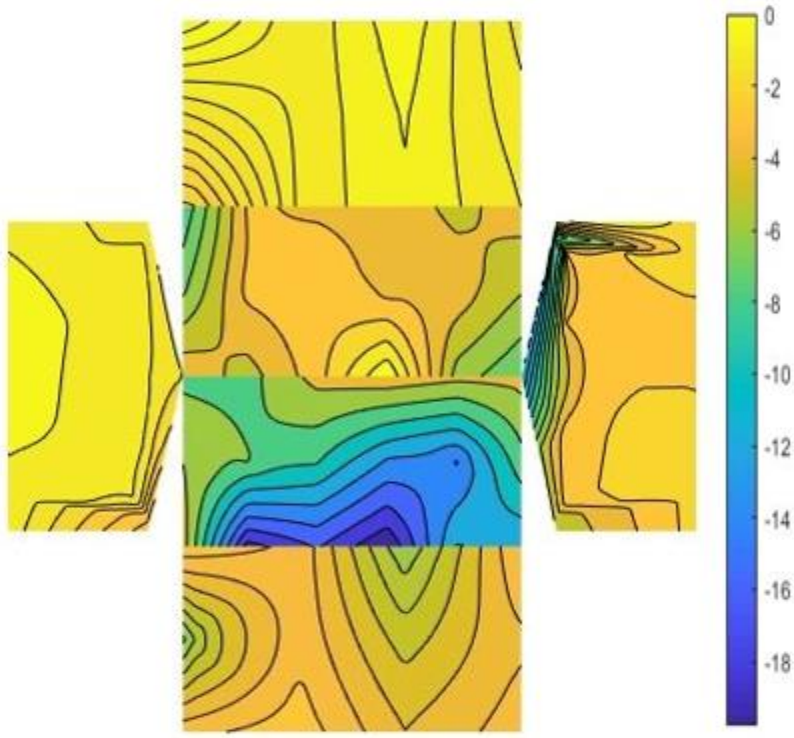

Figure A.3: Model 1, Case 6 (BOA:90°, D:25cm) Peak pressure coefficient contour plot

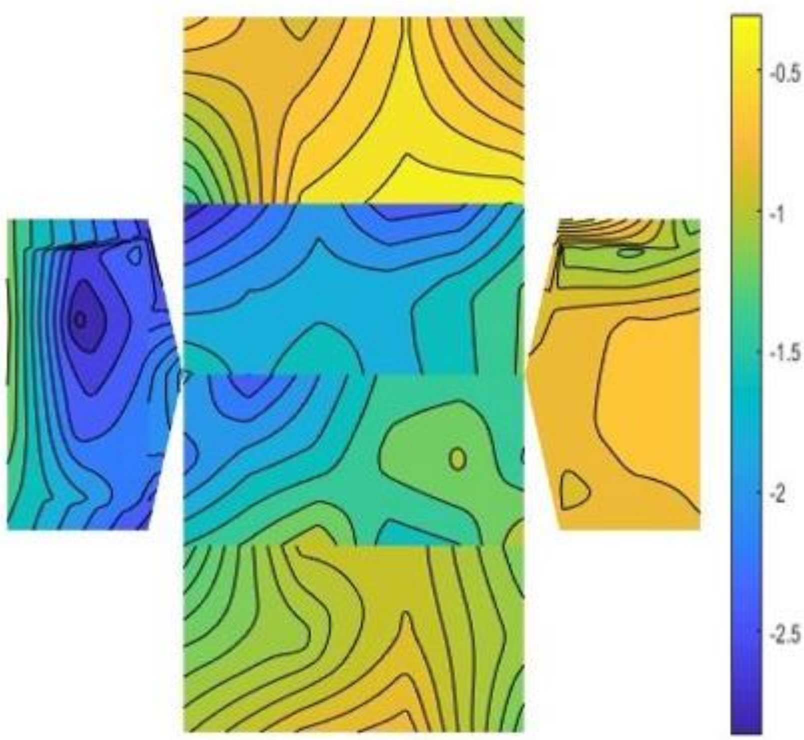

Figure A.4: Model 1, Case 7 (BOA:0 °, D:40cm) Peak pressure coefficient contour plot

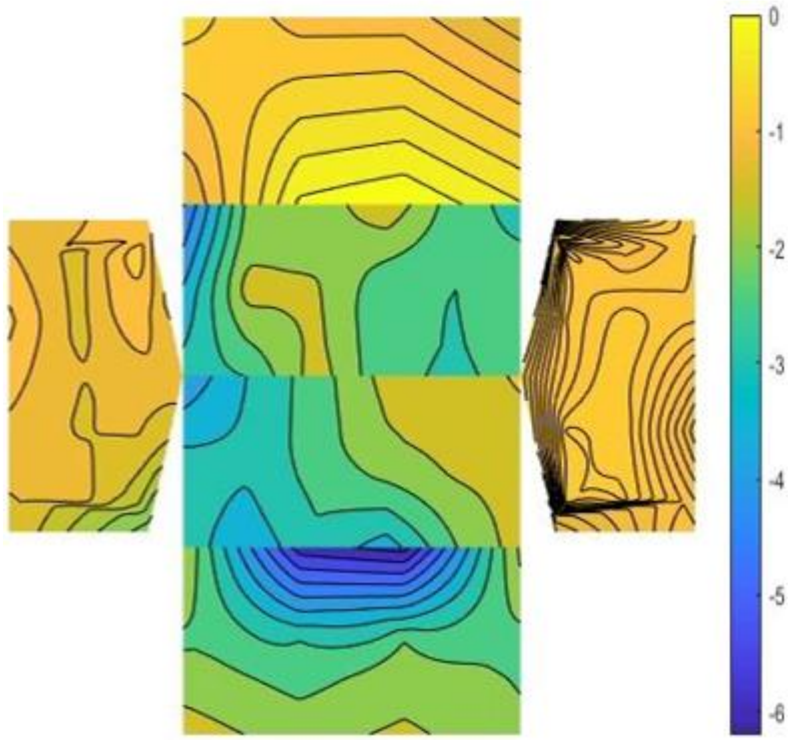

Figure A.5: Model 1, Case 8 (BOA:45 °, D:40cm) Peak pressure coefficient contour plot

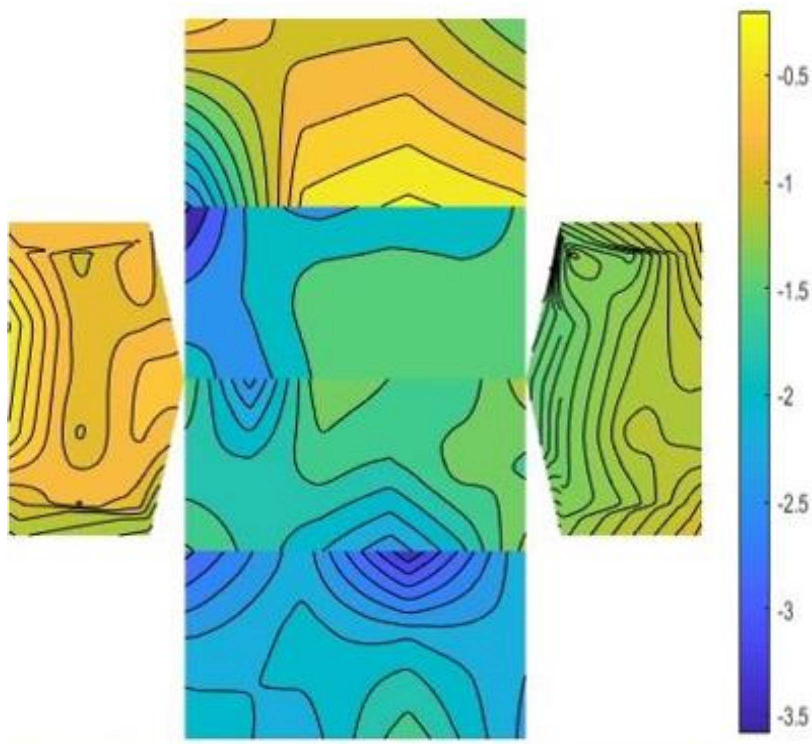

Figure A.6: Model 1, Case 9 (BOA:90 °, D:40cm) Peak pressure coefficient contour plot

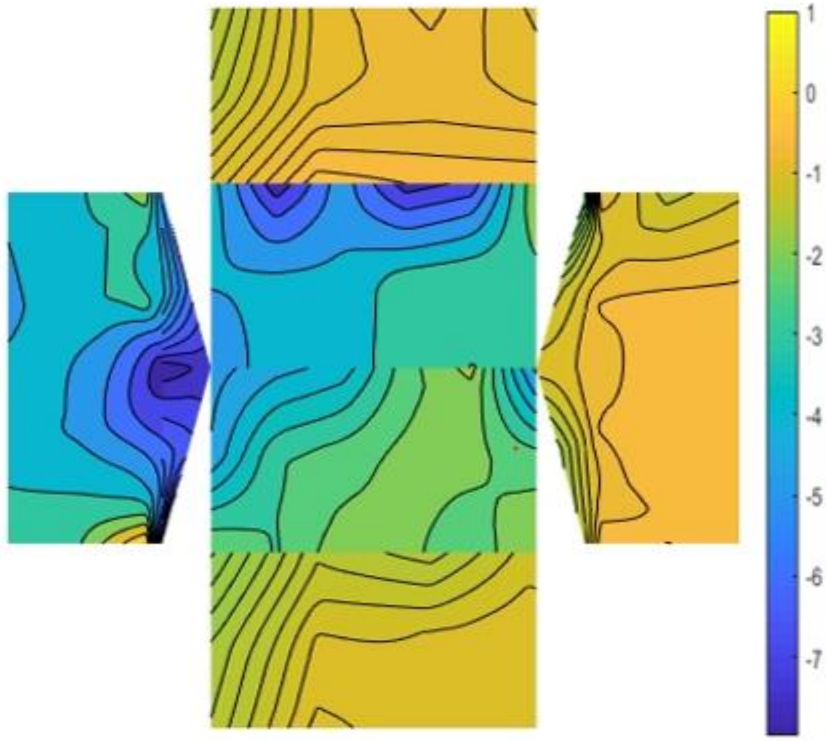

Figure A.7: Model 2, Case 4 (BOA:0 °, D:25cm) Peak pressure coefficient contour plot

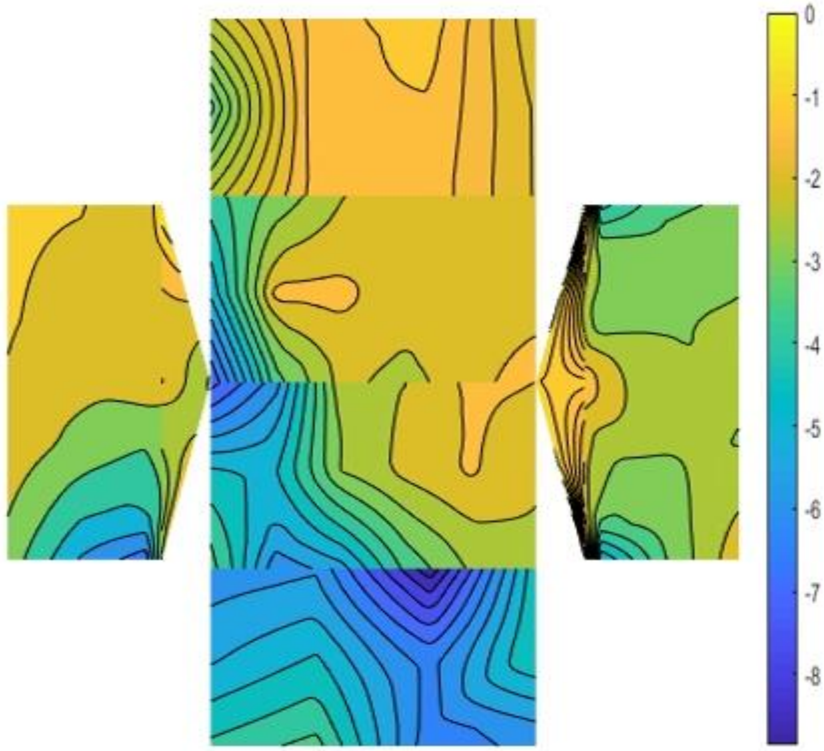

Figure A.8: Model 2, Case 5 (BOA:45 °, D:40cm) Peak pressure coefficient contour plot

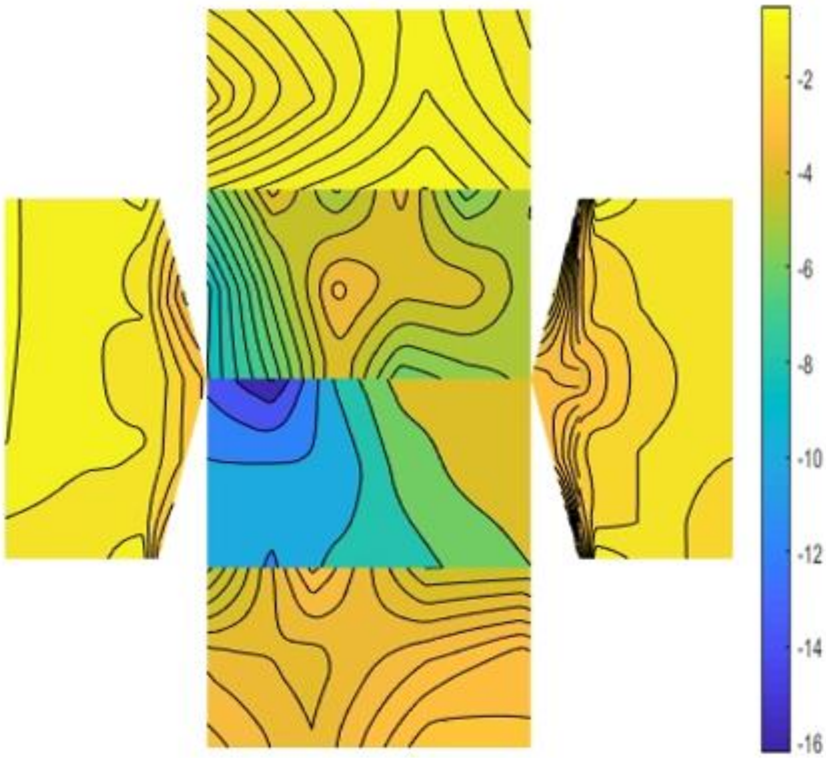

Figure A.9: Model 2, Case 6 (BOA:90 °, D:40cm) Peak pressure coefficient contour plot

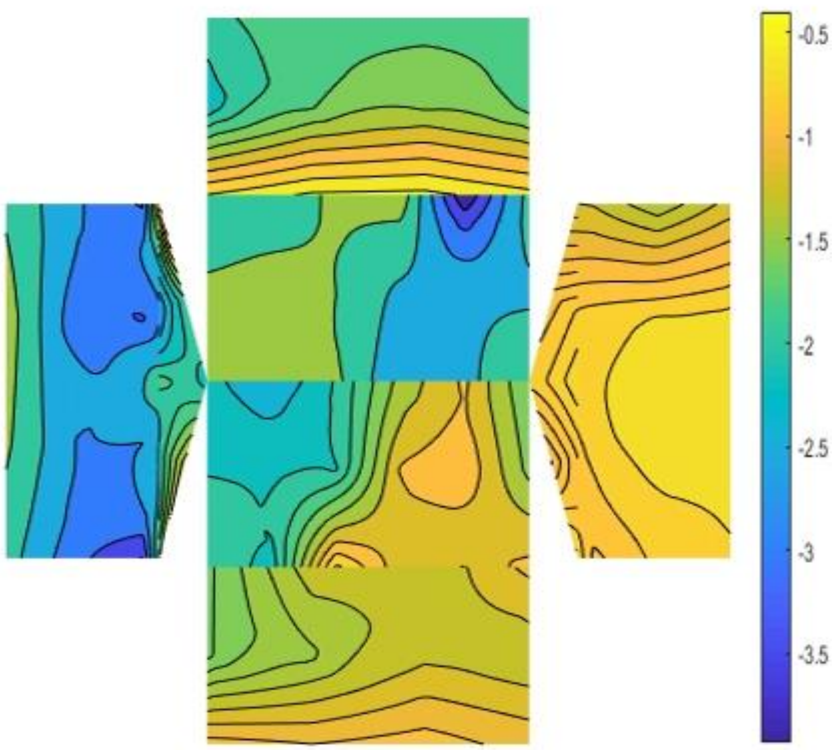

Figure A.10: Model 2, Case 7 (BOA:0°, D:40cm) Peak pressure coefficient contour plot

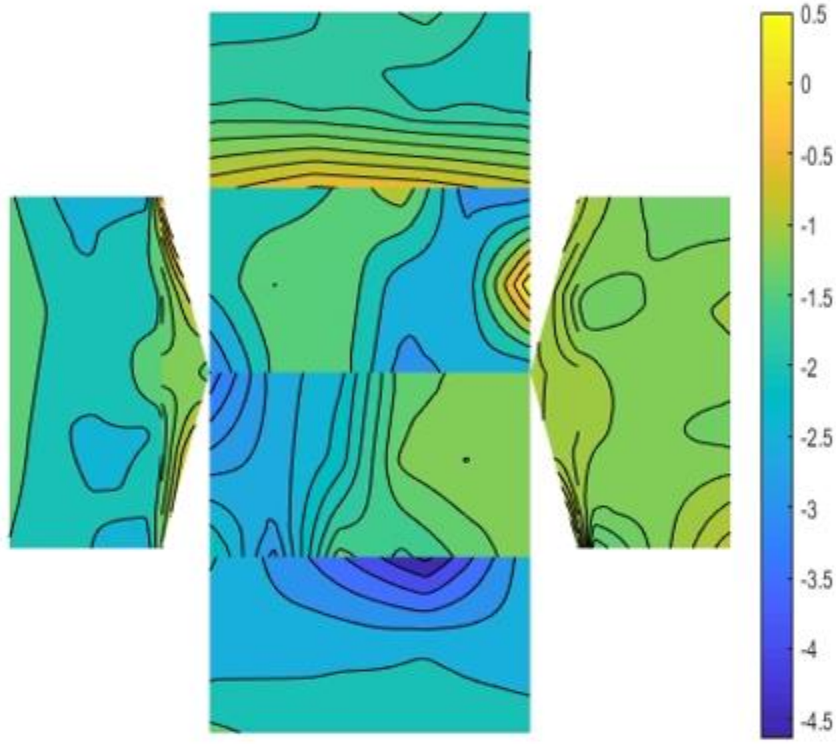

Figure A.11: Model 2, Case 8 (BOA:45°, D:40cm) Peak pressure coefficient contour plot

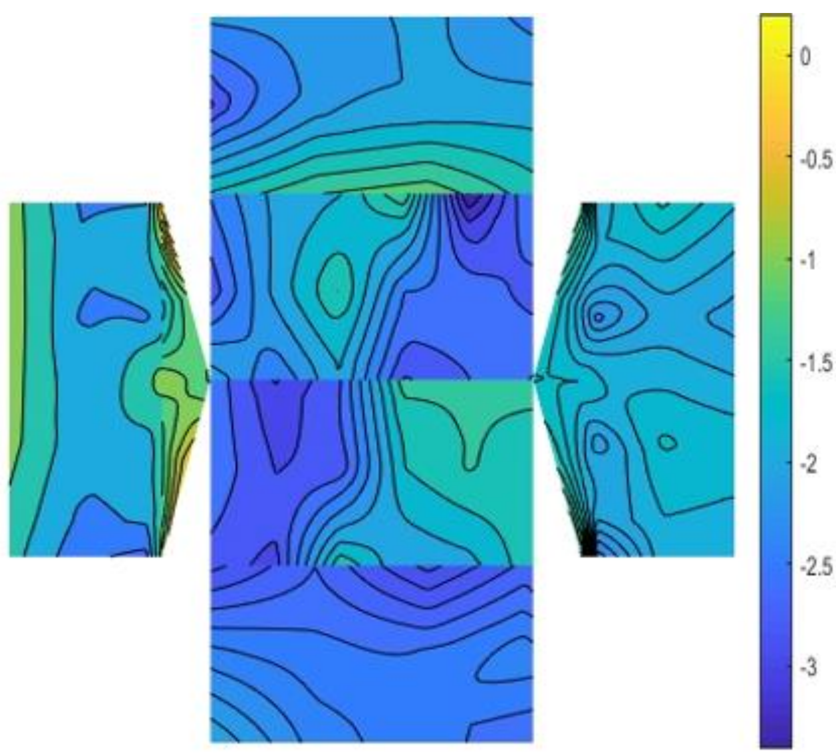

Figure A.12: Model 2, Case 9 (BOA:90°, D:40cm) Peak pressure coefficient contour plot

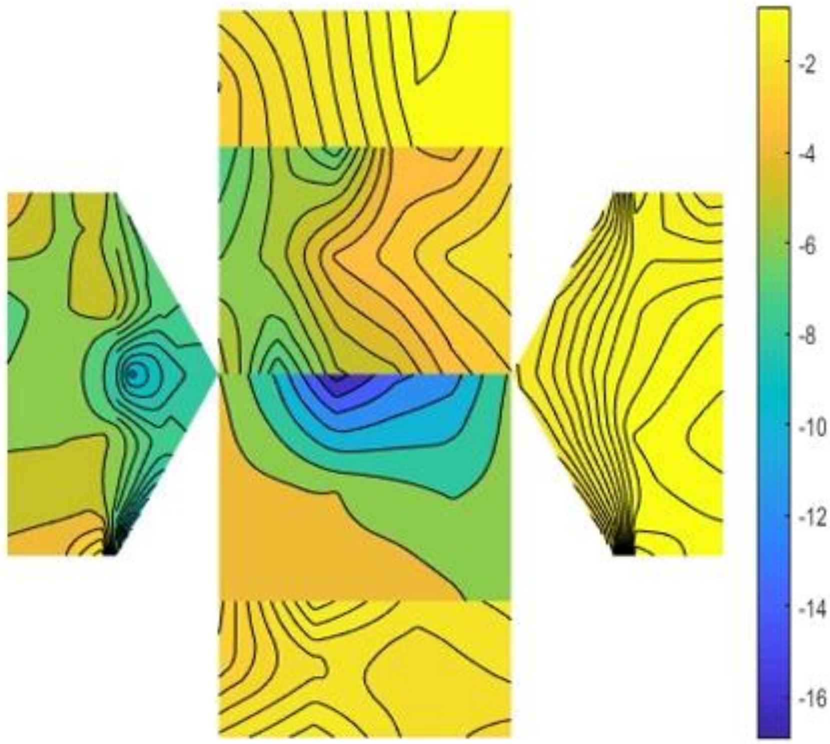

Figure A.13: Model 3, Case 4 (BOA:0°, D:25cm) Peak pressure coefficient contour plot

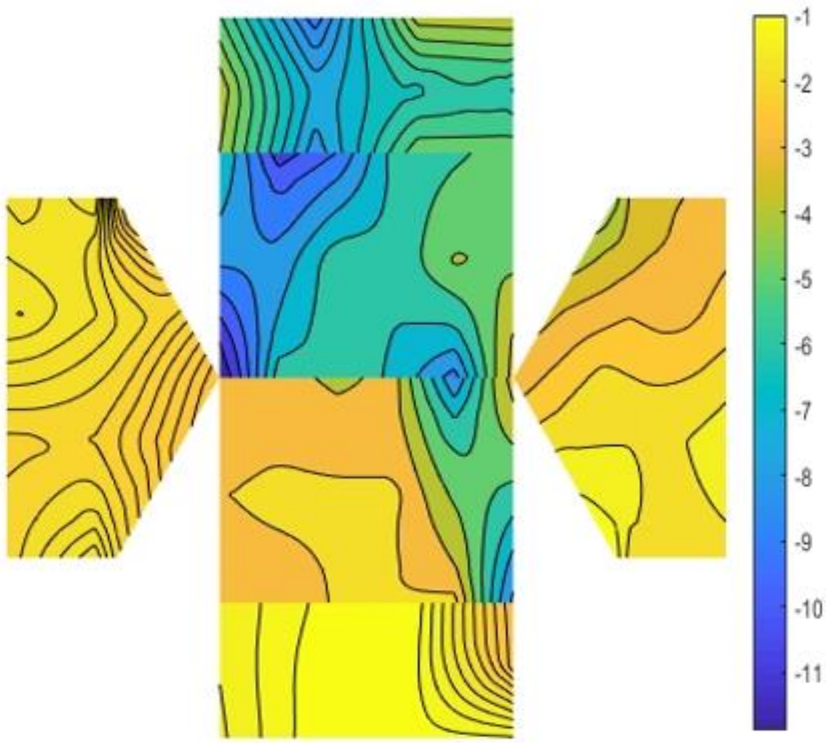

Figure A.14: Model 3, Case 5 (BOA:45°, D:25cm) Peak pressure coefficient contour plot

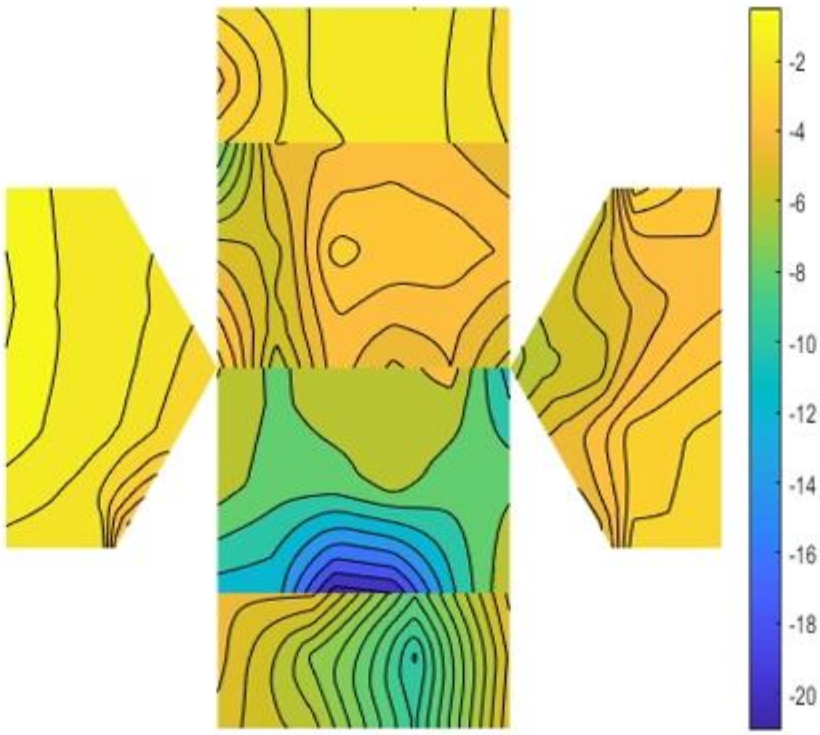

Figure A.15: Model 3, Case 6 (BOA:90°, D:25cm) Peak pressure coefficient contour plot

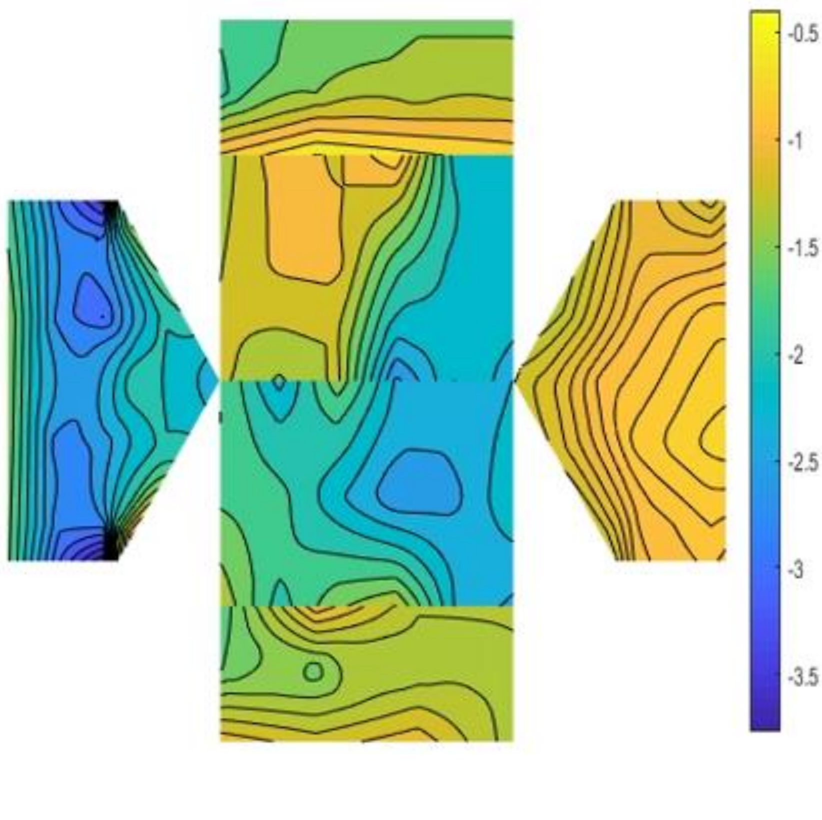

Figure A.16: Model 3, Case 7 (BOA:0°, D:40cm) Peak pressure coefficient contour plot

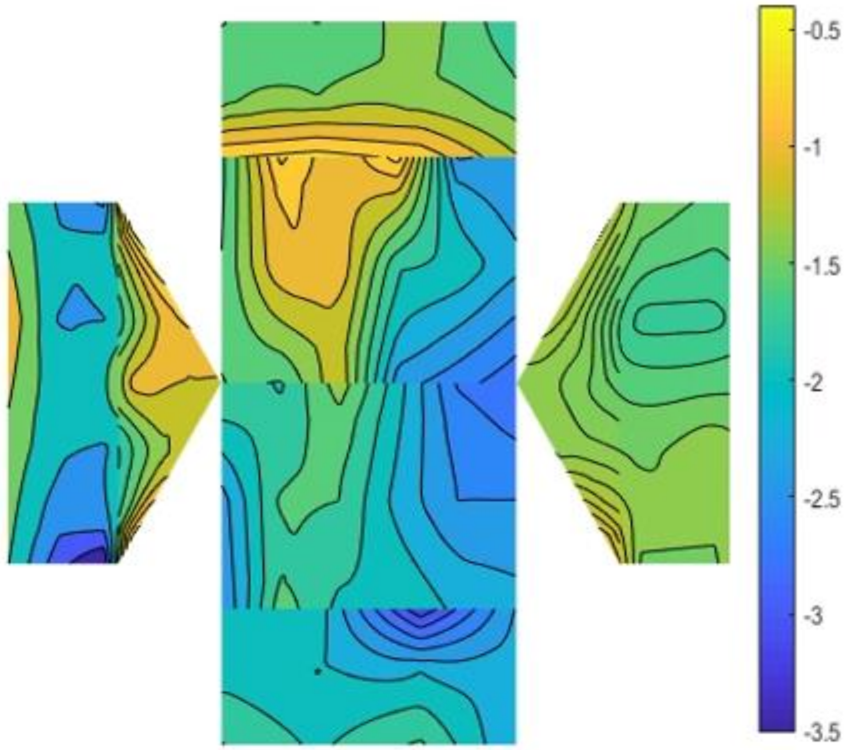

Figure A.17: Model 3, Case 8 (BOA:45°, D:40cm) Peak pressure coefficient contour plot

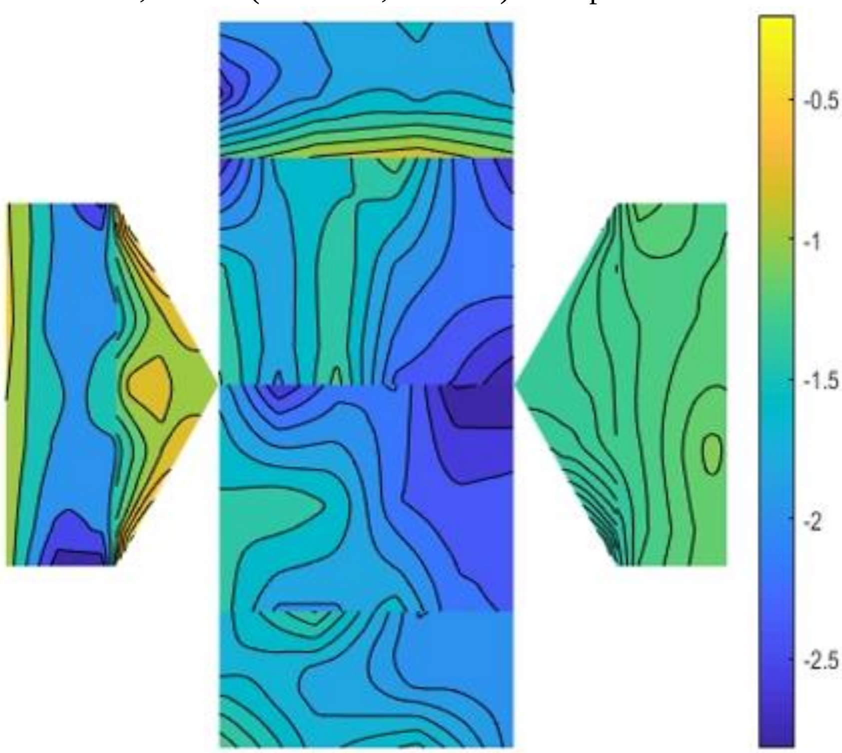

Figure A.18: Model 3, Case 9 (BOA:45°, D:40cm) Peak pressure coefficient contour plot

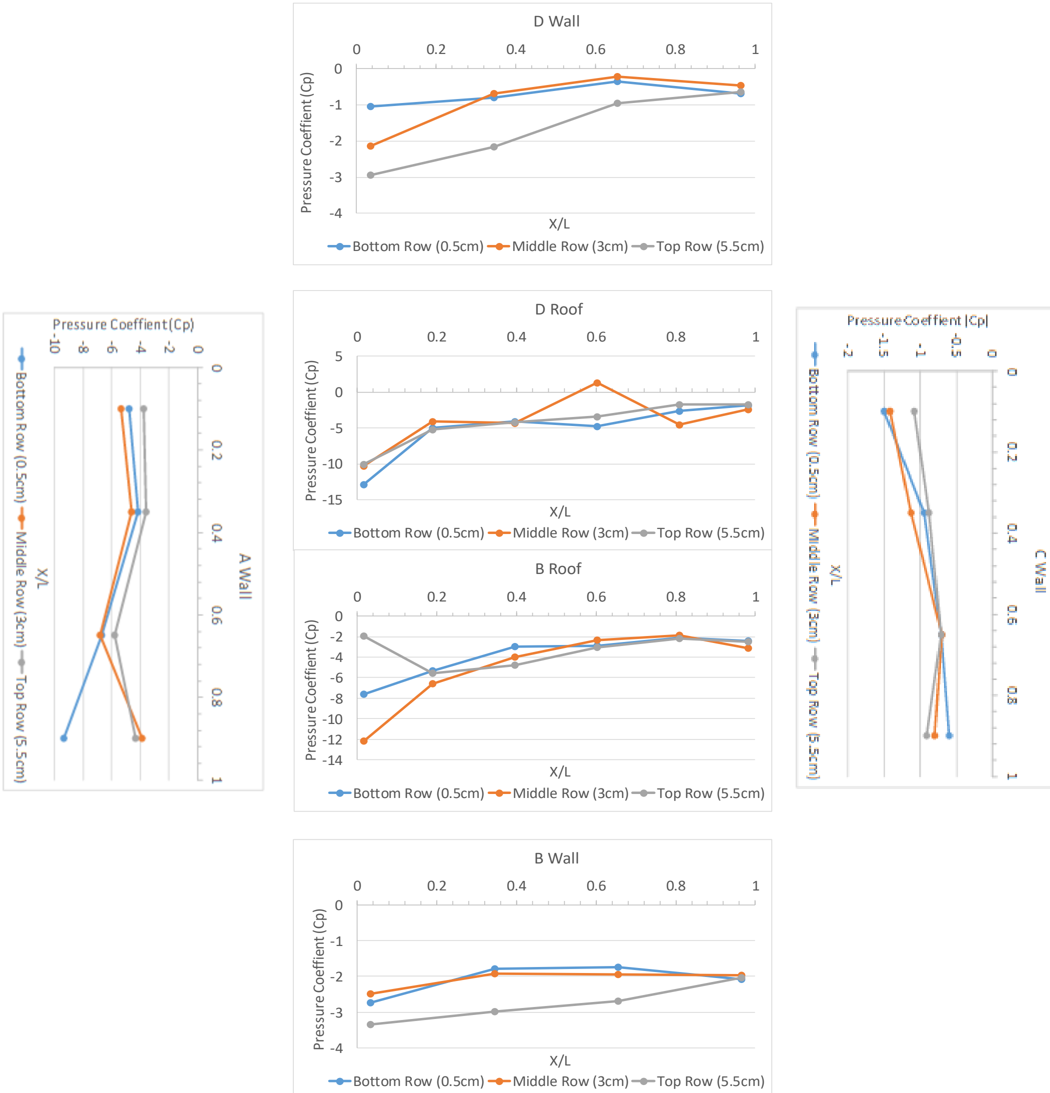

Figure A.19: Model 1, Case 4 (BOA:0°, D:25cm) Peak pressure coefficient plots

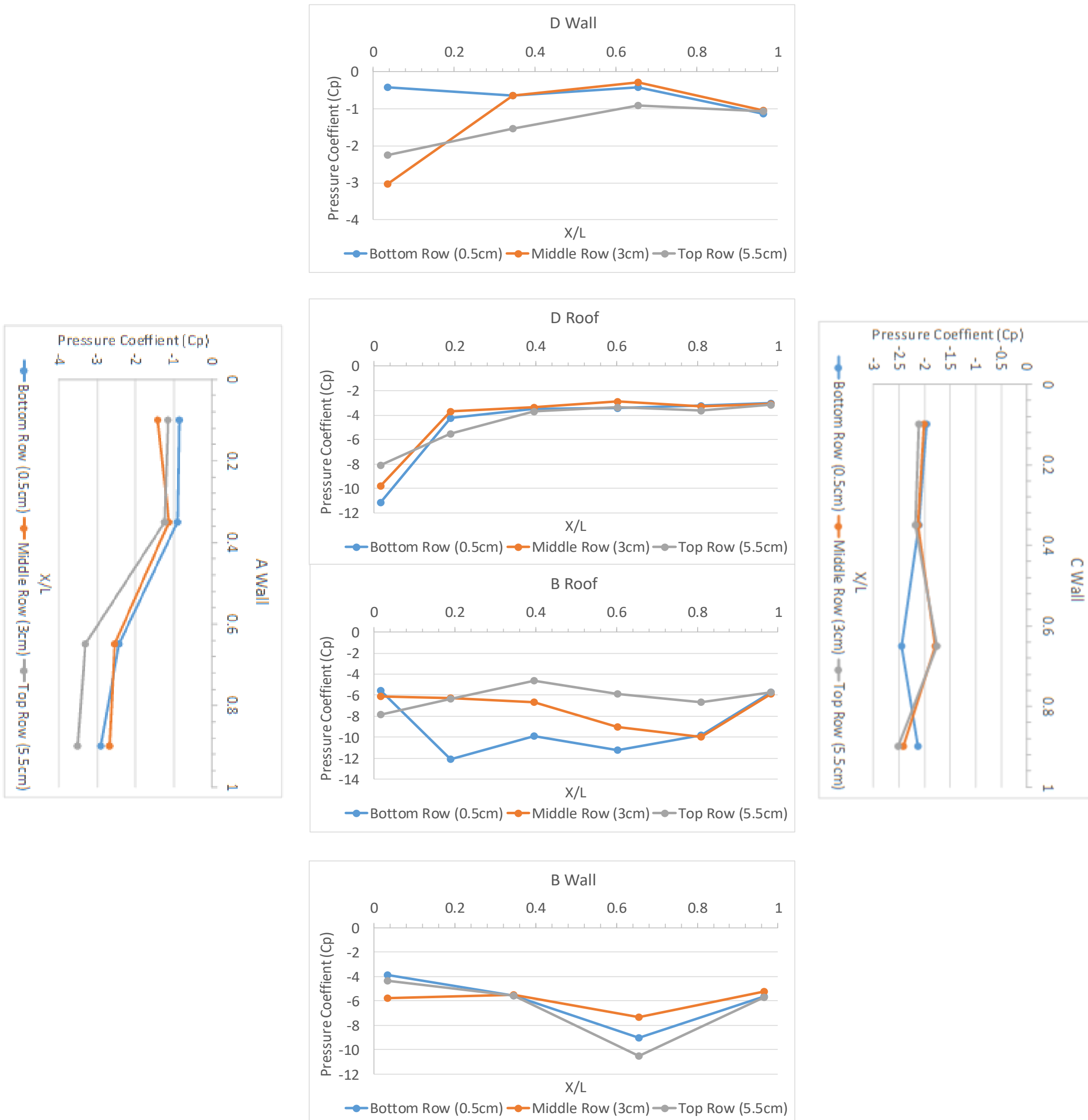

Figure A.20: Model 1, Case 5 (BOA:45°, D:25cm) Peak pressure coefficient plots

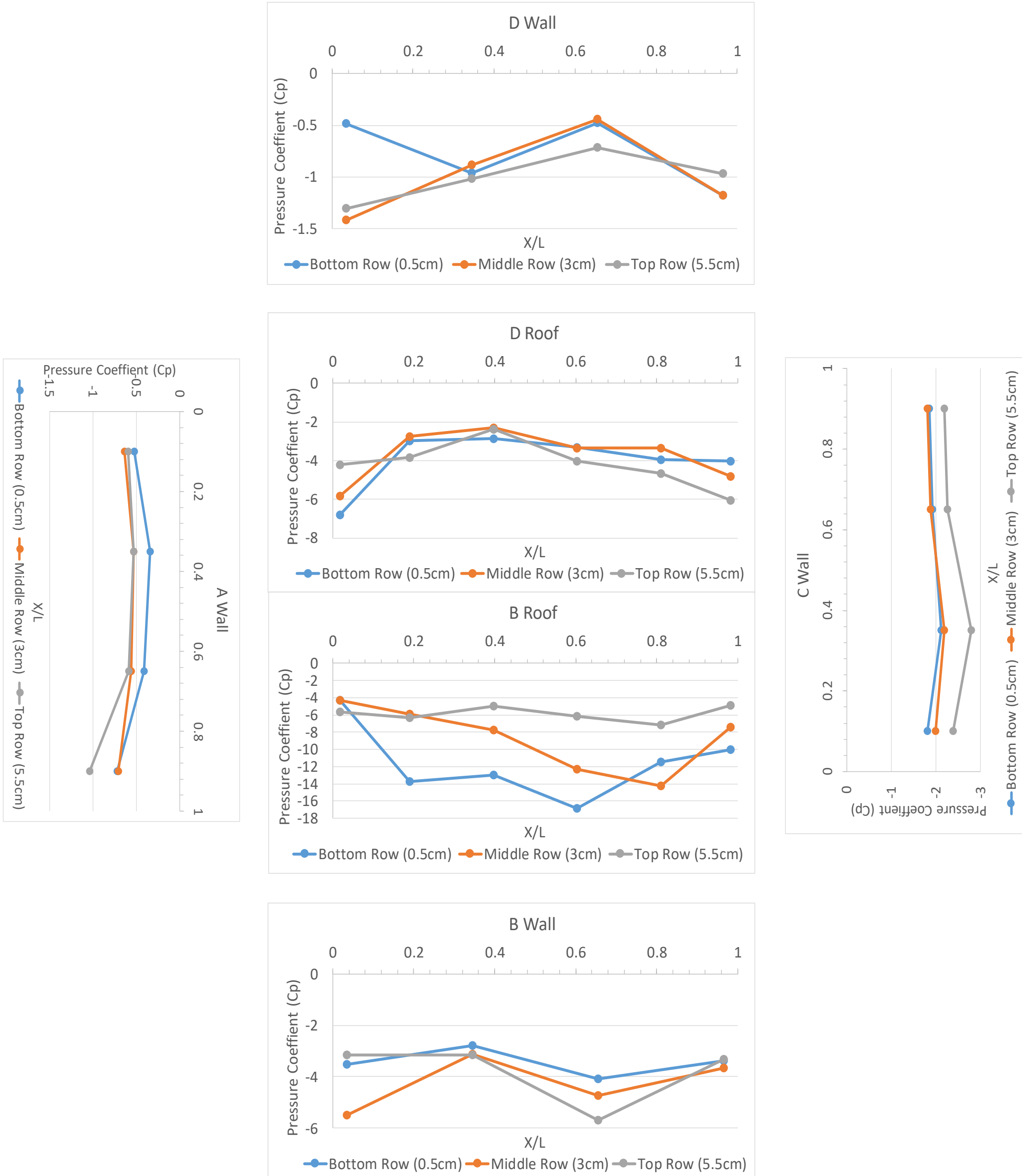

Figure A.21: Model 1, Case 6 (BOA:90°, D:25cm) Peak pressure coefficient plots

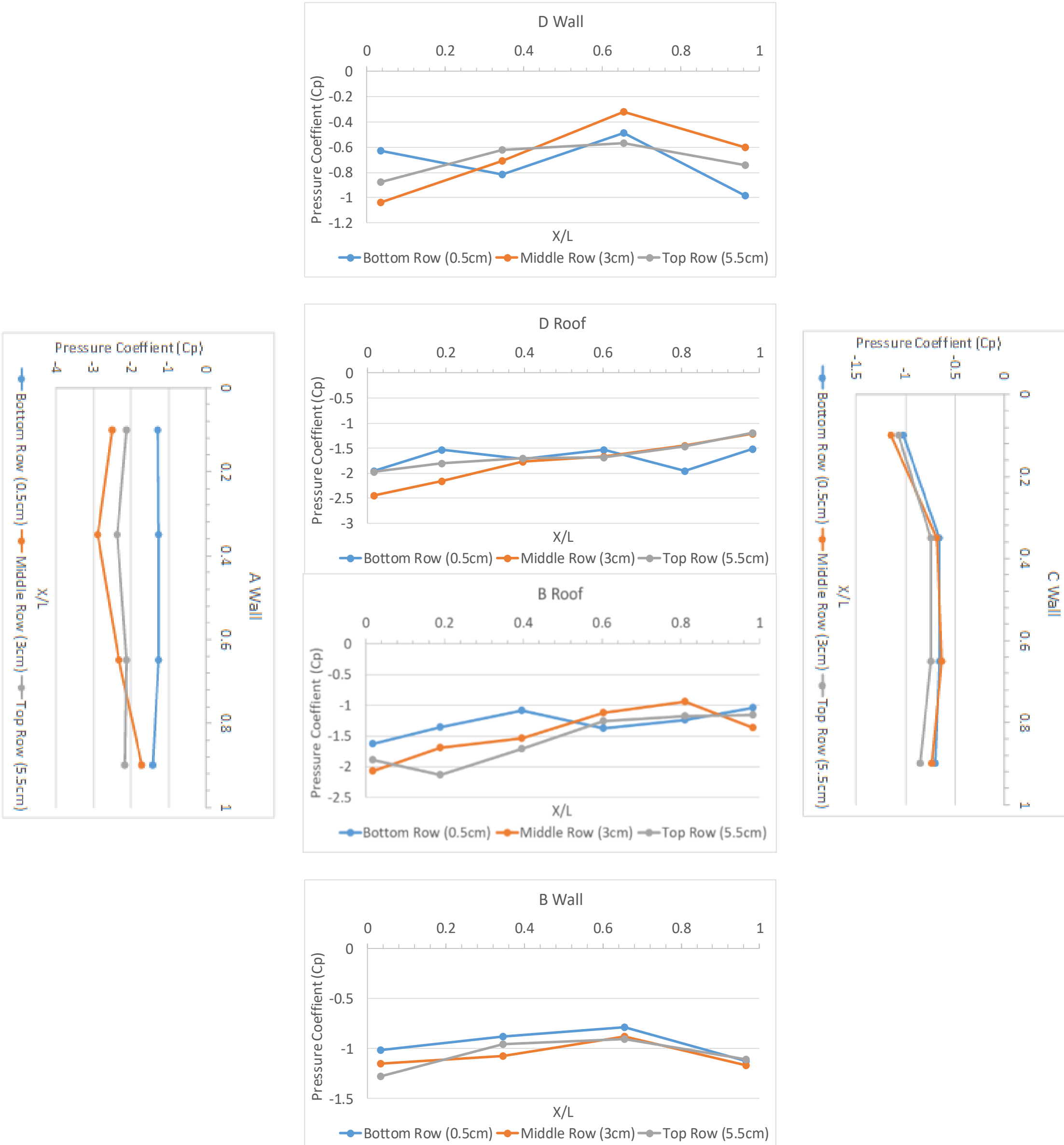

Figure A.22: Model 1, Case 7 (BOA:0°, D:40cm) Peak pressure coefficient plots

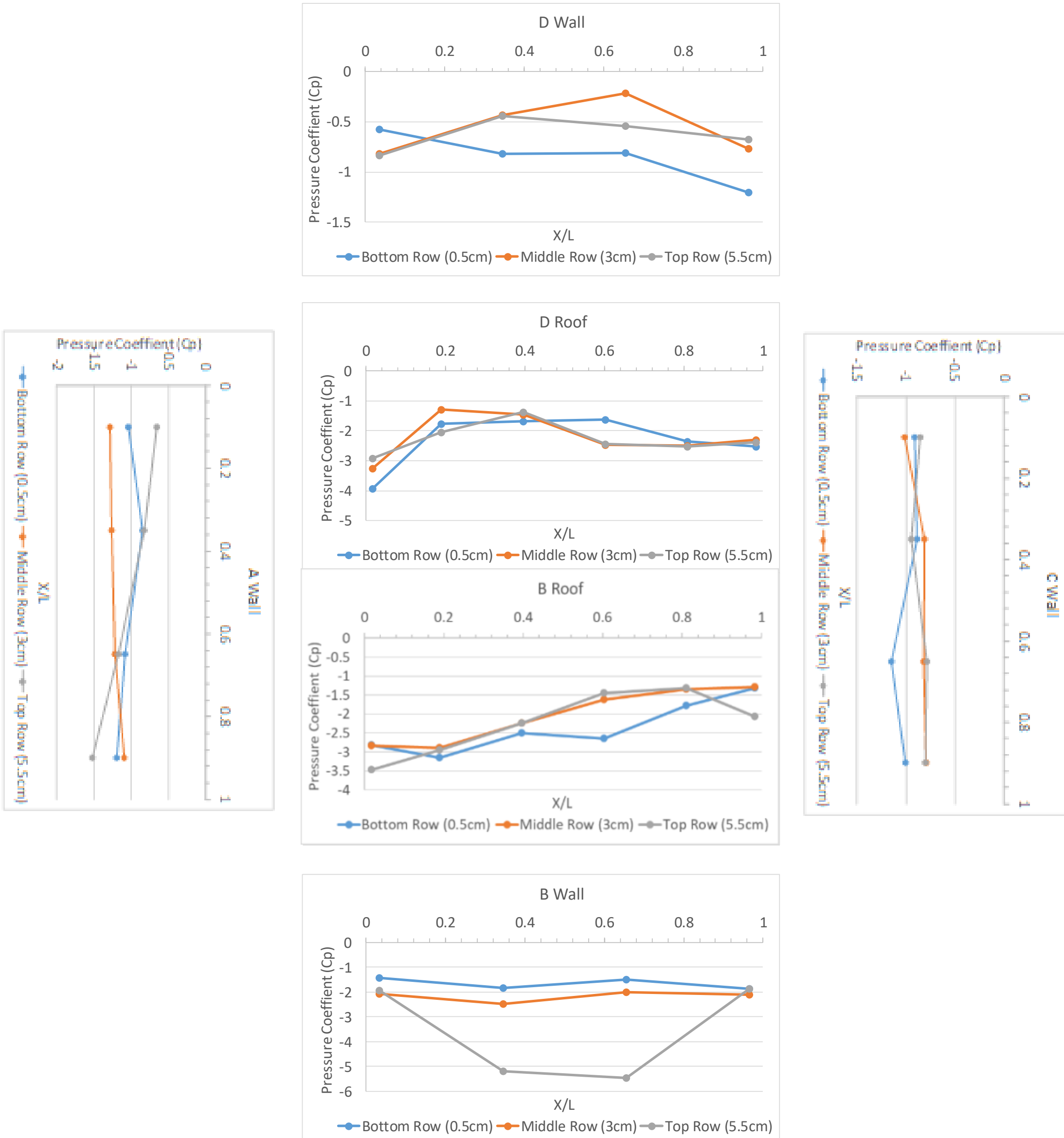

Figure A.23: Model 1, Case 8 (BOA:45°, D:40cm) Peak pressure coefficient plots

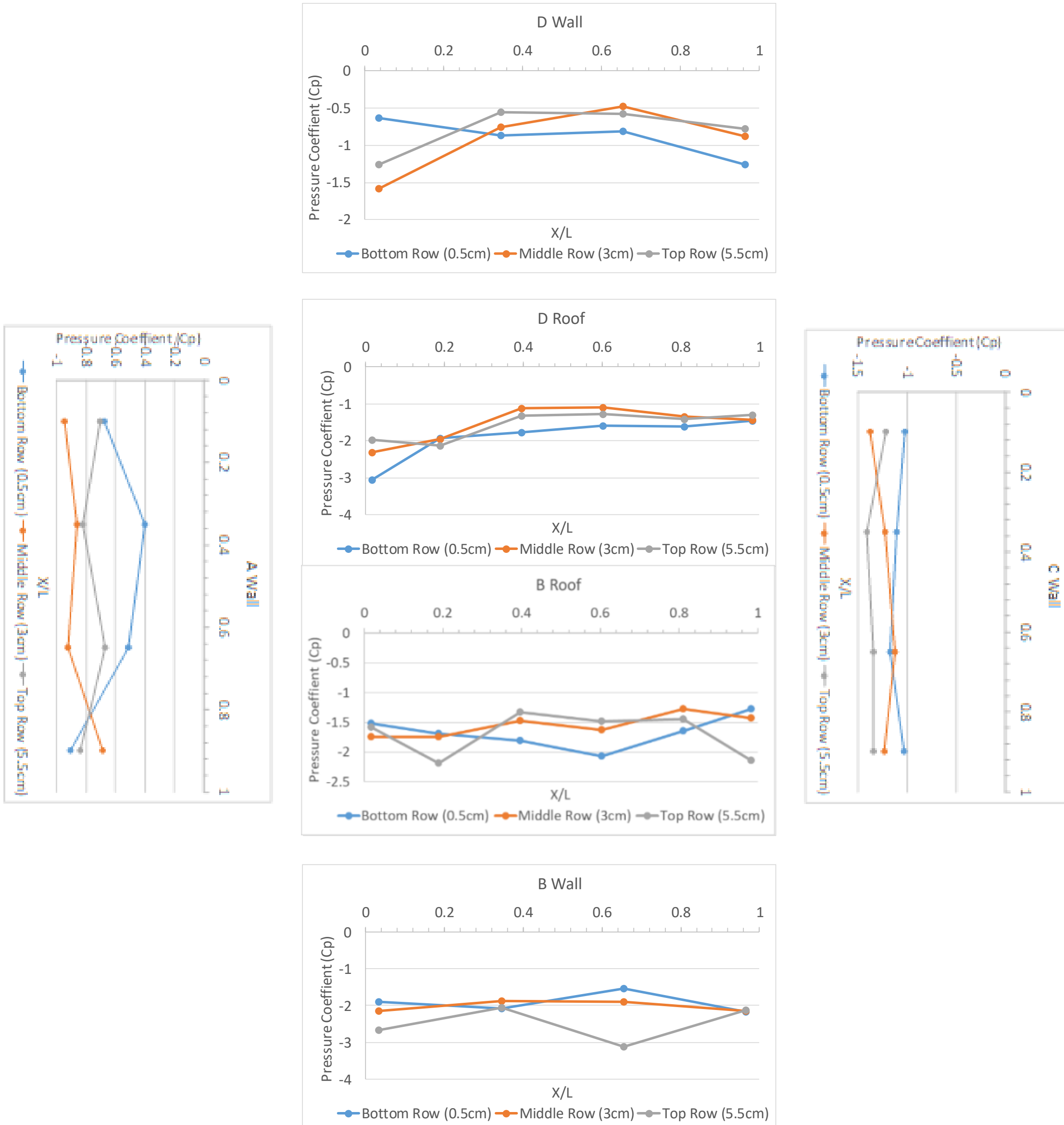

Figure A.24: Model 1, Case 9 (BOA:90°, D:40cm) Peak pressure coefficient plots

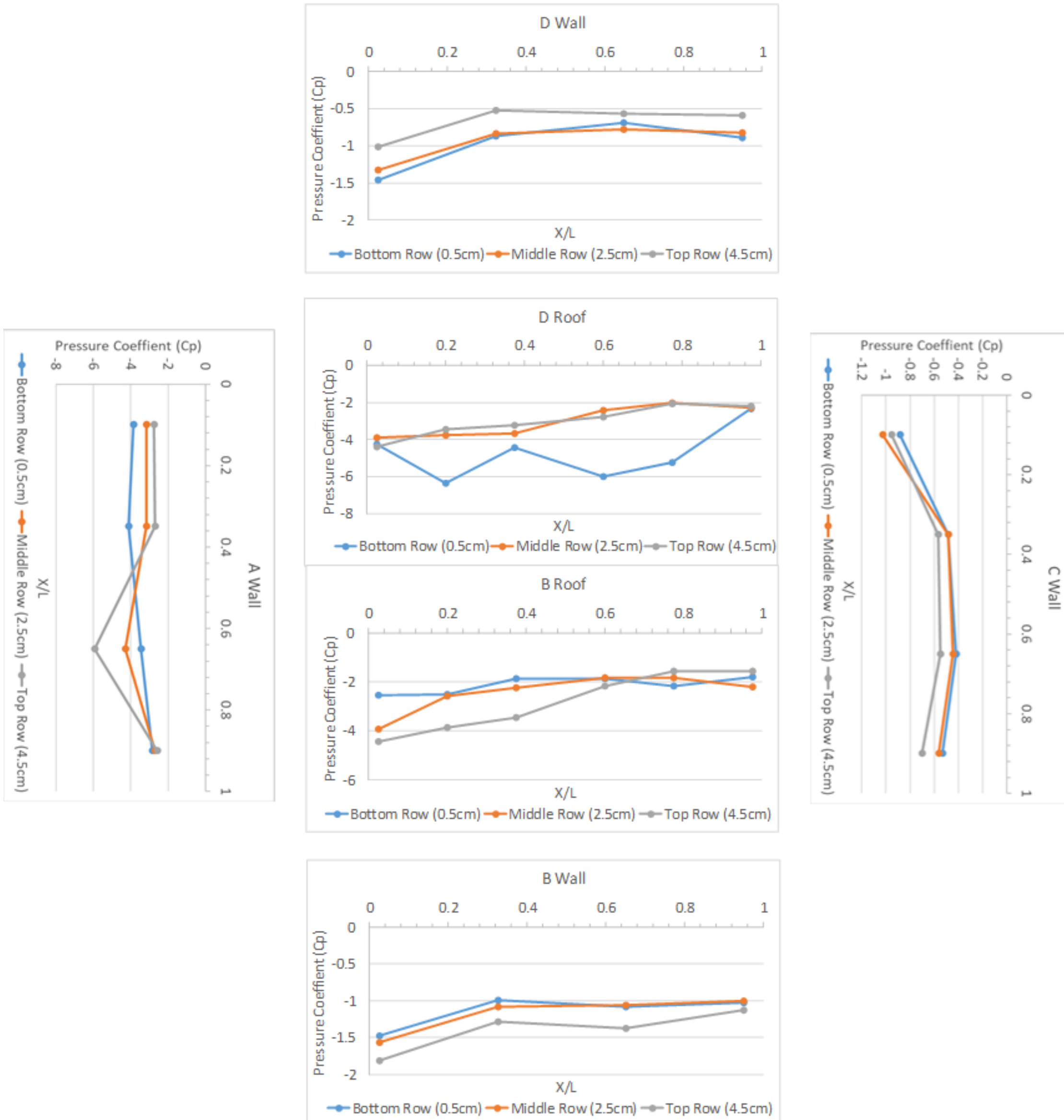

Figure A.25: Model 2, Case 4 (BOA:0°, D:25cm) Peak pressure coefficient plots

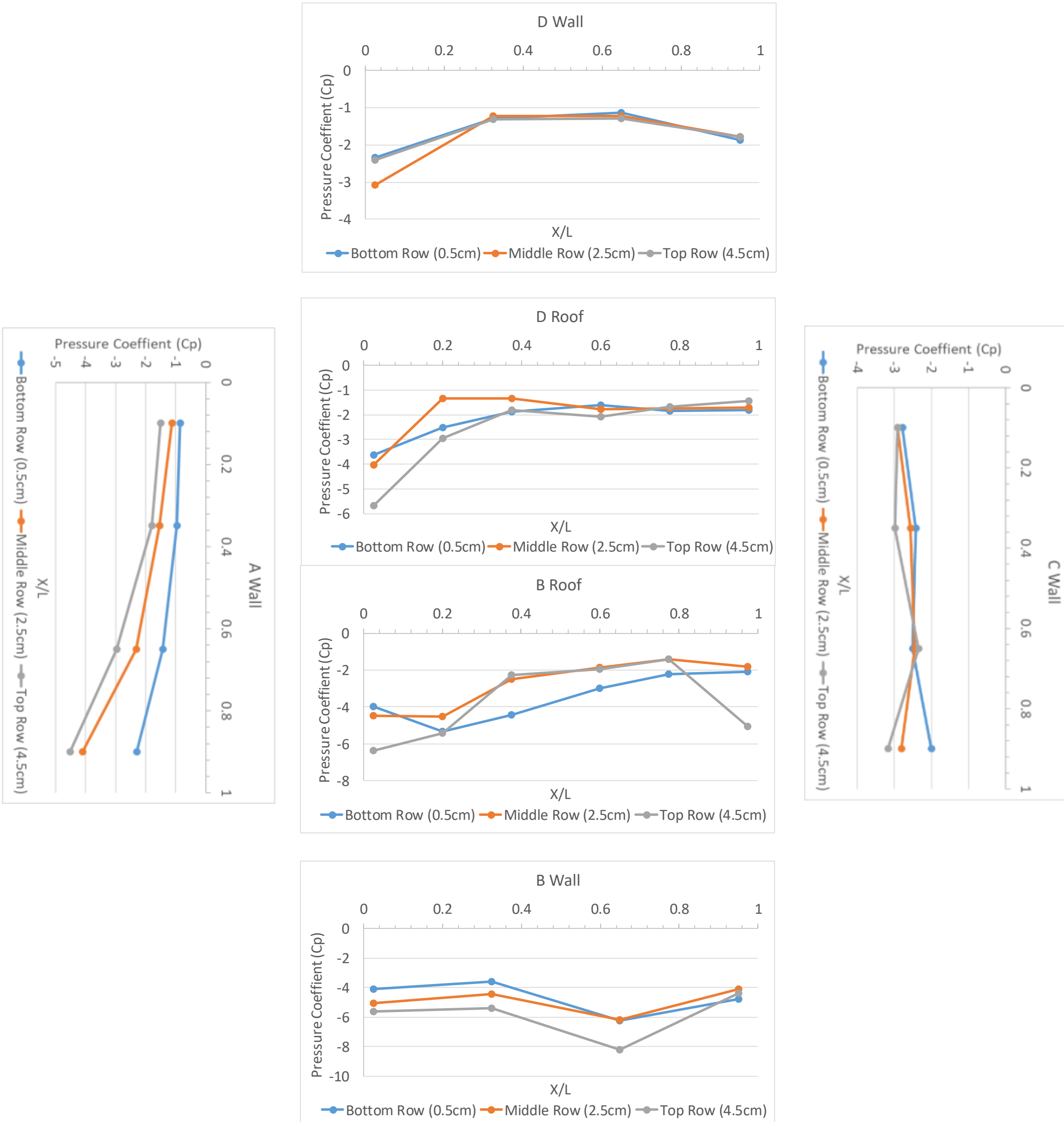

Figure A.26: Model 2, Case 5 (BOA:45°, D:25cm) Peak pressure coefficient plots

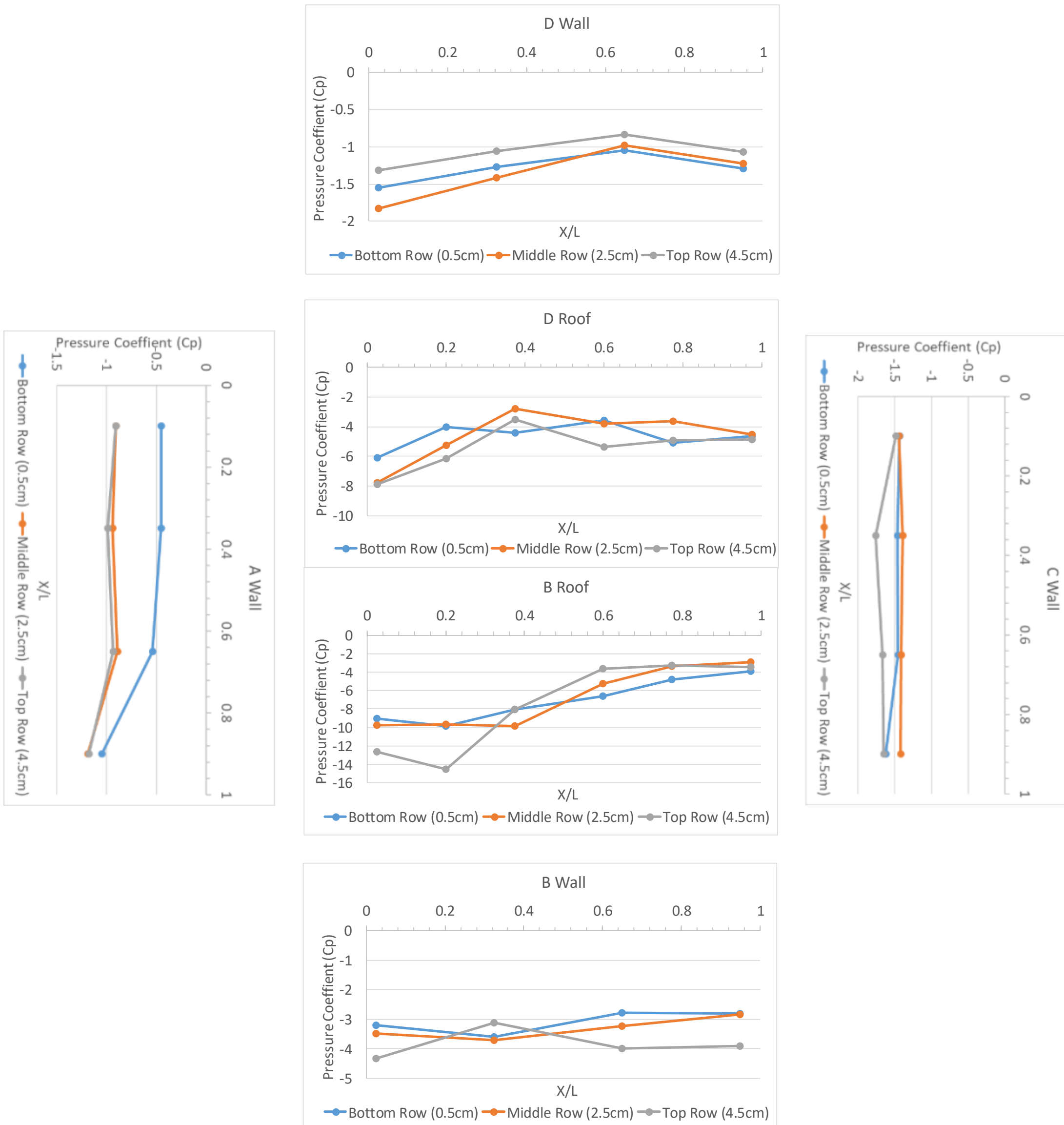

Figure A.27: Model 2, Case 6 (BOA:90°, D:25cm) Peak pressure coefficient plots

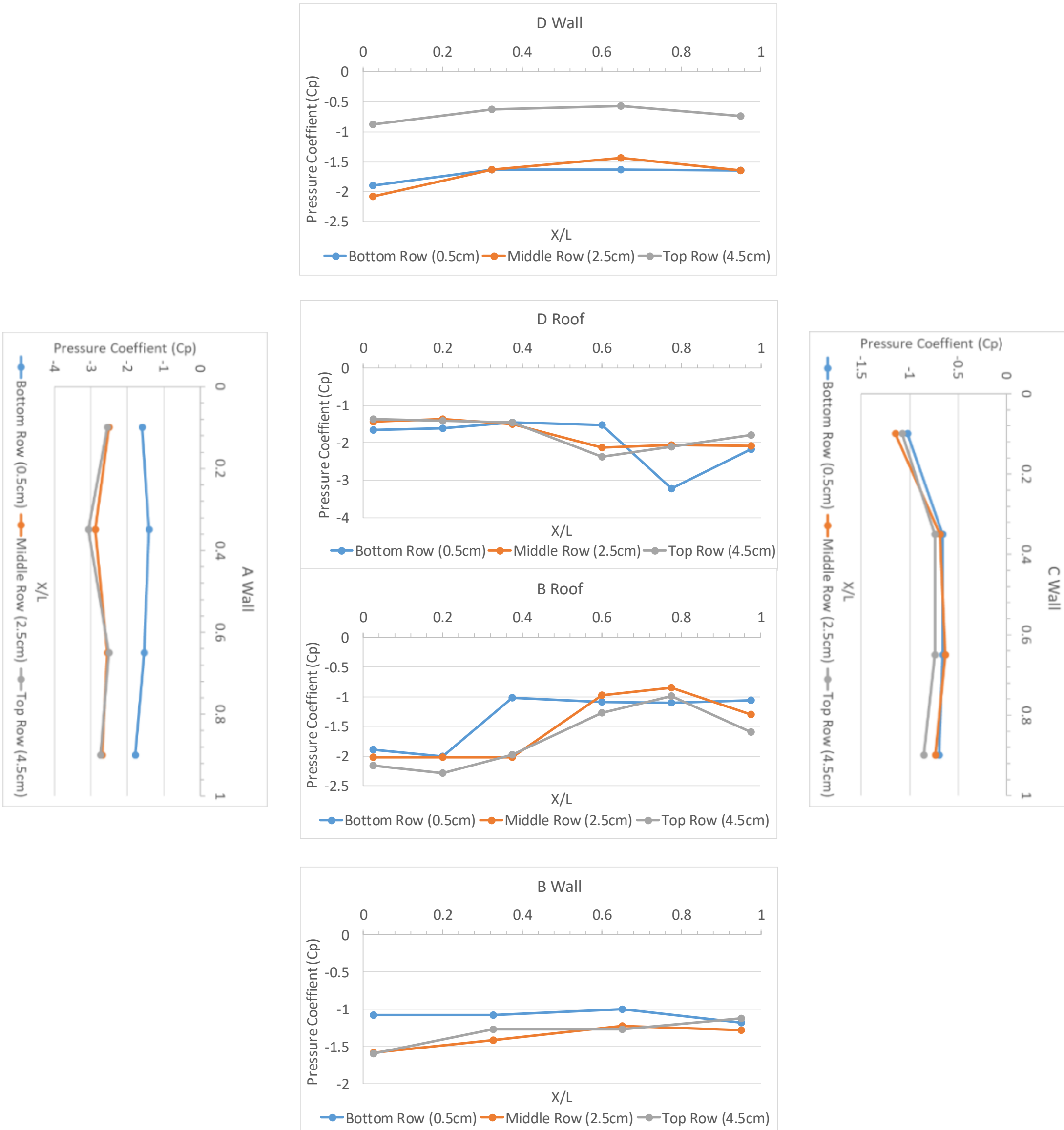

Figure A.28: Model 2, Case 7 (BOA:0°, D:40cm) Peak pressure coefficient plots

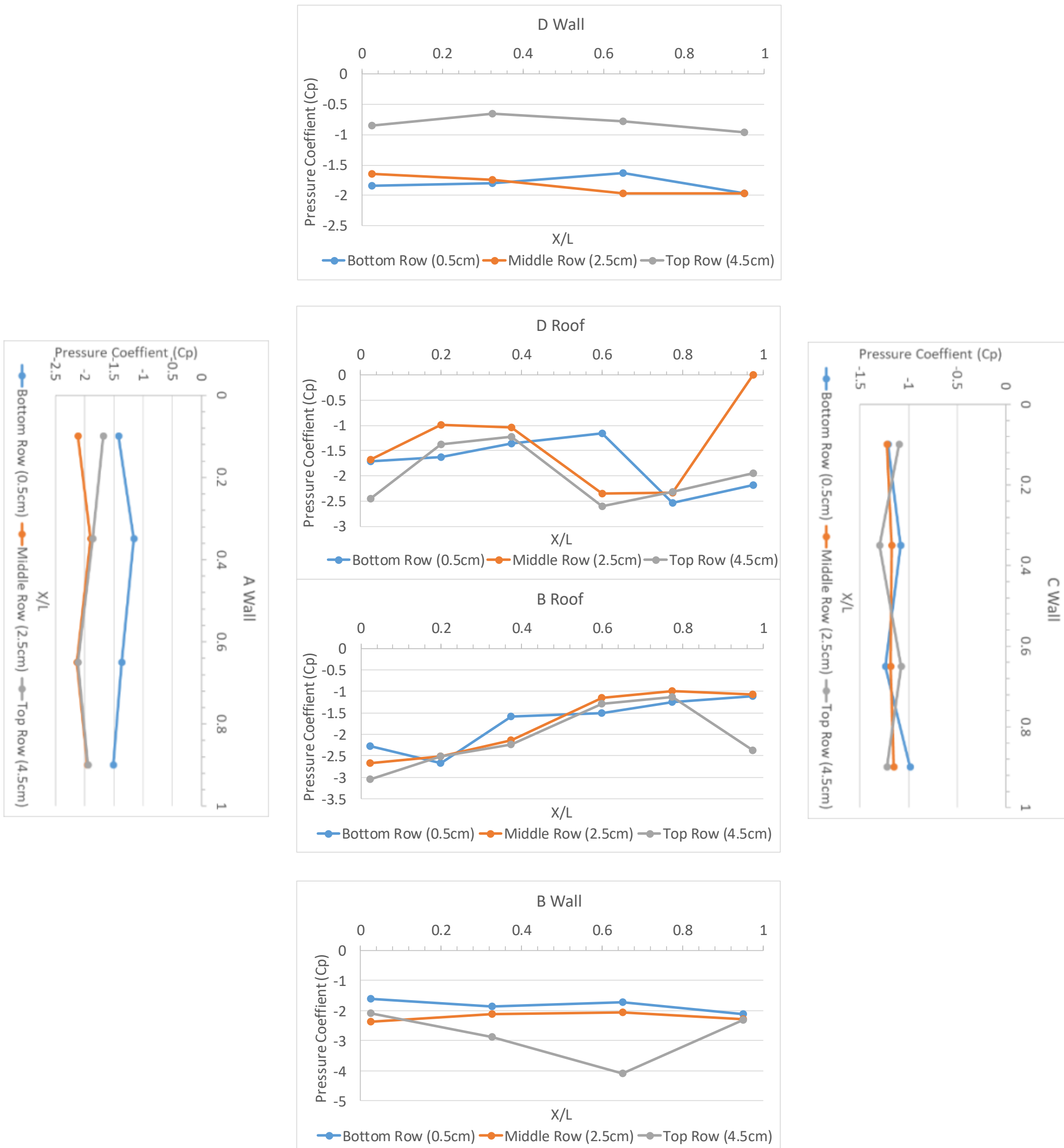

Figure A.29: Model 2, Case 8 (BOA:45°, D:40cm) Peak pressure coefficient plots

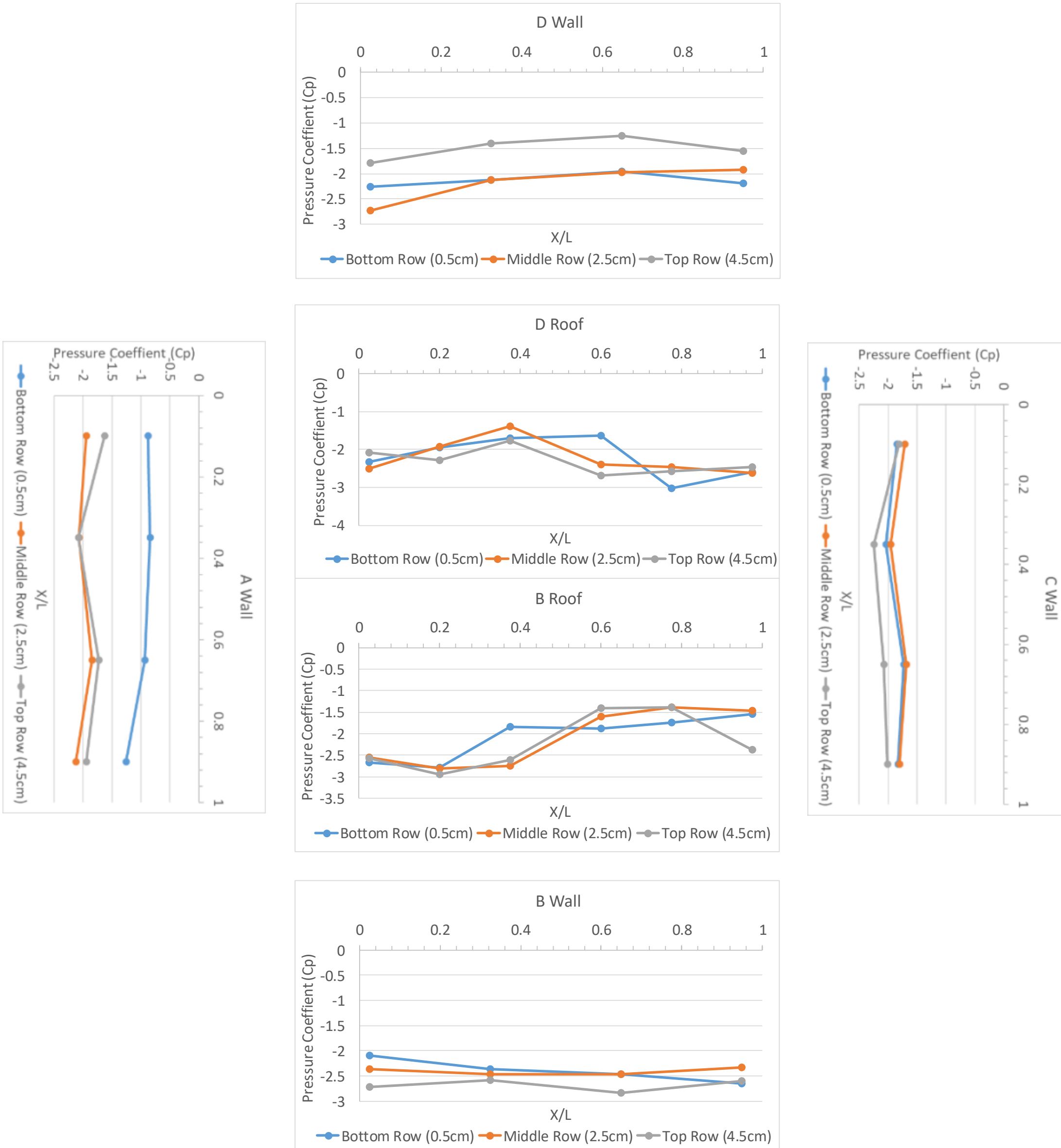

Figure A.30: Model 2, Case 9 (BOA:90°, D:40cm) Peak pressure coefficient plots

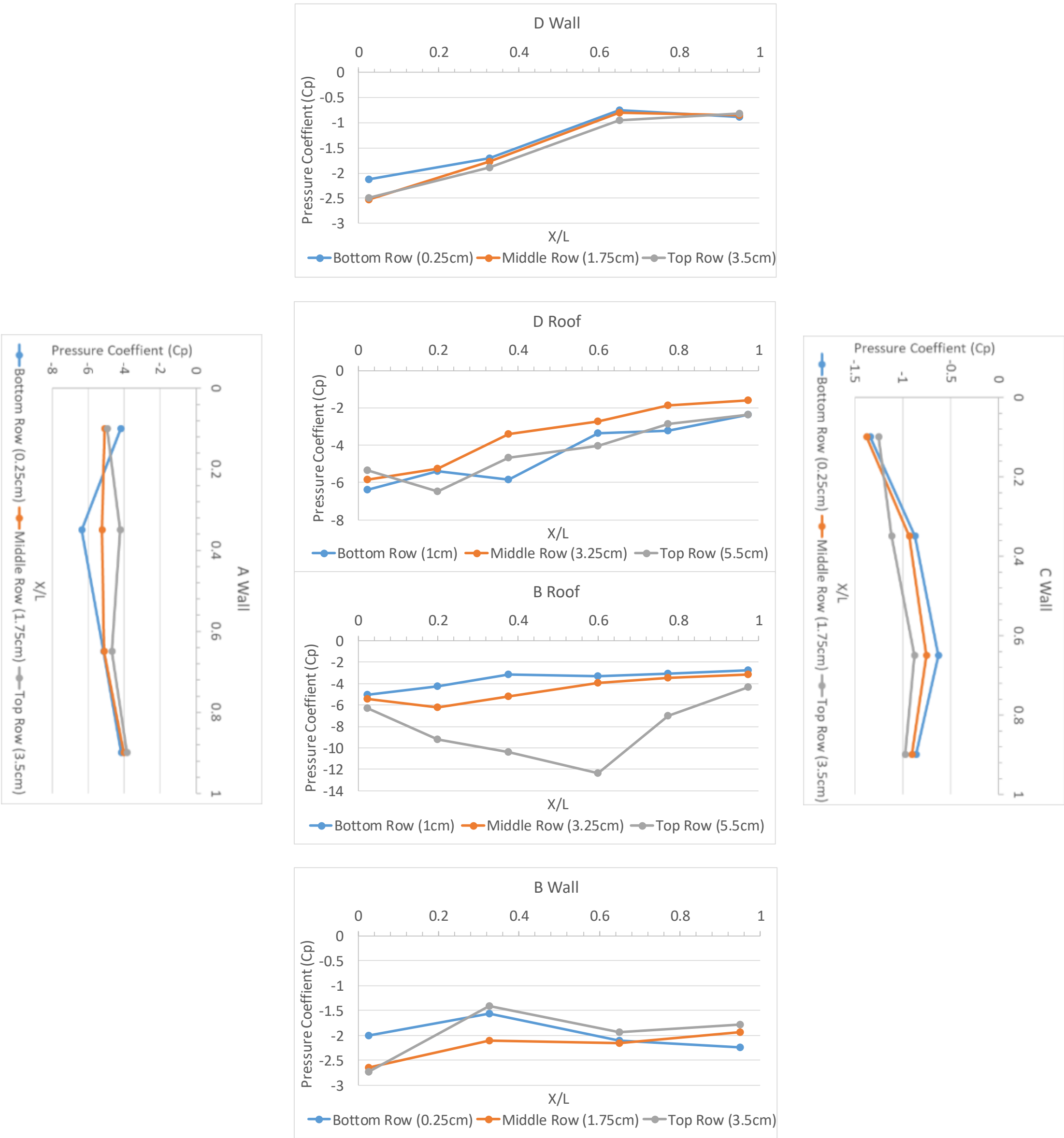

Figure A.31: Model 3, Case 4 (BOA:0°, D:25cm) Peak pressure coefficient plots

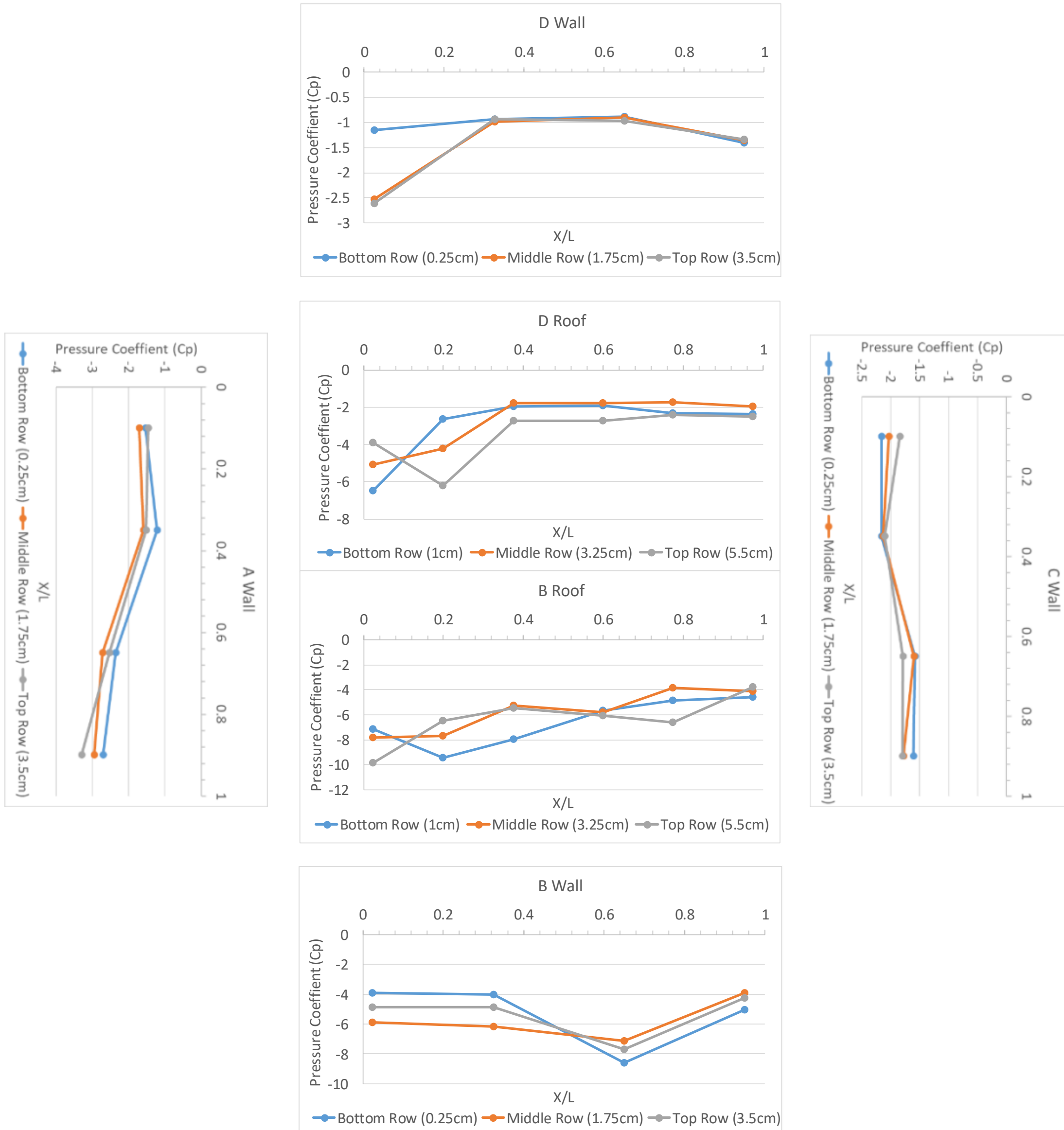

Figure A.32: Model 3, Case 5 (BOA:45°, D:25cm) Peak pressure coefficient plots

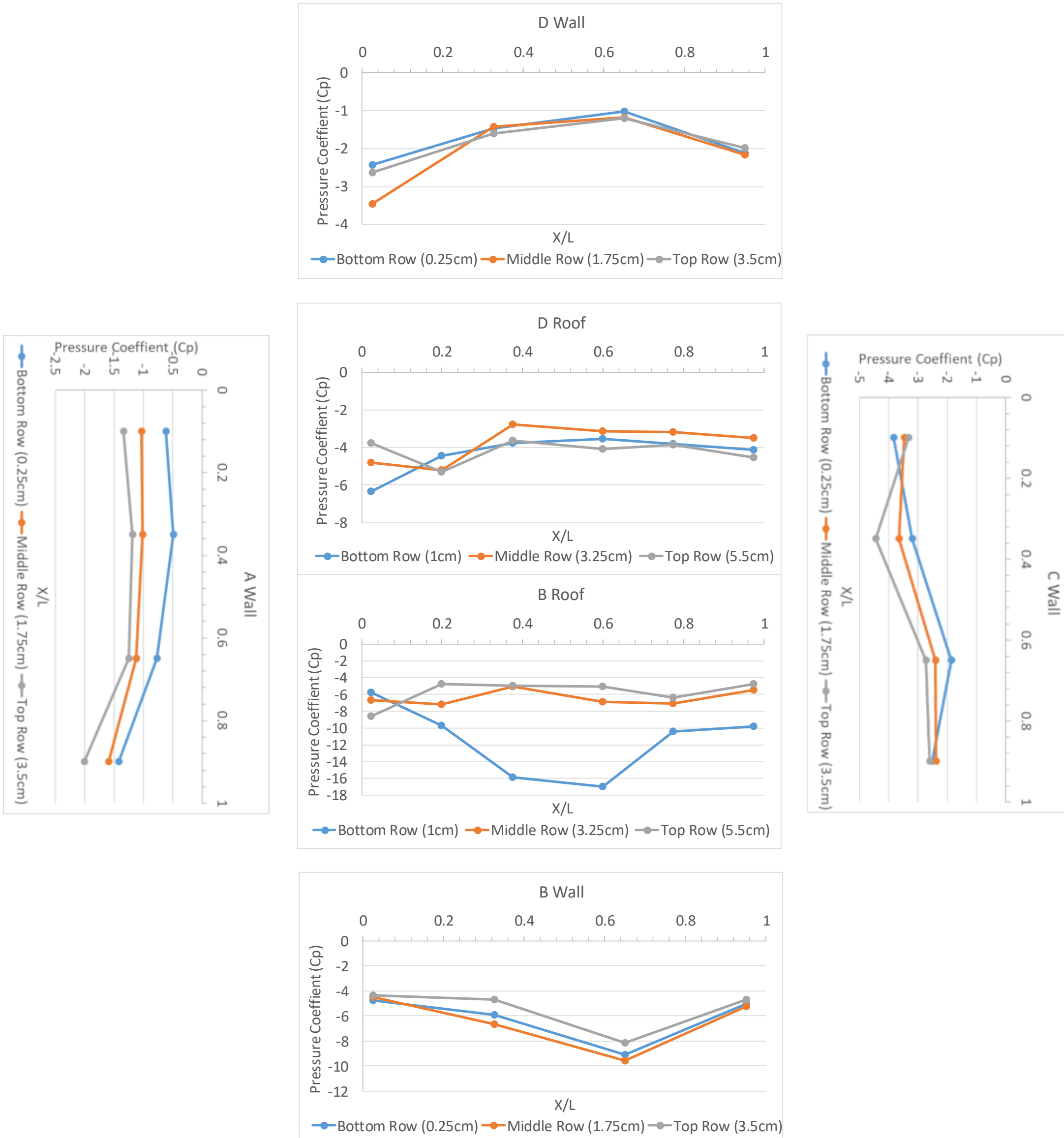

Figure A.33: Model 3, Case 6 (BOA:90°, D:25cm) Peak pressure coefficient plots

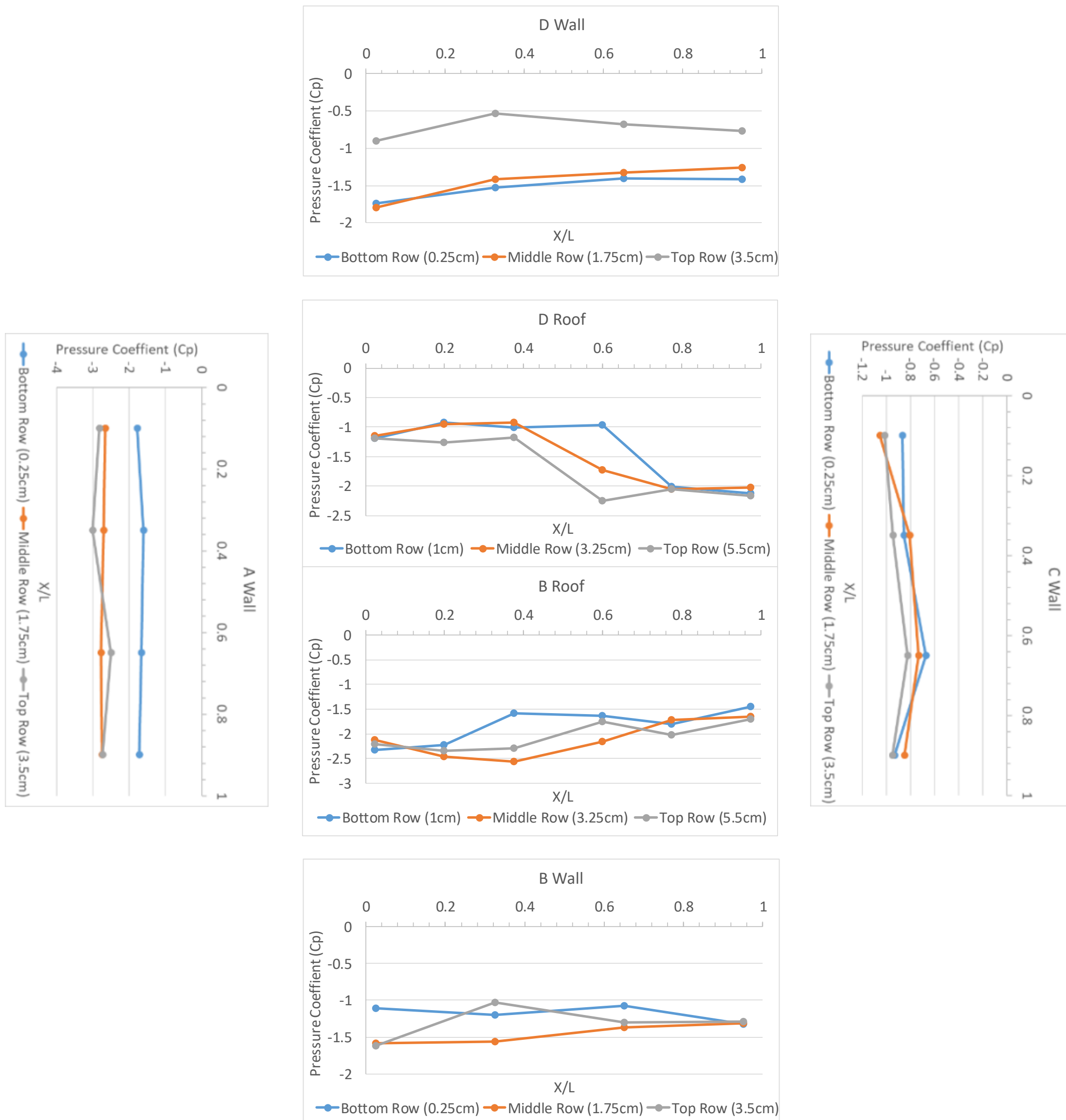

Figure A.34: Model 3, Case 7 (BOA:0°, D:40cm) Peak pressure coefficient plots

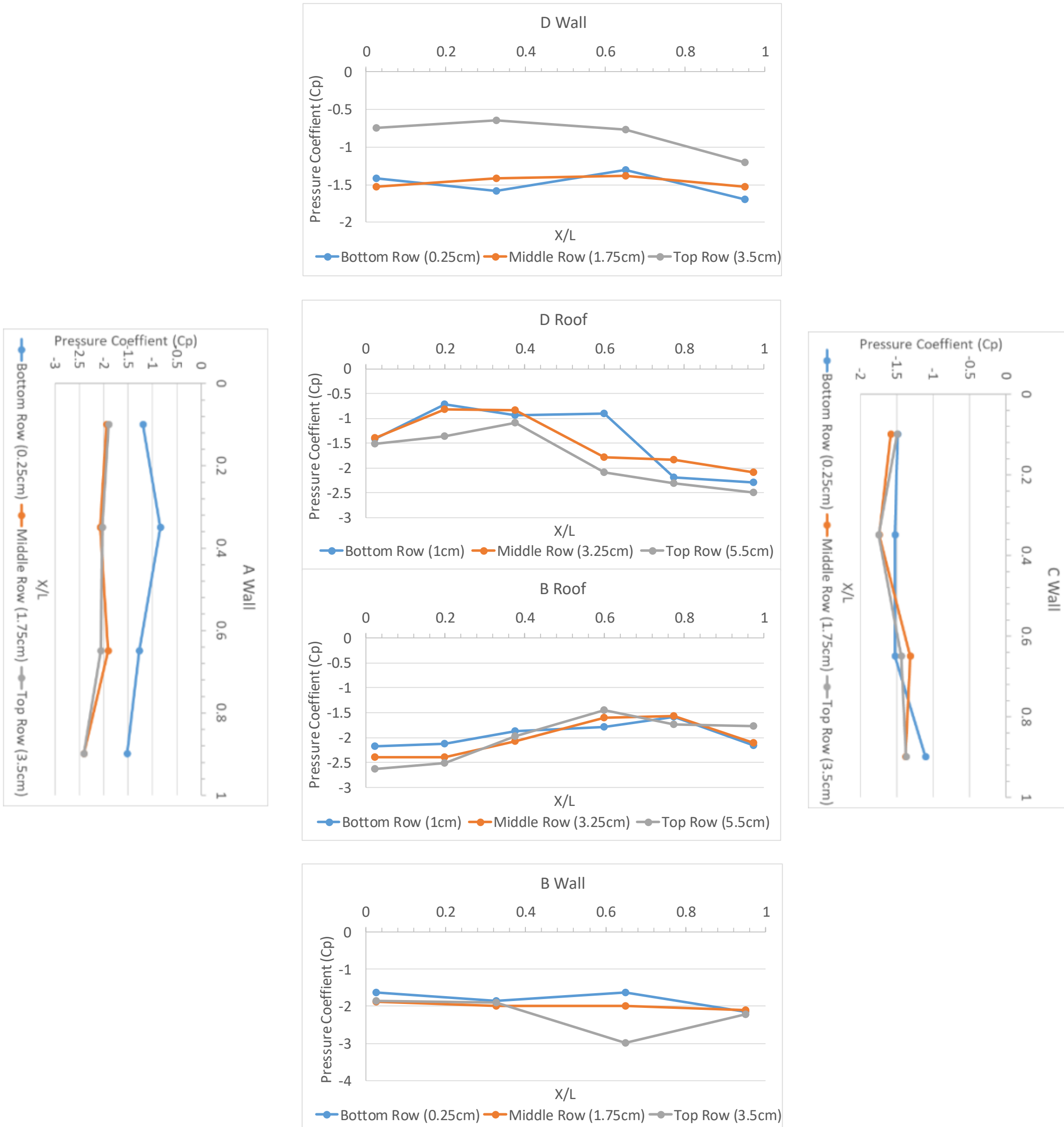

Figure A.35: Model 3, Case 8 (BOA:45°, D:40cm) Peak pressure coefficient plots

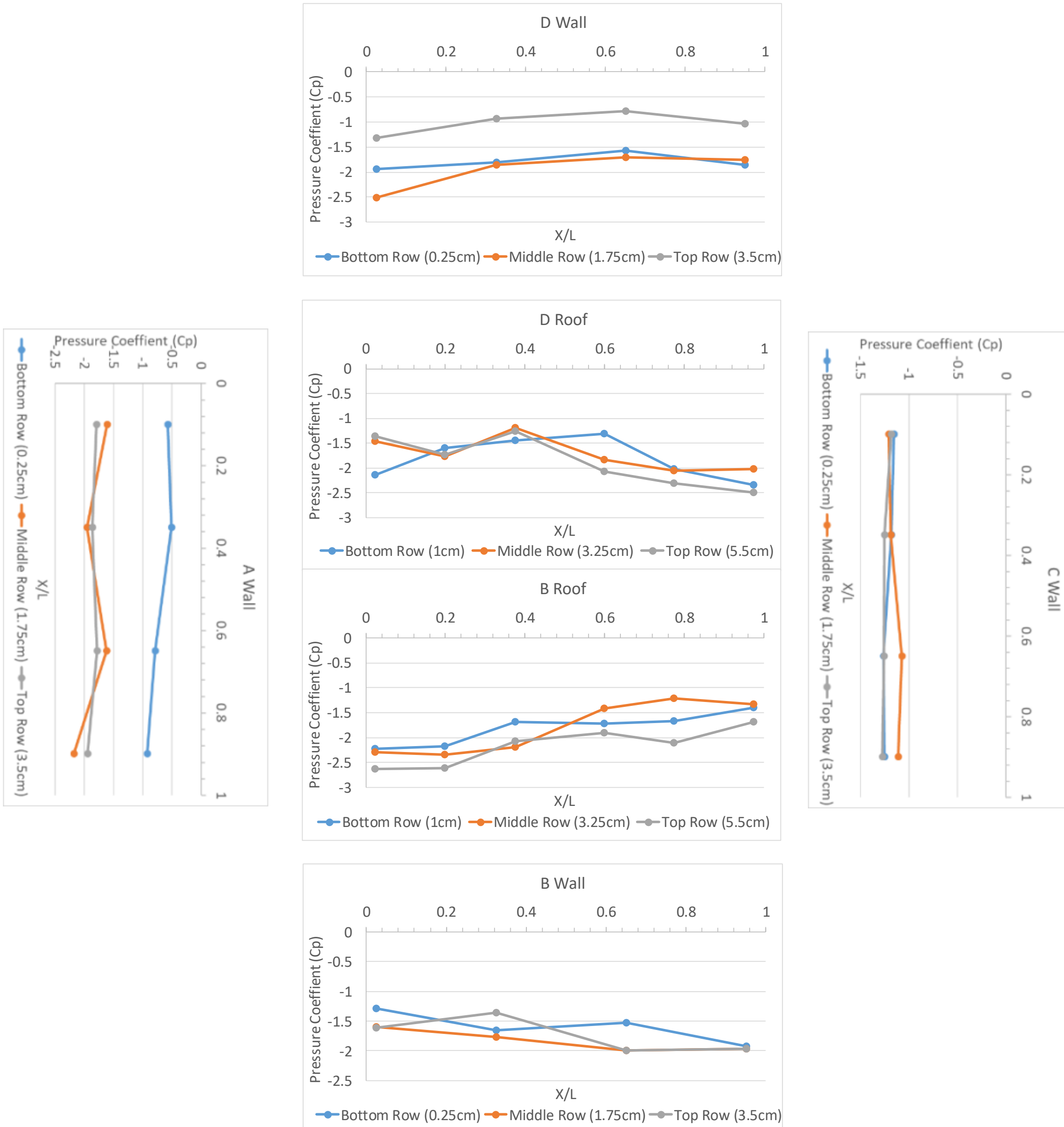

Figure A.36: Model 3, Case 9 (BOA:90°, D:40cm) Peak pressure coefficient plots

Appendix B: Exposure duration analysis

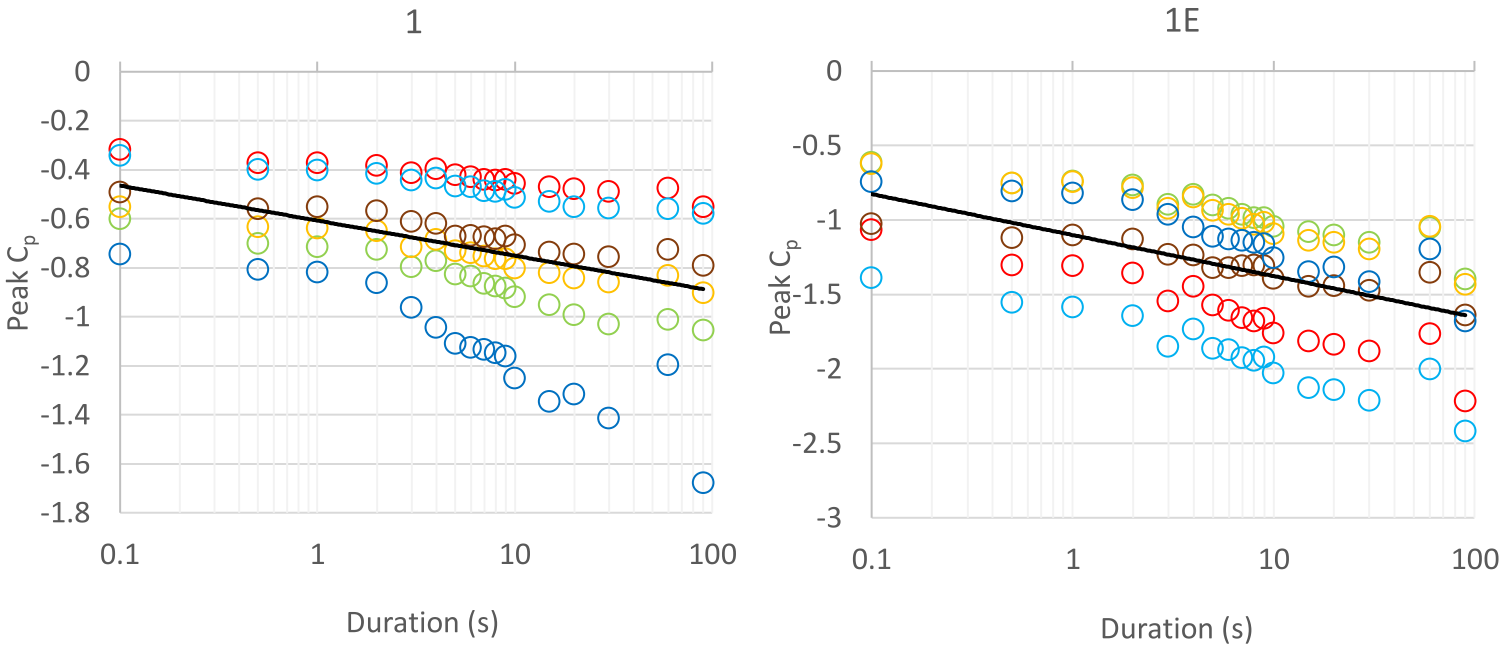

Figure B.1: Peak C_T for different durations in the zones 1 and 1E of 4.1.7.6-A Load Case A for primary structural actions from wind loads acting simultaneously on all surfaces

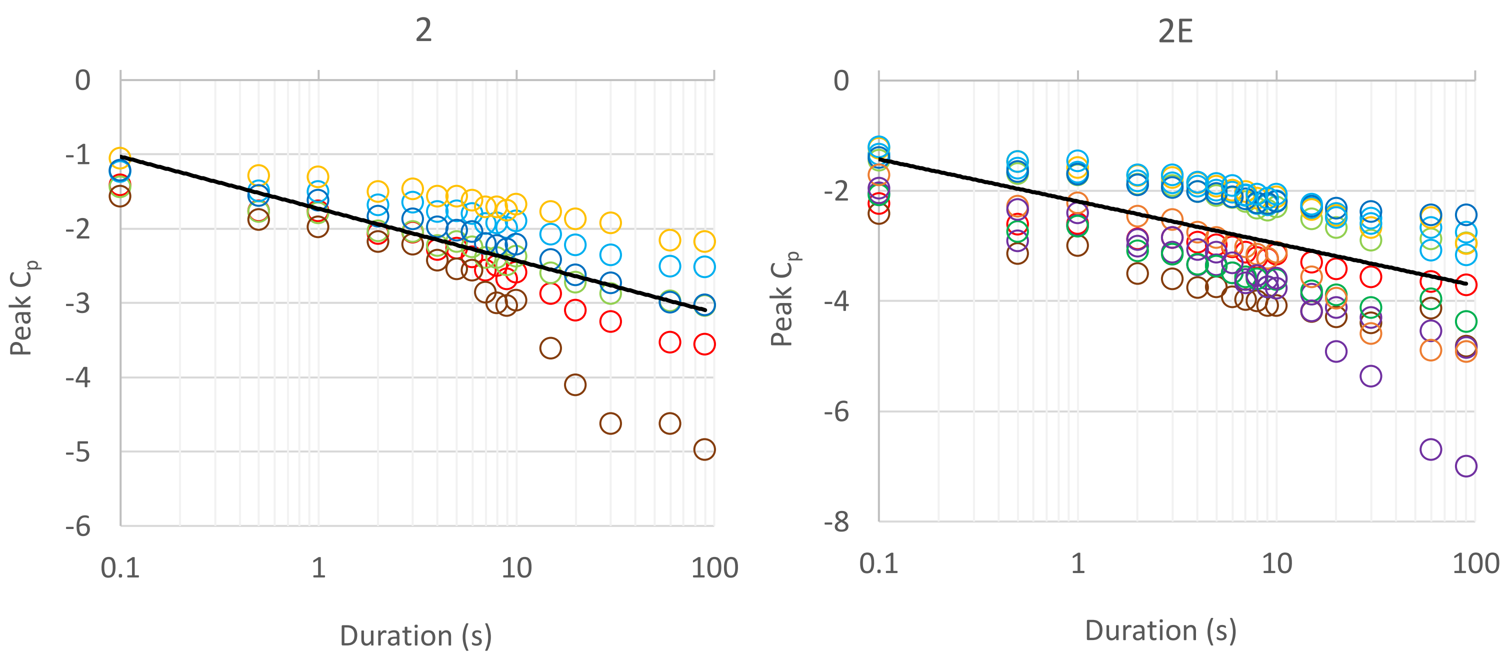

Figure B.2: Peak C_T for different durations in the zones 2 and 2E of 4.1.7.6-A Load Case A for primary structural actions from wind loads acting simultaneously on all surfaces

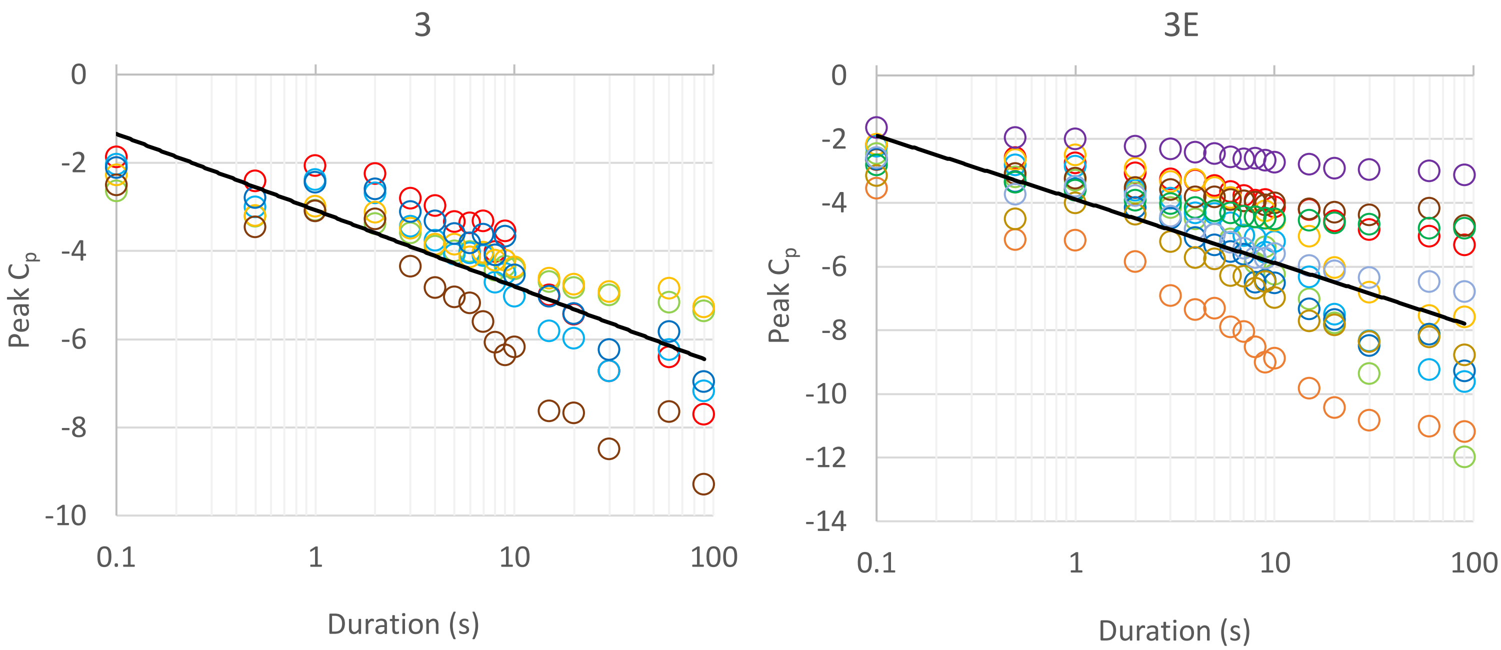

Figure B.3: Peak C_T for -different durations in the zones 3 and 3E of 4.1.7.6-A Load Case A for primary structural actions from wind loads acting simultaneously on all surfaces

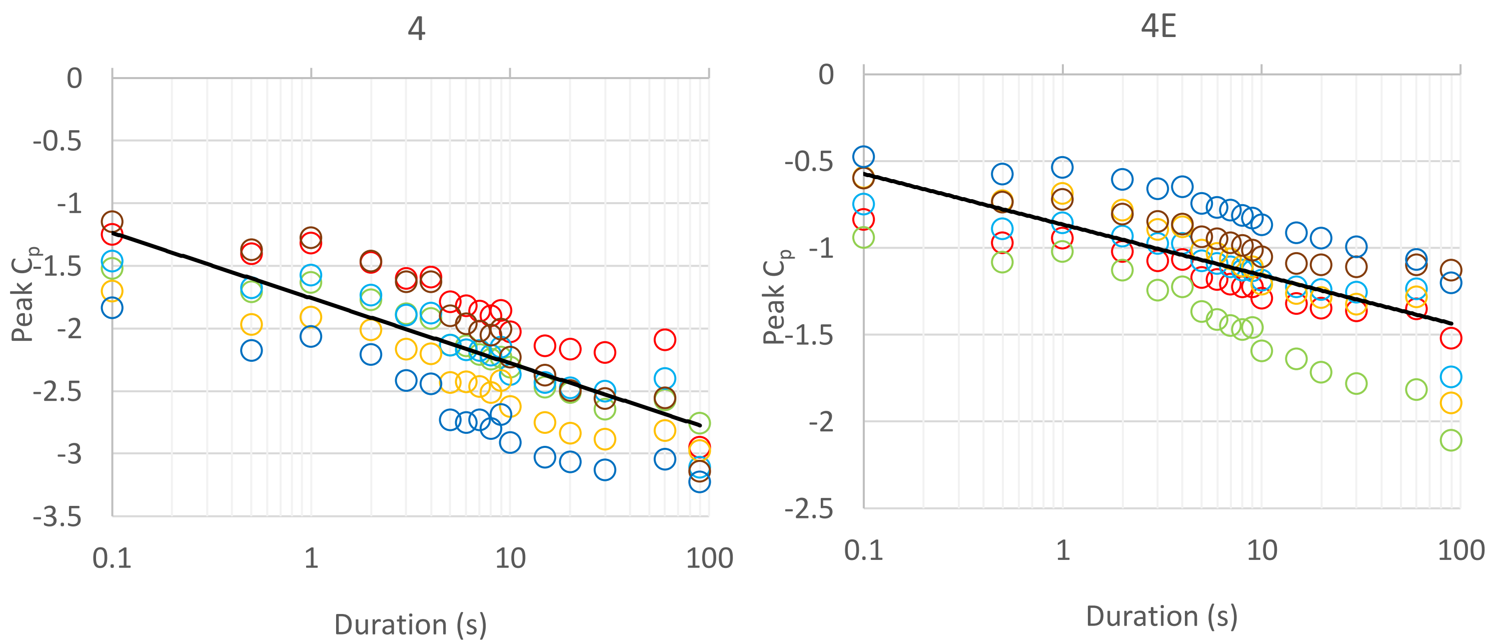

Figure B.4: Peak C_T for different durations in the zones 4 and 4E of 4.1.7.6-A Load Case A for primary structural actions from wind loads acting simultaneously on all surface

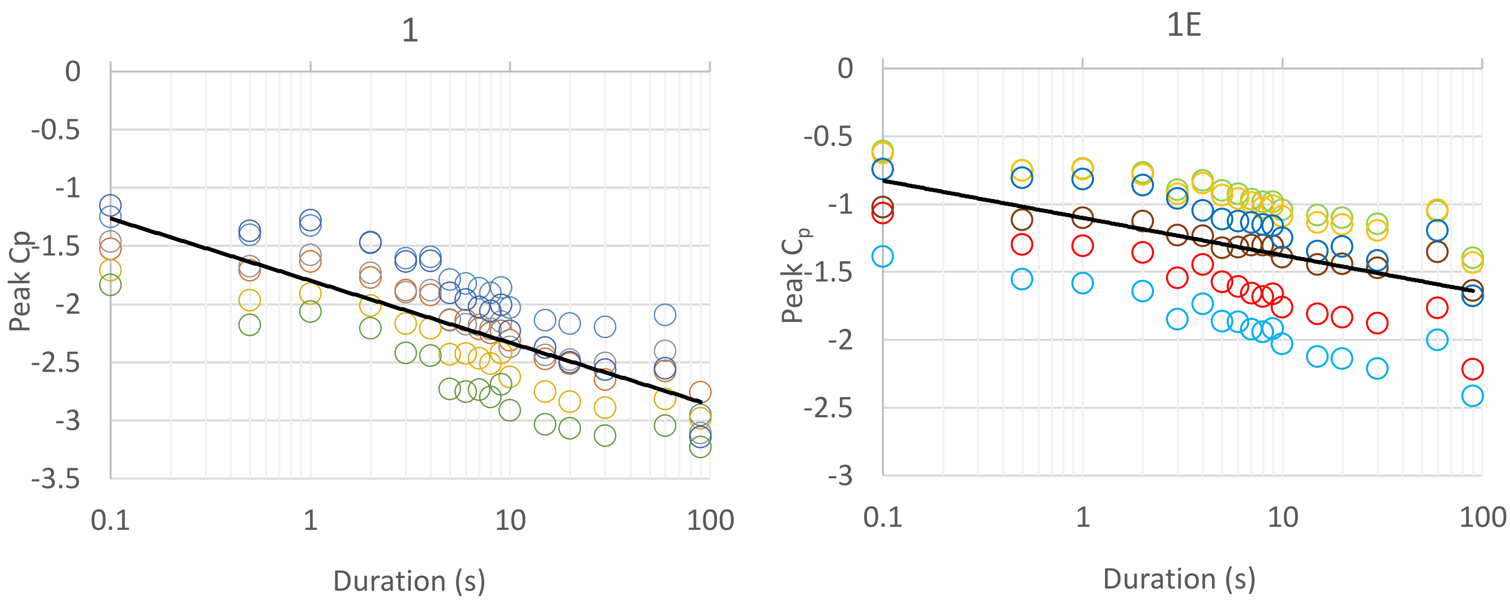

Figure B.5: Peak C_T for different durations in the zones 1 and 1E of 4.1.7.6-A Load Case B for primary structural actions from wind loads acting simultaneously on surfaces

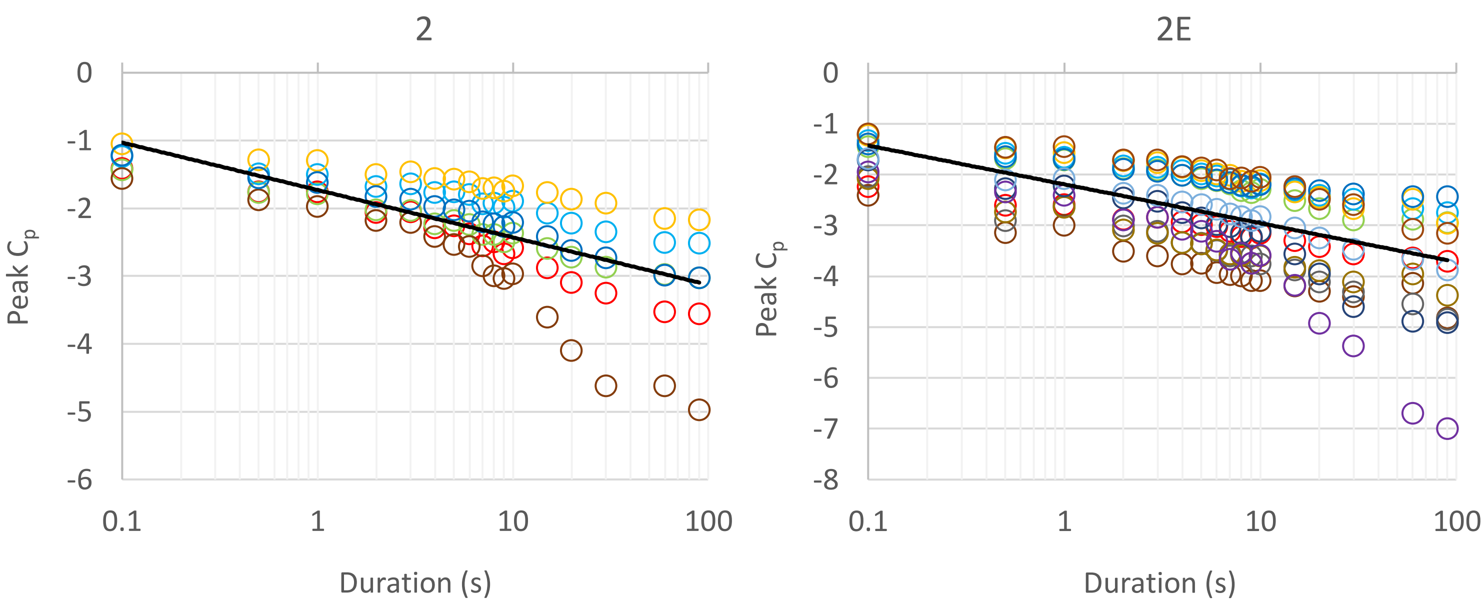

Figure B.6: Peak C_T for different durations in the zones 2 and 2E of 4.1.7.6-A Load Case B for primary structural actions from wind loads acting simultaneously on all surfaces

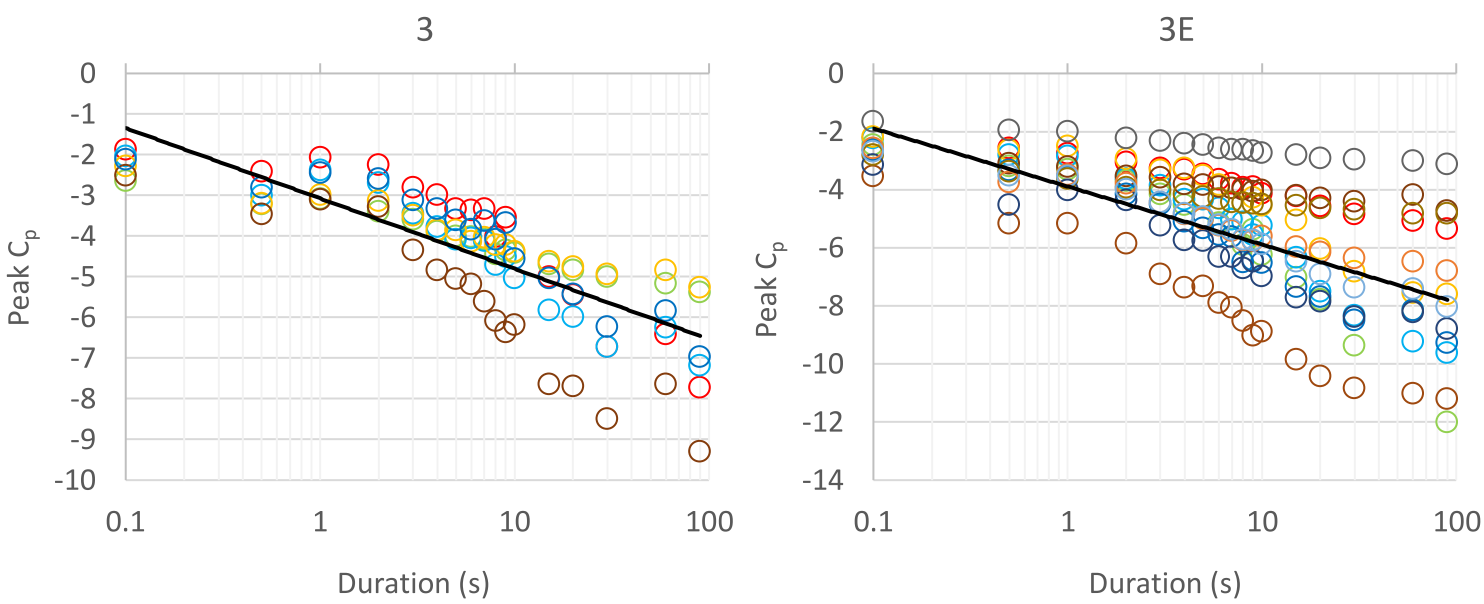

Figure B.7: Peak C_T for different durations in the zones 3 and 3E of 4.1.7.6-A Load Case B for primary structural actions from wind loads acting simultaneously on all surface

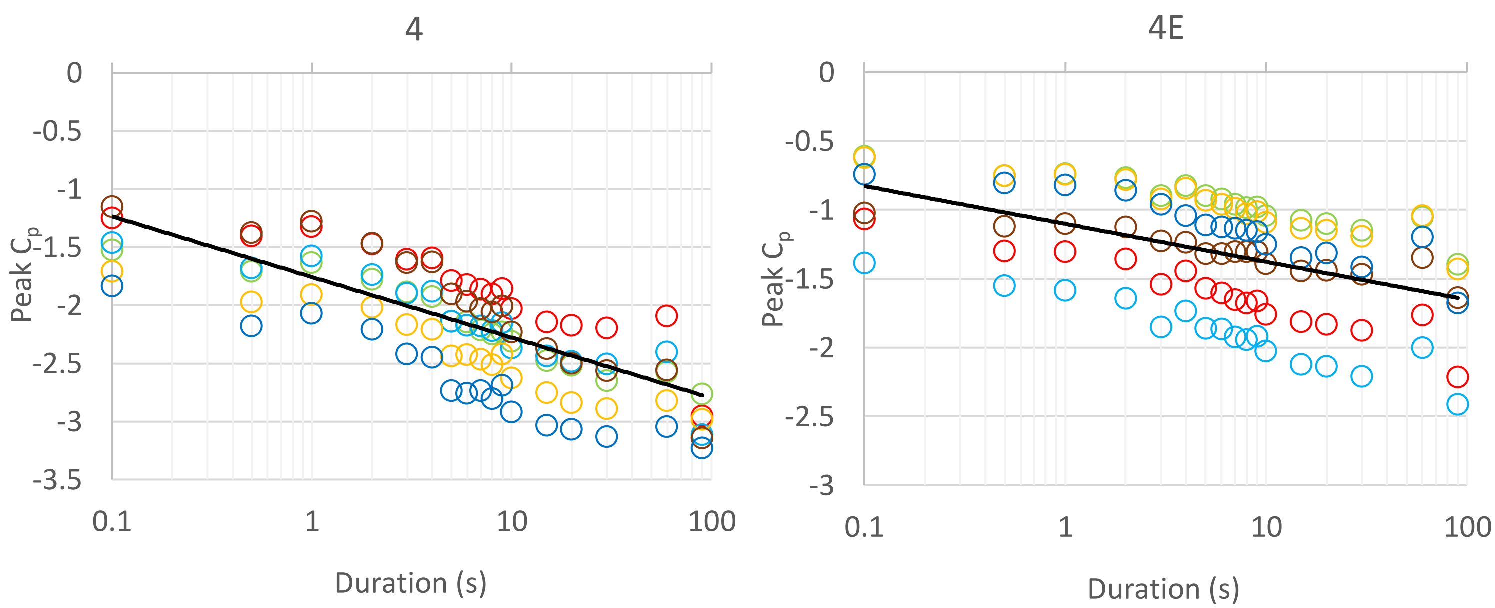

Figure B.8: Peak C_T for different durations in the zones 4 and 4E of 4.1.7.6-A Load Case B for primary structural actions from wind loads acting simultaneously on all surfaces

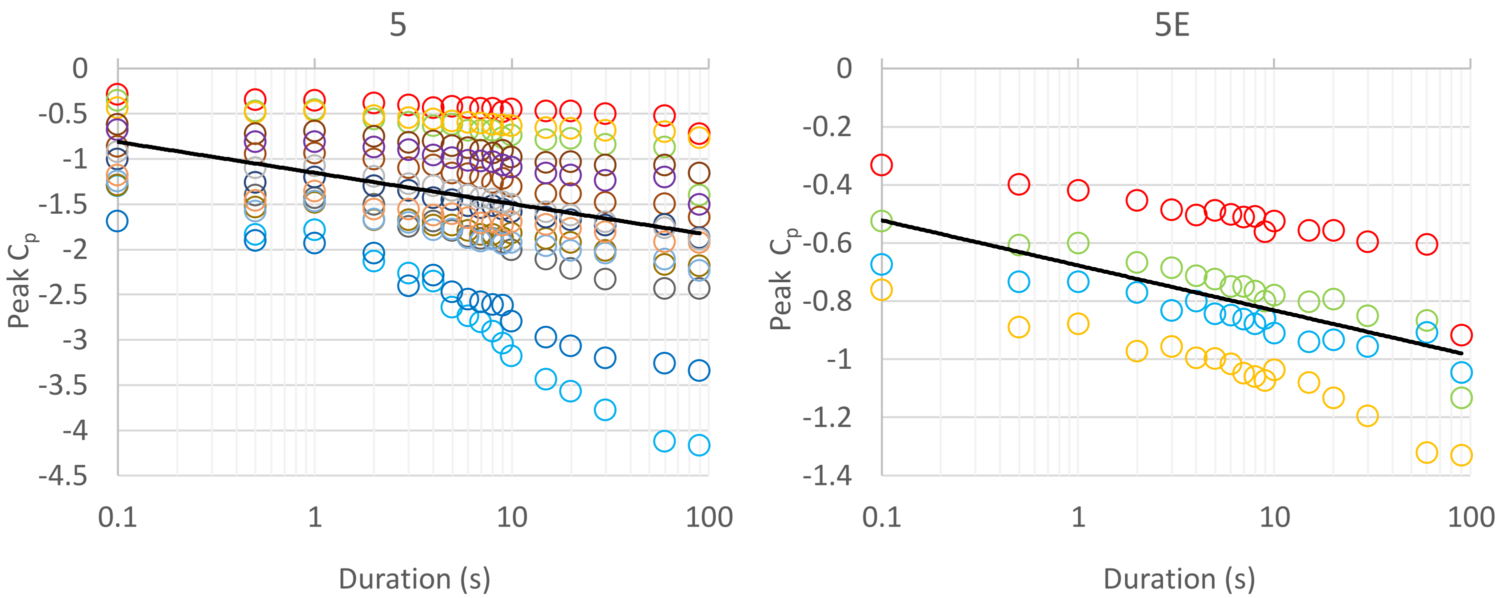

Figure B.9: Peak C_T for different durations in the zones 5 and 5E of 4.1.7.6-A Load Case B for primary structural actions from wind loads acting simultaneously on all building surfaces

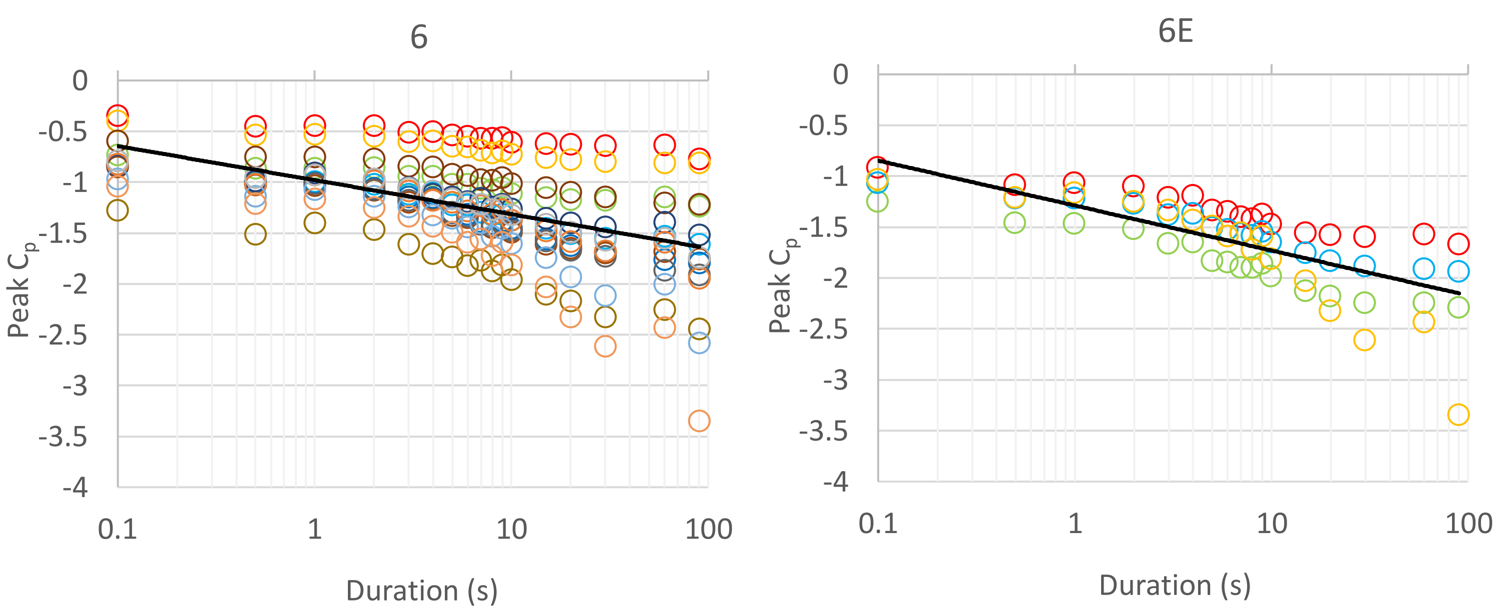

Figure B.10: Peak C_T for different durations in the zones 6 and 6E of 4.1.7.6-A Load Case B for primary structural actions from wind loads acting simultaneously on all building surfaces

Table B.1 : Multiple of the highest to lowest magnitude of the C_T value for zones of figures 4.33 to 4.36 for house 2, case 2 (NBCC 4.1.7.6-A Load Case A)

	0.1s	0.5s	1s	2s	3s	4s	5s	6s	7s	8s	9s	10s	15s	20s	30s	3-pk Avg
1	2.3	2.2	2.2	2.3	2.3	2.6	2.6	2.6	2.6	2.6	2.6	2.7	2.9	2.8	2.9	2.7
1E	2.3	2.1	2.1	2.1	2.1	2.1	2.1	2.0	2.0	2.0	2.0	1.9	2.0	1.9	1.9	2.0
2	1.5	1.5	1.5	1.4	1.5	1.5	1.6	1.6	1.7	1.8	1.7	1.8	2.0	2.2	2.4	2.2
2E	2.1	2.3	2.1	2.3	2.3	2.3	2.2	2.2	2.2	2.1	2.1	2.2	2.1	2.3	2.3	2.2
3	1.4	1.4	1.5	1.5	1.5	1.6	1.5	1.5	1.7	1.5	1.8	1.4	1.6	1.6	1.7	1.6
3E	2.5	3.0	2.9	3.0	3.3	3.7	3.7	3.6	3.9	4.1	4.1	4.0	4.5	4.4	4.4	4.4
4	1.6	1.6	1.6	1.5	1.5	1.5	1.5	1.5	1.5	1.5	1.4	1.4	1.4	1.4	1.4	1.3
4E	2.0	1.9	1.9	1.9	1.9	1.9	1.8	1.8	1.8	1.8	1.8	1.8	1.8	1.8	1.8	1.8

Table B.2: Multiple of the highest to lowest magnitude of the C_T value for zones of figures 4.37 to 4.42 for house 2, case 2 (NBCC 4.1.7.6-A Load Case B)

	0.1s	0.5s	1s	2s	3s	4s	5s	6s	7s	8s	9s	10s	15s	20s	30s	3-pk Avg
1	1.6	1.6	1.6	1.5	1.5	1.5	1.5	1.5	1.5	1.5	1.4	1.4	1.4	1.4	1.4	1.3
1E	2.0	1.9	1.9	1.9	1.9	1.9	1.8	1.8	1.8	1.8	1.8	1.8	1.8	1.8	1.8	1.8
2	1.5	1.5	1.5	1.4	1.5	1.5	1.6	1.6	1.7	1.8	1.7	1.8	2.0	2.2	2.4	2.2
2E	2.5	3.0	2.9	3.0	3.3	3.7	3.7	3.6	3.9	4.1	4.1	4.0	4.5	4.4	4.4	4.4
3	1.4	1.4	1.5	1.5	1.5	1.6	1.5	1.5	1.7	1.5	1.8	1.4	1.6	1.6	1.7	1.6
3E	2.1	2.3	2.1	2.3	2.3	2.3	2.2	2.2	2.2	2.1	2.1	2.2	2.1	2.3	2.3	2.2
4	2.3	2.2	2.2	2.3	2.3	2.6	2.6	2.6	2.6	2.6	2.6	2.7	2.9	2.8	2.9	2.7
4E	2.3	2.1	2.1	2.1	2.1	2.1	2.1	2.0	2.0	2.0	2.0	1.9	2.0	1.9	1.9	2.0
5	4.5	4.6	4.2	4.3	4.2	4.1	4.3	4.3	4.3	4.3	4.0	4.3	4.1	4.3	4.1	3.8
5E	1.4	1.4	1.4	1.4	1.5	1.4	1.6	1.7	1.6	1.7	1.8	1.9	2.0	2.0	2.1	2.2
6	3.2	2.8	2.8	2.7	2.8	2.9	2.8	2.8	2.8	2.7	2.7	2.7	2.8	3.0	3.3	2.9
6E	3.0	2.7	2.5	2.6	2.5	2.7	2.6	2.6	2.5	2.6	2.6	2.6	2.7	2.7	2.9	2.8